Characterisation of the Two Pore Domain Potassium Ion Channels, TASK1 and TASK3, Associated with Pulmonary Arterial Hypertension and *KCNK9* Imprinting Syndrome

Robyn Grace Holden

A thesis submitted in partial fulfilment of the requirements of the University of Kent and the University of Greenwich for the Degree of Doctor of Philosophy

November 2019

Declaration

I certify that this work has not been accepted in substance for any degree and is not concurrently being submitted for any degree other than that of the Doctor of Philosophy being studied at the Universities of Greenwich and Kent. I also declare that this work is the result of my own investigations except where otherwise identified by references and that I have not plagiarised the work of others.

Candidate

Signed: Robyn Grace Holden

Date: November 2019

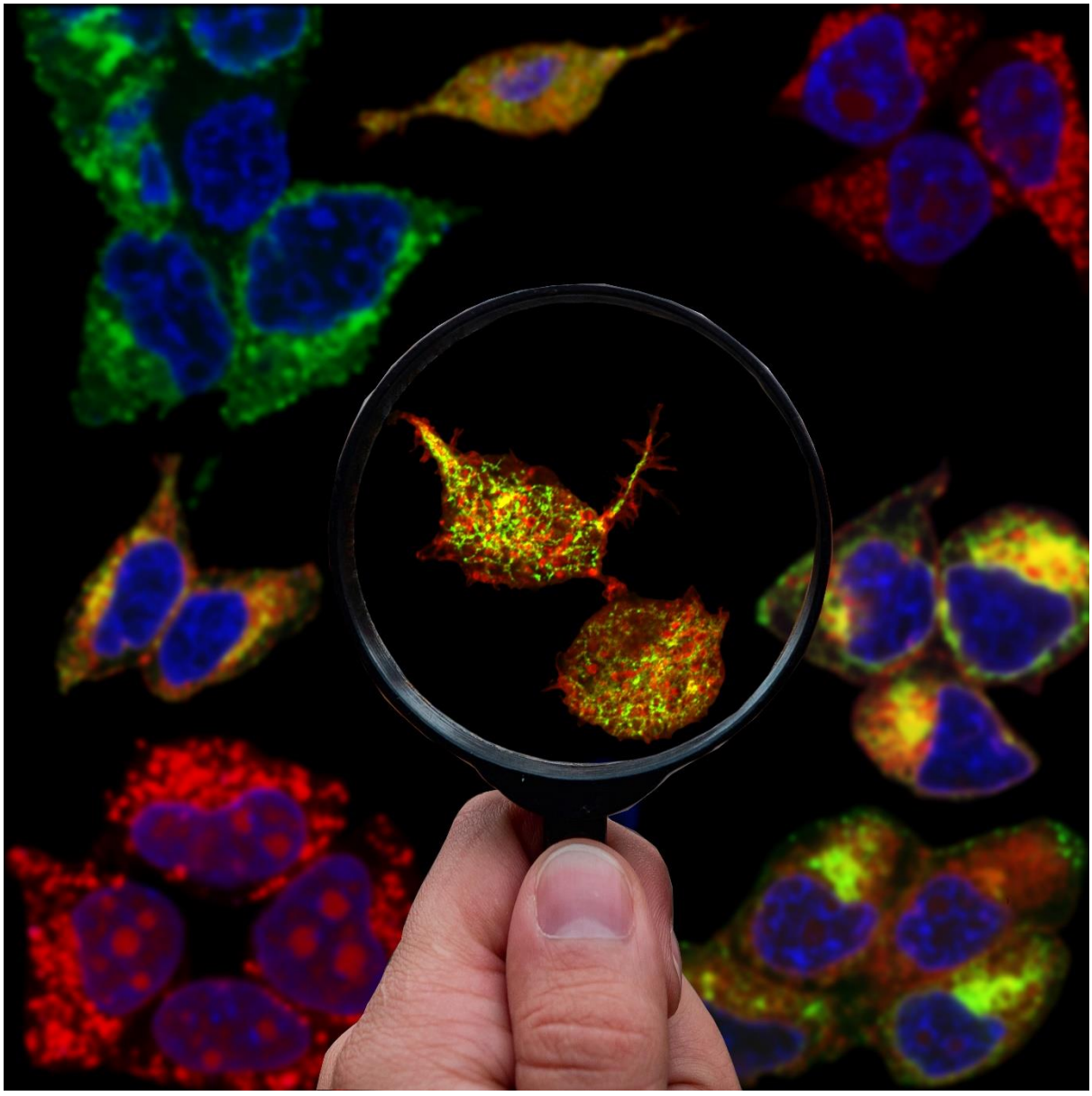

Acknowledgements

First, I would like to thank my PhD supervisors, Dr Emma Veale and Professor Alistair Mathie for supporting me these past three years. To Alistair, I always looked forward to our meetings. Your calm demeanour, extensive knowledge and steadfast advice always made the biggest hurdles seem manageable. To Emma, I apologise for all the times that I have told you that the item was not in the place you told me it was, only for you to find it exactly where you said it would be (standard 'mum' move). Whilst I am grateful for your unwavering patience and unlimited scientific knowhow, I will miss our intense bake-off debriefs, scandalous chatter and good fun. It has been a privilege to work with you both.

I would like to thank the laboratory team, extending a special thanks to Kevin and Yvonne. Kevin, thanks for making me laugh every day. I will never forgive you for planting the 'BB' seed deep into my brain the night before presenting at an international conference. Yvonne, thank you for always being so wise and a continuing voice of reason.

I offer sincere apologies to my family. I apologise to my mum, my dad and my brother for all the years leading up to this point where you have put up with my 'dementor-like' tendencies, for which I now have no more excuses. Your continual support has never failed me, and I am forever grateful for all the times I heard your voices down the phone over the last 6 years of my academic journey, pushing me forward when I felt that I couldn't do it alone. Likewise, thank you to my closest friends Vaishalee Kanjaria and Alexandra Hope, who must also feel like they have lived through the emotional turmoil of a PhD.

Finally, I am indebted to this PhD for crossing my path with that of Vilius Savickas: care provider, joker, husband-to-be and all-round cheerleader. Running into you on the first day was the best thing to happen during this time. I could never have finished this mammoth task without your unwavering support, your perseverance through the worst of my writing-induced emotional storms and continual willingness to fetch snacks. To you I am most grateful. The end of this chapter only marks the beginning of many more to come.

Abstract

This study investigated the regulation and function of two-pore domain potassium (K2P) channels in disease. TASK family of K2P ion channels are predominantly expressed at the cell surface where they maintain the resting membrane potential to regulate neuronal excitability. TASK channel variants associated with diseases such as pulmonary arterial hypertension (PAH) (TASK1_G106R/L214R) and *KCNK9* Imprinting Syndrome (TASK3_G236R/Y205C/Y205Δ) demonstrate reduced activity. Due to the constitutively active nature of TASK channels expressed at the plasma membrane, changes in the level of surface expression can alter current density and subsequently function. Using a combination of imaging, biochemical and electrophysiological techniques, this study explored the effects of pathogenic variants on channel trafficking to the plasma membrane and other organelles. The findings presented here show that the reduced plasma membrane expression of the *KCNK9* Imprinting channel mutation, TASK3_G236R cannot explain all the pathogenic consequences of this mutation. The G236R channels expressed were functionally altered when compared to WT, as interaction with activated $G\alpha_{q/11}$ remains, yet G protein-coupled receptor (GPCR) inhibition is lost. The plasma membrane expression of Y205C and Y205Δ pathogenic variants was unaffected, but the channels were electrophysiologically silent. Low arousal is one symptom of *KCNK9* Imprinting Syndrome which is linked to mitochondrial dysfunction. As membrane expression of TASK3 variants were indistinguishable from the WT, this symptom is potentially a consequence of an inability to respond to GPCR activation by wakeful neurotransmitters such as histamine. TASK3 is regulated by hormones and transmitters acting through GPCR via the $G\alpha_{q/11}$ subclass. Without a crystal structure, TASK3 functional mechanisms remain subjective. Removal of an extreme proximal [VLRFLT] motif from the cytosolic C-terminus abolishes regulation, reminiscent of that seen in *KCNK9* Imprinting syndrome. Since it is unclear whether this motif behaves as a binding site for regulatory molecules or is essential for intracellular signal transduction, this study details the production of the C-terminal fragment. Synchrotron radiation circular dichroism confirmed that the produced fragment was conformationally correct proven by the direct binding of $G\alpha_{q/11}$ to the C-terminus, although the role of the VLRFLT as a binding site or transducer of signal remains to be elucidated.

Reduced activity of TASK1 is a key event in PAH pathogenesis. In this study I show that the non-functional G106R and L214R TASK1 channel variants are translated and expressed at the plasma membrane as efficiently as the WT. This study also explored the hypoxic characteristics inherent to PAH. TASK1 expression in mitochondria was investigated and confirmed for the first time. The expression of the G106R and L214R mutations appeared to be no different to the WT, implying that the presence of these mutations in the mitochondria may not contribute to the progression of PAH.

Table of Contents

List of Figures

List of Tables

Abbreviations

2-AG	2-Arachidonoyl-Glycerol
5ptase IV	Phosphoinositide-Specific Inositol Polyphosphate 5-Phosphatase IV
Ach	Acetylcholine
ANOVA	Analysis of Variance
AP	Action Potential
APP	Amyloid Precursor Protein
ARF	ADP-Ribosylation Factor
BFCN	Basal Forebrain Cholinergic Neurons
BIM	Bisindoylmaleimide-1-Hydrochloride
BRPM2	Bone Morphogenic Protein Receptor Type II
Ca^{2+}	Calcium
CART	Cocaine- and Amphetamine Regulated Transcript Peptide
CD	Circular Dichroism
CF	Cystic Fibrosis
CGN	Cerebellar Granule Neurons
CIE	Clathrin-Independent Endocytosis
CLASP	Clathrin-Associated Sorting Proteins
CME	Clathrin-Mediated Endocytosis
CNS	Central Nervous System
COPI	Coatomer Protein Pomplex 1
Ct	C-Terminus
CFTR	Cystic Fibrosis Transmembrane Regulator
DAG	Diacylglycerol
DLS	Dynamic Light Scattering
DMEM	Dulbecco Minimum Essential Medium
DMSO	Dimethylsulfoxide
DNA	Deoxyribose Nucleic Acid
DPSS	Diode-Pumped Solid State
DTNB	5”-Dithio-*bis*(2-nitrobenzoic acid)
DTT	Dithiothreitol
EAE	Experimentally Induced Autoimmune Encephalomyelitis
EAG	Ether-A-Go-Go Related Gene
EC	Extracellular
***E.* Coli**	*Escherichia* Coli
EEG	Electroencephalogram
EIP	Extracellular Ion Pathway

ER	Endoplasmic Reticulum
ERSD	ER Storage Diseases
FFA	Flufenamic Acid
GDP	Guanosine-Diphosphate
GFP	Green Fluorescent Protein
GHK	Goldman-Hodgkin-Katz
GIRKs	G Protein-Gated Inward Rectifier Potassium Channels
GPCR	G-Protein Coupled Receptor
GTP	Guanosine-Triphosphate
Gö6976	12-(2-Cyanoethyl)-6,7,12,13-Tetrahydro-13-Methyl-5-Oxo-5*H*-Indolo(2,3-a)-Pyrolo(3,4-c)-Carbazole
H1	Histamine Receptor 1
HA	Hemagglutinin
HEK	Human Embryonic Kidney
HEPES	4-(2-Hydroxyethyl)-1 Piperazineethanesulfonic Acid
HIV	Human Immunodeficiency Virus
hPAH	Heritable Pulmonary Arterial Hypertension
HPV	Hypoxic Pulmonary vasoconstriction
HUGO	Human Genome Organisation
IC	Intracellular
IDP	Intrinsically Disordered Protein
IDPR	Intrinsically Disordered Protein Region
IK_{SO}	Standing Outward Potassium Current
IP_3	Inositol-Triphosphate
iPAH	Idiopathic Pulmonary Arterial Hypertension
K^+	Potassium
K2P	Two Pore Domain Potassium Channel
K_{ATP}	ATP-Sensitive Potassium Channel
K_{Ca}	Calcium-Activated Potassium Channel
K_{IR}	Inwardly Rectifying Potassium Channel
K_{Na}	Sodium-Activated Potassium Channel
K_V	Voltage-Gated Potassium Channel
KO	Knock Out
LTP	Long Term Potentiation
MBP	Mannose-Binding Protein
MOC	Mander's Overlap Coefficient
mRNA	Messenger Ribonucleic Acid

MS	Multiple Sclerosis
MTSES	Sodium-(2-Sulfonatoethyl)-Methanethiosulfonate
Na^+	Sodium
NAchR	Nicotinic Acetylcholine Receptor
Na_v	Voltage-gated sodium channel
NMDAR	Anti-N-Methyl-D-Aspartate Receptor
NSAID	Non-Steroidal Anti-Inflammatory Drugs
NTS1	Neurotensin Receptor 1
P	Probability Level
PA	Phosphatidic Acid
PAH	Pulmonary Arterial Hypertension
PASMC	Pulmonary Arterial Smooth Muscle Cells
PBS	Phosphate-Buffered Saline
PCC	Pearson's Correlation Coefficient
PD	Pore Domain
PDI	Poly Dispersity Index
PDL	Poly-D-Lysine
PFA	Paraformaldehyde
PIP_2	Phosphatidylinositol-4,5-Bisphosphate
PKA	Phosphokinase A
PKC	Phosphokinase C
PLC	Phospholipase C
PNS	Peripheral Nervous System
QC	Q-Column
REM	Rapid Eye Movement
RNA	Ribonucleic Acid
ROI	Region of Interest
ROS	Reactive Oxygen Species
RT	Room Temperature
SCN	Superchiasmatic Nuclei
SDS-PAGE	Sodium Dodecyl Sulphate Polyacrylamide Gel Electrophoresis
SEC	Size Exclusion Chromatography
SEM	Standard Error of the Mean
SF	Selectivity Filter
SNPs	Single Nucleotide Polymorphisms
SR	Seizure-Resistant
SRCD	Synchrotron Radiation Circular Dichroism
SRP	Surface Recognition Particle
SS	Seizure-Sensitive
SUR-1	Sulfonylurea-1

TALK	Twik-Related Alkaline pH Activated K^+ Channel
TASK	Twik-Related Acid-Sensitive K^+ Channel
TC	Thalamocortical
TEA	Tetraethylammonium
TGN	Trans-Golgi Network
THIK	Tandem Pore Domain Halothane-Inhibited K^+ Channel
TM	Transmembrane
tMCAO	Transient Middle Cerebral Artery Occlusion
TMN	Tuberomammillary Nucleus
TREK	Twik-Related K^+ Channel
TRESK	Twik-Related Spinal Cord K^+ Channel
TRH	Thyrotropin-Releasing Hormone
TRHR1	Thyrotropin-Releasing Hormone Receptor 1
tRNA	Transfer Ribonucleic Acid
TRP	Transient Receptor Potential
TRPA1	Transient Receptor Potential Ankyrin 1 Channel
TTX	Tetrodotoxin
TWIK	Tandem of P domains in a Weakly Inwardly Rectifying K^+ Channel
UV	Ultraviolet
V	Voltage
VSD	voltage-sensing domain
WHO	World Health Organisation
WT	Wildtype
ZEN	Zeiss Efficient Navigation

CHAPTER 1: Introduction

1.1 Background: Theory to Fruition

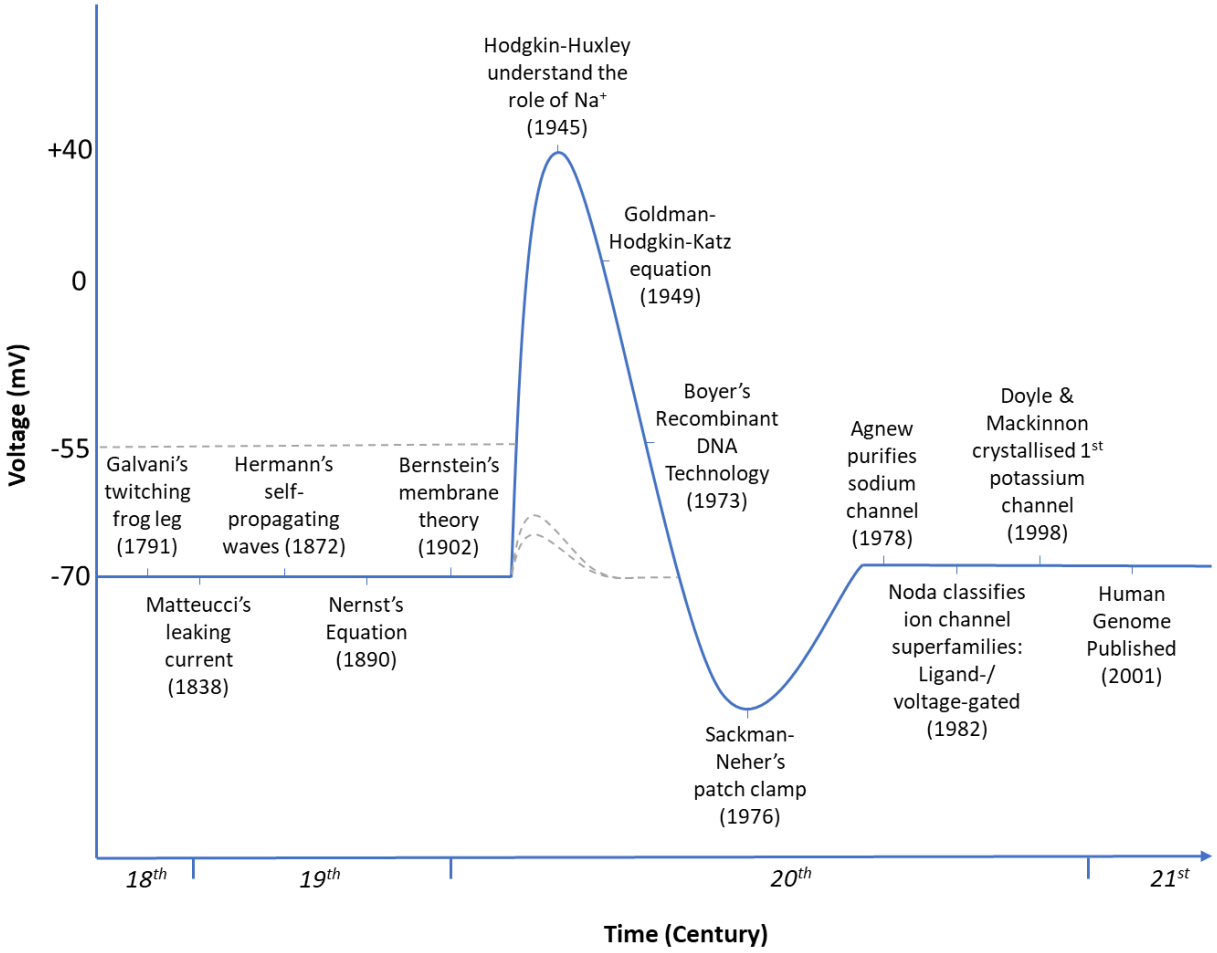

Figure 1 A timeline of discoveries

Thankfully, our scientific predecessors were curious. So curious that the twitching leg of a dead frog in 1791 was enough to lay the foundations of knowledge which now underlie multiple scientific disciplines (Verkhratsky *et al.*, 2006). From physiology and biophysics to biochemistry and structural biology, all have been involved in the extensive exploration of the 'ion channel' throughout history.

By the mid-19th century, much was clear. Hermann, building upon those before him (Figure 1), announced that biological membranes had the ability to generate '*self-propagating waves of negative charge which advances in steps along the tissue*,' a phenomenon reliant upon the permeability of the membrane to ions (Behrends, 2012). For heart muscle to contract it required specific ions: sodium (Na^+), potassium (K^+) and calcium (Ca^{2+})) at specific concentrations, dictated by the highly selective nature of the membrane, a mechanism which could be regulated and altered locally by electrical and

chemical stimuli (Miller, 2004). All of which we now know to be functions of ion channels, involved in every movement, every thought and every heartbeat however, history shows that the ion channel was never truly recognised as responsible in a grand unveiling of a new entity, rather as a hypothesis which developed slowly over time.

It began as a concept, postulated on theoretical and experimental grounds to try and explain mechanisms of osmosis. Theories went back and forth from 'capillary canals' in apple skins (Loeb, 1912) and more dead frogs, but the overriding principle was that the 'pore' was a channel through which water molecules and other particles smaller than the pore diameter could pass.

In 1902 a German physiologist, Julius Bernstein, considered the recent works of physical chemist Walther Nernst. Nernst had developed a formula aptly known as the 'Nernst equation,' used to describe changes in potential during an electrochemical reaction (Equation 1). Bernstein pondered over the clarification of the cellular resting potential (described previously by his tutor Emil du Bois-Reymond). Taking a Nernstian approach, he settled to define this as the 'diffusion potential' involved in excitation and conduction of cells which came to be known as Bernstein's 'membrane theory,'(Bernstein, 1912). He hypothesised that if the membrane is selectively permeable to K^+, these ions will flow down a diffusion gradient carrying charge, creating an excess of positivity on the extracellular (EC) side. This generation of an 'electrical field' will repel ions of same charge, opposing diffusion and so reaching an electrochemical equilibrium described as the 'membrane potential' where there is no net flow of a specific ion across the membrane. He concluded that excitable cells remain permeable to K^+ ions at rest. Following excitation, membrane permeability to other unknown positively charged ions increases allowing the diffusion of charge from the cytoplasm to the EC space, allowing the propagation of an action potential (AP). This is described by the Nernst equation:

$$E_{ion} = \frac{RT}{zF} 1n \frac{[extracellular\ ion]}{[intracellular\ ion]}$$

Equation 1 – Nernst Equation

Where E_{ion} is the ion reversal potential, R is the universal gas constant (8.314 K^{-1} mol^{-1}), T is temperature (Kelvin), z is the electron charge of the ion and F is Faraday's constant (C mol^{-1}).

Regardless, Irwin went on contemplating the possibility of protein transporters (Irwin, 1931) and Davson and Danielli deliberated over the 'Pauci-molecular model,' (Danielli and Davson, 1935) all prominent theories for almost a century but they remained just that, theories – due to the lack of biological tools available at the time.

Cole, Curtis, Mormont, Hodgkin, Huxley, Katz and Goldman were a key force in 20th century biophysics. The introduction of the voltage clamp technique allowed scientists to measure and control the membrane potential of the whole cell, providing crucial insight into the electrical properties and conductivity of the cell membrane which underlie and drive neuronal APs. Further tweaks and refinements of the technology identified that the AP was not simply a relaxation back to zero but an overshoot of membrane potential to much more positive values. With the help of a squid giant axon, Hodgkin and Huxley learned that the depolarisation phase was attributed to a Na^+ influx whilst the repolarisation phase back to a steady state resting membrane potential was achieved by a K^+ efflux (Figure 2) earning them the Nobel prize in 1963 (Cole, 1949, Hodgkin A. L., 1949, Marmont, 1949). Perhaps most significant was the development of the Goldman-Hodgkin-Katz (GHK) voltage equation which built upon the Nernst equation (Equation 1) that only factored for a single permeable ion (Hodgkin and Katz, 1949). The GHK equation allows for the calculation of membrane reversal potential of a membrane which is permeable to multiple ions, simultaneously (Equation 2).

$$V_m = \frac{RT}{F} \ln\left(\frac{P_{Cl}[Cl^-]_i + P_K[K^+]_o + P_{Na}[Na^+]_o}{P_{Cl}[Cl^-]_o + P_K[K^+]_i + P_{Na}[Na^+]_i}\right)$$

Equation 2 – Goldman-Hodgkin-Katz Voltage Equation

For calculation of membrane reversal potential, factoring the difference in multiple ion concentrations on either side of the membrane. V_m is the membrane potential, R is the universal gas constant (8.314 K^{-1} mol^{-1}), T is temperature (Kelvin), F is Faraday's constant (C mol^{-1}), P_{ion} is permeability of that specific ion (m/s), $[ion]_I$ is the intracellular concentration of that ion and $[ion]_o$ is the extracellular concentration of that specific ion.

Whilst this work described the changes observed in Na^+ and K^+ membrane permeability during an AP, they remained unable to elude to any specific mechanism for permeability. Hodgkin, partnered with Keynes, investigated this further using an isotopic K^+ flux-ratio set-up but their unexpected results were only explainable if "*ions cross the membrane along a chain of negative charges or through narrow tubes or channels… in which they are constrained to single file [with] several ions in the channel at any moment,"*(Hodgkin and Keynes, 1955).

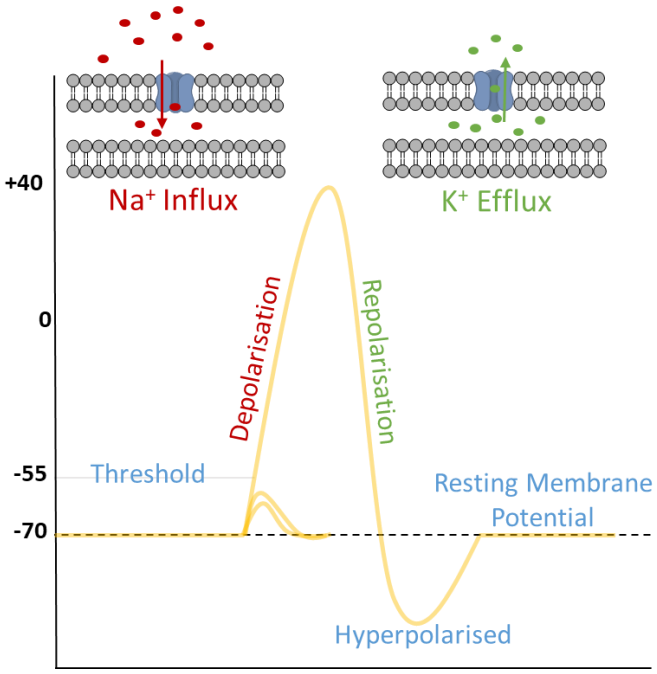

Figure 2 Example action potential.

Following a stimulus exceeding the threshold potential, the membrane is depolarised caused by an influx of Na+ ions, allowing the propagation of the action potential. The membrane is repolarised following a K+ ion efflux as the membrane returns to the steady negative state resting membrane potential.

It was the discovery of selective inhibition of Na^+ and K^+ ion conductance following the application of compounds including tetrodotoxin (TTX) and tetraethylammonium (TEA) of respectively which provided evidence for the presence of selective protein pores facilitating ion passage (Hille, 1975). The problem with making such structural hypotheses regarding ion channels as molecular pores was that no known structures existed. In 1978, Agnew presented the first biochemical purification of a voltage-gated Na_V ion selective pore from electroplax membranes, confirming the presence of selective ion pores (Agnew *et al.*, 1978). Then in 1988, Doyle and Mackinnon crystallised the first full structure of a K^+ channel (Doyle *et al.*, 1998).

In 1991, Sackman and Neher were awarded the 'Physiology and Medicine' Nobel prize for the invention of the patch clamp technique which allowed the recording of current through a single ion channel, a technological advancement which led to a boom in discoveries in the world of pharmacology, physiology and ion channel biophysics (Neher *et al.*, 1978). Combined with the development of recombinant DNA techniques (Boyer and Roulland-Dussoix, 1969), Noda *et al.* (1983) cloned, sequenced and characterised the complete primary structures of the nicotinic acetylcholine receptor (NAchR) and voltage-gated $Na^+{}_V$ channel (Noda *et al.*, 1984, Noda *et al.*, 1983). It was this

discovery that truly began to unravel the extent of mammalian ion channel diversity, prompting classification systems based upon sequence homology, gating properties, phylogeny and was the advent of the first two ion channel super families: voltage- and ligand-gated ion channels.

1.2 Ion channels

The landmark unveiling of the crystal structure of the bacterial K^+ channel, KcsA, by Doyle *et al.* (1998) rapidly increased the tempo of ion channel research with regards to structure and function, swiftly becoming one of the most well-studied families in heterologous expression systems. A plethora of studies documented the role of ion channels from higher organisms down to the lowest prokaryote and demonstrated their importance in functions such as cell growth, cell survival and neuronal signalling. At a basal level, ion channels are proteins which span membranes (plasma and intracellular organelles) to form a pore allowing the passage of specific ions, providing a means of tight cellular temporal control over ion flux and cell permeability. Consider the following example, the neuronal cell in Figure 3 has a total volume of approximately 10^{-12} mL and an intracellular potassium ion concentration of 100 mM, equivalent to 10^8 ions. If potassium crosses the membrane through the ion channel pore at a speed of 10^7 ions per second, the opening of only 10 channels at the cell membrane would drain the cell of potassium in about 1 second (Choe, 2002). Therefore, ion channels have been evolutionarily equipped to alter membrane potential via swift opening and closing of specific channels for rapid ion conduction, with mechanisms such as highly selective filters, gating regions and inactivation switches in response to internal and external environmental stimuli such as pH, temperature, voltage and ligands amongst others (Hille, 2001).

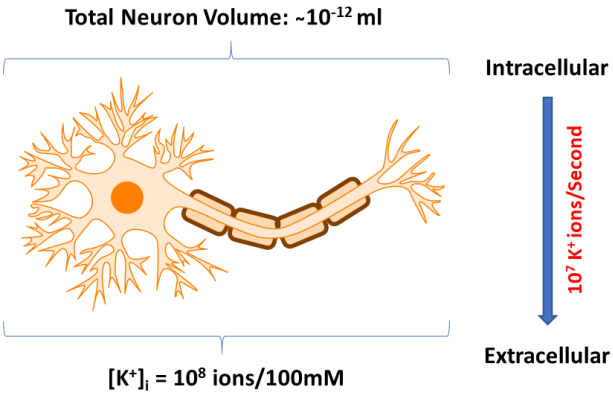

Figure 3 The costly event of ion channel opening in absence of inactivation mechanisms

If ions cross the membrane through an ion channel at a speed of 10^7 ions per second, a neuronal cell with a volume of 10^{-12} mL and an intracellular potassium ion concentration ($[K^+]_i$) of 100 mM or 10^8 ions would be drained of potassium within 1 second of 10 channels opening.

Despite challenges associated with studying ion channels due to the many hydrophobic transmembrane domains, the question became focused upon the cause of selectivity. Atomic resolution provided by X-ray crystallographic characterisation of KcsA identified the presence of a carbonyl group backbone (Doyle *et al.*, 1998), confirming the signature 'XXTVGYGXX,' amino acid sequence to be highly conserved amongst K^+ ion channels (Heginbotham *et al.*, 1994). It can be seen in Table 1, that an 8 amino acid sequence containing 'XXTTXGYG' as a minimum to be required for potassium selectivity, which is reduced as conservation of ion sequence is lost (MacKinnon, 2004). Furthermore, disruption to the residues within this sequence have been shown to disrupt the carbonyl backbone in a way which induces a conformational change (Cordero-Morales *et al.*, 2006) which blocks the selectivity filter (SF) and prevents the rapid diffusion of K^+ (Cheng *et al.*, 2011).

Table 1 The highly conserved, minimum pore regions of potassium selective channels throughout the hierarchy of the tree of life.

Highly conserved residues in blue and lesser conserved residues in red. 'Domain #' refers to the number of transmembrane-spanning segments per each respective pore-forming subunit. Amino acids shown in single-letter code. Adapted from (Mackinnon, 2004)

Organism	Domain #	Selective Filter Sequence
Bacteria	2TM	T A T T V G Y G
Archaea	6TM	T A T T V G Y G
Plant	6TM	T L T T V G Y G
Fruit fly	6TM	T M T T V G Y G
Worm	6TM	T M T T V G Y G
Mouse	6TM	S M T T V G Y G
Human	2TM	T Q T T I G Y G
Human	4TM	V I T T I G Y G
Human	6TM	T M T T V G Y G

There are >300 different ion channels expressed in the human ear alone (Gabashvili *et al.*, 2007). Voltage- and ligand-gated family of ion channel genes account for approx. 1.5% of the human genome, consisting of >400 genes and alternatively spliced variants (Lee *et al.*, 2014). Electrophysiological and computer modelling identify channels differing in expression, location, channel-gating mechanisms, and selectivity whilst *in vivo* investigations exhibit more unexpected properties following coupling with secondary messengers, scaffold proteins and signalling pathways. Voltage-gated ion channels form one of the largest protein super-families (containing 143 members to date) and as such, differing amino acid sequences within the minimal pore regions of these structurally related ion channels has led to the derivation of 7 significant groups (Figure 4)(Yu and Catterall, 2004). Such level of diversification leads to the many physiological roles of ion channels but also highlights the extent of potential dysregulation, commonly resulting in pathological states including cardiac arrhythmias, deafness, epilepsy, diabetes and misregulation of blood pressure which can all be attributed to disruption of K^+ channel gene disruption (Miller, 2000).

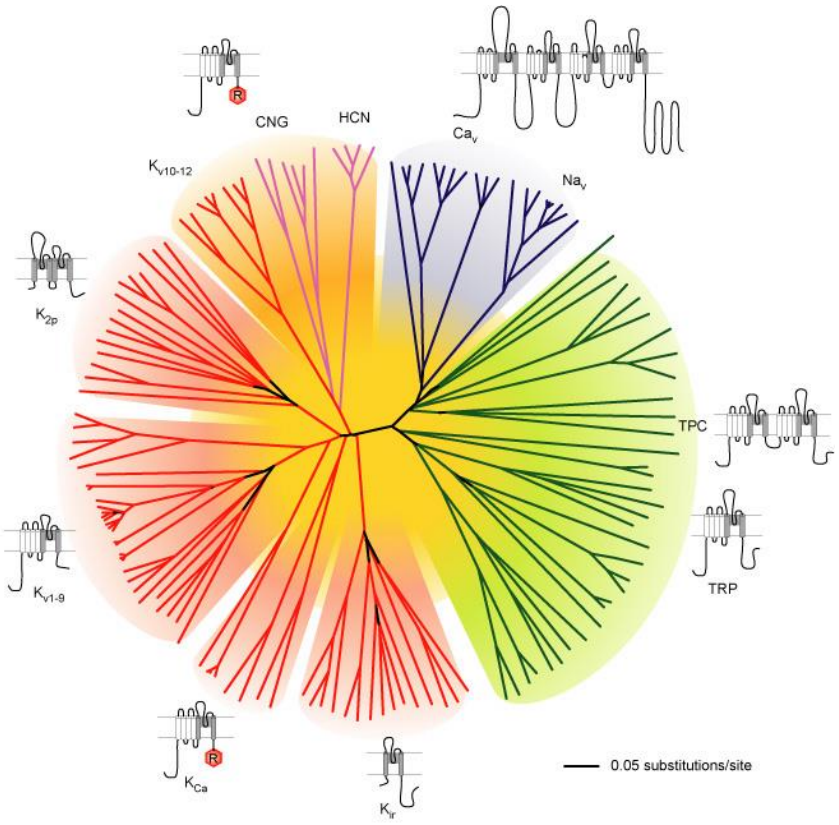

Figure 4 A representation of amino acid sequence diversity within minimal pore regions of related voltage-gated ion channels.

Four domain channels are shown as blue branches; potassium selective channels are red branches; cyclic nucleotide-gated channels are represented by magenta branches and transient receptor potential channels (TRP) and other related channels are shown as green branches. Scale bar represents tree distance corresponding to 0.05 substitutions per site in sequence (Reproduced from Yu and Catterall, 2004).

1.3 Potassium channels

K^+ channels represent a diverse family of membrane proteins and are ubiquitously expressed throughout plant and animal kingdoms in both excitable and non-excitable cells. There are >90 genes present within the human genome encoding principal (α) subunits and many more considering alternate splicing and auxiliary (β) units. For this reason, K^+ channels exercise tight control over an expansive range of duties including cell growth, cell volume, cell death and membrane excitability (Tian *et al.*, 2014).

Common to all K^+ channels are the presence of the canonical K^+ pore (P) architecture formed of two transmembrane (TM) helices and a connecting intracellular (IC) loop, with each channel subunit containing either 1P or 2P domains. K^+ channels contain α subunits, which primarily determine the structure of the channel, and β subunits which modify the functional properties of the channel. In most instances, α subunits do not require the co-expression of β subunits and instead form functional homo-multimeric channel complexes when expressed in heterologous expression systems. In a few cases, it is necessary to express the β subunit for co-assembly with the α subunits to allow for trafficking and functional expression (Wei *et al.*, 1996).

The subunits can be subdivided into at least 8 families based upon structure and function. Three α-subunit families' form 6 TM helices (KQT, voltage-gated K_V, ether-a-go-go related gene (EAG)) which are primarily gated by voltage. Cyclic nucleotide gated channels (CNG) and small/intermediate K^+ conductance (SK/IK) channels also fall within the 6TM family although they are regulated by cyclic nucleotides and Ca^{2+} respectively. The SLO family consists of 7TM channels including big K^+ conductance channels (BK) (Meera *et al.*, 1997) which are regulated by voltage, pH and Ca^{2+} (Schreiber *et al.*, 1998). Inwardly rectifying K^+ channels (K_{ir}) form the bulk of the 2TM family of α subunits which, through tandem repeats, form the final functionally diverse 4TM group, two pore-domain potassium channels (K2P) (Tian *et al.*, 2014). For ease, these channels can be further subdivided into three main groups of K^+ channel: voltage-gated channels (6 or 7TM/P), K_{ir} channels (2TM/P) and K2P channels (4TM/2P) (Figure 5).

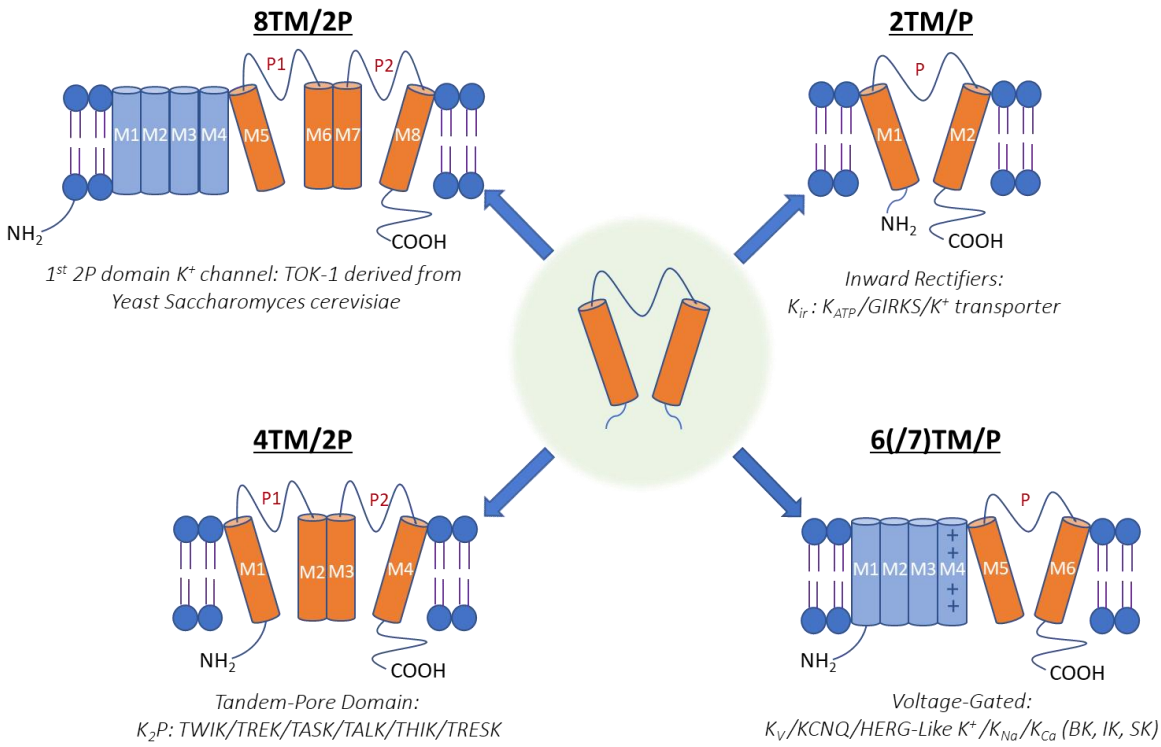

Figure 5 The four main classes of K^+ ion channels containing the signature canonical K^+ pore architecture of the two transmembrane helices and irregular connecting loop

All channels contain at least one prototypical pore structure and two cytosolic amino-/carboxyl terminals. 8TM/2P (8 transmembrane (TM) helices and 2 pore (P) loops) are hybrids of 6TM/P and 2TM/P channels and are not present in humans but represent the first discovery of 2P channels (TOK-1) in yeast. Inward-rectifying K^+ channels (K_{ir}) form the body of 2TM/P; this group may be subdivided further based upon function. 6(/7) TM/P channels contain a voltage-sensing element within TM4 (marked '+') required for the regulation of action potential generation. 4TM/2P channels assemble as dimers to form 'leak' channels and are targets of multiple anaesthetics (Choe, 2002).

1.4 Two pore domain potassium channels

1.4.1 Phylogeny

The *KCNK* gene family encodes the 'two pore domain potassium' channels (K2P). There are 15 genes subdivided into six classes based upon channel sequence homology and functional similarity (Figure 6). The international union of basic and clinical pharmacology (IUPHAR) introduced a numerical nomenclature *(KCNK1-18*) for individual K2P subunits based upon the human genome organisation (HUGO) naming system and the chronological discovery (*KCNK8*, *11* and *14* are omitted). *KCNK7, KCNK15* and *KCNK12* are 'silent channels,' displaying no obvious function when expressed in heterologous systems despite expression in brain tissues (Goldstein *et al.*, 2005). Co-expression studies have shown functional potential for these channels when expressed alongside other K2P channels. Alternately, individual channels may be referred to using the acronym system derived from the salient physiological or pharmacological properties it is characterised by: **TWIK** (*T*andem of P domains in a *w*eakly *i*nwardly rectifying K^+ channel), **TREK** (*T*wik-*re*lated K^+ channel), **TASK** (*T*wik-related *a*cid-*s*ensitive K^+ channel), **TALK** (*T*wik-related *al*kaline pH-activated K^+ channel), **THIK** (*T*andem pore domain *h*alothane-*i*nhibited K^+ channel) and **TRESK** (*T*wik-*r*elated *s*pinal cord K^+ channel).

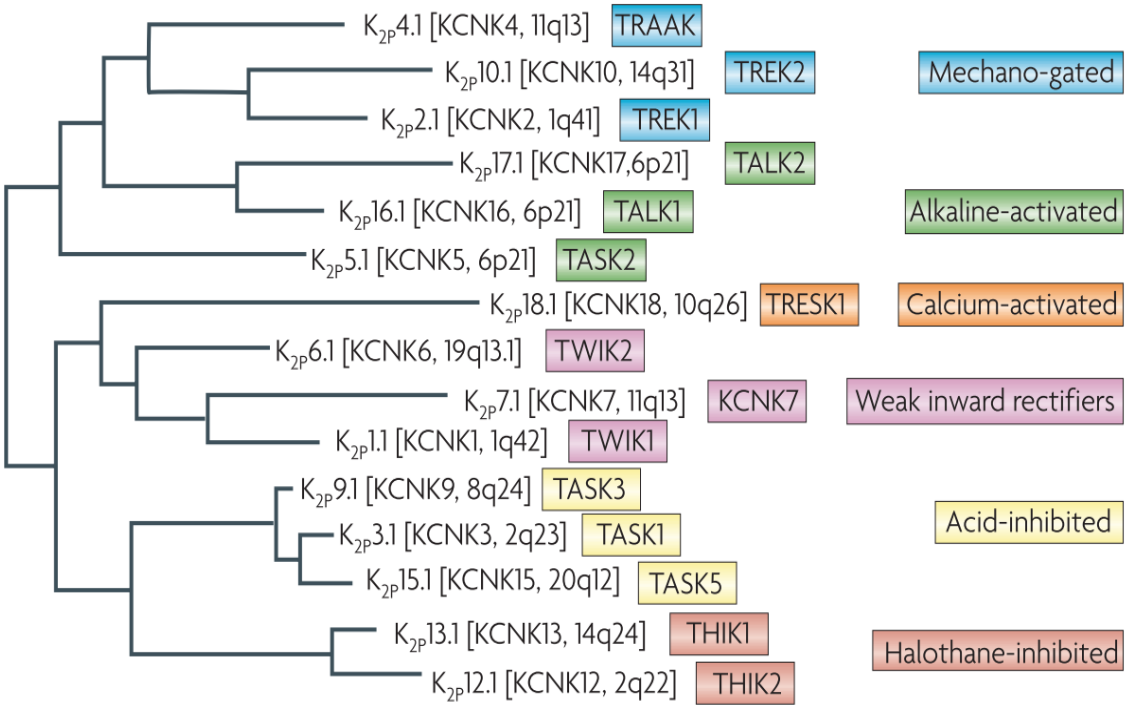

Figure 6 Phylogenetic tree. *Reproduced from (Honore, 2007)*

1.4.2 Structural Features

K2P channel α-subunits form homodimers or heterodimers with closely related members (*i.e.* TASK1:TASK3) and between subgroups (*i.e.* TWIK1:TASK3) to generate channels with functionally distinct properties from the individual parent subunits (Figure 7A); or to allow the functional expression of otherwise silent channels (THIK2 unsilenced by THIK1 co-expression) (Blin *et al.*, 2016). TWIK1 was the first channel identified to contain 4 pore domains. The donation of two pore domains by each dimerised subunit has earnt it the name of 'two pore domain' potassium channel and is the defining feature differentiating the family from the likes of K_V and K_{IR} channels. These channels contribute a single pore per sub-unit to the central pore in a tetrameric conformation, thus, by provision of two P-domains from two subunits, K2P channels are said to be *pseudo*tetrameric. Effectively, if one were to link two K_{IR} subunits and pair with another set of linked subunits, the channel assembles to produce 2 major P-domains (Figure 7C) to form the pseudotetrameric K^+ selective pore (Figure 7B) required to maintain the interior negative resting membrane potential throughout cells of the nervous system. All theories regarding assembly were put to rest following the purification and crystallisation of TWIK (Miller and Long, 2012) and TRAAK (Brohawn *et al.*, 2012) which confirmed Lesage's hypothesised pseudotetrameric symmetry assembly (Lesage *et al.*, 1996a).

Dimerised, the K2P primary topology consists of two short cytoplasmic N-termini (Nt) and two longer cytoplasmic C-terminus (Ct); 2 X four transmembrane α-helical domains (TM1-TM4), 2 X re-entrant pore domains (P1 and P2) and an extended EC 'cap domain,' formed between TM1 and P1, otherwise referred to as the M1P1 loop (Figure 7A and C). It was originally believed that all K2P dimers were connected by a stabilising cysteine-disulphide bridge (Lesage *et al.*, 1996b) however, this is unlikely since the relevant cysteine residues (Cys69) required (with exception of TWIK1) are neither conserved nor required amongst all channels (sub-families: TASK and THIK) (Zúñiga and Zúñiga, 2016). Indeed, TASK1 and TASK3 fail to display a disulphide bond within the dimer, nor does TRESK when in the presence of a long TM2-TM3 re-entrant loop (Enyedi *et al.*, 2012). High resolution crystallographic structures resolved for TWIK1, revealed that the cap forms a structured domain containing two coiled-coiled helices (one from each monomer), sitting approximately 35Å above the lipid membrane, blocking direct entrance to the SF explaining the apparent ineffectiveness of well-known K^+ channel blockers such as TEA, 4AP and toxin (Brohawn *et al.*, 2012, Miller and Long, 2012). Rather than direct pore access, the cap contains two side fenestrations, forming the extracellular ion pathway (EIP) directing K^+ ions to the SF (Brohawn *et al.*, 2012, Miller and Long, 2012).

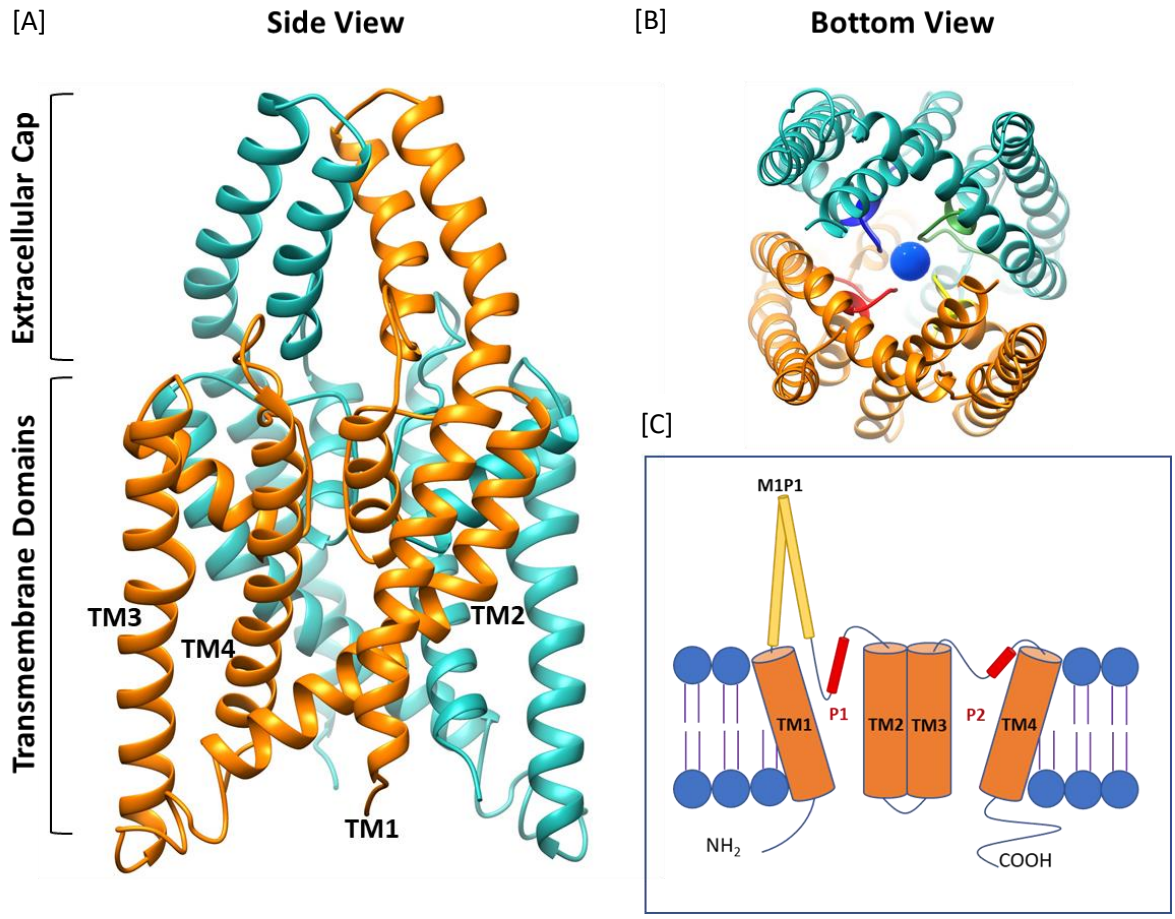

Figure 7 Structural features of K2P channels

[A] Side view of a human TASK3 homology model based upon human TRAAK (PDB ID 3UM7, Brohawn et al. 2012) displaying the dimerization of two inwardly rectifying monomers (blue and orange) as it would in the membrane. Brackets highlight the TM and EC cap portions. Model does not include the IC N-/C-termini. [B] Bottom view of the TASK3 homology model as if underneath and looking through. Model view describes the formation of the channel pore through dimerization. [C] Simple schematic characterising individual domains within the K2P channel.

1.4.3 Channel Gating

Despite access to few crystal K2P structures, the molecular mechanisms involved in channel gating and regulation remain largely unknown. K^+ channels are thought to contain two highly conserved gating mechanisms referred to as the slow 'C-type' inactivation gate,' located at the SF closer to the EC side of the channel (Yellen, 2002) and an activation gate at the bundle-crossing region closer to the IC side (Ben-Abu *et al.*, 2009, Cohen *et al.*, 2009). In K_V and K_{ir} channels, it has been proposed that these structurally distinct gates are tightly coupled with the bundle-crossing gate. The method of action is thought to work like an optical aperture, using the inner TM helices which form the pore to constrict and physically impede the ion pathway (Swartz, 2004, Rapedius *et al.*, 2007, Hibino *et al.*, 2010), with the opening of the lower gate simultaneously closing the upper gate. Less however, is understood regarding the relative importance of the bundle crossing gate and the structural motions involved in the regulation of permeation at the upper C-type gate in K2P channels. Unlike other K^+ channels, the K2P channel contains two long IC Ct which are strongly suspected to play a role in channel gating as a signal transducer between the IC environment and the EC SF, with many supporting a model in which there is no bundle-crossing region present at all (Bagriantsev *et al.*, 2011, Bagriantsev *et al.*, 2012, Piechotta *et al.*, 2011, Brohawn *et al.*, 2012, Miller and Long, 2012). Instead considering a primary activation mechanism which lies close to or within the SF. Through deletional and chimeric analyses, Honore (2007) identified the Ct domain in TREK1 to act as the primary sensor involved in gating. Furthermore, phosphorylation of the Ct by phosphokinase A (PKA) reportedly regulated the number of active channels, whilst agonist-induced phosphatidylinositol-4,5-bisphosphate (PIP_2) hydrolysis at the Ct shifted voltage sensitivity towards depolarized potentials. Taken together, this highlights the Ct's intricate involvement in signalling pathways, polymodal regulation (membrane stretch, intracellular pH, negatively charged lipids, unsaturated fatty acids and temperature) and association/dissociation of the Ct with the lipid membrane (Honore, 2007).

More recently, Piechotta *et al* provided strong evidence suggesting the sole gating mechanism to be at the SF. Using a high-affinity TREK1 channel pore blocker (large quaternary ammonium ions *i.e.* THexA), it has been shown that the bundle-crossing 'activation' gate remains open when the pore is closed, providing free access to the blocking molecule's binding site within (Piechotta *et al.*, 2011). Furthermore, it was demonstrated that the binding kinetics of the blocking agent were very similar, regardless of whether the pore was open or closed. This suggests that the bundle-crossing gate remains constitutively open and does not undergo any obvious structural motion, meaning that the pore remains accessible to cytoplasmic ions right up to the SF which acts as the primary gating mechanism of K2P channels (Piechotta *et al.*, 2011). Such a gating mechanism has been previously reported in cyclic-nucleotide-gated (CNG) channels, which are exclusively gated at the SF (Contreras

et al., 2008). Despite plentiful evidence for ability of SF gating in K^+ channels including K_{ir} (Schulte and Fakler, 2000), K_V (Yellen, 2002) and KcsA (Cuello *et al.*, 2010), these channels are still observed to incorporate some structural adjustments of the bundle-crossing gate that regulates the function of the upper gate and is thus deemed functionally relevant to gating in contrast to K2P (Piechotta *et al.*, 2011).

It is speculated that the extended Ct of K2P channels runs parallel to the lipid bilayer, serving both as a physical link between units at the membrane but also as a functionally important binding site. The Ct and its relationship with the lipid bilayer has been implicated in a broad range of regulatory events, especially in TREK1, involving mechano-gating, intracellular pH, anionic lipids and polyunsaturated fatty acids (arachidonic acid) (Maingret *et al.*, 1999, Honoré *et al.*, 2002, Chemin *et al.*, 2005, Honore, 2007, Piechotta *et al.*, 2011). The question remains that if the bundle crossing gate is 'non-functional' in K2P channels, then the Ct must somehow transduce intracellular signals through the TM domains to the SF in order to inactivate the channel. Whether this occurs through structural motion of the TM domains is yet to be determined.

1.4.3.1 The X-Gate

A preprint paper recently released by Rödström *et al.* (2019) details the discovery of a novel 'X-gate' located intracellularly next to the SF following the crystallisation of the human TASK1 channel and provides evidence for a lower gating mechanism. This structure is formed by the interaction of the Ct regions of both TM4 structures, forming a characteristic 'X' structure at the vestibule entrance. The Ct domain of TASK1 contains a motif formed of six residues (243-VLRFMT-248) which form the key component of this gate structure and are critical to the regulation of the channel by volatile anaesthetics (Patel *et al.*, 1999), G-protein coupled receptors (GPCRs) and other neuromodulatory molecules (Talley and Bayliss, 2002b). Mutations within or around this motif have a significant effect on channel activity, reducing open probability and preventing channel activation by anaesthetics. Until now, strikingly different pharmacological properties of TASK1 and TASK3 channels were unexplainable. Unlike many other K2P channels, TASK1 and TASK3 are uniquely influenced by several high affinity and highly selective inhibitors which demonstrate very low wash out rates following the removal of antagonist compounds. The discovery of this structure unveils a unique phenomenon by which channel inhibitors become trapped within the vestibule, thus offering some explanation to these channel's pharmacological profiles (Rödström *et al.*, 2019).

1.4.3.2 Ion-Flux Gating

Together with K_V and K_{IR} channels, K2P channels regulate cellular excitability. K_V and K_{IR} channels contain a known voltage-sensing domain (VSD) (Schoppa *et al.*, 1992, Aggarwal and MacKinnon, 1996, Seoh *et al.*, 1996) and are recognised as 'voltage-dependent' channels (Hodgkin and Huxley, 1952). In contrast, K2P channels were traditionally identified as 'voltage-independent' due the lack of obvious VSD with outward rectification driven by the asymmetric K^+ gradient across the membrane as predicted by the GHK equation. Excluding TWIK1, many of the K2P channels (TRAAK, TREK1/2, TRESK, TALK2 and TASK1/2/3) have instead been found to display outwardly rectifying currents that are both time- and voltage-dependent despite the absence of the canonical VSD (Schewe *et al.*, 2016). The voltage-sensing ability of K2Ps channels has been attributed to an *ion-flux gating mechanism* that continues to be driven by the K^+ electrochemical gradient, with voltage sensitivity arising from the occupation of ions within the electrical field of the SF (Schewe *et al.*, 2016). In the model suggested by Schewe *et al.* (2016), the SF rapidly switches between inactive and active states (Figure 8) based upon the degree of exposure to electrochemical driving forces. When the electrochemical driving force ($\Delta\mu = V_m - E_{Rev}$) is negative, the SF exists in an inactive, ion-depleted state. As voltages become more positive early into a depolarising event, the SF is gradually occupied with 3 – 4 ions, taking on an occupied but still inactive state which is ready for transformation. Upon reaching full occupation ($\Delta\mu > 0$), the channel switches to the fully active, conductive state, supporting outward rectification. As the membrane repolarises back towards potentials negative to the E_{Rev}, the SF rapidly destabilises as the channel returns to an ion depleted, inactivated state.

It was previously understood that K2P channels remained active at resting membrane potentials where they contribute to the resting potassium permeability leading to reduced excitability at rest. However, the recently established strong voltage-dependency of these channels suggests that unless activated by stimuli, these channels may remain inactive at resting membrane potential however, the rapid kinetics of these ion-flux gated channels makes them critical components to the repolarisation and production of APs in absence of K_V channels (Mackenzie *et al.*, 2015). As such, it is of no surprise that a dynamic mechanism such as this has physiological implications in the likes of sustaining high-frequency action potentials in neurons (Brickley *et al.*, 2007) rather than conforming to the voltage-independent 'leak' K^+ channels as previously believed (Goldstein *et al.*, 2001, Lesage and Lazdunski, 2000).

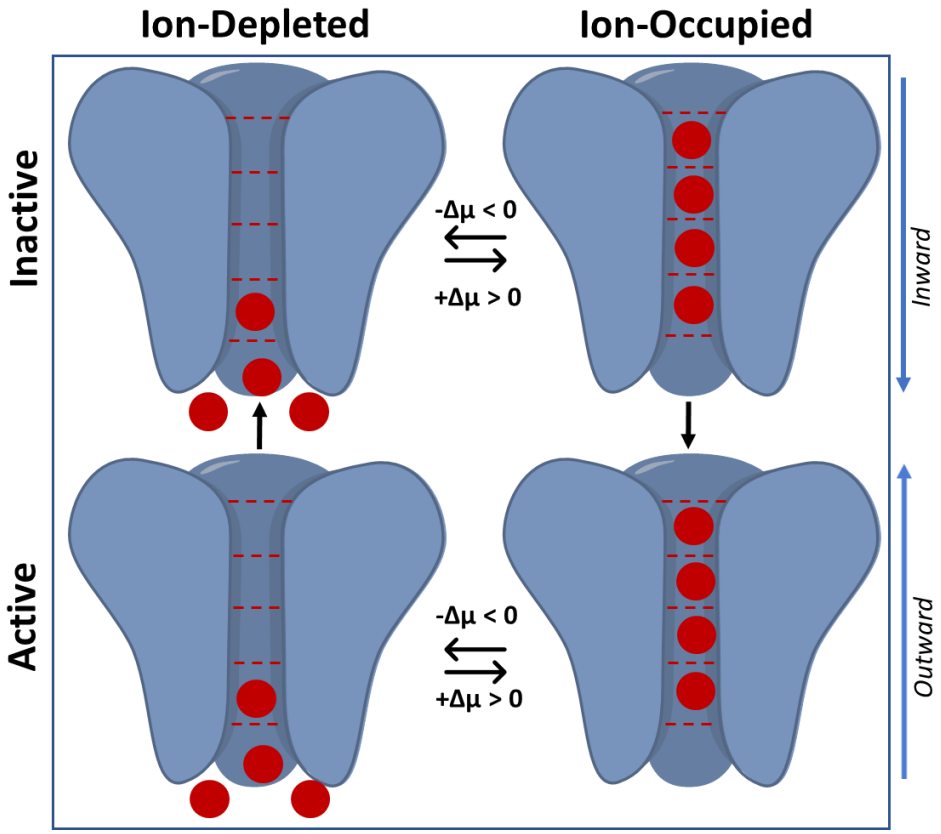

Figure 8 Schematic of the ion-flux gating mechanism proposed by Schewe et al. (2016).

*When the electrochemical driving force (-*Δμ) is *negative (<0) the SF exists in an inactive and ion depleted state. As the electrochemical force becomes more positive (+*Δμ, >0), *an increasing number of channels begin to occupy the inactive SF with* K^+ *ions. Fully occupied, the channel takes on an activated, outwardly rectifying state. Upon reaching the repolarisation phase, Δμ* again becomes negative, inducing inward rectification however, *the activated state of the channel becomes unstable and returns to the ion-depleted, inactive state.*

1.5 TWIK-related acid-sensitive (TASK) K^+ channels

The TASK (TWIK-related Acid-sensitive K^+ channel) subfamily is appropriately named firstly due to its close structural similarity to TWIK1, the first K2P channel member to be characterised, and secondly its functional sensitivity to EC acidification. This subfamily comprises three members sharing >50% sequence identity: TASK1, TASK3 and TASK5, the latter being silent despite differential expression in the brain, particularly auditory nuclei (Ashmole *et al.*, 2001, Karschin *et al.*, 2001). Considering the degree of TASK1 and TASK3 sequence similarity, it is no surprise that these channels share very similar functional kinetics, differences being the degree of pH sensitivity and single channel conductance. TASK channels share the same low time- and voltage-dependency features of other channels within the K2P family and so produce currents in line with the behaviour predicted by the GHK equation for leak K^+-selective pores.

1.5.1 Expression

TASK1 and TASK3 are predominantly expressed throughout the central nervous system (CNS) however they may also be found in abundance within peripheral tissues including the heart and adrenal glands (see Table 2); often forming heterodimers with distinct functional and pharmacological properties (Karschin *et al.*, 2001). The expression patterns of the homo-/heterodimers are variable with certain cell types displaying only one subunit *i.e.* only TASK3 is found in striatal cholinergic neurons however there is vast overlapping expression of TASK3 and TASK1 in cerebellar granule neurons (CGN), motor and sensory neurons, carotid body glomus cells, adrenocortical cells amongst others (Talley *et al.*, 2001a, Ashmole *et al.*, 2001, Karschin *et al.*, 2001, Medhurst *et al.*, 2001).

Table 2 mRNA expression of TASK channels across the central and peripheral systems of the human body

Grey indicates low expression, yellow indicates medium expression, green indicates high expression and red indicates no expression; 'N/A' indicates no data is yet available. Table produced using data collated from the following sources: Talley et al. (2001), Ashmole et al. (2001), Karschin et al. (2001) and Medhurst et al. (2001).

CNS Expression	TASK1	TASK3	TASK5
Amygdala	✓	✓	✘
Caudate nucleus	✓	✓	✘
Cerebellum	✓	✓	✘
Corpus callosum	✓	✓	✘
Frontal cortex	✓	✓	✘
Occipital cortex	✓	✓	✘
Temporal cortex	✓	✓	✘
Hippocampus	✓	✓	✘
Hypothalamus	✓	✓	✘
Nucleus accumbens	✓	✓	✘
Putamen	✓	✓	✘
Substantia nigra	✓	✓	✘
Thalamus	✓	✓	✓
Foetal brain	✓	✓	✘
Spinal cord	✓	✓	✘
Pituitary gland	✓	✓	✘
Whole brain	✓	✓	✘
Peripheral Expression	**TASK1**	**TASK3**	**TASK5**
Heart	✓	✘	✓
Liver	✓	✘	✓
Lung	✓	✘	✓
Skeletal muscle	✘	✓	✘
Kidney	✓	✓	✓
Pancreas	✓	✓	✓
Spleen	✓	✓	✓
Small intestine	✓	✓	✓
Placenta	✓	✘	✓
Testis	✓	✓	✓
Stomach	✓	✓	N/A
Prostate	✓	✓	✓
Uterus	✓	✓	N/A

1.5.2 Regulation

TASK channels contribute to the standing outward potassium current (IK_{SO}) within CGN to produce the characteristic hyperpolarised resting membrane potential (Watkins and Mathie, 1996). Constitutively active under physiological conditions, TASK3 channels are inhibited by EC acidification (Duprat *et al.*, 1997, Kim *et al.*, 2000, Rajan *et al.*, 2000) and activation of G-protein-coupled receptors (GPCRs), coupled primarily to the $G\alpha_{q/11}$ subunit (Chen *et al.*, 2006) (see Table 3 for summary). Very few activators for the channel are known with only pharmacological agents like inhalational anaesthetics (halothane/isoflurane) (Maingret *et al.*, 1999, Talley and Bayliss, 2002b) and terbinafine (Wright *et al.*, 2017).

Table 3 Displaying natural and chemical regulators of TASK channel function

[1] (Duprat et al., 1997), [2] (Patel et al., 1999), [3] (Talley and Bayliss, 2002b), [4] (Kemp et al., 2004), [5] (Gruss et al., 2004), [6] (Czirják and Enyedi, 2003), [7] (Kim et al., 2000), [8] (Rajan et al., 2000), [9] (Chen et al., 2006), [10] (Girard et al., 2002), [11] (Renigunta et al., 2006), [12] (Renigunta et al., 2014), [13] (Zuzarte et al., 2009) and [14] (Cunningham et al., 2019).

Channel	Activators		Inhibitors		Interacting Partners	
TASK1	Alkaline pH_O [*1]	Volatile Anaesthetics (Halothane, Isofluorane) [*2, 3]	Hypoxia [*4]	Acid pH_O [*1, 7, 8] Gαq [*9]	P11 [*10, 11] Syntaxin-8 [*12]	14-3-3 [*13] COPI [*13]
TASK3			Copper [*5] Zinc [*5] Ruthenium Red [*6] Doxapram [*14]			

1.5.2.1 pH Regulation

All channels, excluding THIK1/2 and TRESK, display a degree of sensitivity to changes in environmental pH (Feliciangeli *et al.*, 2015). TASK channels are primarily affected by EC acidification, with TASK1 and TASK3 displaying differential sensitivity. TASK1 is inhibited with a pKa of 7.3 whilst TASK inhibits at pKa 6.7 (Duprat *et al.*, 1997, Kim *et al.*, 2000, Rajan *et al.*, 2000). TASK1 and TASK3 sensitivity to pH depends upon a histidine residue within PD1 (His98) (Kim *et al.*, 2000, Rajan *et al.*, 2000, Morton *et al.*, 2003).

1.5.2.2 Hypoxic Regulation

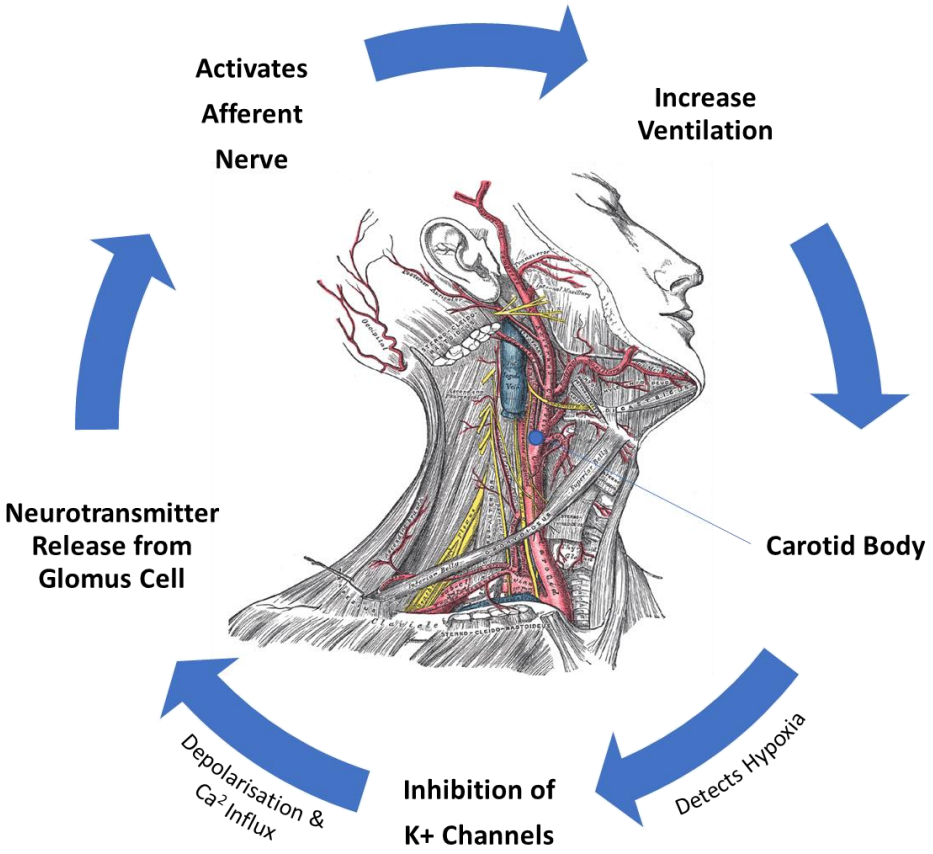

Figure 9 'Membrane model' of the carotid body's response to hypoxia.

An oxygen-sensitive potassium current was first identified in rat carotid body type 1 cells (Buckler, 1997) and since then the notion of a chemosensory function of TASK channels has been widely discussed. The carotid body consists of a small cluster of chemoreceptors and is found at the bifurcation of the carotid artery as it runs along both sides of the throat. This structure monitors the compositions of the arterial blood, detecting change in pH, temperature as well as O_2 and CO_2 partial pressures (Prabhakar and Peng, 2017). The generally accepted 'membrane model' states that carotid body glomus (BG) cells detect hypoxic environment and signal to the medulla oblongata (respiratory centre) to adjust ventilation. How this is achieved remains unclear. It is thought that upon the detection of hypoxia, K^+ channels are inhibited resulting in depolarisation and subsequent influx of Ca^{2+} leading to the release of neurotransmitter from the BG in turn activating the afferent nerve which commands the increase of ventilation (Figure 9) (López-Barneo *et al.*, 2008). Using rats, it was found that the inhibition of the TASK-like current displayed channel kinetics like TASK1. The whole cell K^+ current appeared to be O_2 sensitive but insensitive to TEA, 4-AP and toxin (Buckler, 1997). It displayed

a flickering unitary conductance of ~14-16 pS with short open duration and mild inward rectification and was characteristically, of TASK1, inhibited by acid, zinc, quinidine and bupivacaine (Buckler *et al.*, 2000). Further investigations identified that the channel is also sensitive to EC magnesium (Mg^{2+}) (Williams and Buckler, 2004) which is not typical of TASK1 and is instead suggestive of TASK3. Indeed, it has been shown that the heterodimers of TASK1 and TASK3 are the predominant form present in the carotid bodies (Kim *et al.*, 2009a, Turner and Buckler, 2013) and mice lacking either channel have impaired carotid body function (Ortega-Saenz *et al.*, 2010, Trapp *et al.*, 2008).

A recent study by O'Donohoe *et al.* (2018) has shown that they can evoke membrane depolarisation and subsequent voltage-gated calcium entry in isolated neonatal type 1 cells, using selective pharmacological inhibitors of TASK, supporting a role of these channels in chemosensing. There is reasonable evidence to suggest that these channels may function under many physiological and pathophysiological conditions (Kim *et al.*, 2009a).

1.5.2.3 G-Protein Coupled Receptor Regulation

Receptor-mediated inhibition closes the pore, increasing neuronal excitability and encourages the firing of APs. This form of modulation is not restricted to CGN and is well documented in regulation of K_V, K_{IR} and Ca_V channels amongst others (Chen *et al.*, 2006). In these channels, inhibition appears to occur via a classical $G\alpha_q$ cascade (see Figure 10). In summary, external activation of GPCRs triggers de-phosphorylation of a bound, intracellular tri-subunit G-protein ($\alpha\beta\gamma$) as guanosine-diphosphate (GDP) is phosphorylated to form guanosine-triphosphate (GTP). $G\alpha_q$ is detached from the G-protein complex and may then activate membrane-bound phospholipase C (PLC) to hydrolyse plasma membrane phospholipid phosphatidylinositol-4, 5-bisphosphate (PIP_2) into the secondary messengers: inositol-triphosphate (IP_3) and diacylglycerol (DAG). Secondary messenger IP_3 acts directly at the endoplasmic reticulum (ER) where it stimulates the release of calcium stores, raising intracellular calcium concentrations. In combination with calcium, DAG serves to activate phosphokinase C (PKC) phosphorylation at the carboxyl terminus of the channel in question, leading to inhibition (Mathie, 2007). TASK dependence upon a linked G-protein secondary messenger was originally determined via IC application of a non-hydrolysable, constitutively active form of GTP (GTPγS) (Fink *et al.*, 1996, Kim *et al.*, 2000, Czirják *et al.*, 2001, Chemin *et al.*, 2003). The G-protein isotype involved in TASK inhibition was found to be the $G\alpha_{q/11}$ subunit (Chen *et al.*, 2006). Experiments using fibroblasts from the $G\alpha_{q/11}$ knock out (KO) mice showed that cells co-transfected with TASK3 and G-protein-linked thyrotropin-releasing hormone receptor 1 (TRHR1) in absence of the linked G-protein constituent were insensitive to the application of agonists, confirming that in the absence of the $G\alpha_{q/11}$, inhibition cannot occur

(Chen *et al.*, 2006). The downstream events and the intermediaries involved following $G\alpha_q/_{11}$ activation in TASK remain elusive.

Broadly, there exists three primary hypotheses (Figure 10):

1. Hydrolysis of PIP_2 following isozyme PLCβ activation, generating IP_3 and DAG (Besana *et al.*, 2004, Wilke *et al.*, 2014)
2. Depletion of PIP_2 (Czirják *et al.*, 2001, Chemin *et al.*, 2003, Lopes *et al.*, 2005)
3. Direct inhibition of $G\alpha_q/_{11}$ with TASK3 (Chen *et al.*, 2006, Veale *et al.*, 2007b, Zhang *et al.*, 2016)

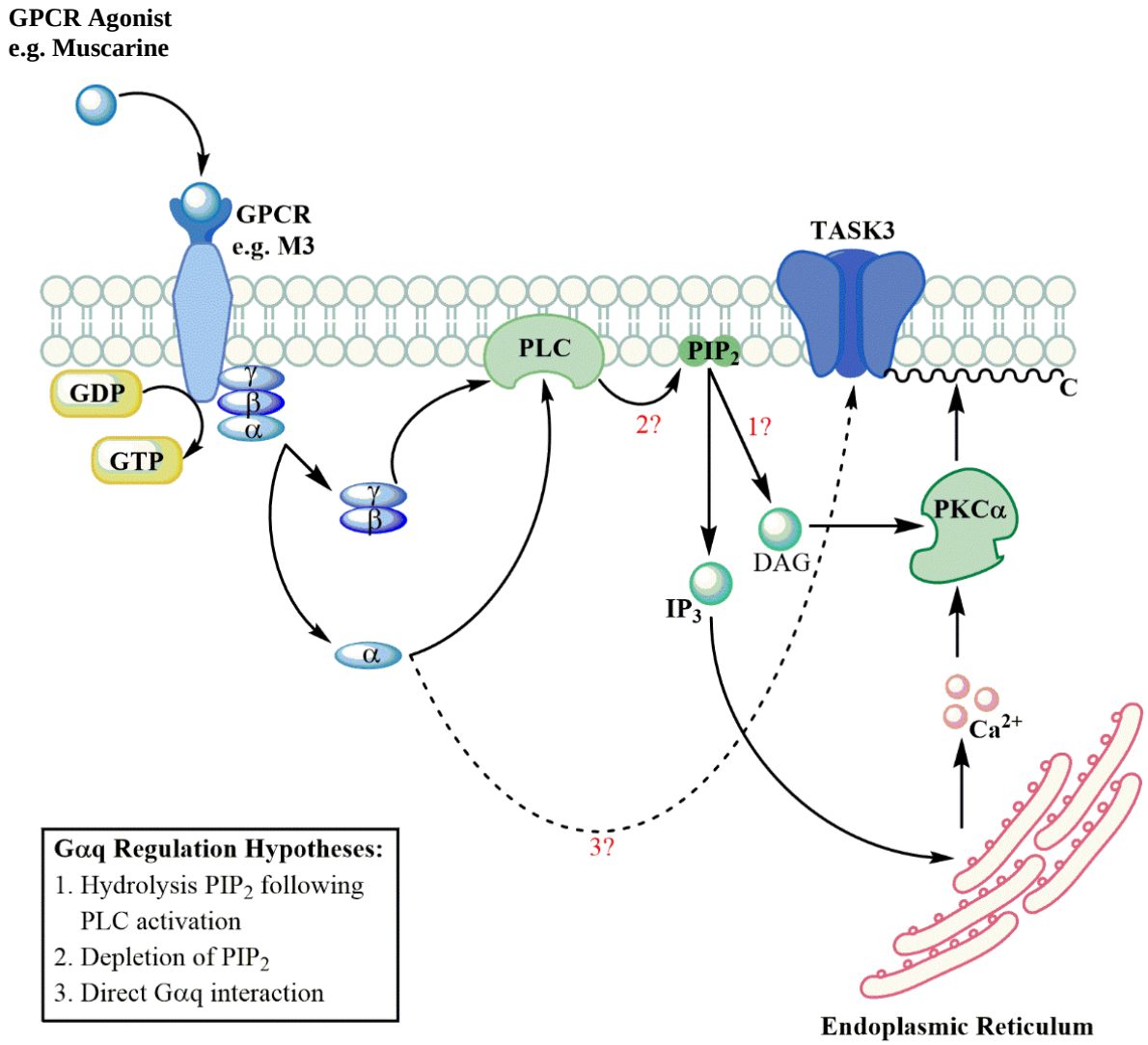

Figure 10 Schematic diagram highlighting possible regulatory mechanisms of TASK3 following activation of GPCR channels.

1.5.2.3.1 Hypothesis 1: Hydrolysis of PIP_2 following PLCβ activation

Following suit of K_V, K_{IR} and Ca_V channels etc., prevailing hypotheses suggested $G\alpha_q$ activation would in turn induce hydrolysis of PIP_2 through the action of PLC. In absence of evidence suggestive of a significant role of IP_3 necessitating intracellular Ca^{2+} release as a primary transducer of inhibition, there is a wealth of data that argues PLC-independent, receptor-mediated inhibition. Chen *et al.* (2006) showed that inhibition of TASK channels through $G\alpha_q$-coupled protein receptors may proceed unabated in the absence of PLC activity following the manipulation of G-protein expression and PIP_2 levels (Chen *et al.*, 2006), although this is debatable. Transient co-transfection of a PLCβ1ct mini construct induced a small, yet significant, decrease in inhibition. This construct impedes PLC-mediated PIP_2 hydrolysis by $G\alpha_q$ coupled receptors. On the other hand, co-transfection of a constitutively active, mutated form of $G\alpha_q$ ($G\alpha_q$*AA) bearing a Ct substitution deeming it deficient in PLC activation capability, strongly inhibited TASK3. This would suggest that inhibition through PLC activity is not the primary mechanism of action but does not rule out its involvement entirely in inhibition of transduction.

Contrary to this, Wilke *et al.* (2014) suggested that PLC is required for TASK channel inhibition as a key regulator of DAG homeostasis (Wilke *et al.*, 2014). Activation of the isozyme PLCβ occurs through the activation of GPCRs which signal via the $G\alpha_{q/11}$ subclass of the Gα protein family following direct interaction (Kadamur and Ross, 2013). DAG is a resident membrane protein believed to function through direct binding to the target protein or via recruitment of effector proteins, such as PKC, to the membrane via a cysteine-rich C1-binding domain. Recognised as an activator of canonical transient receptor potential (TRP) cation channels, details of the binding sites or mechanisms of activation remain unclear (Dietrich *et al.*, 2005). Like TRP channels, TASK channels do not contain a C1-binding domain. As has been observed for other stimuli of TASK channels (Talley and Bayliss, 2002a), removal of a proximal 6 amino acid Ct motif (VLRFLT) proved deleterious to DAG interaction as channel inhibition was abolished (Wilke *et al.*, 2014). Mirroring the hypothesis of direct $G\alpha_{q/11}$ binding, Wilke *et al* promoted the possibility of DAG binding directly to the α-subunits of the pore, rather than an abundant and ubiquitously expressed accessory protein, which in turn interacts with the pore-forming units. Following multiple assays, it was determined that of all the PLC's downstream messengers, only DAG induced channel inhibition. Acceleration of DAG turnover resulted in a reduction in channel inhibition, suggesting that the production of DAG is necessary for regulation. In cell-free systems using excised patches, direct application of DAG was shown to rapidly induce channel inhibition. In such systems, there is unlikely to be rapid recruitment of cytoplasmic DAG effector proteins; activation of kinase signalling cascades or conversion of DAG to downstream intermediaries like (lipid metabolites: 2-arachidonoyl-glycerol (2-AG) and phosphatidic acid (PA)). Significance of DAG involvement is further

supported via the reduction of inhibition following enzymatic conversion of DAG to 2-AG/PA. In excised patches derived from *Xenopus* oocytes, it was discovered that 2-AG was unable to fully abolish GPCR-induced inhibition. This would hint at a potential minor contribution of 2-AG to channel regulation (Wilke *et al.*, 2014).

Whilst DAG regulation had not been previously suggested, knowledge of other lipid compounds known to robustly inhibit TASK was apparent in the form of endocannabinoid: anandamide and its synthetic analogue, methanandamide which are known to interact directly with the channel (Veale *et al.*, 2007a). DAG and these lipid compounds share similar chemical properties, all containing arachidonic acid bound to a mildly polar head group containing a hydroxyl group as seen in Figure 11. It therefore stands that DAG is likely to interact in a similar manner. In conclusion of this hypothesis, Wilke *et al* present a convincing study supportive of cellular DAG concentration dynamics regulated via PLC clearance rate of DAG as an important mediator of TASK activity (Wilke *et al.*, 2014) and therefore a potential factor to consider in pathophysiological processes. Of the 10 mammalian DAG kinase (DGKs) isoforms identified (Shulga *et al.*, 2011), mutations of DGKδ isoform expressed predominantly within the brain resulted in reduced potassium conductance caused by elevated DAG levels, has been linked to epilepsy in both mice and humans (Leach *et al.*, 2007). Furthermore, KOs of other isoforms have resulted in similar neuronal and behavioural alterations (Rodriguez de Turco *et al.*, 2001) commonly reflected in pathology associated with TASK channel mutations, such as Birk Barel Mental Retardation Syndrome. It therefore stands that this theory should be highlighted as a significant potential mechanism.

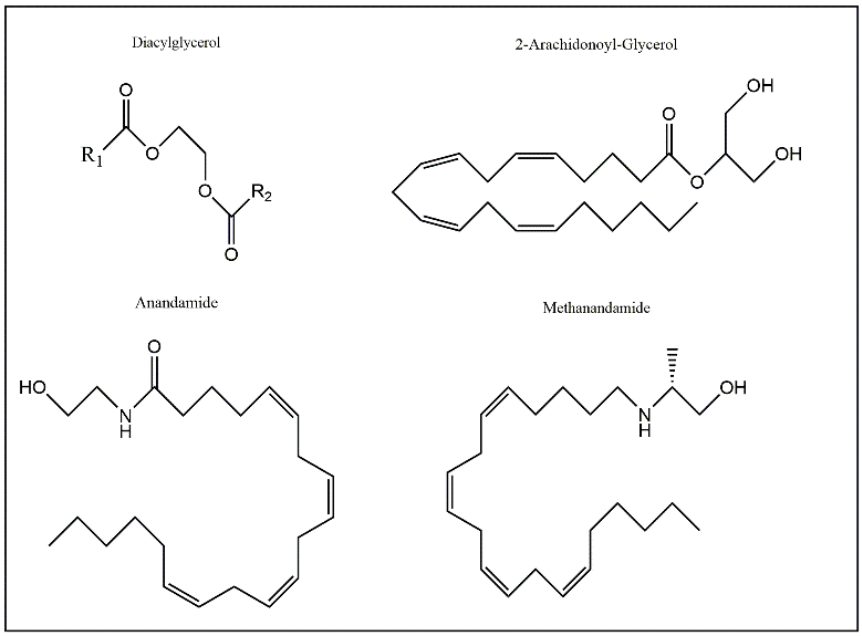

Figure 11 Schematic displaying structural similarities between DAG and other directly acting compounds.

1.5.2.3.2 Hypothesis 2: Depletion of PIP_2

In evaluation of the PIP_2 depletion theory, Chen *et al.* (2006) further rule out PLC involvement in receptor-mediated inhibition (Chen *et al.*, 2006). K_{IR} and K_V channels have been shown to rely upon the presence of PIP_2 in the membrane to support an open, active conformation with agonist inhibition occurring with localised reduction of PIP_2 (Lopes *et al.*, 2005). In light of this, it was proposed that transduction of $G\alpha_{q/11}$ inhibition was achieved through hydrolytic depletion of PIP_2 via $G\alpha_{q/11}$ activation of PLC (Chemin *et al.*, 2003, Lopes *et al.*, 2005). A prediction supported by diminished recovery of TASK3 current observed in the presence of Wortmannin, a PIP_2 re-synthesis inhibitor and a poly-lysine PIP_2 scavenger – evidence arguing for TASK dependence on PIP_2 for inhibition (Czirják *et al.*, 2001, Lopes *et al.*, 2005). This is a disputed hypothesis as it raises the question, is inhibition of recovery by Wortmannin solely attributable to decreased intracellular PIP_2 or, is there a reduction in PLC-induced PKC activation which in turn limits $G\alpha_q$-mediated inhibition (Veale *et al.*, 2007b)? Indeed, PKC has confirmed involvement in channel inhibition, targeting an identified phosphorylation site, threonine 341 (Thr341) in the Ct of the channel. Application of PKC inhibitors bisindoylmaleimide-1-hydrochloride (BIM) and 12-(2-cyanoethyl)-6,7,12,13-tetrahydro-13-methyl-5-oxo-5*H*-indolo(2,3-a)-pyrolo(3,4-c)-carbazole (Gö6976), and a small interfering RNA sequence against PKCα isomers are all reported to block PKC inhibition. Yet a PKC-insensitive mutant channel, co-expressed with a muscarinic M3 receptor can still undergo inhibition following agonist stimulation of the receptor, ruling out PKC as the primary transducer (Veale *et al.*, 2007b). Furthermore, Veale *et al.* (2007) go on to theorise a negative regulatory role for PKC following M3 activation in which, following PLC activation, PKC resists inhibition as opposed to transducing it to '*prevent prolonged current inhibition,*' and support channel recovery (Veale *et al.*, 2007b). Application of PLC blockers; cell lines naturally expressing low PIP_2 and mutated $G\alpha_q$ unable to activate PLC, were all proven unable to completely abolish TASK3 inhibition (Chen *et al.*, 2006).

As a positive control, Chen *et al.* (2006) examined effects of thyrotropin-releasing hormone (TRH) on TASK and compared it to a confirmed PIP_2, pore-mutated $K_{IR}3.4^*$ (S143T) construct, known to depend upon PIP_2 depletion. As expected, inhibition was substantially reduced in $K_{IR}3.4^*$ upon co-transfection with the PLCβct construct when activated by TRHR1. Under the same conditions, TASK inhibition following TRHR1 activation occurred much faster with less sensitivity to the PLCβct, questioning TASK sensitivity to PIP_2 depletion and therefore the second hypothesis. To test this further, TASK channels were expressed in a cell line stably expressing the lipid phosphatase: phosphoinositide-specific inositol polyphosphate 5-phosphatase IV (5ptase IV) under tetracycline control. Upon induction, this lipid phosphatase reduces PIP_2 levels in the cell membrane by up to 15-fold yet TASK inhibition remained undiminished following TRHR1 activation (Chen *et al.*, 2006). This would suggest that inhibition can

occur in an altogether different intermediary pathway that is both predominantly independent of PLC/PKC activity and PIP_2 hydrolysis.

1.5.2.3.3 Hypothesis 3: Direct inhibition of $G\alpha_{q/11}$ with TASK3

Considering these findings, it was postulated that $G\alpha_q$ could co-associate directly with TASK channels independently of the signalling pathway (Chen *et al.*, 2006, Veale *et al.*, 2007b, Zhang *et al.*, 2016). Chen *et al.* (2006) showed that co-transfecting cells with hemagglutinin (HA)-tagged TASK channels and a constitutively active $G\alpha_q$* results in $G\alpha_q$* co-immunoprecipitating with the HA-tagged TASK channels, whilst an inactivated form of $G\alpha_q$ did not interact. Whilst data from this lab using a selective Gαq inhibitor, YM-254890, constitutively active $G\alpha_q$* and a mutated $G\alpha_q$* that no longer has an action on PLC ($G\alpha_q$*RT) was in strong agreement with the Chen *et al*.(2006) theory of direct interaction of $G\alpha_q$ with TASK3 channels (Veale *et al.*, 2007b). More recently, work by Zhang *et al.* (2016) describes enhanced action potential firing frequency upon activation of $G\alpha_{q/11}$-coupled neurotensin (NTS1) receptors in dentate gyrus fibres that is both PLC, Ca^{2+} and PKC independent thus supporting the hypothesis of direct interaction (Zhang *et al.*, 2016). Using co-immunoprecipitation experiments they were able to show that immuno-precipitates treated with neurotensin resulted in the direct association of $G\alpha_{q/11}$ with TASK3, whilst no interaction was observed in TASK3 KO mice.

1.6 TASK Pathologies

Following the discovery of TASK channels over 20 years ago, our knowledge surrounding channel function, regulation and role in disease has grown exponentially. Under normal physiological conditions, TASK channels are regulated by common pathophysiological hallmarks such as reduced oxygen and pH. Due to their pivotal role in apoptosis (Lauritzen *et al.*, 2003) and proliferation (Prevarskaya *et al.*, 2010), the consequences in event of dysfunction are naturally the likes of cancer, (autoimmune) inflammation, ischaemia and epilepsy as well as many developmental conditions (Table 4).

Table 4 Literature overview of TASK channel activity in pathology. Adapted from (Bittner et al., 2010).

Pathology	Channel	Implication	Example	References
Oncology	TASK3	Overexpressed breast, lung and colorectal cancers	Melanoma	(Mu *et al.*, 2003, Kim *et al.*, 2004, Pei *et al.*, 2003, Liu *et al.*, 2005, Pocsai *et al.*, 2006, Rusznák *et al.*, 2008, Kosztka *et al.*, 2011)
		Increased survival in pro-apoptotic conditions		
		Mitochondrial dysfunction		
Ischaemia	TASK1	Increased ischaemic damage in $^{-/-}$mice	Ischaemic stroke	(Meuth *et al.*, 2009) (Bittner *et al.*, 2009)
		TASK1 activity has a neuroprotective effect		
Inflammation	TASK1/ TASK3	Critical roles in T-cell activation	Multiple Sclerosis	(Bittner *et al.*, 2009, Meuth *et al.*, 2008a)
Epilepsy	TASK1	Expression on interneurons reduces neural activity	Temporal lobe epilepsy	(Taverna *et al.*, 2005, Kim *et al.*, 2007)
		Down-regulation in astrocytes has an anti-epileptic effect		
Developmental	TASK3	Neuronal migration	Birk Barel Mental Retardation Syndrome	(Bando *et al.*, 2014) (Barel *et al.*, 2008) (Perry *et al.*, 2014)
			Age at menarche	
Endocrine	TASK1/ TASK3	TASK1 $^{-/-}$ mice: sexual dysmorphic hyper-aldosteronism (HA)	Hyper-aldosteronism	(Davies *et al.*, 2008, Bandulik *et al.*, 2013, Heitzmann *et al.*, 2008, Nogueira *et al.*, 2010, Czirjak and Enyedi, 2002) (Guagliardo *et al.*, 2012, Penton *et al.*, 2012)
		TASK3 $^{-/-}$ mice (neonate): high adrenal renin and severe HA; adults display low renin hypertension and mild HA		
Cardiac Conduction and Repolarisation	TASK1	Alters atrial action potential duration	Long QTS syndrome	(Decher *et al.*, 2011) (Limberg *et al.*, 2011, Petric *et al.*, 2012, Liang *et al.*, 2014)
			Atrial fibrillation	
Increased Body Mass Index	TASK3	Single polymorphisms linked to parent of origin effects	N/A	(Hoggart *et al.*, 2014)
Cardiovascular	TASK1	Loss of function mutations contribute to vascular remodelling and ventricular hypertrophy	Pulmonary Arterial Hypertension	(Ma *et al.*, 2013) (Cunningham *et al.*, 2019, Navas *et al.*, 2016)

1.6.1 TASK channels in Oncology

TASK channels are critically implicated in regulation of cell proliferation and apoptosis. For example, programmed cell death is essential in the first post-natal week of cerebral development (Wood *et al.*, 1993, Lossi *et al.*, 2002). Beginning with intense proliferation of millions of granule neurons (GN) within the external granule layer which then migrate across the molecular and Purkinje layers to the inner granule layer, where they undergo mass apoptosis to numerically match each GN with a post-synaptic Purkinje neuron (Wood *et al.*, 1993, Lossi *et al.*, 2002). The mechanisms by which K^+ channels alter the cellular proliferative state remains unclear however, TASK dysfunction has been inarguably linked to unregulated apoptosis and resulting oncogenesis (see review by (Bittner *et al.*, 2010b)). Following an initial report of a 3 - 10-fold increase of TASK3 expression in 10% of breast cancer samples (Mu *et al.*, 2003), overexpression of TASK3 has now been implicated in 10 - 50% of breast, lung, colorectal and melanoma cancer cells, identifying the channel as a novel proto-oncogene (Mu *et al.*, 2003, Kim *et al.*, 2004, Pocsai *et al.*, 2006, Rusznák *et al.*, 2008). Investigations into overexpression of TASK3 in various cell types and mouse models have described heightened oncogenic potential of the channel to promote the survival of malignantly transformed cells in pro-apoptotic conditions such as reduced serum and hypoxia (Mu *et al.*, 2003, Liu *et al.*, 2005). Interestingly, cells transfected with a mutant TASK3 channel with abolished activity have been shown to reduce the oncogenic potential, thus directly linking TASK3 channel function with tumorigenesis (Pei *et al.*, 2003). Considering the biophysical properties of TASK1 and TASK3 channels, both are inhibited by acidic pH and TASK1 by hypoxia also (Patel and Lazdunski, 2004), it is thus unsurprising to find these channels in solid tumours where the micro-environment is often acidic and hypoxic (Bittner *et al.*, 2010b). Contradictory to the above, TASK1 function and expression on the other hand has been associated with the prolonged survival of patients with late stage colorectal cancer (Cavalieri *et al.*, 2007). It can therefore be broadly summarised that the effect of TASK channels on varying cancers is dependent upon which channel subunit is expressed on which cell type under the control of which pathophysiological stimuli (Patel and Lazdunski, 2004).

1.6.1.1 TASK in the Mitochondria and Cancer

The expression of TASK3 on the inner mitochondrial membrane of melanoma and keratinocyte cells (Szewczyk *et al.*, 2009) has been well documented as it plays a role in the protection of the membrane integrity alongside other ion channels including K^+_{ATP}, BK_{Ca2+} and Kv1.3. Together, these channels support the energy transducing process and the synthesis of reactive oxygen species (ROS) (Laskowski *et al.*, 2016, Szewczyk *et al.*, 2009). Regarding function, the mitochondrial membrane has an intrinsically low permeability to ions in order to preserve oxidative phosphorylation coupling and to prevent energy dissipation through depolarisation of the membrane. As such, the coupling of an energy generating system such as the respiratory chain, alongside an appropriate energy dissipating system, like potassium channels, introduces a tightly regulated mechanism which perpetuates mitochondrial metabolism and energy homeostasis and underlies the primary mitochondrial functions described in Figure 12 (Szabo and Zoratti, 2014).

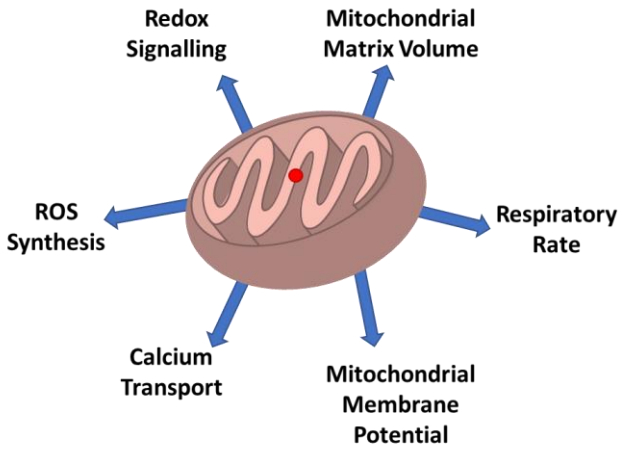

Figure 12 The mitochondrial functions supported by mitochondrial potassium channels

Dysfunctional mitochondria have been linked with several potassium channels including K^+_{ATP}, Ca^{2+}-activated BK_{Ca2+} channel, $K_V1.3$ and TASK3 (Szewczyk *et al.*, 2009). Whilst it is recognised that the TASK3 channels localised at the plasma membrane have a crucial role in the regulation of apoptosis and tumorigenesis, more recently the presence of TASK3 within the mitochondria has been implicated in the development of cancer. A melanoma cell TASK3 knock down model exhibited compromised cell morphology and decreased DNA content; whilst metabolic and mitochondrial activity were significantly reduced as evidenced by diminished ROS production when compared to WT. (Kosztka *et al.*, 2011). Taken together, this suggests that TASK3 is functionally present in a melanoma cell's survival, supporting cellular integrity and viability. Whether this decrease in ROS production is in line with the apoptosis-resistant nature of cancer cells remains to be discovered (Szabo and Zoratti, 2014).

1.6.2 TASK channels in Ischemia

An ischemic stroke will occur following the interruption of blood supply to the brain, starving it of oxygen and glucose, beginning a series of interrelated cascades leading to often fatal neuronal cell death or persisting neurological deficits and disability (Deb *et al.*, 2010). Hypoxia and acidic pH are some of the first pathophysiological markers following an arterial occlusion (Bittner *et al.*, 2010b). As such, it is easy for one to implicate TASK channels in the progression of brain damage based upon inhibition by acidification and hypoxia, leading to prolonged membrane depolarisation and subsequent excitotoxic damage. Alternatively, considering the 'leakage' role of TASK channels where the activity at resting membrane potential serves to preserve a negative potential, reducing neuronal excitability and their metabolic demands. In this way, TASK channels may provide a neuroprotective advantage provided they could remain active during the acute ischaemic event should the changes in pH and oxygen not be severe enough to inhibit them (Meuth *et al.*, 2009). It is well established that the neurons of the CNS are well equipped with acute and long-term protective mechanisms to support homeostatic processes and prevent hyperexcitability in the event of hypoxic events provided by potassium channels including: K_{ATP} channels (Ballanyi and Buck, 2004), BK_{Ca} channels (Rundén-Pran *et al.*, 2002), Kv2.1 (Misonou *et al.*, 2005) and now TASK channels are also being considered. Previous studies have focused primarily on the neuroprotective role of TREK during an ischemic insult. The reduction of intracellular pH is a hallmark of ischemia and inflammation. In such conditions, the open probability of TREK1 and TREK2 is found to be significantly increased with a $TREK^{-/-}$ mouse model, causing reduced neuronal survival rates during an ischemic event (Maingret *et al.*, 1999, Bang *et al.*, 2000). Similarly, $TASK1^{-/-}$ mice models saw the generation of much larger infarct volumes following a transient middle cerebral artery occlusion (tMCAO) (Meuth *et al.*, 2009). As such, due to the similarities observed in the sequence homologies and biophysical properties of these channels and TASK3, it was theorised that the membrane depolarisation and subsequent AP generation by TASK3 channels may be altered under ischemic conditions as a neuroprotective mechanism (Bittner *et al.*, 2010b). Indeed, in *vivo* application of the TASK3 inhibitor anandamide increased the speed of neuronal damage following an tMCAO, mimicking the effect of the $TASK1^{-/-}$ model (Meuth *et al.*, 2009). From the key limited resources available (see: (Meuth *et al.*, 2009, Ehling *et al.*, 2010, Ehling *et al.*, 2013) it has come apparent that TASK channels have a dual purpose which evolves throughout the stages of an ischemic pathophysiological event. During the early phases of a moderate enduring pathophysiological stimuli, such as a transient ischemic attack, TASK channels retain their hyperpolarising function to reduce neuronal excitability and prevent Ca^{2+} overload and excitotoxicity. However, once a certain damage threshold is breached during a more long-lasting event, such as chronic inflammatory ischemia, TASK channels induce neuronal apoptosis as they overcompensate K^+

-efflux which is an indicator of apoptosis. As such, whilst TASK channels may be neuroprotective in the acute stage of an ischemic insult, therapeutics targeting the inhibition of TASK channels in the short term may be effective at preventing neuronal cell death (Bittner *et al.*, 2010b).

1.6.3 TASK channels in (Autoimmune) Inflammation

The diverse expression of ion channels on human T-lymphocytes has been long recognised however, the mechanisms of their dysfunction in autoimmune diseases such as multiple sclerosis (MS), rheumatoid arthritis and type 1 diabetes mellitus (Beeton *et al.*, 2006) is not well understood but their presence alone highlights them as potential therapeutic targets (Kleinschnitz *et al.*, 2007, Wulff and Zhorov, 2008). For appropriate T-cell activation, lymphocytes require the establishment of an increased intracellular Ca^{2+} ion concentration to support the transcription-dependent steps of the activation process (Lewis, 2001, Negulescu *et al.*, 1994, Prakriya and Lewis, 2003). The presence of outwardly rectifying K^+ channels is therefore necessary to maintain the electrochemical gradient to support this (Panyi *et al.*, 2004). Of the K^+ channels expressed: $K_V1.3$ (DeCoursey *et al.*, 1984), BK_{Ca} (Leonard *et al.*, 1992) and TASK channels (specifically TASK1/2/3) (Bittner *et al.*, 2010a, Meuth *et al.*, 2008a) are thought to play prominent roles in disease progression (Beeton *et al.*, 2005, Beeton *et al.*, 2006). In experimentally induced autoimmune encephalomyelitis (EAE) models, specific blocking of $K_V1.3$ led to an improved disease state as cytokine production and proliferation rates were reduced leading to a delayed-type hypersensitivity response (Beeton *et al.*, 2001, Koo *et al.*, 1997). When T-lymphocytes were found to express TASK1, TASK2 and TASK3 in human, rodent and murine species, it was found (ex *vivo*) that similar to $K_V1.3$ inhibition, following application of anandamide and the subsequent inhibition, cytokine production and proliferation were reduced, a phenomenon which was reproducible in the in *vivo* EAE model (Meuth *et al.*, 2008a). This amelioration of disease state was replicated following the selective blockade of TASK channels on myelin basic protein-specific (MBP)T cells (T cells which have been activated following the presentation of an autoantigen such as MBP) (Meuth *et al.*, 2008a). Application of anandamide was observed to reduce the activity of the immune system of WT(EAE) mice resulting in delayed disease onset and severity >50 days but also proved to be equally effective when treatment was began following the onset of symptoms (Bittner *et al.*, 2009). Interestingly, lesion analysis of EAE rodent brain samples identified increased neuronal expression of TASK1 and TASK3 in the optic nerve and decreased expression in the spinal cord. Further lesion analysis in human samples discovered a similar down regulation of TASK 1 and 3 but the upregulation of TASK2 in MS patients during an active disease episode (Meuth *et al.*, 2008b). Taken together, this suggests a regulatory role of TASK channels in pathophysiological states and highlights the ion

channels as an attractive therapeutic target for the treatment of autoimmune diseases (Bittner *et al.*, 2010b).

1.6.4 TASK in Epilepsy

Epilepsy is one of world's oldest recognized disorders with records dating back to 4000 BC and today affects up to 50 million people worldwide. With 10% of the world's population experiencing a single episode of spontaneous neuronal discharge in their lifetime (WHO, 2019), epilepsy is defined as recurrent abnormal and excessive synchronous activity in the brain with at least two unprovoked seizures (Rakhade and Jensen, 2009). For some, seizures may occur less than once a year whilst many live with seizures that occur several times a day. With nearly 80% of patients who live with this condition residing in low-/middle income regions, it has been predicted that up to 70% of those afflicted could live seizure-free should they receive correct diagnosis and treatment (WHO, 2019).

The causes are of epilepsy are many and diverse, ranging from structural abnormalities as a result of malformations in cortical development (i.e. mesial temporal sclerosis) to metabolic irregularities (i.e. epileptic encephalopathies), autoimmune states (i.e. anti-NMDAR encephalitis) and are genetic (Sazgar and Young, 2019). Several of the infantile syndromes associated with epilepsy have been linked to mutations within genes encoding ion channels. As a result, it is unsurprising that the abnormal synaptic transmissions that occur correspond with poor modulation of transmembrane potential following a shift in the brain's extracellular pH. Seizure activity can be described as a biphasic pH shift in which an initial period of extracellular alkalinisation gives way to delayed acidification (Xiong and Stringer, 2000). Due to the regulatory nature of TASK channels, it figures that these channels were prominently investigated to determine a possible role in epilepsy. Much of the available literature focuses upon the role of TASK in temporal lobe epilepsy (Nadler, 2003). Using rodent models, differential expression of TASK channels in various sub regions has been observed, leading researchers to suspect a cell-type specific sensitivity to extracellular acidification in epilepsy (Bittner *et al.*, 2010b). The expression of TASK1 has been noted in astroglial cells of the gerbil hippocampus (Kim *et al.*, 2009b). Gerbils are recognised as a well-established model of inherited epilepsy (Buchhalter, 1993). Whilst there was no difference in hippocampal TASK1/TASK2 expression between seizure-sensitive (SS) and seizure-resistant (SR) strains, an upregulation of TASK1 expression in astrocytes of SS models compared to SR models was observed. The expression of TASK1 in astrocytes of SS animals was found to be very dynamic throughout an episode (Kim *et al.*, 2007). In the acute phase (post-seizure) TASK1 was upregulated, affecting the cellular buffering capacity via increased outward rectification of K^+; increasing cellular excitability as the EC environment pH is reduced. Then

follows a rapid downregulation of TASK1 in attempt to diminish seizure activity by decreasing outward rectification (Bittner *et al.*, 2010b). For these reasons, there are several anti-epileptic drugs on the market today (i.e. Carbamazepine and Vigabatrin) which are known to decrease the number of TASK1 positive astrocytes in the hippocampus by up to 50% (Kim *et al.*, 2007).

In health, the thalamocortical (TC) neural network regulates wakefulness by altering oscillatory states between fast active (awake or rapid eye movement (REM) sleep) and slow inactive states (natural or anaesthesia-induced sleep or absence epilepsies) (Timofeev, 2011). As neuronal firing rates change, there is a concomitant shift in the membrane potential as the TC relay neuron is depolarised following inhibition of TASK1 and TASK3 channels (Meuth *et al.*, 2003). Following the localisation of TASK3 to the 8q24 chromosomal region, mutational analysis in patients diagnosed with absence epilepsy identified an exon-2 polymorphism however, this was found not to be functional in this disease (Kananura *et al.*, 2002). Whilst other anomalies have been found in TALK1 and TASK2 (Saez-Hernandez *et al.*, 2003), a clear association between epilepsy and TASK channels is yet to be revealed.

1.6.5 Pulmonary Arterial Hypertension

Pulmonary arterial hypertension (PAH) is a progressive and incurable pulmonary vasculopathy (Simonneau *et al.*, 2013) affecting 15 - 50 people per million of the population (Humbert *et al.*, 2014), of which 34% will survive 5 years post-diagnosis (Tang *et al.*, 2016). The pathogenic drivers of PAH are complex (Kumar and Graham, 2018). PAH may be idiopathic (iPAH), heritable (hPAH) or may arise as a secondary condition to multiple pathologies including: autoimmune diseases (i.e. scleroderma or systemic lupus erythematosus) (Dib *et al.*, 2012, Rabinovitch *et al.*, 2014, Trad *et al.*, 2006); infectious disease (i.e. human immunodeficiency virus (HIV) and schistosomiasis) and other pro-inflammatory diseases (i.e. digital ischemia in scleroderma and portal hypertension in schistosomiasis) (McMahan and Hummers, 2013, Wilson *et al.*, 2007, George *et al.*, 2013). PAH occurs following the pathological remodelling of the pulmonary arteries causing vasoconstriction and a consequential increase in pulmonary vascular resistance, preluding to a possibly fatal right-sided ventricular heart failure (Gaine and McLaughlin, 2017). As it stands, there are three prominent pathways contributing to cell proliferation and vasoconstriction in the lead up to PAH: the prostacyclin, endothelin and nitric oxide pathways. The clinical treatments currently available target the appropriate up-/down-regulation of these pathways in attempt to slow disease progression and prolong life expectancy (Hill *et al.*, 2016).

Previously, both hPAH and iPAH forms of the disease had been linked to a defective copy of the bone morphogenic protein receptor type II (BRPM2) which, under healthy physiological conditions, regulates vascular cell proliferation (Machado *et al.*, 2015). Ion channels have also been identified as key risk factors for hPAH and iPAH. TASK1 channels play a critical role in the regulation of vascular tone and excitability of pulmonary arterial smooth muscle cells (PASMCs) (Yuan *et al.*, 1998, Boucherat *et al.*, 2015, Hemnes and Humbert, 2017). The TASK1 channel was first implicated in PAH following the discovery of six heterozygous mutations by Ma *et al.* (2013) in patients expressing either iPAH or hPAH forms of the disease. This finding was followed by the discovery of two novel homozygous missense mutations: L214R and G106R in exon 2 of *KCNK3* of patients, which precipitates a particularly aggressive forms of PAH (Navas *et al.*, 2016). Electrophysiological characterisation of these mutants found the functional currents to be significantly reduced when compared to the WT (Cunningham *et al.*, 2019, Ma *et al.*, 2013).

The pharmacological phospholipase A2 inhibitor (ONO-RS-082) has been shown enhance the current of WT TASK1 channels (Girerd *et al.*, 2014). Application of ONO-RS-082 in rat PAH models identified the inhibitor to have reversing effects on proliferation, vasoconstriction and inflammation associated with PAH (Antigny *et al.*, 2016). Furthermore, ONO-RS-082 was able to restore the current in a couple of the heterozygous mutations previously identified by Ma *et al.* (2013), including T8K and E182K, but not the others. Additionally, the reductions in current observed with the mutations could not be attributed to trafficking defects (Cunningham *et al.*, 2019). Riociguat, a guanylate cyclase activator commonly prescribed to PAH patients, increases the synthesis of cGMP down-stream of the nitric oxide pathway and has been shown to improve the pulmonary vascular haemodynamics (Hill *et al.*, 2016, Ghofrani *et al.*, 2017). Despite being previously shown to enhance current in WT TASK1 channels, it was also unable to rescue current in mutated channels (Cunningham *et al.*, 2019). As such, the mutations implicated in PAH display significantly different functional properties. It is currently unclear whether the therapeutics presently available act primarily through the activation of TASK1 channels however, enhancement of current through TASK1 channels continues to be a popular therapeutic strategy (Cunningham *et al.*, 2019).

1.6.6 TASK in Developmental Disorders

Neural activity is vital in the embryonic development of cerebellar granule neurons (CGNs). Cortical development follows a distinctive activity pattern in the early phases (Khazipov and Luhmann, 2006, Allene and Cossart, 2010), driving a series of proliferation (Weissman *et al.*, 2004, Liu *et al.*, 2010), differentiation (Borodinsky *et al.*, 2004) and migratory processes (Komuro and Rakic, 1993, Nakanishi and Okazawa, 2006, Bortone and Polleux, 2009). Alterations in neural activity in relation to TASK3 has been associated with disturbances in cortical arrangement and is therefore suspected to participate in cognitive developmental disorders (Bando *et al.*, 2014). One such disorder is *KCNK9* imprinting syndrome.

1.6.6.1 KCNK9 Imprinting Syndrome

Mendel's theory of genetic inheritance states that an individual receives two alleles of a gene, one from each parent. Certain autosomal genes are inherited in such a way that only one allele is expressed and the other is silent. For instance, a mutation in a gene imprinted with paternal silencing will have no effect whilst a mutation on the maternal gene will be expressed as a dysfunctional gene. This is *'genomic imprinting,'* an epigenetic phenomenon in which dysfunction has been linked with only a few human phenotypes. The most studied imprinted syndromes include Prader-Willi and Anglemann, which are paternal and maternal imprinting syndromes respectively, on chromosome 15q11-q13; Beckwith-Wiedemann and Russel-Silver of chromosome 11p15.5 (Temple, 2007).

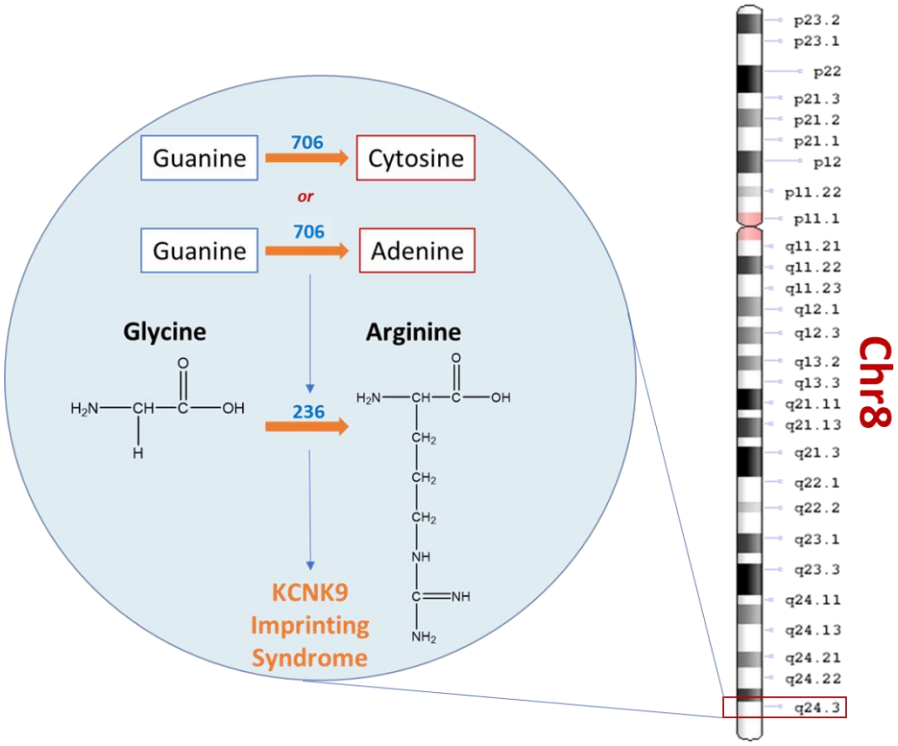

Figure 13 Displaying the location of the gene defect associated with *KCNK9* Imprinting Syndrome.

The KCNK9 gene is expressed on chromosome 8. Base pair variants (706G>C and 706G>A) at exon 2 of 8q24 lead to the G236R amino mutation resulting in the rare disorder.

TASK3 channels are the only genetically imprinted K2P channels. The *KCNK* gene is expressed from the maternal allele with the paternal allele silenced via methylation within the gene promoter region (Barel *et al.*, 2008). Whole genome exome sequencing mapped *KCNK9* imprinting syndrome (Birk Barel Mental Retardation Syndrome) to two individual base changes (guanine>cytosine (706G>C) and guanine>adenine (706G>A)) in exon 2 of chromosome 8q24 (see Figure 13). These changes in turn, resulted in an hydrophobic glycine (Gly, G) being replaced by an hydrophilic, positively charged arginine (Arg, R) at position 236 (G236R) in the maternal allele which is imprinted with paternal silencing (Barel *et al.*, 2008) (Figure 13). *KCNK9* imprinting syndrome is a rare developmental disorder characterised by intellectual and development disability, hypertonia and dysmorphisms (Figure 14). Barel *et al.* (2008) concluded that the G236R mutation was a loss-of-function variant, displaying an abolished functional current in *KCNK9* homodimers or TASK3/1 heterodimers resulting in a non-functional channel (Barel *et al.*, 2008). Overexpression of the dominant-negative G236R mutation was shown to hinder migration of cortical neurons in association with increased Ca^{2+} transients, leading Bando *et al.* (2014) to believe that TASK channels regulate cortical pyramidal neurons by maintaining intracellular calcium concentrations (Bando *et al.*, 2014).

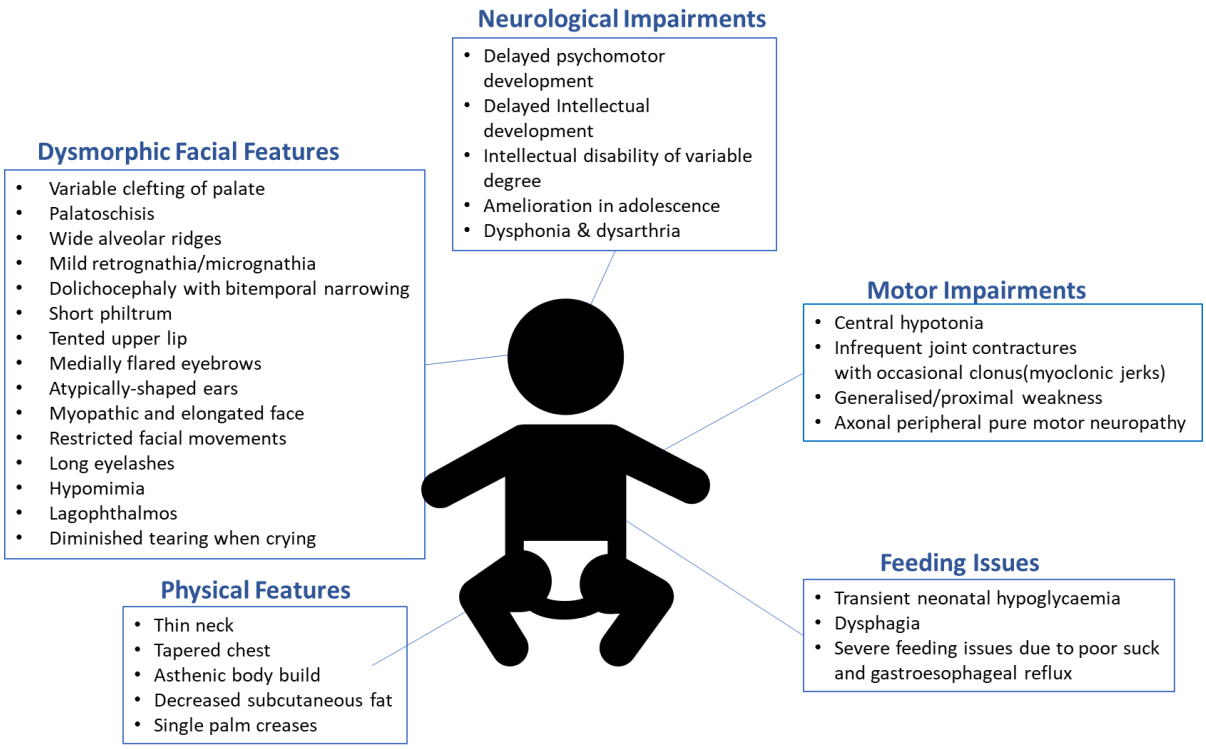

Figure 14 Neurological, physiological and developmental features of *KCNK9* Imprinting Syndrome.

Only 6 families worldwide, mapped with one or the other base changes resulting in a G236R mutation are recorded in literature so far. More recently however, a novel variant (c. 710C>A) occurring within the 2nd exon of the TASK3 gene has been reported in a patient (Šedivá *et al.*, 2019). The consequence of this base change is the mutation of an Alanine (Ala, A) at position 237 to an Aspartic acid (Asp, D) at position 237 (A237D) resulting in the same clinical phenotype as the G236R patients. This would suggest that *KCNK9* Imprinting Syndrome may be caused by nucleotide variants other than those resulting in the G236R mutation (Šedivá *et al.*, 2019).

1.6.6.2 Therapeutic Approach

TASK3 channels remain open across the physiological resting membrane potential in order to maintain the hyperpolarised resting membrane potential of the cell (Goldstein *et al.*, 2001). Through TASK3 inhibition, neuronal excitability may be increased to aid long term potentiation; alternatively, through opening more channels, an AP may be decreased/abolished. Surprisingly, unlike Barel *et al.* (2008), Veale *et al.* (2014) found that in their experimental conditions the TASK3 G236R mutation gave rise to a measurable but significantly reduced current that showed pronounced inward rectification and a slight reduction in K^+ selectivity when compared to the WT-TASK3 channel (Veale *et al.*, 2014). This G236R mutation was also found to be differentially sensitive to regulators such as the selective inhibitors (i.e. synthetic cannabinoid methanandamide or ruthenium red and zinc) – all of which are thought to be effective through altering the channel gating. Reduced currents through these mutant channels could be partially overcome by introducing a gain of function mutation (A237T) (Ashmole *et al.*, 2009) to the mutant channel or by application of non-steroidal anti-inflammatory (NSAID), flufenamic acid (FFA) (Veale *et al.*, 2014). However, currents were not restored to WT levels. Another interesting observation by Veale *et al.* (2014), was that the GPCR mediated inhibition of the mutant channel was also altered. Activation of muscarinic (M3) receptors co-expressed with the TASK3-G236R mutant channel, showed no concurrent inhibition regardless of the muscarine concentration applied. Furthermore, the direct inhibitory effects of constitutively active $G\alpha_q$* was abolished, suggesting a complete loss of $G\alpha_q$ regulation (Veale *et al.*, 2014). Whilst there have been significant positive effects observed following *in vivo* application of fenamate derivatives (mefenamic acid) with regards to developmental acceleration and improvements in feeding difficulties (*i.e.* poor calorie intake), it has proven clinically difficult to measure therapeutic effects as patient numbers are so limited and with vast differences in severity and phenotypical traits (Šedivá *et al.*, 2019, Graham *et al.*, 2016).

One explanation for the reduced current recorded at the cell membrane for this and for other TASK channel mutations may be as direct consequence of impaired trafficking of the channels to the plasma membrane. In the next chapter I will discuss the trafficking of integral membrane proteins, with focus upon potassium channels, and the implications of mutations which impair trafficking and promote disease (Cobbold *et al.*, 2003). I will also investigate the trafficking of the TASK3_G236R mutation, plus two novel unpublished TASK3 variants identified in patients, tyrosine to cysteine at position 205 (Y205C) and a Y205 truncation (Y205Δ) in which a simple substitution of cytosine to adenine at position 604 introduces a stop codon resulting in a channel that is truncated within PD2. These mutations are both clinically and functionally like G236R. Finally, I shall also study two TASK1 mutations (G106R and L214R) that have been implicated in PAH (Navas *et al.*, 2016).

Chapter 2:

Exploration of TASK trafficking in tsA201 cells in association with novel pathological mutations

2.1 Introduction

TASK channel regulation of cellular membrane potential has been implicated in a vast range of physiological and pathological pathways including: regulation of cell proliferation (i.e. oncogenesis and PAH), neuroprotection (i.e. ischemia and epilepsy), immune response (i.e. inflammatory conditions) (Enyedi and Czirjak, 2010, Buckler *et al.*, 2000), neurological diseases such as *KCNK9* imprinting syndrome (Barel *et al.*, 2008, Veale *et al.*, 2014) and many others. Due to the leak nature of TASK channels expressed at the plasma membrane, alterations in expression at the cell surface directly affects current density of the neuronal membrane and therefore function (Mathie *et al.*, 2010). Regardless of function, all integral membrane proteins must embark upon a pathway consisting of biogenesis, assembly and membrane insertion, with quality assurance checks at every stage to ensure that only correctly folded proteins will reach their destination. Whilst there are many genetic polymorphisms present in transmembrane proteins that induce no obvious effect, there are as many disease-causing genetic mutations which do alter trafficking properties.

2.1.1. Biogenesis

K^+ ion channel biogenesis and trafficking begins with transcription of the gene in the nucleus to messenger ribonucleic acid (mRNA) that is exported into the cytosol where it forms a complex with cytosolic ribosomes and transfer RNA (tRNA). Translation, directed by mRNA codon sequence, is facilitated by the delivery of amino acids associated with tRNA. As the nascent peptide elongates it enters a ribosomal tunnel approximately 100Å in length and 10 - 20Å in width, which is sufficiently large enough to support formation of secondary structure. Upon completion of translation, the ribosome-peptide complex is targeted to the endoplasmic reticulum (ER) via the inclusion of a specialised signal recognition motif within a hydrophobic helical region of the Nt. The recognition motif binds a signal recognition particle (SRP) which is in turn bound to the cytosolic side of the ER. In $K_v3.1$ of the potassium ion *Shaker*-family, it has been shown that multiple TM domains are involved in the targeting process with the second segment (S2) acting as the SRP motif (Tu *et al.*, 2000). This process occurs in a matter of minutes and emphasises the importance of translational regulation and protein topology in determination of traffic destination during even the early stages of synthesis.

2.1.2 ER: Translocation, Folding, Assembly, Quality Control and Disease.

The ribosome-peptide complex binds specifically to a multi-protein complex termed, the translocon (composed of the heterotrimeric Sec61 complex), which forms an aqueous pore. A hydrophobic motif present within the Nt directs the nascent peptide through the pore so that it may cross the lipid bilayer of the ER. Opening of the pore is initially governed by length of the peptide which in turn dictates translocation and membrane integration of the protein. Whilst the protein continues to be translated, the peptide simultaneously undergoes modification by translocon-associated proteins which cleave the SRP motif and drive glycosylation and the addition of glycans to the Nt (N-glycans). Carrying out the translation and translocation processes synchronously avoids premature folding and ensures the safe delivery of the peptide into the ER lipid bilayer where ER machinery choreographs the folding events that arranges transmembrane topology into the hydrophilic cytoplasmic and hydrophobic TM domains (Deutsch, 2002). It is speculated that oligomerisation of proteins to form functional units occurs at this stage. K_v channels form functional tetramer units and have been observed to oligomerise via coupling of two dimer units as opposed to sequentially as individual subunits (Tu and Deutsch, 1999). This occurs via a highly conserved tetramerisation domain within the Nt, although oligomerisation is not restricted to this domain (Kosolapov and Deutsch, 2003). Studies involving mutated K_v channels in which this domain is missing still display oligomerisation but with considerably lower efficiency. Alternately, other potassium channels contain oligomerisation domains within the Ct (Schwappach, 2008) or in the case of TASK3, the M1P1 loop. At this stage within the ER lies the first of many quality control sites along the secretory pathway which is tightly regulated by ER-associated chaperones that identify unfolded or misfolded polypeptide chains and prevents anterograde movement (Ellgaard *et al.*, 1999). On the one hand, chaperone proteins like calnexin and calreticulin lectins co-ordinate with thiol-dependent oxidoreductase ERp57 to dictate folding events occurring within the lumen (Swanton and Bulleid, 2003, Rutishauser and Spiess, 2002, Ellgaard *et al.*, 1999). On the other hand, these proteins recognise and bind monoglucosylated intermediates of the N-glycans attached to the peptide. The trimming of these glycans signals that the protein is ready to exit the ER and begin transport to the Golgi apparatus for further modification. If the protein is incorrectly folded, a glucose residue is reattached to the protein thus preventing exit from the ER (Aebi *et al.*, 2010, Appenzeller-Herzog and Hauri, 2006). TASK1 and TASK3 contain a conserved N-glycosylation site: asparagine (Asn, N) residue at position 53 (N53) (Mant *et al.*, 2013b). Channel glycosylation of this residue in TASK1 is confirmed to be critical for cell surface expression and function. For TASK3 channels, glycosylation is not required for expression however it does have a negative impact on the degree of membrane expression, displaying only a 40% reduction of a TASK3_Asn53 mutation at the surface compared to the WT, whilst patch clamp analysis proved function to be indifferent (Mant *et*

al., 2013b). This suggests that in absence of glycosylation, the rate of retrograde recycling of the channel is increased.

2.1.2.1 ER Storage Diseases

Here occurs the first of many trafficking diseases occurring in the first ER compartment due to early defects in biogenesis: ER storage diseases (ERSD) which all present with a similar phenotype caused either by reduced expression at the plasma membrane or indirect toxicity caused by aggregates which impair cell function and may lead to cell death (Cobbold *et al.*, 2003). One example of an ERSD is the retention of the chloride channel and cystic fibrosis transmembrane regulator (CTFR). A deletion mutation of phenylalanine at position 508 [F508_Del] is observed in approximately 70% of all patients diagnosed with cystic fibrosis (CF) and is characterised by the retention of the mutant protein in the ER (Bertrand and Frizzell, 2003). Consequently, patients display with an accumulation of sticky mucus within the lungs due to the reduced secretion of chloride ions from the epithelial cells. The chaperone protein calnexin has been observed to interact with both WT and the CTFR (F508_Del) however, the interaction with WT is only transient and is released from this interaction prior to ER exit. For CTFR (F508_Del), calnexin remains bound to the mutant peptide and it is this association which is thought to drive the mislocalisation of the protein in CF (Pind *et al.*, 1994). Other ERSDs associated with impaired ion channel trafficking include Long QT-2 syndrome following ER retention of potassium HERG channels in which several mutations may result in irregular electrical cardiac impulses and ventricular tachycardia (Ficker *et al.*, 2000, Kupershmidt *et al.*, 2002); another example would be a deletion mutation [F1388_Del] (Cartier *et al.*, 2001) within the sulfonylurea-1 (SUR-1) subunit of K_{ATP} leading to ER retention and fatal hypoglycaemia in children diagnosed with congenital hyperinsulinism (Meissner *et al.*, 1999).

2.1.3 ER to the Golgi

Following departure from the ER lumen, newly modified proteins may associate with cytosolic chaperones forming transient interactions to aid further modification and trafficking, preventing misfolding during transport and retaining dysfunctional channels. These proteins are suspected to work in competition, with binding of the 14-3-3 adaptor protein promoting forward traffic from the ER to the plasma membrane, whilst binding of coatomer protein complex 1 (COPI) encourages retrograde transport from the Golgi apparatus toward the ER for retention and degradation. These proteins are critical in the transport of TASK channels with interaction observed in both native and

recombinant forms (O'Kelly *et al.*, 2002, Rajan *et al.*, 2002, Coblitz *et al.*, 2005, Zuzarte *et al.*, 2009). Mutational studies of TASK found that all seven isoforms of 14-3-3 (β, γ, ε, ζ, η, τ, δ) bound to TASK1 and TASK3 with 14-3-3β binding with highest affinity in a phosphorylation-dependent manner (O'Kelly *et al.*, 2002). 14-3-3 are more recently emerging as 'switch proteins,' due to their dynamic ability to induce conformational changes and restraints depending upon their target and are recognised in many interactions, predominantly involving phosphoserine-containing motifs (Mackintosh, 2004). There are currently three hypotheses surrounding 14-3-3 and COPI interactions and their involvement in the regulation of TASK trafficking: "clamping," "scaffolding" and "masking" (Mathie *et al.*, 2010). Originally, the clamping hypothesis was favoured (O'Kelly *et al.*, 2002), but more recently, evidence supports the masking mechanism of action (Zuzarte *et al.*, 2009).

2.1.3.1 Anterograde Movement: The 'Clamping' Hypothesis

The clamping hypothesis describes a process by which 14-3-3 binding infers a conformational change that prevents binding of COPI via inactivation of COPI-interacting motifs. Indeed, initial experimental data supported the inhibition of COPI binding through binding of 14-3-3 in a non-competitive nature. Binding appeared to occur at separate dibasic sites on TASK1 in a 'mutually exclusive' manner with COPI thought to bind at the TASK Nt [(M)KR] motif and 14-3-3 to the [RR(K/S)SV] motif at the Ct, see Figure 15. It was also determined that, for 14-3-3 interaction to occur at TASK1 channels, a distal serine residue must be phosphorylated. This discovery prompted the theory that COPI is constitutively bound to the channel at the Nt dibasic motif that dictates retrograde transport from the Golgi to the ER for retention in the absence of 14-3-3 binding. 14-3-3 interaction may then possibly induce the dissociation of COPI by conformational change, inhibiting the ER retention motif and promoting forward traffic to the plasma membrane (O'Kelly *et al.*, 2002). This theory proposes an attractive mechanism by which surface expression may be regulated dependent upon IC 14-3-3 concentration.

There are three recognised 14-3-3 binding motifs: Type I/II which are dependent upon a proline residue and may be localised anywhere within cytoplasmic domains and Type III in which proline is absent from the motif and may be found anywhere within the extreme Ct (Coblitz *et al.*, 2005). As seen in Figure 15, both TASK1 and TASK3 contain a type III 14-3-3 binding motif [xRRKS^{p}V]. WT and truncated proteins involved in a yeast GST-pulldown assay determined that only channels that interacted with 14-3-3 were present in the membrane whilst interaction with βCOP1 resulted in reduced surface expression and the channels were observed to accumulate within the ER (O'Kelly *et al.*, 2002).

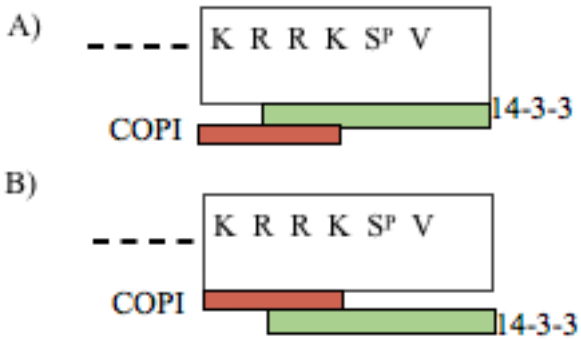

Figure 15 Schematic displaying the masking theory of channel translocation from ER to membrane.

A) Binding of 14-3-3 to the RRKSV motif prevents COPI binding to the KRR retention motif promoting forward translocation. B) Binding of COPI to xKRRx retention motif prevents 14-3-3 binding and the channel is retained within Golgi/ER thus promoting retrograde translocation.

2.1.3.1 Anterograde Movement: The 'Masking' Hypothesis

Evidence in support of the masking theory shows 14-3-3 binding [xRRKS^{P}V] masks tribasic [xKRR] retention motif (Figure 15) in a way that differs functionally from the classical canonical arginine-based [RxR] and lysine-based [KKxx] retention sorting signals and present as a novel retention motif. More recently, Zuzarte *et al.* (2009) confirmed 14-3-3 binding may occur at the Ct motif of both TASK1 and TASK3. The data acquired indicates the Nt retention signal functions independently of 14-3-3 binding. Rather than 14-3-3 binding to the Ct as a prerequisite to forward transportation to the membrane, they suggest that either COPI or 14-3-3 binding at the Ct retention motif is a dominant interaction and so the Nt is not involved in COPI binding and retention, thus discounting the clamping theory (Zuzarte *et al.*, 2009). Such a mechanism is not novel and closely resembles that of the $GABA_B$ receptor in which forward trafficking is mediated by competitive binding of COPI and 14-3-3 as opposed to regulation by conformational change (Brock *et al.*, 2005). It was found that through disabling the 14-3-3 motif and exposing the [xKRRx] motif, retrograde translocation was upregulated as observed by an accumulation of GFP-tagged channels within the Golgi network (Zuzarte *et al.*, 2009). TASK1 ability to bind with 14-3-3 had been previously demonstrated in co-immunoprecipitation investigations in which 14-3-3 ability to bind was lost upon mutation of the Ct phosphoserine (Shikano *et al.*, 2005). It was observed that TASK1 and TASK3 mutants that could still bind 14-3-3 and displayed increased surface expression when compared to those that could not. It was therefore hypothesised that COPI binding and the predicted reduction in surface channel number would be directly proportional to the reduction in potassium current amplitude and vice versa in absence of the conserved [xKRR] motif. Indeed, in channels in which the final 5 amino acids (including the KRR motif) was removed (ΔC_5), current amplitude was 33.3±3% less compared to WT; alternately, when only the extreme valine of

the Ct (TASK1/TASK3), was removed and the retention motif retained (ΔC_1), current amplitude was only 5.9±0.3% less than that of WT channels (Zuzarte *et al.*, 2009).

GST-pull down assays have confirmed COPI interaction occurs at the Ct with ΔC_1 mutants whilst no interaction was observed with ΔC_5. In live-cell imaging investigations, 24 hours following transfection, WT-TASK3 is mostly localised at the cell membrane with partial co-localisation with βCOPI in the juxtanuclear Golgi region. There appeared to be no ΔC_1 membrane localisation as the channel appeared to co-localise almost exclusively with βCOPI in the juxtanuclear region and some partial localisation within the Golgi and IC COPI-coated vesicles thus supporting the notion of COPI mediated Golgi retrieval and ER retention (Zuzarte *et al.*, 2009). Following confirmation of TASK3 ΔC_1 localisation within the Golgi network, cells were incubated with the drug, Brefeldin A. Brefeldin A prevents protein transport via inhibition of guanine-nucleotide exchange factor which in turn prevents the GTP-binding ADP-ribosylation factor 1 (ARF1) from associating with the Golgi membrane. βCOPI requires ARF1 association in order to form a vesicular coat (Helms and Rothman, 1992). Following this treatment, TASK3 ΔC_1 mutants appeared to disperse to the ER. Lack of active ARF1 protein, subsequent vesicle formation and SNARE build-up results in the collapse of the Golgi into the ER causing stress and eventual apoptosis (Nebenführ *et al.*, 2002). Therefore, apparent dispersion of TASK3 ΔC_1 throughout the ER in presence of Brefeldin A otherwise confirms the transport of channels from the Golgi to the ER via βCOPI-coated vesicles. Interestingly, TASK3 ΔC_5 mutants were observed to localise in large, vesicular/tubular structures throughout the cell (Zuzarte *et al.*, 2009). This is likely to be aggregated protein that cannot be scavenged by COPI since it is lacking the retention motif and is instead directed to a degradative pathway. It should be noted that the mediation of TASK trafficking to the membrane is not exclusive to the [xKRRx] and [xRRK[S/K]SV] binding motif. Further motifs such as the conserved di-acidic [EDE] motif at the proximal Ct (Figure 16) (Zuzarte *et al.*, 2007) have been identified to participate in ER-export and promote trafficking to the membrane in the case of TASK3 via interaction with COPII complexes. Mutations of the EDE motif resulted in a significantly reduced current density indicative of limited surface expression in comparison to WT TASK3 (Zuzarte *et al.*, 2007). Whilst apparent that this motif certainly has a role in the efficiency of forward trafficking, interaction with the EDE motif is not able to overcome those occurring at the extreme Ct. Considering these investigations, regulation at post-translational levels is crucial to plasma membrane channel expression and is directly proportional to current amplitude of neuronal cells and level of excitability. Whilst knowledge of membrane insertion itself is poor, surface expression appears to be predominantly mediated via retention/promotion of ER trafficking via the Golgi complex through interaction of specialised ER export motifs and COPI/II mediated vesicles.

2.1.4 Transport through the Golgi Network to the Plasma Membrane

Once the protein reaches the Golgi, it must navigate through the *cis-*, *medial-,* and *trans*-Golgi cisternae and the tubulo-vesicular *trans*-Golgi network (TGN) (Cobbold *et al.*, 2003) where the glycosylation processes and other modifications are completed and the protein matures. Within the TGN, proteins are sorted based upon their ultimate residence (Steele *et al.*, 2007). Plasma membrane proteins are concentrated into clathrin-coated vesicles prior to Golgi export before SNARE-mediated fusion conducts insertion into the membrane – a process which is well documented in K_V 1.1 and K_V2.1 for example (Steele *et al.*, 2007, Mathie *et al.*, 2010). Whilst the exact mechanics of this process remain unknown, it is suspected that upon interaction of the exocytotic vesicle with the membrane-bound SNARE protein leads the deformation of membrane, disturbing the hydrophobic/hydrophilic interactions and allowing the direct insertion of the protein (Jahn and Scheller, 2006, Steele *et al.*, 2007). Defective post-Golgi trafficking is becoming increasingly apparent following association with human diseases such as Hermansky-Pudlak syndrome. In such conditions, it is not the protein itself that's dysfunctional, rather a mutation within an adaptor protein (i.e. AP-3) which causes defects in membrane localisation (Starcevic *et al.*, 2002).

2.1.5 Endocytosis: Recycle, Redistribute, Remove

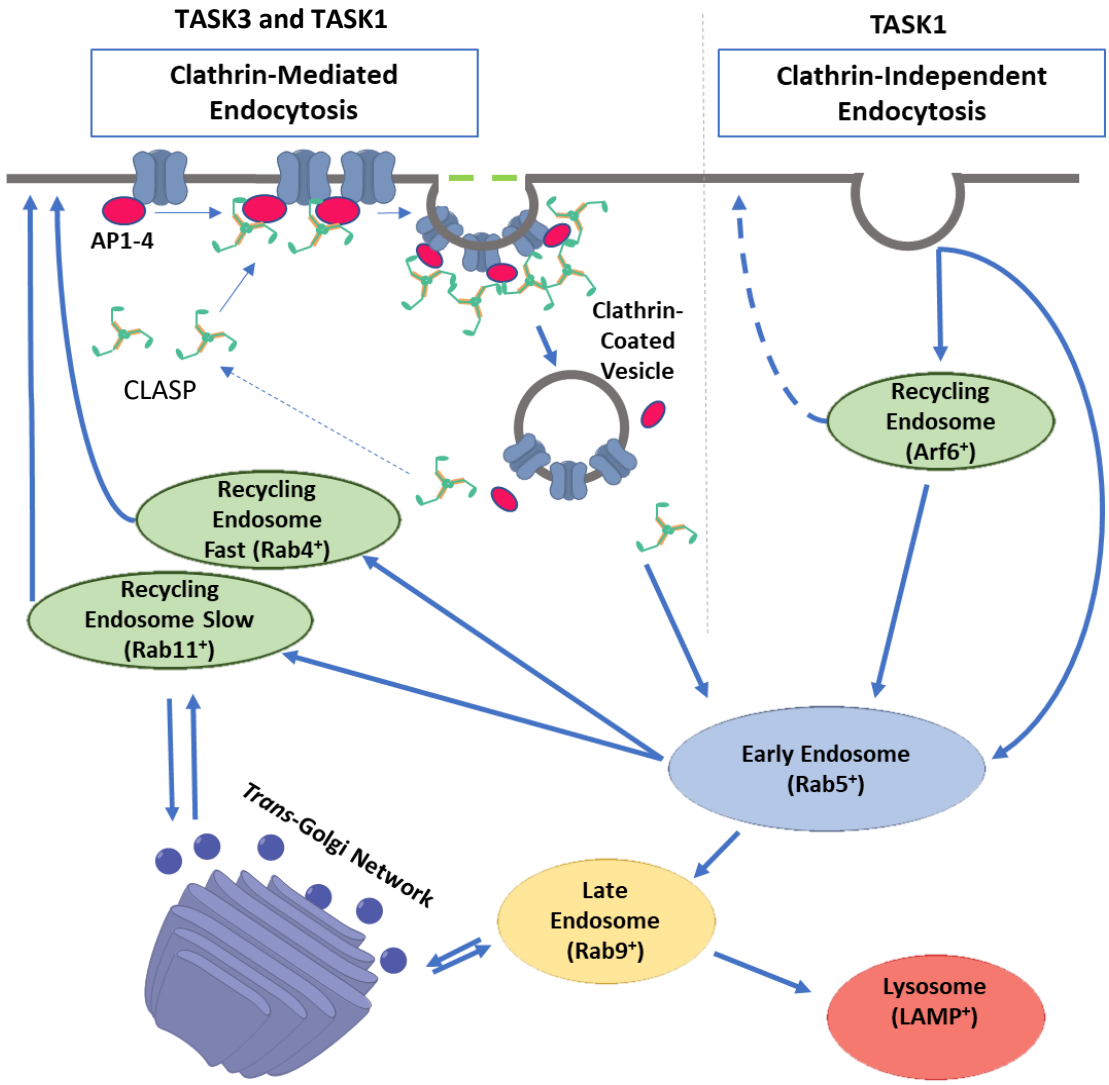

Figure 16 Pathways involved in TASK1 and TASK3 endocytosis.

Both TASK3 and TASK1 can utilise the CME mechanism of internalisation. In the CME pathway, Adaptor proteins 1-4 (not exclusive) and clathrin-associated sorting proteins (CLASPs) gather proteins into clathrin-coated pits that are internally excised from the membrane by dynamin GTPase allowing the vesicle to be sorted into relevant endosomes for recycling or degradation (green-dashed line).TASK1 may also undergo endocytosis through the CIE pathway, where the cargo may either be delivered to early endosomes prior to transport to lysosomes or the trans-Golgi network or, it may be targeted to ARF6^{+} recycling endosomes and return directly to the cell surface or back to the early endosome and into the endocytic pathway.

The process of endocytosis is now understood to be a crucial component in the control of cell surface expression of membrane proteins in response to environmental triggers or internal stimulation (O'Kelly, 2015). Such a process is tightly regulated by the presence of discrete structural features and sorting motifs within the Ct which allow channel binding partners to direct proteins into the correct pathway (O'Kelly, 2015). Despite the high degree of similarity both in homology, regulation (Bittner *et al.*, 2010b, Duprat *et al.*, 1997, Kim *et al.*, 2000, Rajan *et al.*, 2000) and forward processing (Czirják and Enyedi, 2002, Girard *et al.*, 2002, Mant *et al.*, 2013b, O'Kelly and Goldstein, 2008, O'Kelly *et al.*, 2002, Rajan *et al.*, 2002, Renigunta *et al.*, 2006, Zuzarte *et al.*, 2009), the endocytic processes of TASK1 and TASK3 diverge significantly (O'Kelly, 2015) with TASK1 shown to utilise both the clathrin-mediated endocytic (CME) and clathrin-independent endocytic (CIE) pathways. TASK3 on the other hand has only been associated with CME (Figure 16) (Mant *et al.*, 2013a, Renigunta *et al.*, 2014). This is likely because the sorting processes depends on motifs within the Ct of which TASK1 and TASK3 only share 34% sequence homology (Rajan *et al.*, 2000).

Table 5 Putative motifs identified in TASK1 and TASK3 channels that are considered necessary for endocytosis

The number represents the position of the critical (bold) or first residue within motif. N/A represents the absence of sequence. Table adapted from (O'Kelly, 2015).

Channel	**Y**XX**ϕ**	DEXXXL[L/I]	Short Acidic Cluster
TASK1	**Y**$_{138}$LL**H** **Y**$_{300}$AE**V** **Y**$_{323}$SI**P** **Y**$_{353}$SD**T**	**E**HRA**L**$_{263}$**L**	E$_{252}$DEKRD
TASK3	N/A	N/A	E$_{252}$DERRDAEE

As shown in Figure 16, the CME pathway relies upon the work of adaptor proteins (AP, most likely 1-4 but this is not exclusive) and clathrin-associated sorting proteins (CLASPs) to cluster channels on the surface plasma membrane into clathrin-coated vesicles prior to fission (O'Kelly, 2015). Recruitment of AP and CLASPS in the CME pathway depends upon sorting motifs within the cytosolic Ct of the channels (see Table 5) (Bonifacino and Traub, 2003). For example, the AP-2 protein requires the presence of either a tyrosine motif (YXXϕ: X represents a variable; ϕ is a hydrophobic residue) or a di-leucine motif (DEXXXL[L/I]) (Bonifacino and Traub, 2003) for recruitment to the vesicle which is subsequently targeted for lysosomal degradation. In absence of these, TASK3 may still be endocytosed through the CME pathway following recognition of a short acidic cluster (252-EDERRDAEE) (see Table 5) by ADP-ribosylation factor 1 (ARF1) protein. ARF1 localises endocytic cargo to the *trans*-Golgi network (TGN) and drives AP1 recruitment at the membrane (Doray *et al.*, 2012, Nakai *et al.*, 2013).

The CIE pathways, however, consist of multiple pathways which are considerably less defined with only a few motifs associated with a single pathway. The CIE pathways are broadly categorised into groups based upon their general regulators: ARF6, Cdc42/ARF1 and Rho A, although it is unclear how many CIE pathways exist (O'Kelly, 2015). In unprovoked conditions, both TASK1 and TASK3 have been observed to localise within early $Rab5^+$ endosomes however, a >50% increase in vesicles containing TASK3 compared to TASK1 (Mant *et al.*, 2013a) was observed suggesting that TASK3 is either more readily endocytosed or that it remains in the endocytic pathway for longer. As shown in Figure 16, both channels are able to interact with clathrin in the CME pathway but application of dynasore, a dynamin GTPase inhibitor which prevents the cleavage of the clathrin pits, saw the number of endocytosed vesicles positive for both clathrin and channels reduced by over half but endocytosis was not abolished (Mant *et al.*, 2013a, Renigunta *et al.*, 2014). This hints at an alternative pathway being utilised either in the absence of, or in conjunction with, the CME pathway. This observation is supported by further studies, in which TASK3 was commonly found in fractionation samples alongside the transferrin receptor, a recognised cargo of the CME pathway. Whilst TASK1 channels were also present in these fractions, they were equally present in fractions containing flotillin, a cargo of the CIE. Eventually the pathways must converge as TASK1 and TASK3 may both be found in the recycling $Rab11^+$ and degradative $Lamp1^+$ pathways (O'Kelly, 2015).

Dysregulation of endocytosis has been implicated in several very prominent human diseases. Abnormal endocytosis occurring through the CME pathway is situated at the pathophysiological core of Alzheimer's disease (Wu and Yao, 2009). The accumulation of the amyloid-β (Aβ) peptide is now a recognised hallmark of this neurological degenerative disease. Aβ is the product of the processing of type 1 membrane glycoprotein, amyloid precursor protein (APP), which under normal physiological conditions plays many roles in the development and function of the neuron (Mattson, 1997, Young-Pearse *et al.*, 2007). Following CME, APP may either undergo non-amyloidogenic processing (by α and γ secretases) or amyloidogenic processing (by β secretase) producing the infamous Aβ peptide (Mattson, 1997, Thinakaran and Koo, 2008). As it is the endocytic sorting process which ultimately determines which of pathways APP goes through (Nordstedt *et al.*, 1993, Vassar *et al.*, 1999, Lah and Levey, 2000) and that amyloidogenic processing occurs within the endosome (Koo and Squazzo, 1994), it is clear that the process of endocytosis makes a very significant contribution to disease pathology.

2.2 Objective

The objective of these experiments was to identify if there were any differences in the trafficking of WT-TASK3 channels and the TASK3_G236R mutation implicated in *KCNK9* Imprinting Syndrome (Barel *et al.*, 2008) to the plasma membrane using confocal microscopy that would account for the reduced current and function, observed for this variant in electrophysiological experiments. In addition, two novel TASK3_Y205 patient mutations (Y205C and truncated Y205Δ) with clinical symptoms similar to the original G236R variant, were also investigated. Expression of these channels in the endoplasmic reticulum and mitochondria was also explored.

In addition to this, confocal imaging and protein quantification was used to determine whether novel TASK1 disease causing mutations: TASK1-G106R and TASK1-L214R are trafficked to the cell membrane as efficiently as WT-TASK1, following the discovery of decreased TASK1 expression in PASMCs of patients diagnosed with PAH and reduced current observed in patch clamp electrophysiology experiments using heterologous expression systems (Cunningham *et al.*, 2019).

2.3 Methods

2.3.1 Molecular biology

Human wild-type (WT) TASK1 and TASK3 cDNA was originally cloned into pcDNA3.1 vector (Invitrogen, Carlsbad, CA, USA). WT sequence was cut from this vector and cloned into the multiple cloning site (MCS) of pAcGFP1-N1 vector (Clontech-Takara Bio Europe, Saint-Germain-en-Laye, France) to create a fusion construct with the Nt of pAcGFP1. Terminating stop codons were removed by site-directed mutagenesis using a QuikChange site-directed mutagenesis kit and procedure (Stratagene, La Jolla, CA) and maintained within the same reading frame with the start codon of pAcGFP1. Constructs were fully sequenced to ensure correct sequence incorporation (Eurofins MWG Operon, Huntsville, AL, USA). Point mutations were introduced into both pcDNA3.1 and pAcGFP1-N1 encoding TASK1 and TASK3 cDNA by site-directed mutagenesis. A pair of complementary oligonucleotide primers (25-35 bases) incorporating the intended mutation (either G236R, Y205C, Y205Δ, G106R or L214R) were synthesised (Eurofins MWG Operon, Ebersberg, Germany). All constructs were fully sequenced to ensure correct mutation incorporation. For in-cell and on-cell western assays, the TASK1 channel was tagged with hemagglutinin (HA) on the M1P1 loop between Alanine 50 (A50) and Arginine 51 (A51).

2.3.2 Cell Culture

TsA201 cells, modified human embryonic kidney 293 cells which are stably transfected with the SV40 larger T antigen (ECACC; Sigma Aldrich, Missouri, USA), were grown as a monolayer in a tissue culture flask. The cells were maintained in Dulbecco Minimum Essential Medium (DMEM) constituted with 88% minimum essential media with Earle's salts, 2mM L-glutamine, 10% heat-inactivated foetal bovine serum, 1% penicillin (10,000 units mL^{-1}) and streptomycin (10mg/mL^{-1}) , and 1% non-essential amino acids (Sigma-Aldrich, Missouri, USA; Pan Biotech, Aidenbach, Germany; Fisher Scientific, Pittsburgh, PA, USA). Cells were incubated at 37^{o}C in a humidified atmosphere of 95% air and 5% CO_2. Upon reaching 80 – 90% confluency, cells were split and resuspended in a four-well plate containing glass coverslips (13 mm diameter) coated with Poly-D-Lysine (1mg/mL^{-1}) at a density of 7 x 10^4 cells in 0.5 mL of media. Cells were incubated at 37^{o}C in a humidified atmosphere of 95% air and 5% CO_2.

2.3.3 Transfection

Following 24 – 48 hours incubation, cells were transfected using TurboFect transfection reagent (Thermofisher, Loughborough, UK) upon reaching approximately 90% confluency. Briefly, 0.5 µg of the pAcGFP-N1 vector encoding the relevant cDNA was diluted in 100 µl serum-free DMEM prior to the addition of 1.5 µl of the transfection reagent. The DNA mixture was vortexed immediately and then incubated at RT for 20 minutes. Following incubation, 100 µl was added to the appropriately labelled well of the plate and incubated for 24 hours at 37^{o}C in a humidified atmosphere of 95% air and 5% CO_2.

2.3.4 Cell Membrane Staining

A fresh 1X working solution of Cell Mask Deep Red (Thermofisher Scientific, Loughborough, UK) plasma membrane stain was prepared in pre-warmed 1X PBS (1:1000) from a concentrated stock solution prior to use. Transfected cells were washed 3 times with 1X PBS and submerged in 1 mL of the prepared staining solution for 10 minutes (37°C/5% CO_2). The staining solution was removed and the coverslips washed 3X in PBS ready for fixation.

2.3.5 Mitochondria Staining

A 1 mM stock solution of MitoTracker® was prepared by dissolving the lyophilized product in anhydrous dimethylsulfoxide (DMSO). Serum-fee DMEM was pre-warmed in a water bath set at 37 ^{o}C. The 1 mM stock solution was diluted to a working concentration of 400 nM in serum-free DMEM. The media on the cells was removed and replaced with the media containing the staining solution. Cells were incubated for 45 minutes at 37^{o}C/95% air/5% CO_2. After staining, cells were washed in pre-warmed PBS, fixed and mounted as described below (2.3.7 – 2.3.9).

2.3.6 Endoplasmic Reticulum Staining

The endoplasmic reticulum was stained using the CytoPainter ER kit (red fluorescence) by abcam®(Cambridge, UK). Cells were washed in the 1X assay buffer (diluted in ddH_2O) from the 10X buffer provided by the kit. The buffer covering the cells were removed and they were fixed as described below. After fixation, the cells were rinsed 3 times in the 1X assay buffer. Enough dual detection reagent for number of samples was prepared. For every 1mL of 1X assay buffer, 1 µl of red

detection agent and 1 µl of Hoechst 33342 nuclear stain was added. Enough volume of the dual detection agent was added to cover the cells. Cells were then incubated for 25 minutes at 37°C/95% air/5% CO_2. Following incubation, the cells were washed 3 times in 1X assay buffer and mounted as described below.

2.3.7 Cell Fixation

All PBS from the previous washing step was removed and the cells were fixed in 1 mL of 2% paraformaldehyde (PFA) solution and incubated at RT for a maximum of 20 minutes in the dark to protect from exposure. Following incubation, cells were immediately washed 3 times with 1X PBS.

2.3.8 Nuclei Staining

To stain the nucleus, 500 µl of freshly prepared Hoechst 33258 (1:500 dilution in PBS; Sigma Aldrich (Missouri, USA) was added to each well and was incubated at 37°C for 10 minutes. Cells were washed 3 times with 1X PBS following incubation to remove traces of stain.

2.3.9 Mounting

Glass slides (Thermofisher Scientific, Loughborough, UK) were washed with pure ethanol and allowed to dry. Coverslips were mounted face down onto the slides containing a droplet of Vectashield anti-fade mounting medium (Vector Laboratories, Peterborough, UK).

2.3.10 Confocal Microscopy

Images were obtained using the Zeiss™ Laser Scanning 880 (Carl Zeiss, Jena, Germany) confocal microscope using an oil 63x 1.4 NA objective lens. This unit contains a Diode (405nm) laser, an Argon (458, 488, 514nm) laser, a Diode-Pumped Solid State (DPSS)(561nm) laser and a Helium-Neon (He-Ne) (633nm) laser. The experimental workflow and acquisition settings used consistently throughout all the experiments are displayed in Figure 17. Depending on the fluorophore being visualised, the laser used was selected based upon the individual excitation/emission spectra, see Table 6. Zeiss Efficient Navigation (ZEN) (Version: Black) was used for projections (XY).

Table 6 Fluorescent properties of the fluorophores and the Zeiss LSM 880 laser lines/filter sets used.

Fluorophore	Laser line	Excitation/Emission (Ex/Em)	Filter Set
Green-fluorescent protein (GFP)	Argon (488 nm)	495/519	eGFP
Hoechst-33258 (Nuclear)	Diode (405 nm)	354/461	Hoechst-33258
Cell Mask Red™ (Plasma Membrane)	He-Ne (633 nm)	650/655	Cy5
MitoTracker™ (Mitochondria)	DPSS (561 nm)	579/599	Texas Red
CytoPainter™ (ER)	DPSS (561 nm)	570/670	Rhodamine

Switch on Zeiss LSM880 equipment. Load Zen Black software & warm up lasers

Configure experiment & apply following acquisition settings:

Configuration	Setting
Quality	Best Signal
Scan Mode	Frame (Unidirectional)
Frame Size (X*Y)	764 x 764
Line Step	1
Speed Setting	5
Averaging (Mean)	X8 (Line Mode)
Image Bit Depth	12-Bit
Zoom	X2
Pin holes	1 Airy Unit

Select 63x oil objective lens with 1.4 numerical aperture

Place a drop of oil onto slide & arrange face-down on the slide. Adjust stage as necessary

Using the fluorescent microscope setting, select a channel & find region of interest

In acquisition, enter 'live mode' & individually adjust field of focus (Z) & gain settings as necessary for each channel

Stop live view & take 'snap shot' image. For collected image set cross-hair thresholds according to single-stain controls

Figure 17 Experimental set up and standard workflow of image collection using the Zeiss LSM880 confocal microscope

For colocalization analysis, care was taken to avoid detector saturation and crosstalk between channels. Crosshair thresholds were applied within the Zen Black software (Zeiss), prior to any image editing. To accurately set the cross hairs, regions of interest (ROI) were drawn around single label controls (i.e GFP or CellMask (CMR) alone) to prevent artificial inflation, which were prepared and imaged under the same settings as the double-labelled samples (i.e. TASK3_GFP and CMR). The single labelled samples were still scanned for in two channels (i.e. for the GFP only sample, the CMR channel will also be imaged). Examination of the pixel distribution of the GFP-only scatter plot allowed the setting of the horizontal crosshair just above any background signal and the value was noted. This was repeated in the red channels (i.e. for CMR, MitoTracker and CytoPainter) in order to set the vertical crosshair. The co-ordinates collected from the controls were then applied to all the double-labelled samples collected on that day. By setting these crosshairs, any colocalised pixels are the direct result of significant intensity levels of both labels and not due to any slight changes in sample preparation and image collection. It is important to note that the double-labelled experiments were carried out first to remove potential bias of the user. Following extraction of data from the raw images, simple image editing was carried out using Adobe Photo Shop.

2.3.11 Statistical Analyses for Confocal Microscopy

Whilst superposition of fluorescent images is the most common method for evaluating co-localisation, the results of such experiments are often ambiguous and so the Pearson's correlation coefficient (PCC) was used as the statistic for quantifying colocalization in this study. The PCC formula is defined as:

$$PCC = \frac{\Sigma_i (R_i - \bar{R}) \times (G_i - \bar{G})}{\sqrt{\Sigma_i (R_i - \bar{R})^2 \times \Sigma_i (G_i - \bar{G})^2}}$$

Where R_i and G_i represent individual pixel intensity values of red and green channels respectively, whilst $\bar{R}$ and $\bar{G}$ refer to the mean intensities of red and green fluorescence across the entire image. The correlation 'R' value is measured from -1 to +1, with +1 representing perfect colocalization and -1 is perfectly uncorrelated. A value of 0 is considered random or an absence of relationship. All data was analysed using GraphPad Prism 7 software (GraphPad Software Inc., CA, USA). Values are expressed as mean ± standard error of the mean (SEM). For imaging data, n = number of cells. A minimum of 3 cells were imaged per slide, over a minimum of 3 passages. An unpaired student's t-test was used to determine statistical significance between two different groups of transfected cells. When comparing three or more groups, a one-way ANOVA test followed by an adhoc Tukey's multiple comparison was carried out. Statistical significance was defined as a probability value of $P < 0.05$.

2.3.12 In-Cell/On-cell Assay

TsA201 cells were cultured at a density of 2 x 10^4 cells/well per 100 µl of DMEM media in poly-D-lysine coated 96-well TC plates and incubated for 24 hours (37°C/95% air/5% CO_2). At 80% confluency, cells were transfected as per the Turbofect protocol described previously with concentrations scaled to suit the 96-well arrangement. The cells were transfected with 200 ng of DNA and 0.4 µl of Turbofect prior to incubation overnight (37°C/95% air/5% CO_2). To establish membrane surface expression, this assay utilised a HA-tag positioned on the extracellular M1P1 loop, between alanine 50 (A50) and arginine 51 (R51), which is accessible to antibody detection. The following morning, the media on the plate was removed and the cells were immediately fixed with 40 µl PFA (2%) for 20 minutes at room temperature (RT) with no rocking. After fixation, the cells were washed once with 1X PBS. For membrane expression, cells were washed with 40 µl of 0.1% Tween-20 (TBST) solution. For whole cell expression, the cells were permeabilised with 40 µl of a 0.1% Triton-X-100 solution. Each wash lasted a duration of 5 minutes on a rocking table and this was repeated a total of 5 times. After the last wash, the plate was blocked in a 2.5% non-fat milk blocking solution in 1X TBST at RT for approximately 1 hour to prevent non-specific binding. The blocking buffer was removed, and the cells loaded with 40 µl of the primary monoclonal (mouse) anti-HA antibody which was prepared at a concentration of 1 µg/mL in the 2.5% milk blocking buffer and incubated for 2 hours at RT on a rocking table. Next, the antibody solution was removed, and the wells were washed 5 times for 5 minutes in TBST and patted dry between each wash. The final wash step was then removed and the cells covered in a dual detection of 2.5% milk blocking solution containing secondary goat anti-mouse IRDye (800CW green, Licor, NE, USA) at a concentration of 1:1000 and the DRAQ5 DNA dye which is provided as a 5mM solution and diluted to 1:10’000. After incubating for 1 hour at RT in the dark, the cells underwent a final wash cycle of 5 times of 5 minutes in TBST and the plate was patted until completely dry prior to imaging. The plate was imaged on a LI-COR plate reader at 700nm and 800nm (169 nm resolution, 7 sensitivity and 3.2 mm offset). Integrated intensity values were recorded and analysed. Statistical analyses carried out as described in 2.3.11.

2.4 Results

2.4.1 The G236R mutation displays reduced current at the membrane compared to WT

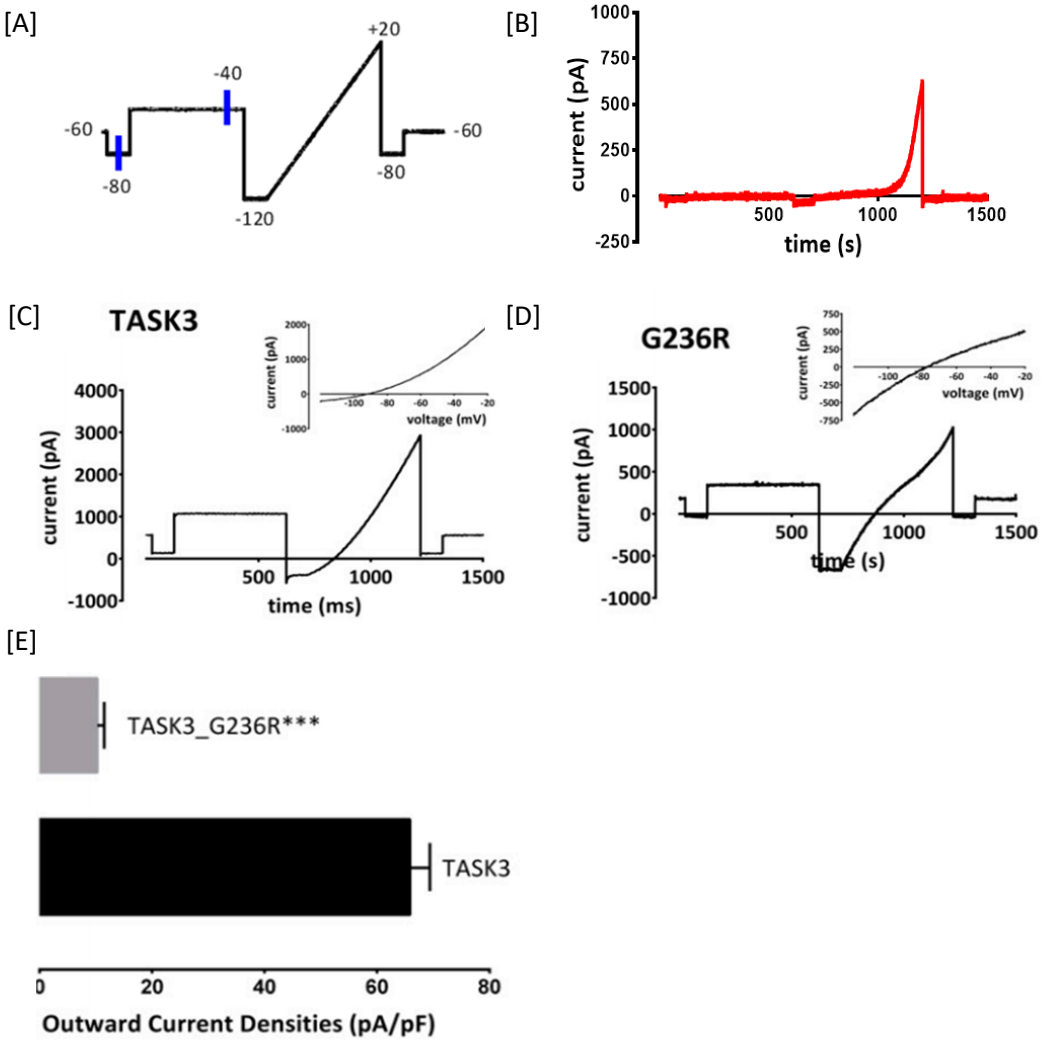

Figure 18 Electrophysiological profile of TASK3 and TASK3_G236R

[*A] Example "step-ramp" voltage protocol (cells are hyperpolarised from a holding voltage of -60 mV to -80 mV for 100 miliseconds (ms) then stepped to -40 mV for 500 ms. For the ramp, cells were then stepped to -120 mV for 100 ms, followed by a 500 ms voltage ramp to +20 mV and a step back to -80 mV for another 100 ms, before being returned to the holding voltage of -60 mV. This protocol was composed of sweeps that lasted 1.5 seconds (including sampling at the holding voltage) and was repeated once every 5 seconds). [B] Trace of an untransfected tsA201 cell displaying no endogenous currents between the -80mV to -40mV voltage range to be analysed. [C] Exemplar trace for WT TASK3 channel in control conditions using the step-ramp voltage protocol. Inset: current-voltage graph in control conditions. [D] Trace for TASK3_G236R channel in control conditions exposed to the step-ramp voltage protocol. Inset: current-voltage graph in control conditions. [E] A histogram comparing current densities (pA/pF) of WT-TASK3 and TASK3_G236R measured as the difference current between -80 and -40 mV in normal (2.5 mM potassium) external. Error bars represent (SEM) and * statistical significance (P<0.001). Work carried out by Dr E L Veale (see: (Veale, et al., 2014)).*

In a paper released by our lab group (Veale *et al.*, 2014) it was discovered that following transient transfection in tsA201 cells, whole-cell patch-clamp electrophysiological techniques recorded a significantly reduced outward current density ($P<0.001$) in cells expressing the TASK3_G236R mutation compared to the WT. Figure 18E displays the 85% reduction in outward current density from 66 ± 3 p*A*/p*F* (n = 56 cells) for WT_TASK3 to 10 ± 1 p*A*/p*F* (n = 17 cells) in TASK3_G236R when measured between –40 mV and –80 mV (see *Materials and Methods: Whole-cell Patch-Clamp Electrophysiology (Veale et al., 2014)).* It was also noted that unlike WT_TASK3 which is typically outwardly rectifying (Figure 18C), the TASK3_G236R mutant displays altered function and becomes predominantly inwardly rectifying when measured at currents between –40 mV and –80 mV (Figure 18D).

Following this observation, this study aimed to investigate whether this difference in current density arises from altered expression of the mutant channel at the membrane due to trafficking issues, using confocal microscopy. For confocal microscopy, the channels were Ct tagged with green fluorescent protein (GFP) (ex/em: 488/507nm). It is necessary to note that similar electrophysiological findings observed in Figure 18, were obtained from the WT and G236R GFP-labelled constructs. The plasma cell membrane was viewed with the application of a plasma membrane-specific stain: CellMask™ Deep Red (ex/em: 649/666 nm) and nuclei were stained blue (ex/em: 352/461 nm). To initially assess the degree of colocalization, the red and green channels may be scanned separately and overlapped giving in a yellow appearance in the event of colocalization. To quantify this, the 'Pearson's Correlation Coefficient' (PCC) statistical analysis was employed on a drawn ROI to quantify the degree of overlap, where 'N' represents number of cells (minimum of 9 cells, from 3 plates made from 3 different cultures). For each set of experiments an example of the single-labelled control samples are included.

In Figure 19, image sets [Ai-iii] and [Bi-iii] display examples of the single-label control samples of CMR and GFP respectively, employed throughout the plasma membrane localisation experiments. [Ci-iii] confirms that GFP alone does not localise at the membrane by lack of yellow signal in [Ciii], confirming that any colocalising effect observed in the channel studies are a direct result of the channel and not the GFP it is attached to. Images [Di-Diii] confirm that in the presence of CMR stain [Ei-iii] expression of the WT-TASK3_GFP is unaffected. As expected, WT-TASK3_GFP is seen to be expressed at the membrane with both red and green fluorescence exhibiting similar profiles in [Ei] and [Eii] respectively. The overlap image in [Eiii] confirms the colocalization of the channel by presence of the yellow signal. Despite this, a degree of intracellular localisation of WT-TASK3_GFP is still made apparent as observed by the remaining green presence in [Eiii] alongside the yellow signal.

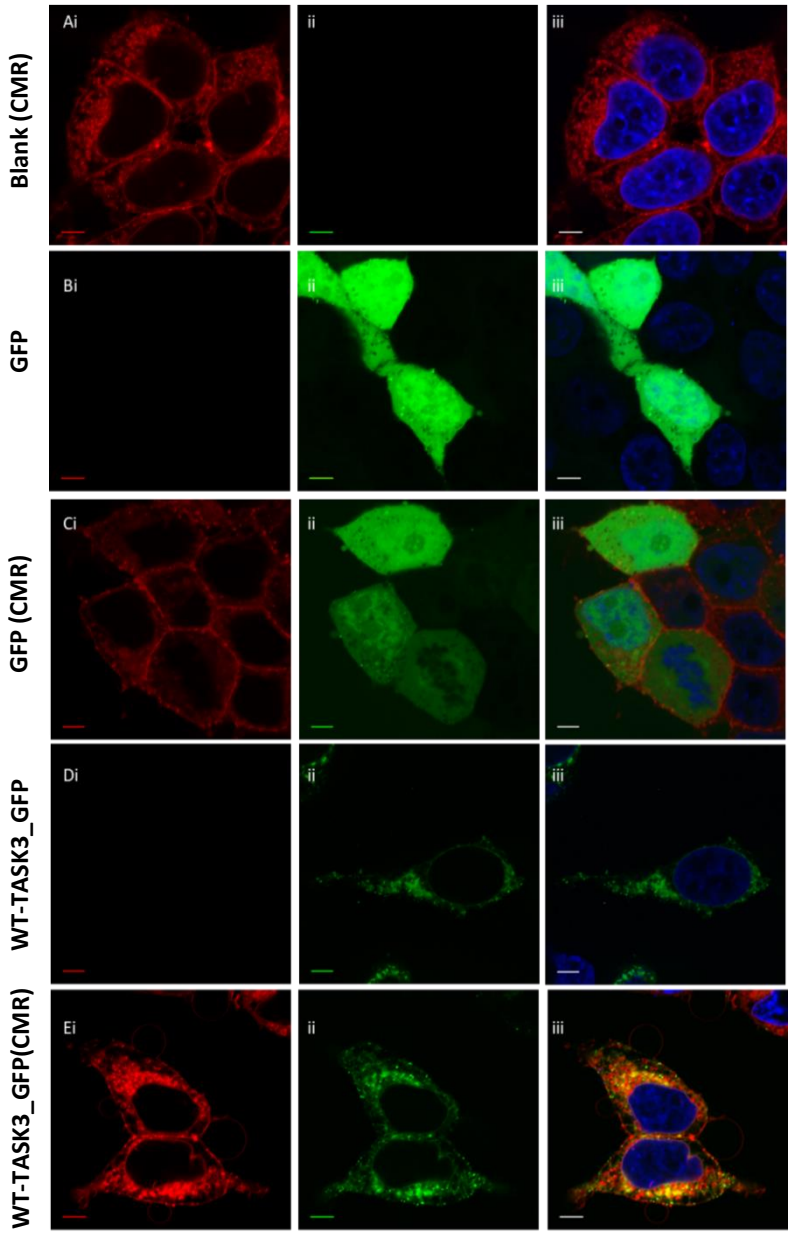

Figure 19 A photomicrograph displaying the plasma membrane localisation of GFP-labelled TASK3.

Confocal images [Ai-iii] represent a single-stain control image consisting of membrane stained, untransfected tsA201 cells. [Ai] Displays the red stained plasma membrane; [Aii] no green autofluorescence and [Aiii] is the overlap of [Ai] and [Aii]. Nuclei are blue. [Bi-iii] represent a single-stain control image consisting of tsA201 cells transfected with GFP only. [Bi] No red autofluorescence; [Bii] green GFP fluorescence and [Biii] an overlap of [Bi] and [Bii]. [Ci-iii] Confocal images of tsA201 cells with the red plasma membrane stain [Ci] and transiently transfected with GFP [Cii]; the overlay of [Ci] and [Cii] in [Ciii] show that GFP does not localise with the plasma membrane and that any yellow colocalization signal observed in the following images is a function of the associated channel trafficking and not GFP. Images [Di-iii] Show the unstained [Di] WT-TASK3_GFP [Dii] and the overlap [Diii]. Set [Ei-iii] Display the localisation of WT-TASK3_GFP at the plasma membrane. [Ei] the red stained plasma membrane; [Eii] transiently transfected WT-TASK3_GFP and [Eiii] an overlay of images [Ei] and [Eii] resulting in a yellow signal indicative of channel colocalisation at the plasma membrane. All scale bars are calibrated to 5 µM.

For the TASK3_G236R_GFP however, Figure 20 [Biii], by qualitative assessment it would appear that there is less expression of the mutant at the plasma membrane due to the reduced degree of yellow signal in the overlap image. Indeed, WT-TASK3_GFP PCC (± SEM) displayed a moderately strong, positive linear correlation of 0.55 ± 0.02 (n= 25 cells, 95% confidence interval (CI): 0.50 – 0.60). Conversely, TASK3_G236R displayed a reduction in linearity despite the apparent yellow signal in Fig[Diii], obtaining a PCC value of 0.40 ± 0.04 (n = 25 cells, 95% CI: 0.32 – 0.48), denoting a weaker correlation (Figure 21[A]). Using an unpaired student's t-test, a significant reduction (P<0.001) of TASK3_G236R expression at the cell plasma membrane was confirmed, when compared to WT.

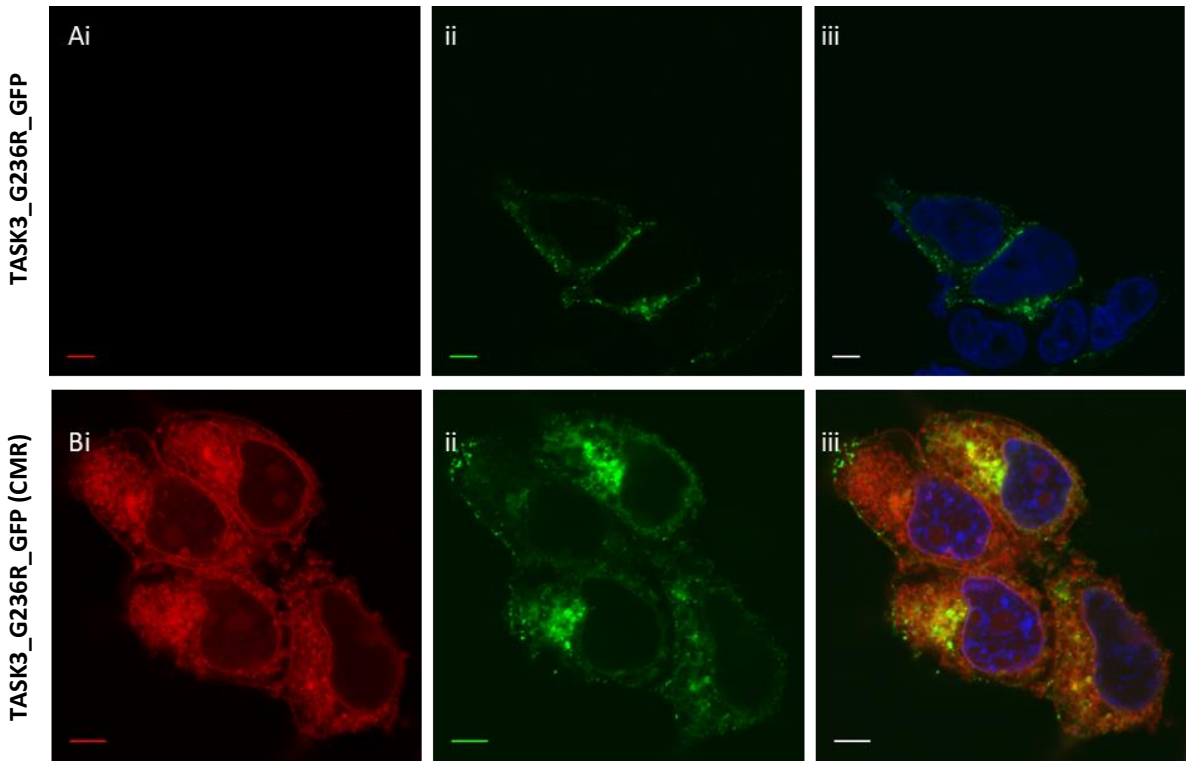

Figure 20 A photomicrograph investigating differences in plasma membrane localisation of GFP labelled TASK3 and the TASK3_G236R mutation

Confocal images [Ai-iii] represent unstained tsA201 cells transfected with TASK3_G236R_GFP. Nuclei are blue. [Bi-iii] Display the localisation of TASK3_G236R_GFP at the plasma membrane. [Bi] the red stained plasma membrane; [Bii] transiently transfected TASK3_G236R_GFP and [Biii] an overlay of images [Bi] and [Bii] resulting in a yellow signal indicative of channel colocalisation at the plasma membrane. On initial qualitative assessment there appears to be less yellow overlap signal compared to [Biii]. All scale bars are calibrated to 5 µM.

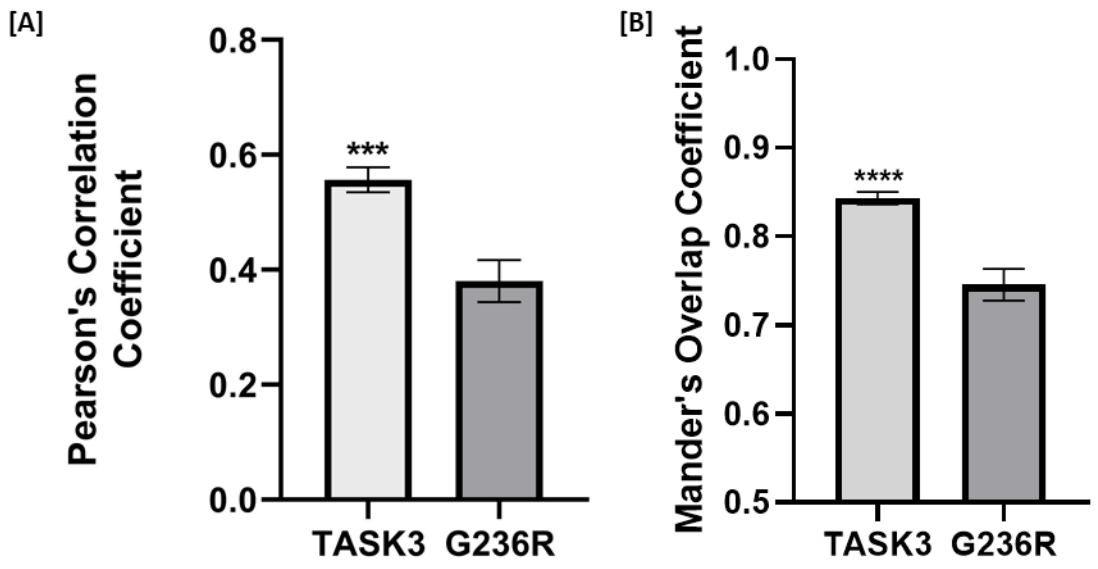

Figure 21 Comparison of two methods used to quantify the degree of colocalization between fluorophores. [A] Pearson's Correlation Coefficient (PCC) and [B] Mander's Overlap Coefficient (MOC)

Mathematically very similar, MOC uses absolute pixel intensities whilst PCC uses the deviation from the mean. PCC measures colocalization from -1 to +1 in which +1 represents perfect colocalization, -1 is perfect inverse (or no) colocalization and 0 is random localisation. MOC is measured 0 to +1. Error bars represent standard error of the mean (SEM).

Presently, there are many different methods available to quantify biological colocalisation experiments. Whilst PCC analysis appears to be the most used in literature, the Mander's overlap coefficients (MOC) were also considered for the quantification of colocalization since they are both mathematically similar and may be defined as:

$$\frac{\Sigma(Ch1_i)(Ch2_i)}{\sqrt{(\Sigma)(Ch1_i)^2(Ch2_i)^2)}}$$

This equation was developed to dismiss the possibility of obtaining a negative value in colocalization studies which were considered hard to interpret. MOC uses the absolute pixel intensity (*i*) and is measured on a scale of 0 to 1, in which 1 represents perfect colocalization. Whilst both analytical methods are mathematically very similar and are independent of changes in gain, the MOC is sensitive to changes in offset and may be falsely inflated, whilst PCC remains unchanged in the event of signal shifts. The effect of this may potentially be seen in the increased significance observed following MOC analysis in Figure 21 [B]. The term 'colocalisation' is often used loosely however, it may be defined either as co-occurrence or correlation based upon the chosen method of analysis. Correlation focuses upon the extent of the relationship between signal (i.e. a pixel with high intensity level in channel 1 is

likely to have a high intensity in channel 2; whilst low correlation could be a pixel that has high intensity in channel 1 but is likely to have low intensity in channel 2); co-occurrence considers the fraction of overlap from a spatial point of view. Whilst it may seem relevant to apply the MOC to these experiments, the MOC complicatedly combines both correlation and co-occurrence which typically overlooks low intensity interactions by favouring those that are high intensity and ignores 'blank' pixels, whilst PCC only measures correlation. For these reasons amongst others, PCC is considered more relevant, accurate, and reliable. For the purpose of this study, PCC was measured for individual cells on which a ROI was drawn to prevent the under representation of correlation.

2.4.2 Non-functional TASK3 variants: Y205C and Y205Δ traffic to the plasma membrane as efficiently as WT-TASK3_GFP

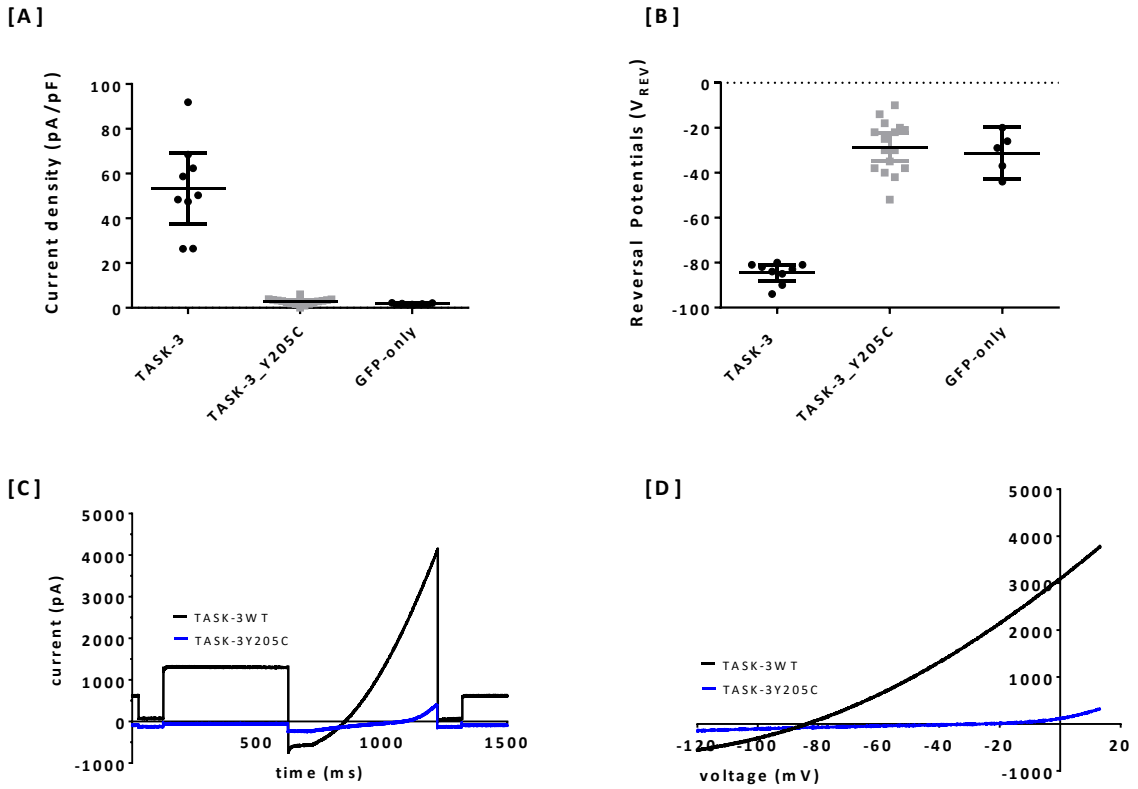

Figure 22 Comparison of current density (pA/pF) of WT TASK3 and Y205C variant.

Panel [A] a comparison of current density between WT TASK3, TASK3 mutant channel Y205C and GFP-only. The average whole-cell current of the Y205C mutation measured as a difference between that seen at -40 mV and -80 mV. Panel [B] is a comparison of zero current potentials (V_{REV}) observed at 0 mV in a physiological extracellular solution containing 2.5 mM $[K^+]_o$ for WT TASK3, Y205C and GFP-only transfected cells. Panel [C] is averaged raw data traces (n=6) from human wildtype (WT) TASK3 channel (black line) and TASK3_Y205C (n=16) (blue line), when transiently expressed in tsA201 cells, using a step-ramp voltage protocol. Panel [D] is averaged currents (as for [C]) recorded through TASK3_WT and TASK3_Y205C mutant channels evoked by ramp change in voltage from -120 mV to +20 mV. This work was carried out by Dr E L Veale.

Whole-cell patch-clamp electrophysiology confirmed that the mutation of tyrosine to cysteine at position 205 in TASK3 resulted in a channel that is non-functional when 500 ng of the appropriate cDNA was transiently expressed in tsA201, as it appears to have a similar current density to that of GFP-only transfected cells (Figure 22[A]) when measured as the difference in current between –40 mV and –80 mV. For TASK3_Y205C the average whole cell current, in physiological extracellular solution of 2.5 mM $[K^+]_o$, was reported at 2.7 p*A*/p*F* (n = 16 cells, 95% CI: 1.9 – 3.5). This is significantly reduced (P <0.05) when compared to WT-TASK3 which has an average whole cell current of 53 p*A*/p*F* (n = 9 cells, 95% CI: 38 – 69) when measured under the same conditions. As mentioned above, the average whole cell current of TASK3_Y205C was not significantly different (P>0.05) when compared to GFP-only transfected controls: 1.9 p*A*/p*F* (n = 5, 95% CI: 1.5 – 2.3). Figure 22 [B] Compared the zero current potentials (V_{Rev}) of WT-TASK3, Y205C and GFP, recorded at 0 mV in the same extracellular solution as mentioned above. An unpaired student's t-test confirmed a significant difference (P<0.05) between the WT-TASK3 (-84 mV (n = 6, 95% CI: -88 to -81)) and Y205C (-29 mV (n = 16, 95% CI: -35 to -22)), but no significant difference (P>0.05) when Y205C V_{Rev} was compared to the GFP-only cells (-31 mV (n = 5, 95% CI: -43 to -20)). Figure 22 [C] displays the averaged raw data traces (n=6) for the human WT-TASK3 channel (black line) and TASK3_Y205C (n=16) (blue line), when transiently expressed in tsA201 cells and measured using a standard step-ramp protocol, see Figure 18 legend. Figure 22 [D] displays the averaged currents (as for [C]) recorded through TASK3_WT and TASK3_Y205C mutant channels evoked by ramp change in voltage from -120 mV to +20 mV. This work was carried out by Dr E L Veale (unpublished data).

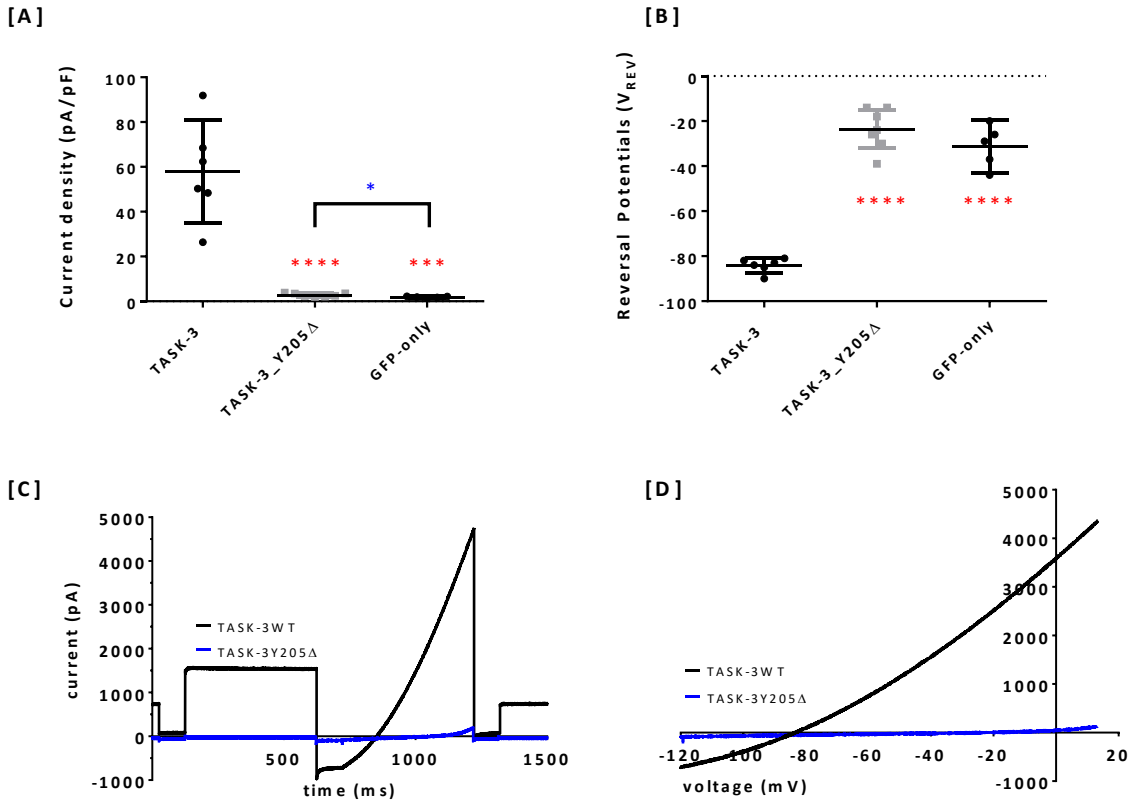

Figure 23 Comparison of current density (pA/pF) of WT TASK3 and Y205Δ variant

Panel [A] a comparison of current density between WT TASK3 and TASK3 mutant channel Y205Δ. The average whole-cell current measured as a difference between that seen at -40 mV and -80 mV. Panel [B] is a comparison of zero current potentials (V_{REV}) observed at 0 mV in a physiological extracellular solution containing 2.5 mM $[K^+]_o$ for WT TASK3, Y205Δ and GFP-only transfected cells. Panel [C] is averaged raw data traces (n=6) from human WT TASK3 channel (black line) and TASK3_Y205Δ (n=7) (blue line), when transiently expressed in tsA201 cells, using a "step-ramp" voltage protocol. Panel [D] is averaged (n=7) currents recorded through WT TASK3 and TASK3_Y205Δ mutant channels evoked by ramp change in voltage from -120 mV to +20 mV. This work was carried out by Dr E L Veale.

A simple substitution of cytosine to adenine at position 614 in human TASK3 was found to introduce a stop codon at position 205, producing a 'non-functional' channel when transiently transfected in tsA201, likely due to substantial truncation within PD2 and only a single pore domain remaining. Figure 23 compares the electrophysiological profiles of WTTASK3 and the Y205Δ truncated mutant. [A] Shows a comparison of current density between WT TASK3 and TASK3 mutant channel Y205Δ. The average whole-cell current measured, in cells transfected with 500 ng of cDNA, as a difference between that seen at -40 mV and -80 mV. For Y205Δ, the recorded current was 2.8 p*A*/p*F* (n=7, 95% CI = 2.0 to 3.5), using a physiological extracellular solution of 2.5 mM $[K^+]_o$. This observed current was significantly different from WT TASK3 whole-cell current (58 p*A*/p*F* (n=6, 95% CI = 35 to 81)). Unlike Y205C (Figure

22[A]) in which no difference is observed between the mutant channel and GFP expressing cells, analysis of data suggests that Y205Δ is significantly different from GFP-only transfected cells (1.9 pA pF^{-1} (n=5, 95% CI = 1.5 to 2.3)), implying the presence of a very small functional current. Comparing zero current potentials (V_{REV}) observed at 0 mV in a physiological extracellular solution containing 2.5 mM $[K^+]_o$ for WT TASK3, Y205Δ and GFP-only transfected cells found a significant difference ($P<0.05$) of zero current potentials between the WT [-84 mV (n=6), 95% CI = -88 to -81) and Y205Δ [-24 mV (n=7), 95% CI = -32 to -15) mutant channels Figure 23 [B]. No significant differences ($P>0.05$) were observed when comparing Y205Δ with GFP-only cells [-31 mV (n=5), 95% CI = -43 to -20). Both the averaged raw data traces (n=6) for the human WT-TASK3 channel (black line) and TASK3_Y205C (n=7) (blue line) (using the standard step-ramp protocol) in Figure 23 and [D], displaying the averaged currents (as for [C]) recorded through TASK3_WT and TASK3_Y205C mutant channels evoked by ramp change in voltage from -120 mV to +20 mV show the channel to be largely unfunctional. This work was carried out by Dr E L Veale (unpublished data).

Considering the reduced expression of TASK3_G236R at the plasma membrane, it seemed necessary to determine the expression patterns of two novel TASK3 variants (Y205C and Y205Δ) that have been shown to elicit the *KCNK9*-Imprinting syndrome phenotype and display abolished function.

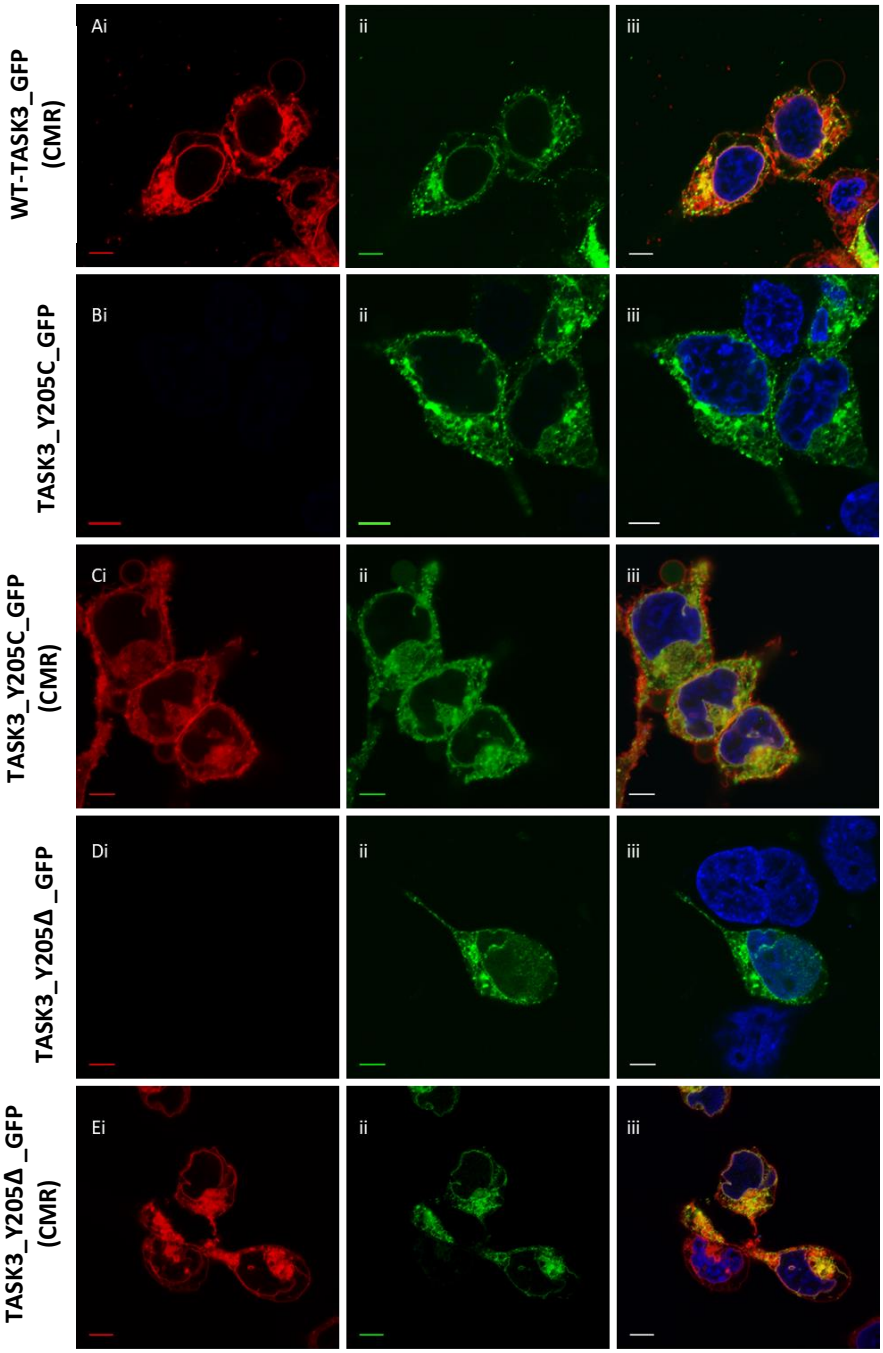

Figure 24 A photomicrograph investigating differences in plasma membrane localisation of GFP labelled WT-TASK3_GFP and the TASK3_Y205C/Y205Δ_GFP mutations

Confocal images [Ai-iii] Display the localisation of WT-TASK3_GFP at the plasma membrane. [Ai] the red stained plasma membrane; [Aii] transiently transfected WT-TASK3_GFP [Aii] and [Aiii] an overlay of images [Ai] and [Aii] resulting in a yellow signal indicative of channel colocalisation at the plasma membrane. Nuclei are stained blue. [Bi-iii] are unstained tsA201 cells transiently transfected with the TASK3_Y205C_GFP mutation. [Ci-iii] displays the location of the TASK3_Y205C_GFP channel relative to the plasma membrane. [Di-iii] are unstained tsA201 cells transiently transfected with the TASK3_Y205Δ_GFP mutation. [Ei-iii] displays the location of the TASK3_Y205Δ_GFP channel relative to the plasma membrane. On initial qualitative assessment there appears to be similar yellow overlap signal in both mutants compared to [Aiii]. All scale bars are calibrated to 5 µM.

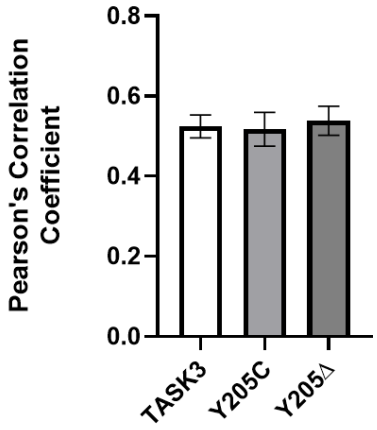

Figure 25 Quantification of colocalization experiment investigating differences in plasma membrane localisation of GFP labelled WT-TASK3_GFP and the TASK3_Y205C/Y205Δ_GFP mutations

A histogram displaying the PCC quantification of colocalization of the above images. Error bars represent standard error of the mean (SEM). No statistical differences (P>0.05) were observed in the expression of WT-TASK3_GFP and the Y205C and Y205Δ mutations following an ordinary one-way ANOVA analysis with adhoc Tukey's multiple comparison. Both TASK3_Y205C_GFP and TASK3_Y205Δ_GFP displayed PCC values comparative of WT_TASK3_GFP with an average PCC (± SEM) of 0.52 ± 0.04 (n = 15 cells, 95% CI: 0.43 – 0.61) and 0.54 ± 0.04 (n = 15 cells, 95% CI: 0.46 – 0.62) respectively when compared to WT_TASK3_GFP PCC: 0.52 ± 0.03 (n = 16 cells, 95% CI: 0.46 – 0.59).

Cellular localisation of WT_TASK3_GFP in tsA201 cells was examined using confocal microscopy. GFP fluorescence was observed at the plasma membrane of cells transiently transfected with either WT_TASK3_GFP or TASK3_Y205C_GFP or TASK3_Y205Δ_GFP. Control images were collected as displayed in Figure 19 and the experimental procedure repeated as described above. From qualitative inspection of Figure 24, it is difficult to identify any clear differences in the overlap images. Instead, an ordinary one-way ANOVA significance test with an adhoc Tukey's multiple comparison comparing each variant against the PCC of the WT_TASK3_GFP was carried out Figure 25. Both TASK3_Y205C_GFP and TASK3_Y205Δ_GFP displayed PCC values comparative of WT-TASK3_GFP with an average PCC (± SEM) of 0.52 ± 0.04 (n = 15 cells, 95% CI: 0.43 – 0.61) and 0.54 ± 0.04 (n = 15 cells, 95% CI: 0.46 – 0.62) respectively when compared to WT_TASK3_GFP PCC: 0.52 ± 0.03 (n = 16 cells, 95% CI: 0.46 – 0.59). As such, there was interestingly no significant difference (P>0.05) observed between WT_TASK3_GFP expression and either of the Y205 variants at the membrane. This suggests that the trafficking and translation of the Y205 variants is at least as efficient as the WT_TASK3 under these experimental conditions.

2.4.3 Functional consequences of TASK3 variants are likely independent of mitochondrial expression

Unlike wakefulness, a conscious state in which an individual can interact with the environment, the term 'arousal' describes the extent of vigilance and alertness whilst in the wakeful state (Pfaff and Kieffer, 2008). As such, vigilance can be regulated depending on environmental stimuli or stressors to initiate responses such as courtship, fight-or-flight and other behaviours vital to behavioural adaptation and survival (de Lecea *et al.*, 2012). Altered arousal states are observed in *KCNK9* imprinting syndrome (Graham *et al.*, 2016) and TASK3 expression in mitochondria has been implicated in human pathologies (Kosztka *et al.*, 2011). Reduced expression of the TASK3_G236R_GFP mutant at the membrane in combination with the altered arousal states naturally directed this study to the mitochondria.

Confocal microscopy was used to determine any differences between WT-TASK3_GFP channels colocalised with the mitochondria and TASK3_ G236R/Y205C/Y205Δ_GFP. As before, the channels were Ct tagged with GFP (ex/em: 649/666 nm). The mitochondria were visible following staining with MitoTracker™ Red CMXRos (ThermoFisher Scientific) (ex/em: 579/599 nm). Nuclei were stained blue (ex/em: 352/461 nm). Statistical significance of colocalization was determined using the PCC values. In Figure 26, image sets [Ai-iii] and [Bi-iii] display examples of the single-label control samples of MitoTracker and GFP respectively, employed throughout the mitochondrial localisation experiments. [Ci-iii] confirms that GFP alone does not localise at the mitochondria by lack of yellow signal in [Ciii], confirming that any colocalising effect in observed in the channel studies are a direct result of the channel and not the GFP it is attached to. The overlap image in [Diii] confirms the colocalization of the WT-TASK3_GFP with the mitochondria by presence of the yellow signal. Initial qualitative analysis of the G236R and Y205 variants in Figure 27 [B – D] would suggest reduced mitochondrial expression of the mutants as there is no obvious overlap when compared to the WT in [Aiii]. Surprisingly, significant difference ($P<0.05$) in expression was only observed between WT-TASK3_GFP and TASK3_ Y205Δ_GFP with mean PCC values of 0.32 ± 0.07 (n = 9, 95% CI: 0.15 – 0.49) and 0.58 ± 0.07 (n = 9, 95% CI: 0.42 – 0.74) respectively, Figure 28. This suggests that truncation of the channel may expose trafficking motifs which are usually buried within the protein, thus allowing forward traffic in absence of the trafficking motifs present within the Ct. TASK3_G236R_GFP and TASK3_Y205C displayed similarly low values to the WT-TASK3_GFP of 0.28 ± 0.07 (n =9, 95% CI: 0.12 – 0.43) and 0.28 ± 0.05 (n = 9, 95% CI: 0.16 – 0.41) respectively. In comparison to the plasma membrane, correlation (and therefore degree of expression) appears to be considerably lower in the mitochondria.

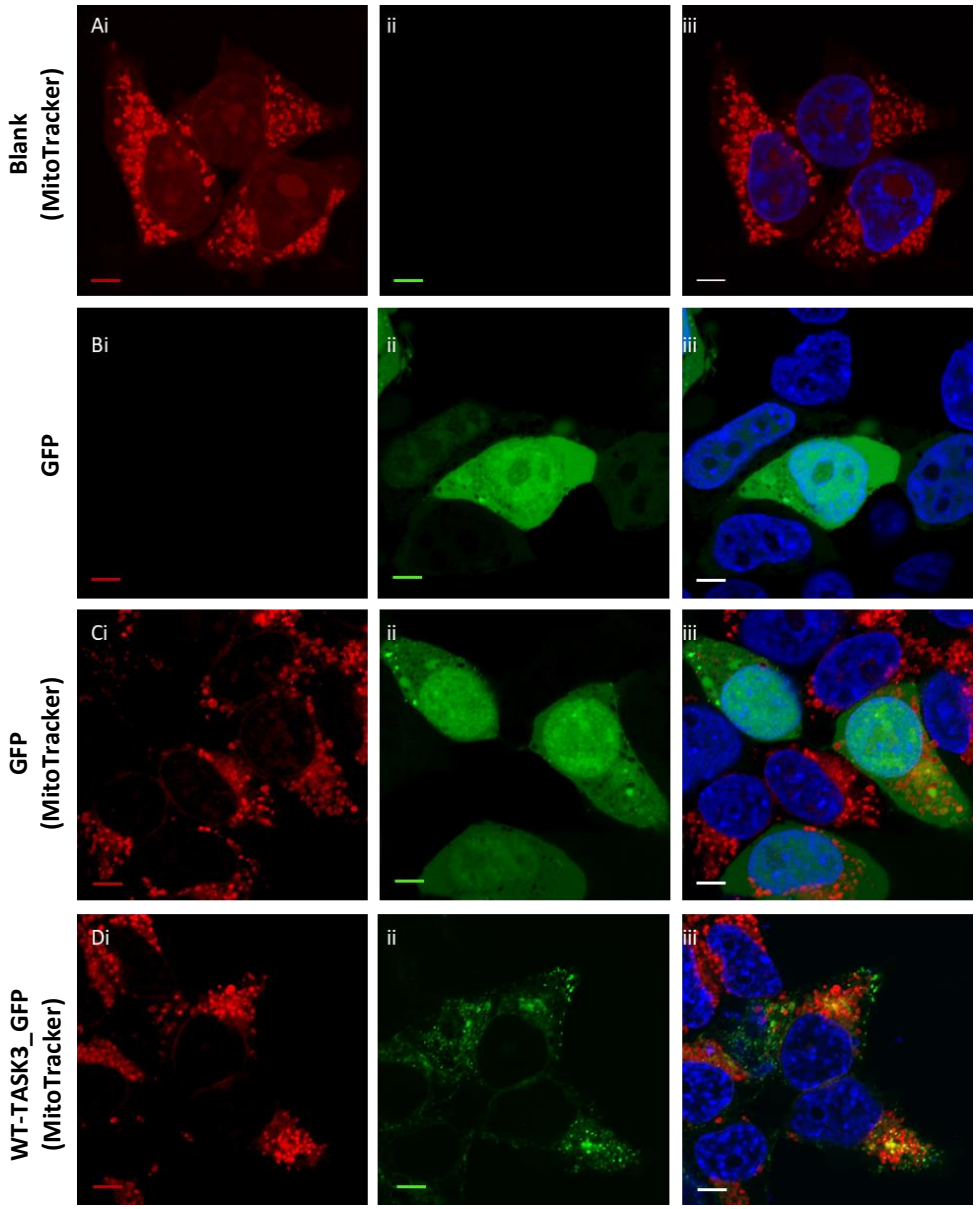

Figure 26 A photomicrograph displaying mitochondrial localisation of GFP labelled TASK3 and controls

Confocal images [Ai-iii] represent a single-stain control image consisting of mitochondrial stained, untransfected tsA201 cells. [Ai] Displays the red stained mitochondria; [Aii] no green autofluorescence and [Aiii] is the overlap of [Ai] and [Aii]. Nuclei are blue. [Bi-iii] represent a single-stain control image consisting of tsA201 cells transfected with GFP only. [Bi] No red autofluorescence; [Bii] green GFP fluorescence and [Biii] an overlap of [Bi] and [Bii]. [Ci-iii] Confocal images of tsA201 cells with the red mitochondria stain [Ci] and transiently transfected with GFP [Cii]; the overlay of [Ci] and [Cii] in [Ciii] show that GFP does not localise with the mitochondria and that any yellow colocalization signal observed in the following images is a function of the associated channel trafficking and not GFP. Images [Di-iii] Display the colocalisation of WT-TASK3_GFP with the mitochondria. [Di] the red stained mitochondria; [Dii] transiently transfected WT-TASK3_GFP and [Diii] an overlay of images [Di] and [Dii] resulting in a yellow signal indicative of channel colocalization with mitochondria. All scale bars are calibrated to 5 µM.

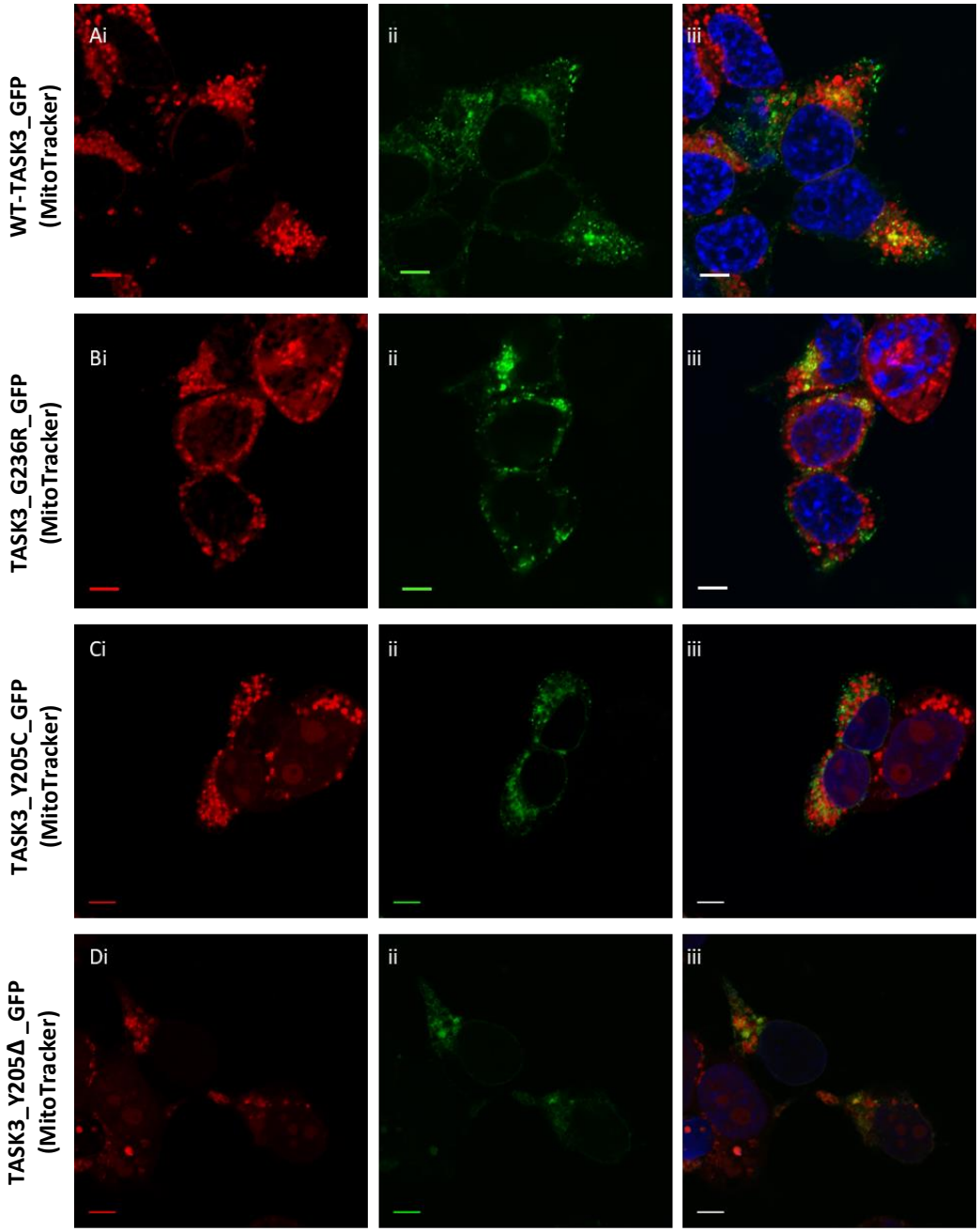

Figure 27 A photomicrograph investigating mitochondrial localisation of GFP labelled TASK3, G236R and the novel Y205 variants

Confocal images [Ai-iii] represent tsA201 cells transfected with WT_TASK3_GFP. [Ai] displays the red stained mitochondria; [Aii] the same cells displaying the green GFP-fused TASK3 and [Aiii] is the overlap of [Ai] and [Aii] displaying the location of the channel relative to the mitochondria as a yellow signal. Nuclei are blue. As [A], images [Bi-iii] display the location of the TASK3_G236R_GFP channel relative to the mitochondria; [Ci-iii] TASK3_Y205C_GFP and [Di-iii] TASK3 Y205Δ_GFP. All scale bars are calibrated to 5 µM.

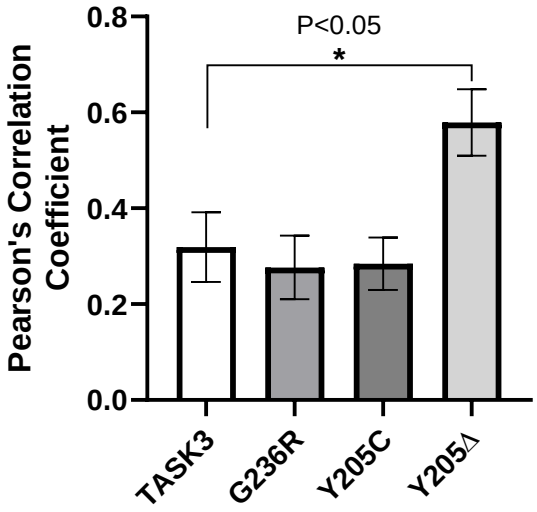

Figure 28 Quantification of colocalization experiment investigating differences in mitochondrial localisation of GFP labelled WT-TASK3_GFP and the TASK3_G236RY205C/Y205Δ_GFP mutations

A histogram displaying the PCC quantification of colocalization of the images in Figure 27. Error bars represent standard error of the mean (SEM). Statistical differences (P<0.05) was observed between the expression of WT-TASK3_GFP and the Y205Δ mutation within the mitochondria following an ordinary one-way ANOVA analysis with adhoc Tukey's multiple comparison.

2.4.4 Increased ER retention of the TASK3_Y205 mutations but not TASK3_G236R

With the TASK3_G236R mutation displaying reduced expression at the plasma membrane, it would be logical to consider increased expression in the ER as the channel is potentially sorted into alternate degradative pathways. Equally, despite the Y205 expression reflecting that of the WT, it is possible that these mutants are recycled as efficiently as they are delivered to the plasma membrane.

As before, channels were Nt tagged with GFP (ex/em: 649/666 nm). The endoplasmic reticulum was made visible following staining with the Cytopainer red staining kit by Abcam (ex/em: 580/677 nm). Nuclei were stained blue (ex/em: 352/461 nm). Statistical significance of colocalization was determined using the PCC values. In Figure 29, image sets [Ai-iii] and [Bi-iii] display examples of the single-label control samples of the red CytoPainter and GFP respectively, employed throughout the ER localisation experiments. [Ci-iii] confirms that GFP alone does not localise at the ER by lack of yellow signal in [Ciii], confirming that any colocalising effect in observed in the channel studies are a direct result of the channel and not the GFP it is attached to. The overlap image in [Diii] confirms the colocalization of the WT-TASK3_GFP with the ER by presence of the yellow signal as expected. For WT-TASK3_GFP and its variants (G236R, Y205C and Y205Δ) expression within the ER is apparent by the yellow overlay signal observed in the image below (Figure 30 [A] – [D]). Ordinary one-way Anova with adhoc Tukey's multiple comparison test confirmed that there was no significant difference ($P>0.05$) observed in the ER between WT-TASK3_GFP and TASK3_G236R_GFP with PCC of 0.51 ± 0.06 (n = 10, 95% CI: 0.36 – 0.65) and PCC of 0.56 ± 0.06 (n = 12, 95% CI: 0.43 – 0.69) respectively. There was a significant ($P<0.01$) increase of the Y205 variants localising at the ER however, when compared to the WT channel, potentially suggestive of increased retrograde recycling or over expression Figure 31. Compared to WT-TASK3_GFP, TASK3_Y205C_GFP and TASK3_Y205Δ_GFP both obtained significantly increased ($P<0.01$) PCC values of 0.75 ± 0.03 (n = 12, 95% CI: 0.69 – 0.80) and 0.76 ± 0.03 (n = 8, 95% CI: 0.70 – 0.83) respectively.

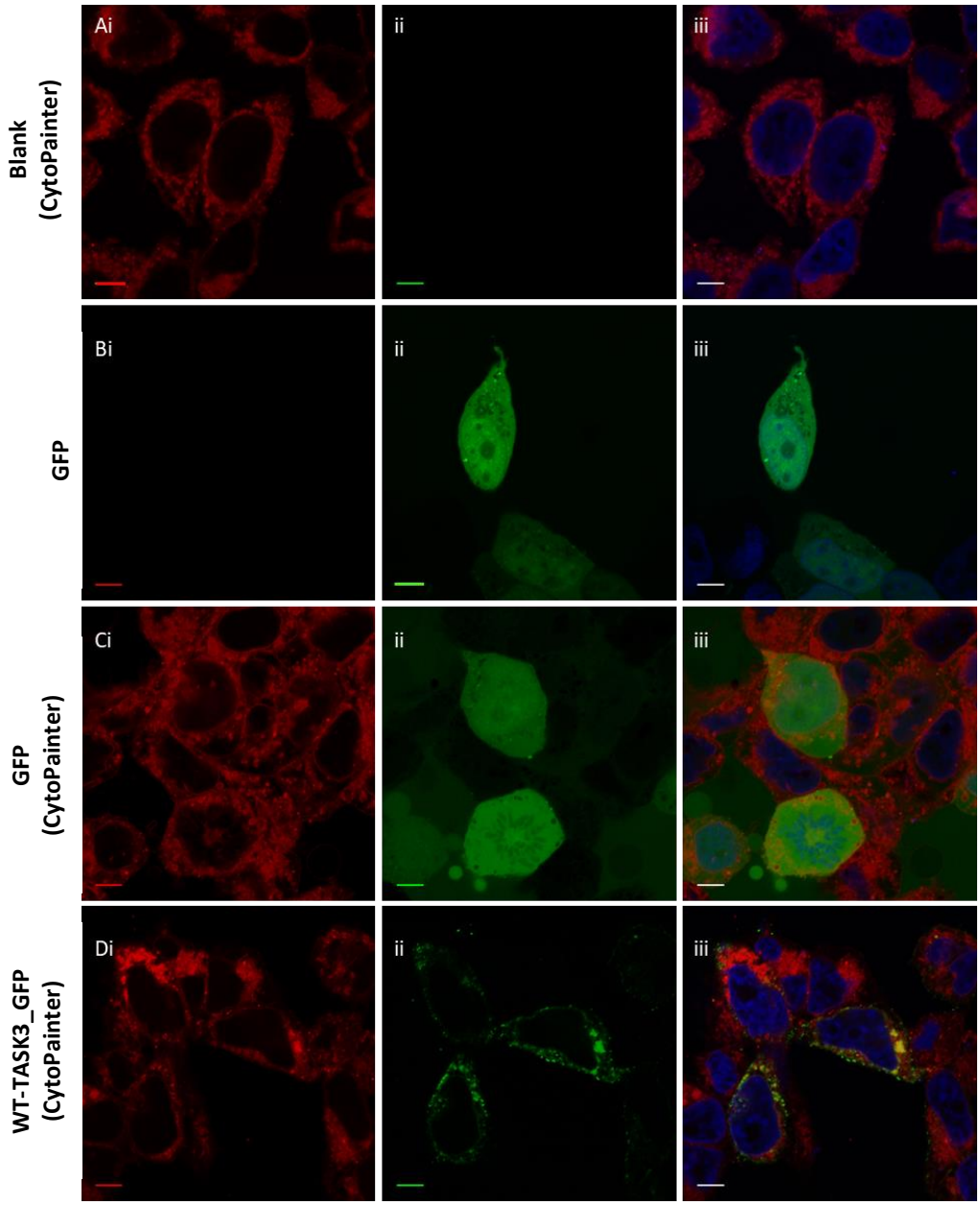

Figure 29 A photomicrograph displaying localisation of GFP labelled TASK3 with the endoplasmic reticulum (ER)

Confocal images [Ai-iii] represent a single-stain control image consisting of stained ER, untransfected tsA201 cells. [Ai] Displays the ER; [Aii] no green autofluorescence and [Aiii] is the overlap of [Ai] and [Aii]. Nuclei are blue. [Bi-iii] represent a single-stain control image consisting of tsA201 cells transfected with GFP only. [Bi] No red autofluorescence; [Bii] green GFP fluorescence and [Biii] an overlap of [Bi] and [Bii]. [Ci-iii] Confocal images of tsA201 cells with the red ER stain [Ci] and transiently transfected with GFP [Cii]; the overlay of [Ci] and [Cii] in [Ciii] show that GFP does not localise with the ER and that any yellow colocalization signal observed in the following images is a function of the associated channel trafficking and not GFP. Images [Di-iii] Display the colocalization of WT-TASK3_GFP with the ER. [Di] the red stained ER; [Dii] transiently transfected WT-TASK3_GFP and [Diii] an overlay of images [Di] and [Dii] resulting in a yellow signal indicative of channel colocalization with the ER. All scale bars are calibrated to 5 µM.

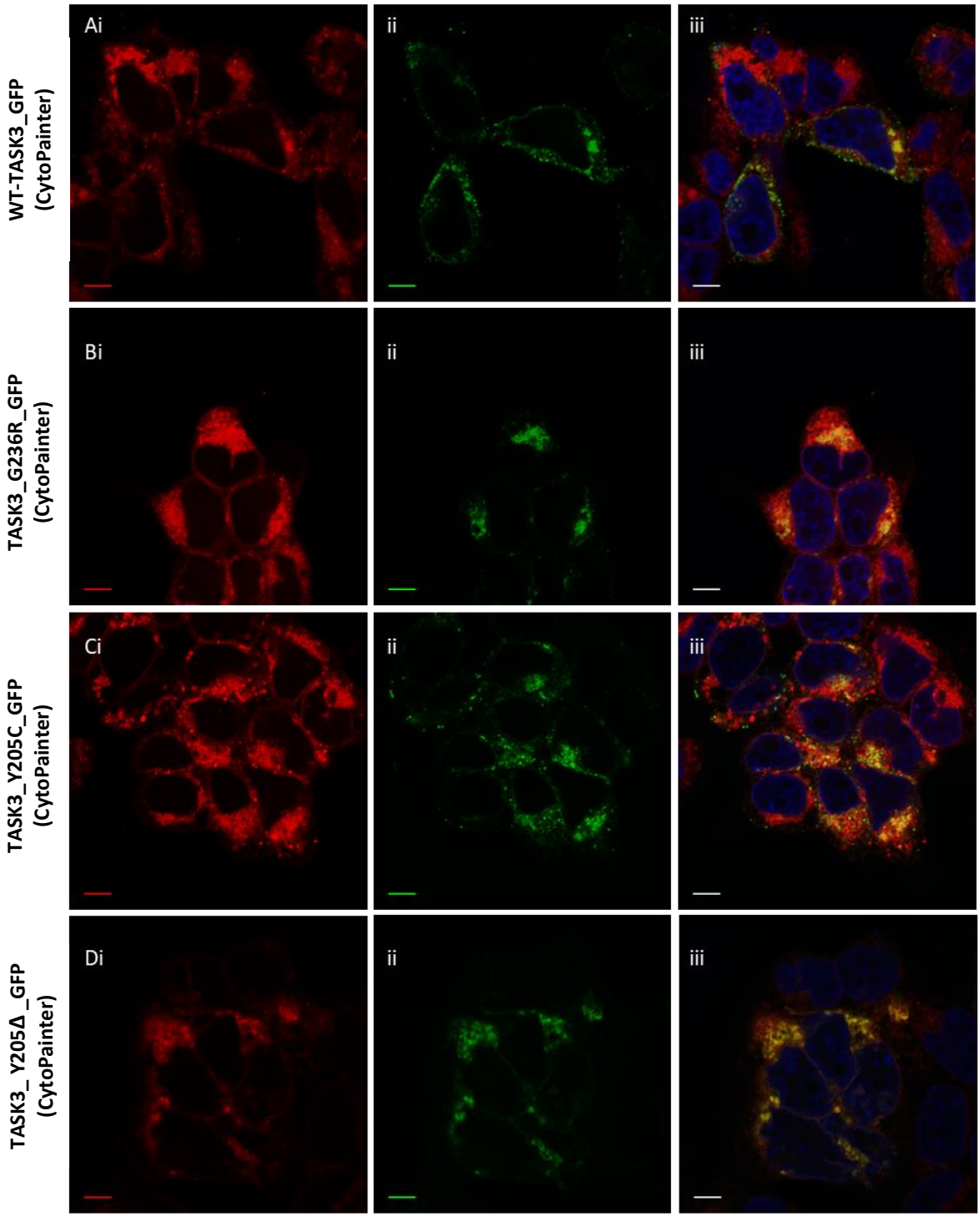

Figure 30 A photomicrograph investigating localisation of GFP labelled TASK3, G236R and the novel Y205 variants with the ER

Confocal images [Ai-iii] represent tsA201 cells transfected with WT_TASK3_GFP. [Ai] displays the red stained ER; [Aii] the same cells displaying the green GFP-fused TASK3 and [Aiii] is the overlap of [Ai] and [Aii] displaying the location of the channel relative to the ER as a yellow signal. Nuclei are blue. As [A], images [Bi-iii] display the location of the TASK3_G236R channel relative to the ER; [Ci-iii] TASK3_Y205C and [Di-iii] TASK3 Y205Δ. All scale bars are calibrated to 5 µM.

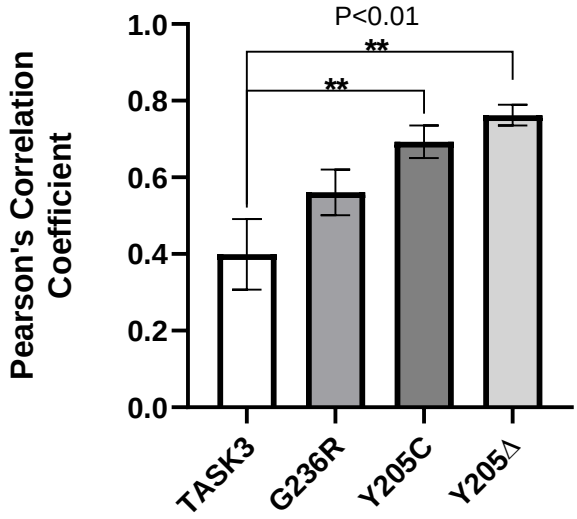

Figure 31 Quantification of colocalization experiment investigating differences in ER localisation of GFP labelled WT-TASK3_GFP and the TASK3_G236R/Y205C/Y205Δ_GFP mutations

A histogram displaying the PCC quantification of colocalization of the images in Figure 30. Error bars represent standard error of the mean (SEM). Statistical differences (P<0.05) was observed in the expression of WT-TASK3_GFP and the Y205 mutations but not G236R within the ER following an ordinary one-way ANOVA analysis with adhoc Tukey's multiple comparison.

2.4.5 TASK1 variants (G106R and L214R) associated with PAH are expressed at the plasma membrane as efficiently as the WT channel

In another paper published by my group (Cunningham *et al.*, 2019) the TASK1 mutations (G106R and L214R) underwent electrophysiological profiling using the whole-cell patch-clamp technique. Measuring the current density between -40 mV and -80 mV in cells transfected with 500 ng of WT-TASK1 or G106R/L214R found TASK1 gave average whole cell currents of 7.8 pA pF–1 (n = 44 cells, 95% CI = 5.8–9.7) (Figure 32 [A]) in physiological extracellular solution of 2.5 mM [K+]o. Ramp changes in holding potential from –120 to +20 mV demonstrate that the current is outwardly rectifying [B and C], with a mean zero current potential of –78 mV (n = 44, 95% CI = –74 to –82) close to the equilibrium potential for potassium ions under these recording conditions. By contrast, mutation of a small uncharged glycine residue at position 106 to a large positively charged arginine residue, resulted in a poorly functioning channel with significantly reduced current, when expressed alone as a homozygous mutant channel in tsA201 cells. The average whole-cell current measured at –40 mV was 1.8 pA pF–1 (n = 38 cells, 95% CI = 1.3–2.4). Similarly, mutation of a small hydrophobic leucine residue at position 214 to a large positively charged arginine residue was found to have substantially reduced current when expressed alone as a homozygous mutant channel in tsA201 cells (Figure 32 [A – B]). The average whole-cell current measured at –40 mV was 1.6 pA pF–1 (n=27, 95% CI = 1.0–2.3). The outward currents recorded from TASK1_G106R and TASK1_L214R channels were statistically significantly reduced ($P<0.05$, one-way ANOVA followed by a Dunnett's multiple comparisons test) from WT TASK1 and not significantly different from untransfected cells. Untransfected tsA201 cells had an average whole-cell current measured at –40 mV of 1.5 pA pF–1 (n = 36 cells, 95% CI = 1.2–1.8) (Figure 32 [A–C]).

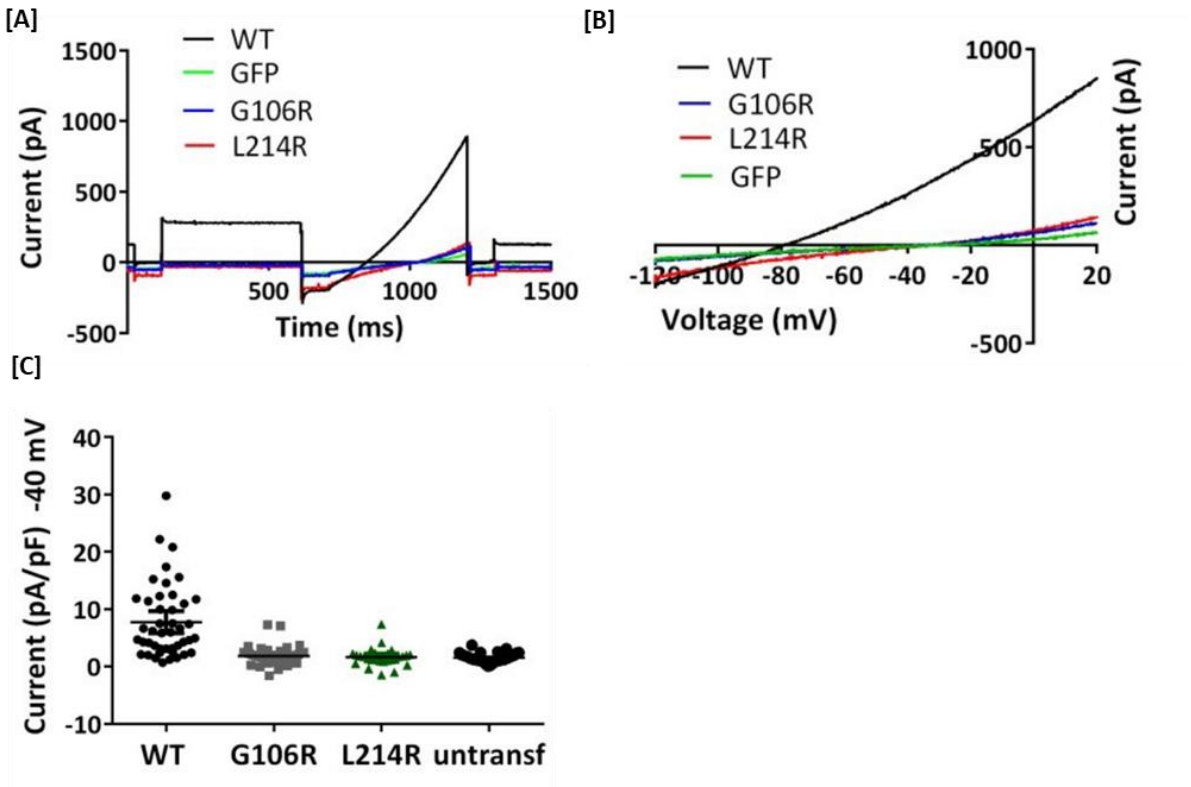

Figure 32 Electrophysiological profile of TASK1 and TASK1 mutants: TASK1_G106R and TASK1_L214R.

[A] shows raw data trace from exemplar human TASK1, TASK1_G106R, TASK1_L214R channel traces and GFP-alone using a step-ramp voltage protocol. [B] illustrates the current-voltage relationship for the WT and mutatnt channels evoked by ramp changes in voltage from -120 to -20 mV. [C] illustrates current density (pA/pF) measured at -40 mV from individual cells transiently expressing WT-TASK1, TASK1_G106R, TASK1_L214R or untransfected cells. Error bars represent 95% CI. This work was carried out by Dr E L Veale.

Following the observation that the G106R and L214R mutations of TASK1 associated with PAH resulted in significantly reduced outward currents similar to that seen with TASK3_G236R, it was important to determine whether this reduction in current was due to reduced expression at the membrane or a consequence of the mutation affecting the structure function of the channel, so that they can no longer pass current. The localisation of WT-TASK1 and its pathogenic variants in relation to the plasma membrane was repeated as discussed in section 2.4.1. Single label controls were carried out as described in Figure 19. It is clear from Figure 33 [Aiii] that WT_TASK1_GFP is principally expressed at the plasma cell membrane from the extent of the yellow overlay observed, as with the variants G106R and L214R which exhibit a similar profile (Figure 33 [B] and [C] respectively). To quantify difference unobvious to the eye, assessment of the PCC values was carried out (Figure 33 [D]). A moderately strong PCC value of 0.65 ± 0.04 (n = 12 cells, 95% CI: 0.57 – 0.73) was obtained for WT_TASK1_GFP. Similarly, G106R and L214R displayed equally strong linearity, acquiring PCC values of 0.75 ± 0.03 (n = 12 cells, 95% CI: 0.69 – 0.81) and 0.72 ± 0.04 (n = 12 cells, 0.64 – 0.80) respectively. One-way ANOVA confirmed no significant differences were observed between WT_TASK1_GFP and G106R/L214R_GFP plasma membrane expression ($P > 0.05$). These data suggest that the trafficking and translation of the G106R and L214R mutations were equal to WT_TASK1 under these experimental conditions.

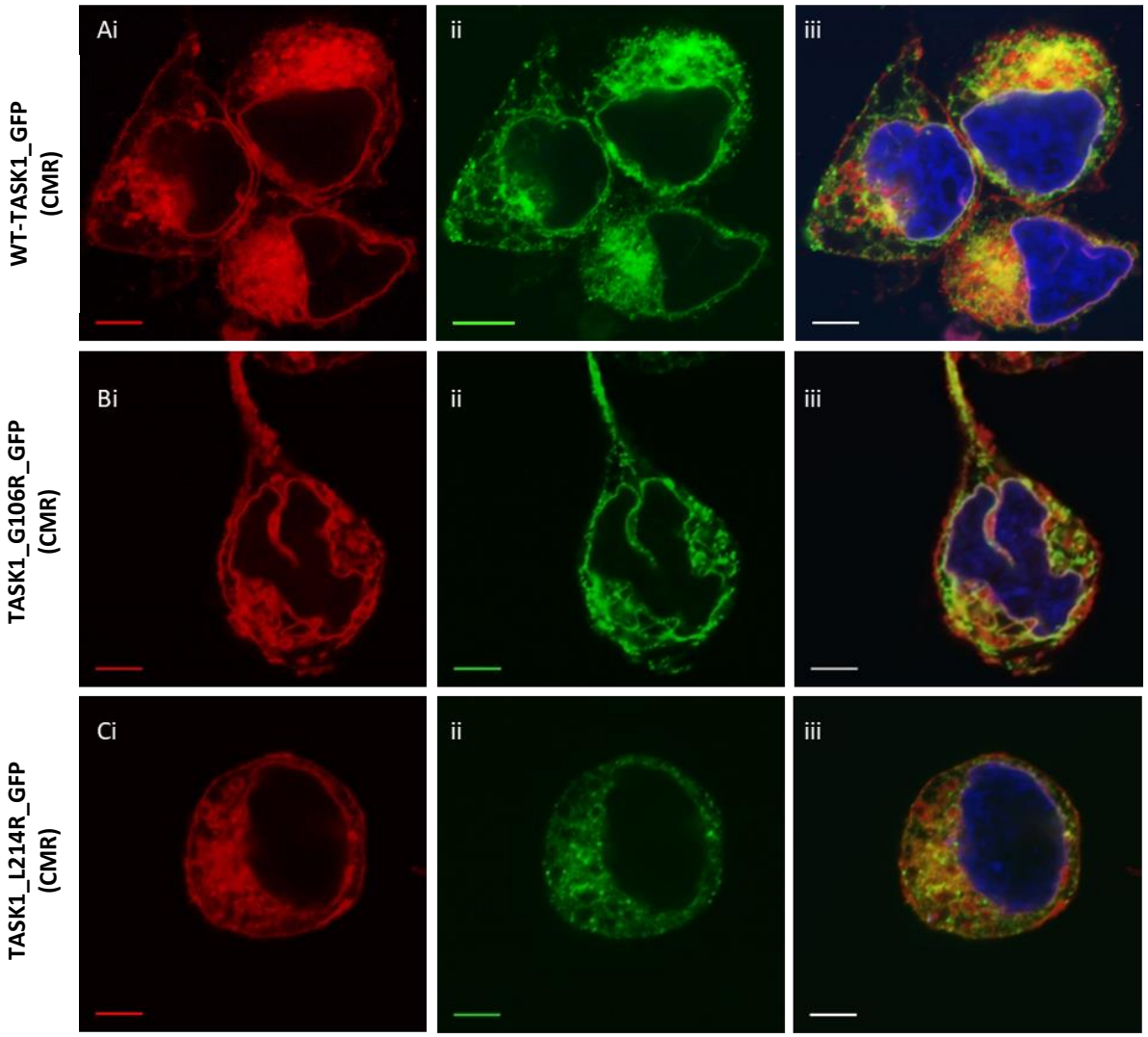

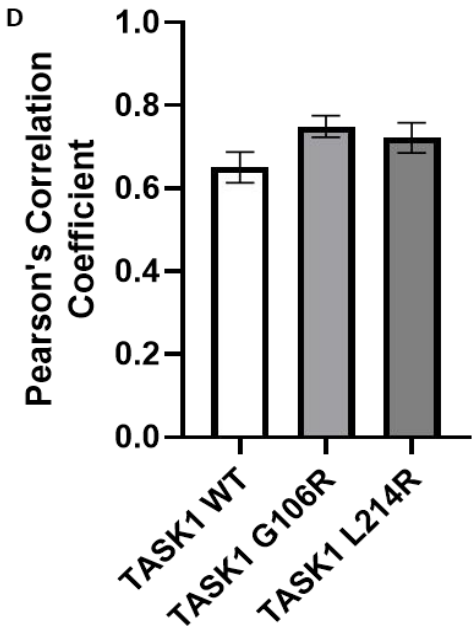

Figure 33 A photomicrograph investigating plasma membrane localisation of GFP labelled TASK1 and the novel G106R and L214R variants

Confocal images [Ai-iii] represent tsA201 cells transfected with WT_TASK1_GFP. [Ai] displays the red stained plasma membrane; [Aii] the same cells displaying the green GFP-fused WT_TASK1_GFP and [Aiii] is the overlap of [Ai] and [Aii] displaying the location of the channel relative to the plasma membrane as a yellow signal. Nuclei are blue. As [A], images [Bi-iii] display the location of the TASK1_G106R_GFP channel relative to the plasma membrane and [Ci-iii] TASK1_L214R_GFP. All scale bars are calibrated to 5 µM. D) A histogram displaying the PCC quantification of colocalization of the above images. Error bars represent standard error of the mean (SEM).

To support these results and investigate translation and trafficking further, an in-cell/on-cell assay was carried out to determine differences in the amount of channel expressed at the plasma membrane surface (on-cell) against proportion of channel expressed throughout the whole cell (in-cell) (Figure 34). Unlike previous confocal experiments, the channels were now tagged upon the externally located M1P1 loop with a human influenza hemagglutinin (HA) which is accessible to the primary mouse anti-HA antibody in order to determine proportion of channel on the membrane. To ascertain whole cell volume, cell membranes were permeabilised with Triton-X-100 allowing access of the anti-HA antibody to channels held within the cell. A goat anti-mouse antibody conjugated to a green dye that is detectable at 778 nm was applied alongside a DNA stain (DRAQ5) to confirm equal cell distribution (Figure 34). Excitation of DRAQ5 confirmed equal cell numbers across all samples (two-way ANOVA, $P < 0.05$) with values of 408 ± 50 ($n = 9$) for WT_TASK1, 341 ± 62 ($n = 9$) for TASK1_G106R and 328 ± 65 ($n = 9$) for TASK1_L214R. On cell assay confirmed no difference in expression on the plasma membrane surface between WT_TASK1, TASK1_G106R and TASK1_L214R: 487 ± 69, 443 ± 114 and 377 ± 27 respectively ($P > 0.05$, two-way ANOVA). This result is reflected in the whole cell expression with no significant differences in total expression between WT_TASK1, TASK1_G106R and TASK1_L214R: 1552 ± 313, 1892 ± 351 and 1219 ± 311 respectively ($P > 0.05$, two-way ANOVA). These observations are in-line with the confocal data collected. It may therefore be said, with a significant degree of certainty, that under such experimental conditions, TASK1_G106R and TASK1_L214R loss of function is not caused by trafficking and translational abnormalities.

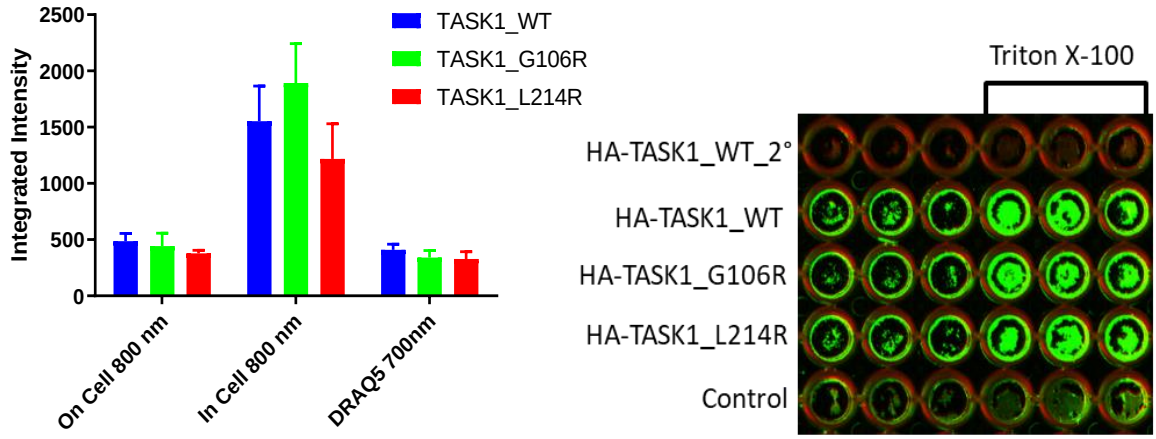

Figure 34 A) A histogram displaying integrated on-cell and whole-cell intensity values of HA-WT_TASK1, HA-TASK1_G106R and HA-TASK1_L214R.

On-cell 800 nm values represent the number of channels present on the plasma membrane cell surface. In-cell 800 nm values represent the total channel expression of the whole cell. DRAQ5 700nm is a measure of total cell numbers per sample. B) Image of the 96-well plate organisation with each row denoted on the left. Columns on the right are permeabilised with Triton X-100. HA-TASK1_WT_2° represents the secondary only antibody control. The control sample is treated with tansfection reagent but is not transfected – these values were subtraces from all samples as non-specific background signal.

2.4.6 Functional consequences of the TASK1 variants are not due to differences in mitochondrial expression

Genetic variants of TASK1 have been implicated in conditions with symptoms relating to possible dysfunction of the mitochondria. For this reason, confocal microscopy was used to determine whether the TASK1 channels colocalised with the mitochondria and if there was any difference the expression of pathogenic variants, as this has never been recorded in the literature before.

As before (section 2.4.3), the channels were Nt tagged with GFP (ex/em: 649/666 nm). The mitochondria were visible following staining with MitoTracker™ Red CMXRos (ThermoFisher Scientific) (ex/em: 579/599 nm). Nuclei were stained blue (ex/em: 352/461 nm). Statistical significance of colocalization was determined using the PCC values. For WT-TASK1_GFP and its variants (G106R and L214R) expression at the mitochondria is apparent by the yellow overlay signal observed in the image below (Figure 35 [A – C]). Single label controls were collected as described in section 2.4.3. No statistical differences ($P > 0.05$) between TASK1 and the mutations expression in the mitochondria was observed following an ordinary one-way Anova with adhoc Tukey's multiple comparison test (Figure 35 [D]). WT-TASK1 PCC of 0.32 ± 0.05 (n = 12, 95% CI: 0.20 – 0.44); TASK1_G106R_GFP PCC of 0.40 ± 0.03 (n = 12, 95% CI: 0.33 – 0.48) and TASK1_L214R_GFP PCC of 0.32 ± 0.04 (n = 12, 95% CI: 0.24 – 0.41). Whilst there is no statistical difference observed between WT-TASK1 and the variants G106R and L214R, these data display both the yellow overlay and PCC values reflective of that of TASK3 (Figure 35 [D]) for which there is confirmed mitochondrial expression recorded in the literature (Rusznák *et al.*, 2008, Stojanovski *et al.*, 2012, Yao *et al.*, 2017). For the first time, this data confirms the expression of TASK1 in the mitochondrial membrane.

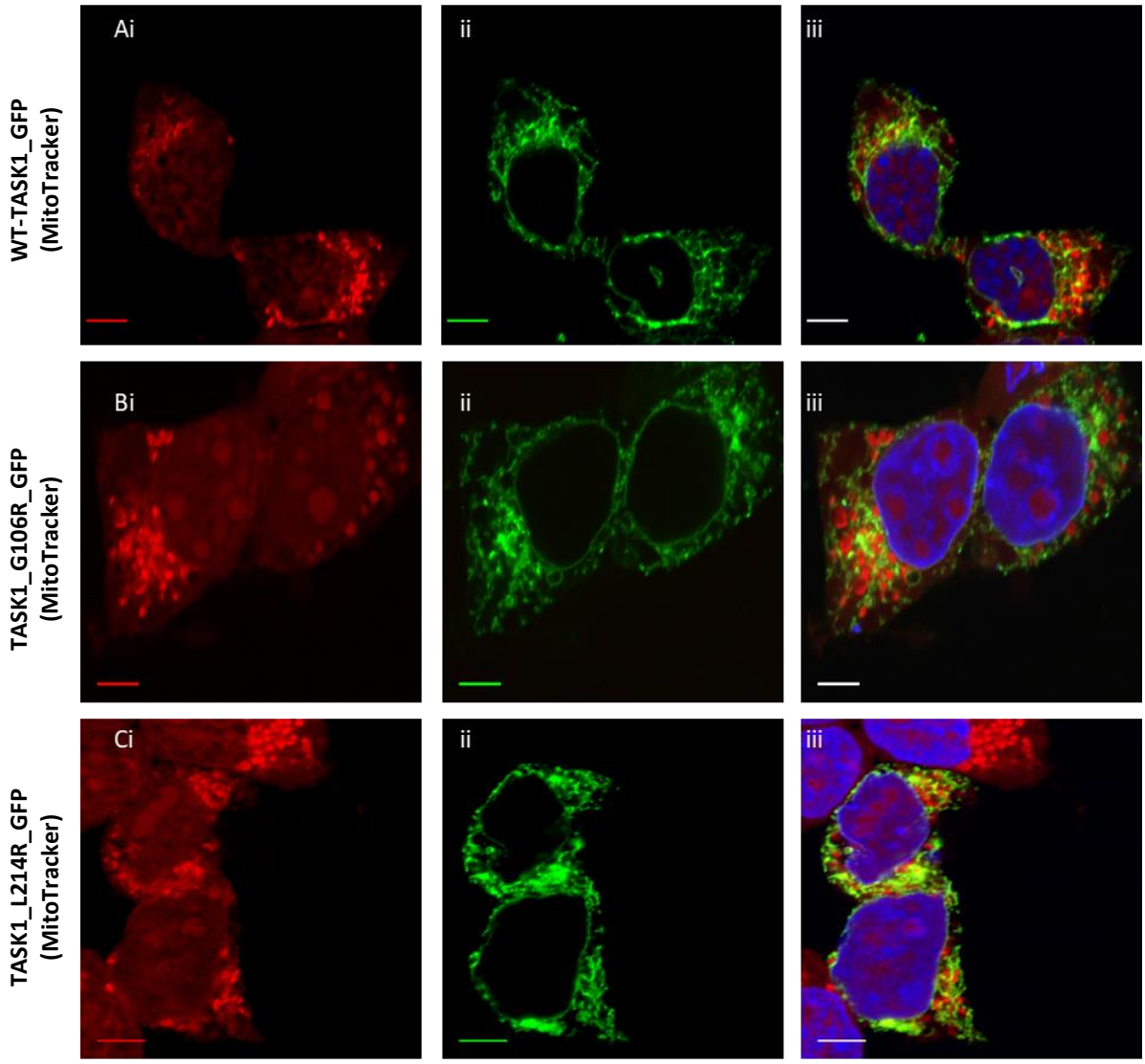

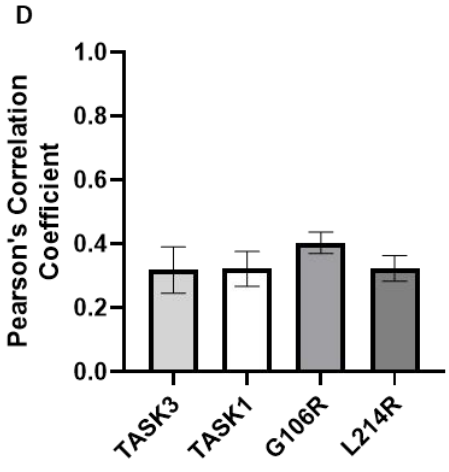

Figure 35 A photomicrograph investigating mitochondrial localisation of GFP labelled TASK1 and the novel G106R and L214R variants

Confocal images [Ai-iii] represent tsA201 cells transfected with WT_TASK1_GFP. [Ai] displays the red stained mitochondria; [Aii] the same cells displaying the green GFP-fused TASK1 and [Aiii] is the overlap of [Ai] and [Aii] displaying the location of the channel relative to the mitochondria as a yellow signal. Nuclei are blue. As [A], images [Bi-iii] display the location of the TASK1_G106R_GFP channel relative to the mitochondria and [Ci-iii] TASK1_L214R_GFP. All scale bars are calibrated to 5 µM. D) A histogram displaying the PCC quantification of colocalization of the above images, including WT-TASK for comparison. Error bars represent standard error of the mean (SEM).

2.5 Discussion

Heterozygous pathogenic variants of the maternal *KCNK9* allele (c.706G>C and 706G>A) have previously been identified to produce a p.Gly236Arg mutation in human TASK3 (Barel *et al.*, 2008, Graham *et al.*, 2016), resulting in loss-of-function channels with a reduced outward current density of approximately 80% in whole-cell patch-clamping investigations (Veale *et al.*, 2014). Advances in whole-exome sequencing helps the discovery of more novel variants, including Y205C and Y205Δ (Šedivá *et al.*, 2019) which are shown to exhibit similar phenotypes to *KCNK9* syndrome. However, a major rate-limiting step to future discovery is the fact that *KCNK9* syndrome has thus far only been reported amongst 6 families worldwide (Barel *et al.*, 2008, Graham *et al.*, 2016). Novel variants G106R and L214R have been shown equally to cause a reduction in TASK1 function, which is reportedly a major event in the pathogenesis of PAH. With recent hypotheses leaning towards reduced expression (Antigny *et al.*, 2016), this study was carried out to determine whether the loss-of-function feature displayed by these mutations is caused by the delivery of dysfunctional channels to the plasma membrane or, whether reduced current is the direct result of improper trafficking.

2.5.1 TASK3: Plasma Membrane Investigations

In this study, the significant reduction of the TASK3_G236R mutation expressed at the plasma membrane, when compared to WT in tsA201 cells, was reported for the first time in support of the reduced outward currents observed in electrophysiological investigations (Veale *et al.*, 2014). In combination with the reduced colocalised appearance of TASK3_G236R_GFP, the PCC of 0.40 was significantly lower than that of WT (0.55). Recently, (Veale *et al.*, 2014) disproved that the G236R mutation gave rise to a non-functional current as previously suggested (Barel *et al.*, 2008), instead providing evidence for a current which was heavily reduced in the outward direction as the channel became predominantly inwardly rectifying (Veale *et al.*, 2014). As such, it must be that at least a small proportion of TASK3_G236R channel are expressed at the membrane and this was apparent from the imaging data and the moderate linearity of the reduced PCC value, although a significant proportion of the GFP signal appeared to be situated within an alternate location within the cytoplasm. This suggests that the presence of TASK3_G236R does have a negative impact on channel trafficking. Despite reduction in plasma membrane expression, subcellular localisation of the G236R mutant is otherwise indistinguishable from the WT in both the ER and the mitochondria suggesting that the channel retains some trafficking function. Considering the location of this mutation within the fourth transmembrane domain, it is important to remember the critical role of signalling motifs within the Ct

in TASK trafficking (O'Kelly *et al.*, 2002, Rajan *et al.*, 2002, Kilisch *et al.*, 2015, Zuzarte *et al.*, 2009). The trafficking of TASK3 relies upon multiple signalling motifs which dictate the transport to and from the membrane. In particular, the high affinity binding of 14-3-3, which promotes forward trafficking, requires the [RRXpS/pTXCOOH] ('p' denotes phosphorylated residue) motif as the last 5 residues of the Ct (Coblitz *et al.*, 2005). Binding of 14-3-3 masks the retention motif [KRR] required by COPI for retention and retrograde transport (Zuzarte *et al.*, 2009). To date, only mutations affecting these signalling motifs have been implicated in trafficking dysfunctions of TASK3 rather than mutations occurring elsewhere within the transmembrane portions. In the case of the G236R mutation, it is more likely that the insertion of a large, positively charged, hydrophilic amino acid like arginine into an otherwise hydrophobic domain in place of a small, uncharged amino acid like glycine has an unfavourable effect on protein stability. Whether this induces a conformational change or is limited to the single transmembrane domain alone is unclear, but it suggests altered trafficking is unlikely to account for all the deleterious effects of the G236R mutation.

The Y205 truncation (Y205Δ) resulted in indistinguishable plasma membrane expression from the WT. This was an interesting finding since the mutation of cytosine to adenine at position 614 introduces a stop codon at position 205, producing a non-functional channel which is cut short part way through PD2. It was discussed above that mutations occurring at these positions were unlikely to impede protein trafficking due to their distance from the signalling motifs present in the Ct. However, in a construct containing the truncation of the last 5 residues of the TASK3 Ct (ΔC5) it was found that, although 14-3-3 binding was inhibited, reducing membrane expression and current density; the retention signal was simultaneously removed and so forward traffic was observed to continue through alternate mechanisms resulting in the same level of expression as WT (Zuzarte *et al.*, 2009). It is therefore clear that trafficking is not regulated exclusively by the motifs mentioned above. For example, in a paper by Schöneberg *et al.* (1995), it was demonstrated that the rodent GPCR, muscarinic acetylcholine receptor (M3), contained several independent units which may regulate localisation, structure and function (Schoneberg *et al.*, 1995).

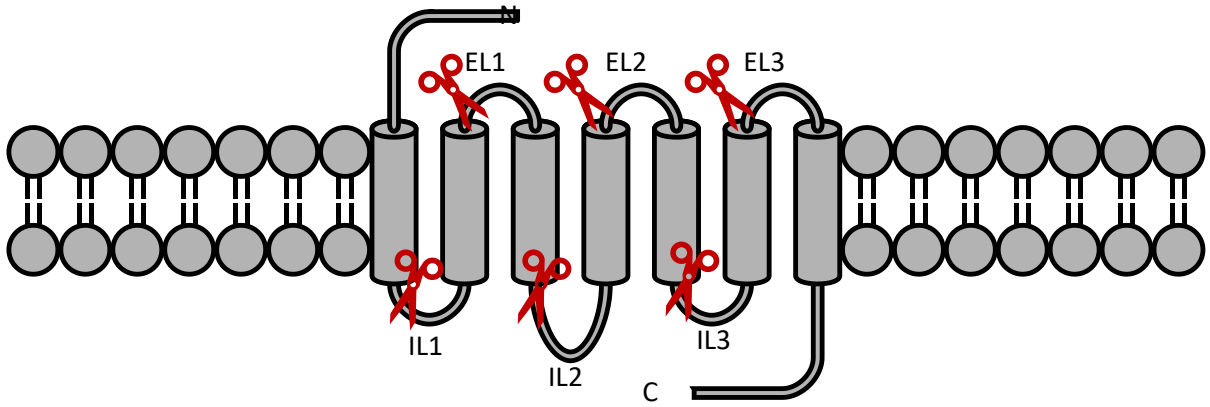

Figure 36 displays the splitting of the murine M3 GPCR at each of the intracellular loops (IL1-3) and extracellular loops (EL1-3), forming 6 truncated fragments of the full protein

This image was adapted from Schöneberg et al., 1995.

The M3 GPCR is composed of seven transmembrane helices that are linked by three IC and three EC loop linkers (Figure 36)**.** Splitting the GPCR into fragments containing either internal or external peptide loops and transiently expressing them in COS-7 cells individually, found that each of the Ct truncated peptides (minus the first IL1 fragment) were expressed within the plasma membrane to the same degree as the whole protein. The fragment containing the first transmembrane domain and the IL1 loop was only observed to localise elsewhere in the cell. Since the first fragment only contained the first 6 amino acids of the IL1 loop (total of 12 amino acids), it was suggested that the structural information required for membrane insertion and orientation of the protein were missing (Schoneberg *et al.*, 1995). These findings suggest that, in the case of the GPCR, the full-length protein is not required for trafficking and that the full protein is composed of multiple structural subunits (Schoneberg *et al.*, 1995). For TASK3, Y205C and Y205Δ, it is then possible that if the intracellular Nt remains intact, the proteins may continue to be trafficked to membrane regardless of these mutations.

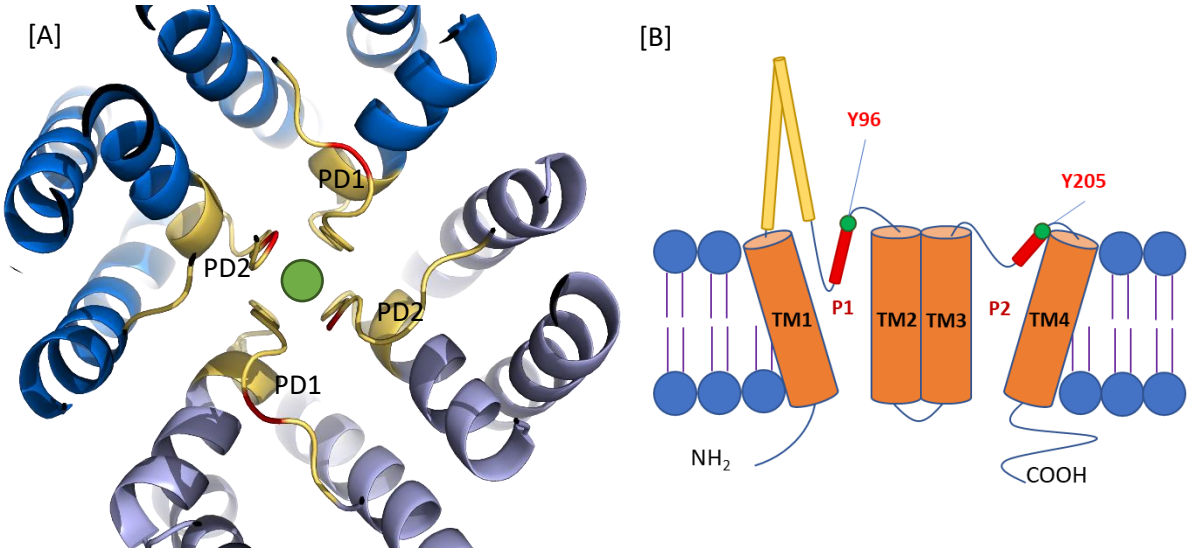

Figure 37 Displaying the ring-like formation of tyrosine residues around the mouth of the pore

[A] TASK3 homology crystal structure based upon TRAAK (PDB ID 3UM7, Brohawn et al. 2012*. The dark and light blue chains represent the two monomer units; pore domains are gold and the position of the relevant tyrosine residues are marked red. The green sphere represents a potassium ion in the pore. [B] A cartoon schematic showing the position of the tyrosine residues with regards to the rest of the channel components.*

The human synaptic $GABA_A$ receptor requires 4 tyrosine (Tyr, Y) residues positioned around an EC binding pocket, where they form an 'aromatic glove,' creating a favourable environment for the formation of cation-π interactions (Zhu *et al.*, 2018). In the full, dimerised conformationally-correct TASK3 channel, there are four Tyr that can be seen to form a ring around the extracellular mouth of the channel just above the SF, with each monomer donating both Y96 (PD1) and Y205 (PD2) residues (Figure 37) (Concha *et al.*, 2018). Tyrosine is amphipathic in nature and is comfortable being situated in contact with the EC aqueous environment. In the event of Y205 being mutated to the hydrophobic cysteine (Cys, C) residue, the channel displays an almost complete loss of function (Figure 22) and a pathogenic phenotype like *KCNK9* imprinting syndrome (Šedivá *et al.*, 2019) although membrane expression remains indistinguishable from WT.

The EC cap of TASK3 prevents inhibition by tetraethylammonium (TEA) channel (Brohawn *et al.*, 2012, Miller and Long, 2012, Concha *et al.*, 2018, Clarke *et al.*, 2008). A TASK 3 construct in absence of the cap structure generated a channel which was highly sensitive to TEA and relied upon the presence of Tyr residues at the mouth of pore (Concha *et al.*, 2018). This sensitivity to TEA is also reflected in the potassium *Shaker* channels (Heginbotham and MacKinnon, 1992). According to Doyle *et al* (1998), the presence of aromatic residues (tryptophan (Trp) and Tyr) at either end of the pore domain loops in KcsA channels are important in determining the final dimensions of the EC mouth (Doyle *et al.*, 1998).

Together, these residues were suspected to form an aromatic cuff around the pore which, through hydrogen bonds (Trp: nitrogen group – Tyr: hydroxyl group) and van der Waals forces, function as a 'molecular spring,' which alters the dimensions of the mouth to aid the selective uptake of K^+ ions (Doyle *et al.*, 1998). In the event of a mutation of Tyr to valine (Val), hydrogen bonds are interrupted and the KcsA channel takes up a persistently C-type inactivated position (Heginbotham *et al.*, 1994, Fan *et al.*, 1999). Mutational investigations carried out to explore whether the C-type inactivation of K_V channels was the result of pore constriction or dilation, found that the mutation of a single Tyr residue within the ring at the mouth of the filter disturbed the pore structure in such a way that generates mutual repulsion between the remaining Tyr residues, leading to a permanent state of pore dilation and C-type inactivation as the residues can no longer come together to complex a K^+ ion (Hoshi and Armstrong, 2013). It is therefore possible that the internal location of the Y205C mutation in TASK3 has no effect on trafficking due to its distance from the signalling motifs in the Ct resulting in a similar plasma membrane expression pattern as the WT however, following mutation of Tyr at the mouth of the pore produces a permanently inactivated channel, hence the loss of function like K_V.

An alternative theory could be that the insertion of the hydrophobic Cys into PD2 allows formation of non-specific disulphide bonds (S-S) which could stabilise the c-inactivated state following the removal of the Tyr (Hoshi and Armstrong, 2013); it is equally possible that the insertion of a hydrophobic residue in place of Tyr causes the pore to collapse in on itself. Indeed, application of Cys-specific oxidising agent: -5"-Dithio-*bis*(2-nitrobenzoic acid) (DTNB or Ellman's) which reacts with the free sulfhydryl chain of Cys to form an S-S bond between the channel and thionitrobenzoic acid residues were unable to rescue current through Y205C (Appendix 1.1). Methanethiosulfonates (MTS) are sulfhydryl-reactive compounds that form mixed disulfide linkages and are commonly used to study Cys residues on proteins; sodium-(2-sulfonatoethyl)-methanethiosulfonate (MTSES) is a negatively charged, membrane impermeant MTS. It is highly reactive with ionized thiolates and targets sulfhydryl groups accessible from the aqueous medium. Application of MTSES was observed to have no effect on Y205C mutant channels, suggesting that 205C was either not accessible from the EC side or was already cross-linked with the 205C mutation on the other monomer or a different Cys (Appendix 1.2). As MTSES had no effect on the protein, the disulphide reducing agent: dithiothreitol (DTT) was used to determine whether the 205C mutation had formed intermolecular S-S between subunits, closing the channel however, DTT acted only to reduce current further at more positive potentials where the activation of a voltage-gated channels is observed (Appendix 1.3). Considering these findings, it is not possible to say that the Y205C mutation does not form a S-S as it is possible that it may cause the pore to collapse, preventing reagents from accessing the bonds.

2.5.2 TASK3: ER Investigations

An increase in localisation of the Y205C and the Y205Δ mutants in the ER was unexpected. As discussed previously, there are multiple signalling motifs contained within the IC terminals of TASK3 which drive retrograde transport from the Golgi to the ER for degradation in the event of protein misfolding (Zuzarte *et al.*, 2009). Whilst it has been concluded that, despite presence of Y205 mutations within PD2, the protein will continue to traffic to the membrane, it is curious to see a concurrent increase in ER expression when one would typically suspect reduced membrane expression in hand with increased ER retention. This is not a novel phenomenon and has been previously experienced with mutations effecting the CFTR gene in cystic fibrosis (Marcorelles *et al.*, 2014). Whilst a portion of the misfolded mutant channel is retained within the ER for degradation, some of these channels continue to be directed to the plasma membrane however, they are observed to have a decreased half-life (Tizzano *et al.*, 1993). Decreased half-lives of ion channels at the membrane have been associated with unstable proteins which are rapidly recycled and sequestered for degradation. Both TASK3 and TASK1 channels have been shown to undergo rapid-dynamin dependent endocytosis (Mant *et al.*, 2013a). In unstimulating conditions, these channels colocalise with $Rab7^{+}$ late endosomes (Mant *et al.*, 2013a). Since both Y205 mutations are non-functional, it is tempting to suggest that the mutant channels which do reach the surface may enter the same degradative pathway as the unstimulated WT channels. Recognition of motifs on misfolded proteins by COPI vesicles at the Golgi induces retrograde translocation to the ER (Zuzarte *et al.*, 2009) where they remain as they undergo multiple rounds of refolding in attempt to correct the structure. When this cannot be achieved, the proteins are destined for ER-associated degradation (ERAD) as they are targeted to the cytosol for ubiquitin-dependent proteasomal degradation (Capera *et al.*, 2019).

2.5.3 TASK1: Plasma Membrane Investigations

The G106R and L214R mutations were found to produce significantly reduced outward currents when compared to the WT-TASK1 (Cunningham *et al.*, 2019). This reduction in function was not caused by translational or trafficking deficiencies following the observation of equal channel distribution at the plasma membrane and was more likely the result of a change in the structural and functional properties. Both G106R and L214R mutations occur in EC positions (Figure 38), between PD1 – TM2 and PD2 – TM4 respectively. Insertion of a large, positively charged, hydrophilic residue like Arg in place of smaller residues like Gly and Leu, is suspected to alter channel arrangement. It has been suggested previously that the arrangement of the histidine (His, H98) and aspartic acid (Asp, D204) residues within the channel are crucial for TASK1 pH-sensitivity and ionic-selectivity (Yuill *et al.*, 2004).

It can be seen in Figure 38 that the H98-D204 residues from each monomer within the channel form a ring just above the mouth of the SF. Whilst the H98 residues are recognised as the direct pH sensor, D204 are suspected to support TASK1 sensitivity by maintaining an optimal conformation. Expression of the G106R and L214R mutations close to this ring inserts a large residue into the cavity of the SF, potentially blocking ion flow through the channel or at least altering the optimal conformation in a way that inhibits function.

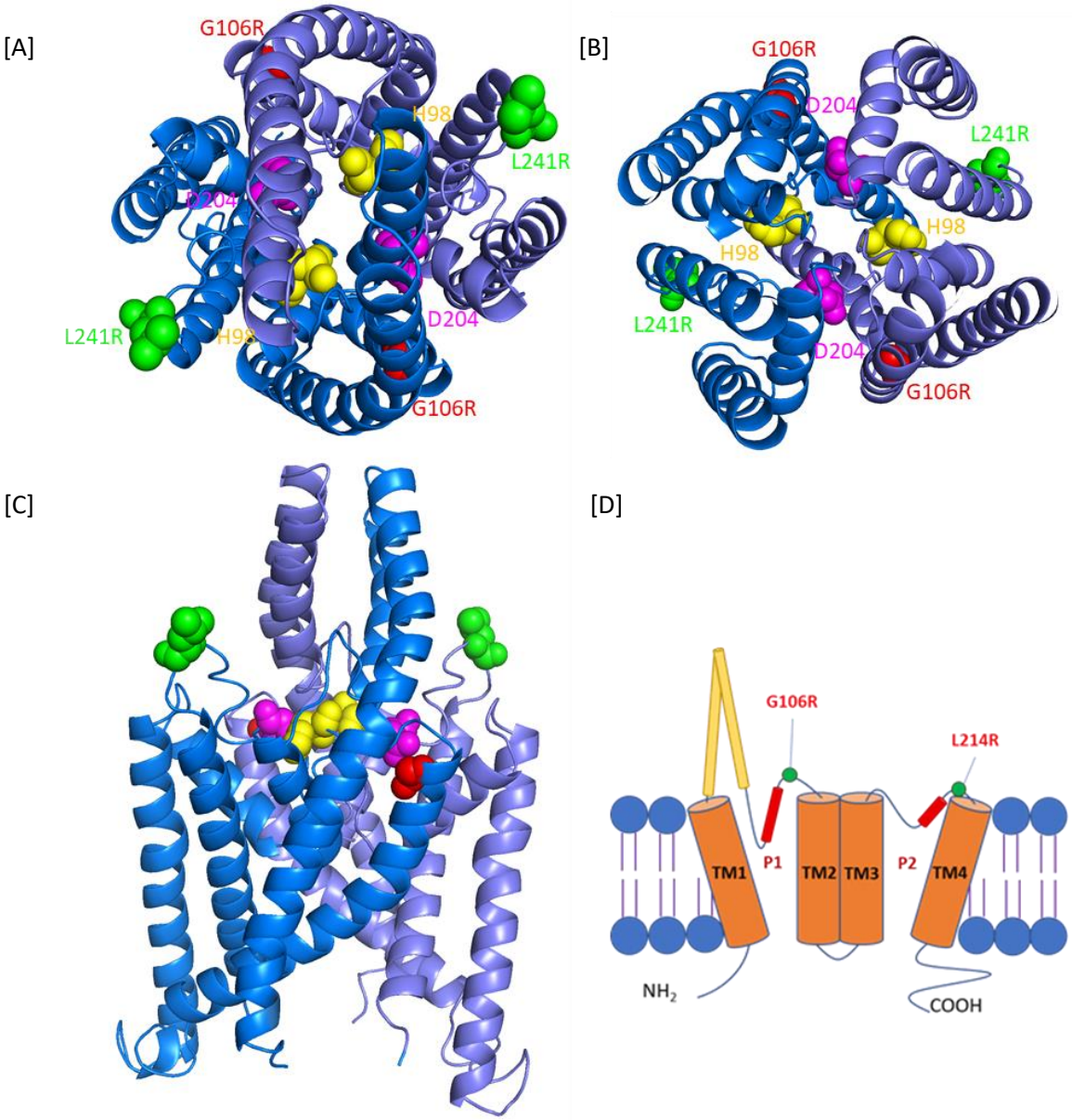

Figure 38 TASK1 homology model based upon the crystal structure of TRAAK (PDB ID: 3UM7, Brohawn et al., 2012)

[A] Top view of the channel; [B] bottom view of the channel and [C] side view of the channel. The G106R mutations are visible in red and L214R mutations in green. Function critical H98 and D204 residues are highlighted yellow and magenta respectively [D] A schematic of TASK1 structure highlighting the position of the mutations relative to the pore domains. Image reproduced and adapted from Cunningham et al., 2019.

2.5.4 TASK1: Mitochondria Investigations

Under normal conditions, the expression of TASK1 in PASMCs is associated with the regulation of resting membrane potential (Lesage and Lazdunski, 2000, Gurney *et al.*, 2003), mediating vascular responses following changes in EC pH and oxygen tension. Simply, inhibition of TASK1 prevents the efflux of K^+ ions which enhances the open probability of Ca^{2+} channels in PASMCs, causing depolarisation and vasoconstriction of pulmonary vessels. In TASK1 KO models, PASMCs were significantly depolarised, sensitive to the effects of hypoxia and insensitive to the effects of pH and chemical inhibitors like anandamide. As such, physiological and pathophysiological conditions including hypo-/hyperventilation or ischemia, or indeed anything that induces a local pH change may increase pulmonary arterial pressure (Olschewski *et al.*, 2006). As shown in these KO experiments, many patients diagnosed with PAH display significantly reduced TASK1 expression (Antigny *et al.*, 2016) or genetic mutations, such as G106R and L214R (Navas *et al.*, 2016) resulting in decreased function. Reduced TASK1 current promotes vasoconstriction, proliferation and inflammation (Antigny *et al.*, 2016).

Considering the sensitivity of TASK1 to changes in oxygen levels in PASMCs and vascular tone, TASK1 is often referred to as an oxygen 'sensor' (Olschewski *et al.*, 2006). Mitochondria within PASMCs of resistance level arteries have also been given this title, responding to reductions in alveolar oxygen tension in their local environment by initiating hypoxic pulmonary vasoconstriction (HPV) (Weir *et al.*, 2005, Archer *et al.*, 1993, Ryan *et al.*, 2015). HPV is an autoregulatory mechanism which matches perfusion to ventilation by shunting perfusion to areas within the lung with better ventilation. This is important in patients suffering with the likes of acute pneumonia (Sylvester *et al.*, 2012). Initiation of the mechanism is suspected to be driven by mitochondria in PASMCs during hypoxic events (Weir *et al.*, 2005). The "*Redox Theory"* hypothesises that a reduction in oxygen levels slows the rate of electron flux through the mitochondrial electron transport chain complexes I and III, decreasing ROS production causing closure of K^+ channels and subsequent activation of Ca_V channels, resulting in vasoconstriction (Archer *et al.*, 1986, Ryan *et al.*, 2015). Unlike mitochondria in renal arteries where changes in oxygen levels have little effect on ROS production, it is a unique ability of PASMCs mitochondria to regulate ROS production for modulation of HPV (Michelakis *et al.*, 2002). Disturbances in mitochondrial redox signalling have been associated with the failure of mitochondria to detect changes in oxygen (Ryan *et al.*, 2015). Considering the implication of TASK1 in PAH as an oxygen sensor and its dysfunction having been associated with depolarisation and vascular remodelling (Olschewski *et al.*, 2006), it is curious that the presence of TASK1 in the mitochondria as a regulator of mitochondrial membrane potential alongside TASK3 has not yet been considered.

The colocalisation data in this chapter showed no significant difference in the degree of mitochondrial expression of TASK1 and the G106R and L214R mutants. Whilst a yellow overlay indicative of colocalisation is not clearly visible, the expression of TASK1 at the mitochondria cannot be conclusively ruled out. The average PCC value of TASK1 and its variants at the mitochondria was 0.35. In the case of WT-TASK3 which has confirmed mitochondrial expression in literature, a low PCC value of 0.3 was also achieved. This data is in support of a possible role of TASK1 in the regulation of mitochondrial membrane potential however, any consequences of the G106R and L214R mutations are not the effect of altered expression but more likely a result of structural and functional changes discussed above in relation to the membrane.

2.5.5 TASK3: Mitochondria Investigations

The presence of TASK3 on the inner mitochondrial membrane in malignant and non-malignant cells has been well documented in the literature for supporting mitochondrial functions and pathologies like cancer (Rusznák *et al.*, 2008). By comparison, investigation into the role of TASK3 channels in arousal and wakefulness and their relationship to sleep disorders, considerably less so. TASK3 channels are ubiquitously expressed throughout the CNS and PNS where they modulate neuronal excitability. The dynamic modulation of TASK channels is suspected to underlie changes in arousal, wakefulness, sleep and general anaesthesia (Bayliss and Barrett, 2008). Particularly, it is the expression of TASK channels in the preoptic and superchiasmatic nuclei (SCN) within the hypothalamus and thalamocortical (TC) relay neurons which implicates their role in the regulation of the sleep-wake cycle (Talley *et al.*, 2001b). During sleep-wake activity, the transition between these states is mediated by neurotransmitter activation of neurons of the ascending brainstem, like the basal forebrain cholinergic neurons which form the main source of acetylcholine (Ach) (Vu *et al.*, 2015). The release of ACH drives a depolarising shift in the membrane potential of TC neurons which inhibits the oscillatory burst activity associated with deep sleep (<15 Hz) and switches to the tonic firing activity associated with wakefulness and rapid eye movement sleep (REMS) (approx. 40 Hz) (Bista *et al.*, 2012, Meuth *et al.*, 2003, Meuth *et al.*, 2006a, Meuth *et al.*, 2006b).

Wakefulness is also supported by the expression of TASK1 and TASK3 within serotonergic dorsal and caudal raphe neurons within noradrenergic cell bodies of the locus coeruleus where the depolarising effect upon acidification contributes to the stimulation of behavioural arousal (Talley *et al.*, 2001b, Washburn *et al.*, 2002, Duprat *et al.*, 2007). Much of this activity is driven by the open and closure of K2P channels like TASK1/TASK3 and TREK which appears to rely critically upon $G\alpha_q$ signalling (Coulon *et al.*, 2010, Steinberg *et al.*, 2015) however, Veale *et al* (2014) have reported previously that cells

transiently expressing the TASK3_G236R mutation fail to respond to Gαq-induced inhibition (Veale *et al.*, 2014). One of the symptoms reported in *KCNK9*-imprinting syndrome is low arousal, or reduced vigilance and alertness during wakefulness (Graham *et al.*, 2016). Orexin neurons function to promote wakefulness (Burdakov *et al.*, 2006). It has recently been shown the that inhibition of these neurons requires regulation of glucose metabolism by TASK3 channels, presenting a novel pathway in the regulation of consciousness and energy balance (Burdakov *et al.*, 2006). There is no literature currently available which explores the expression of mutants associated with *KCNK9* imprinting syndrome in mitochondria.

This study aimed to determine whether there were any differences between expression of WT and mutants in mitochondria which could lead to altered metabolism and the symptoms surrounding arousal in *KCNK9* imprinting syndrome. As expected, TASK3 was found to colocalise with the mitochondria in transiently transfected tsA201 cells, although the degree of expression was low. No significant difference between expression of WT-TASK3, G236R or Y205C variants in the mitochondria confirms that any of the functional consequences of these channels is not due to impaired trafficking or expression within the mitochondria. Interestingly, the expression of the Y205Δ mutant appeared to be almost double that of WT-TASK3. Unlike other organelles, mitochondria contain their own genome, however this only encodes 13 peptides (approx. 1%) of the mitochondrial proteome. The other 99% are encoded on the nuclear genome and are synthesised on cytosolic ribosomes (Stojanovski *et al.*, 2012). Prior to insertion into the inner mitochondrial membrane, the proteins are retained in their nascent, unfolded form to allow passage through the small membrane pores of the mitochondria. This process requires the binding of cytosolic chaperones that stabilise the peptide and guide them to pore (Stojanovski *et al.*, 2012). Whilst TASK3 channels lack the cleavable amino-terminal presequences required for mitochondrial targeting (Yao *et al.*, 2017, Stojanovski *et al.*, 2012), it is suspected to contain non-cleavable internal import signals that target the channel to TOM70 receptors at the mitochondrial outer membrane for internalisation, assembly sorting into the inner membrane (Stojanovski *et al.*, 2012).

With the Y205Δ Nt intact, the channel continues to be trafficked to and from the plasma membrane and the ER in a state which is folded and recognisable. It is currently unclear which cytosolic chaperones are involved in the mitochondrial targeting of TASK3 channels. It is possible that truncation of Y205Δ enhances the exposure of the internal import signals utilised in mitochondrial trafficking, increasing expression at the mitochondria. It is unlikely that this overexpression has implications in arousal since that is a symptom associated with the G236R mutation which was indistinguishable from the WT.

2.6 Conclusions and Further Study

Here I have provided evidence for reduced plasma membrane expression of the TASK3_G236R mutant despite expression within the ER and mitochondria being indistinguishable from the WT. In absence of increased ER retention, it would be useful to expand this colocalisation study to include late endosomes and lysosomes to determine whether TASK3_G236R channels are rapidly recruited into alternate degradative pathways. It is unlikely that the reduction in plasma membrane expression is linked to reduced gene translation as a concurrent reduction would be expected within the ER and mitochondria, although confirmation either by in-cell western or flow cytometry could resolve this. This study confirms that the Y205C and Y205Δ mutations have no effect on plasma membrane expression confirming that channels will continue to be expressed on the plasma membrane provided that the Nt remains intact and is likely dysfunctional due to the insertion of cysteine into the mouth of the pore with blocking or destabilising effects. In absence of resolved TASK3 crystal structure, this is difficult to confirm. Together this data suggests that impaired trafficking to the membrane is unlikely to account for all the deleterious effects of this channel in *KCNK9* imprinting syndrome, as both Y205C and G236R mutations display differing trafficking characteristics but produce the same functional and phenotypic outcomes.

In line with CFTR (Marcorelles *et al.*, 2014), it is suspected that increased retention of Y205C and Y205Δ in the ER, despite efficient membrane expression, is linked to decreased half-lives (Tizzano *et al.*, 1993) of those expressed at the plasma membrane which are retrieved by the same rapid dynamin-dependent endocytosis mechanisms as WT channels. The Y205C and Y205Δ retained within the ER are suspected to undergo refolding attempts until labelled for ERAD and ubiquitin-dependent proteasomal degradation. This could explain the simultaneous expression of these mutants at the plasma membrane and ER although further investigations into these systems looking into interactions between specific pathway proteins are required.

The TASK3_G236R and Y205C mutations implicated in *KCNK9* imprinting syndrome do not exert pathological influence through altered expression at the mitochondria as they are expressed in equal measures to the WT. Whilst these channels lack the discreet signalling motif required for mitochondrial targeting, it is suspected that these channels locate to the mitochondria via an internal sequence similar to the many other proteins which also lack the signalling motif (Stojanovski *et al.*, 2012). For this reason, it is possible that the increased mitochondrial expression of the TASK3_Y205Δ mutation is due to the enhanced exposure of the internal signalling motif following truncation of this channel. It is unlikely that this overexpression has implications in arousal since that is a symptom which has been associated with the G236R mutation however, it remains possible that the presence of a

dysfunctional channel is enough to alter mitochondrial membrane potential.

The reduced function of the G106R and L241R mutations of TASK1 observed in patients with PAH is not caused by translational or trafficking deficiencies following the observation of equal channel distribution at the plasma membrane. It is more likely the result of a change in the structural properties following the insertion of a much larger residues in proximity of structures key to functional roles.

For the first time, this study investigated the localisation of TASK1 within mitochondria. Despite low expression rates, TASK1 channels do appear to localise within mitochondria however, the G106R and L214R mutations displayed no significant difference in expression when compared to WT. Whilst this suggests that differential expression of mutant channels within the mitochondria is unlikely to contribute to the progression of PAH, it cannot be said that the presence of dysfunctional channels do not disturb mitochondrial redox signalling in hypoxic conditions. Unfortunately, the methods used in this study are unable to determine which compartment of the mitochondria TASK1 channels are localised in. As previously described for TASK3, a pull-down assay identifying protein-protein interactions with compartmental-specific proteins could solve this issue and help to understand a functional role of TASK1 in regulation of mitochondria membrane potential in health and disease (Yao *et al.*, 2017).

Chapter 3:

Investigation into the G-Protein Regulation of the TASK3_G236R Mutated Channel

3.1 Introduction

As discussed in Chapter 1, TASK3 channels are regulated by a wide variety of biological and pharmacological stimuli (Talley and Bayliss, 2002b, Lesage and Barhanin, 2011) which may work through GPCR signalling mechanisms (Chen *et al.*, 2006, Mathie, 2007) to mediate the leak conductance underlying cellular excitability, the physiological consequence of which is linked to processes such as motor control (Perrier *et al.*, 2003, Talley *et al.*, 2000, Lazarenko *et al.*, 2010) and aldosterone secretion (Bandulik *et al.*, 2010). Previously our laboratory has demonstrated, in expression systems and native IK_{SO} present in CGNs, pronounced GPCR regulation of TASK3 channels by the muscarinic acetylcholine receptor (M3), which couples through the G-protein: G_q. This effect could not be replicated with the M2 receptor, which couples through $G_{i/o}$. In addition, we were able to show that a selective $G\alpha_q$ antagonist, YM-254890, abolished the inhibition of TASK3, suggesting that GPCR regulation of TASK3 channels occurs through $G\alpha_q$ (Veale *et al.*, 2007b). Indeed, co-expression of the constitutively active form of the G-protein ($G\alpha_q$*) in the absence of the M3 receptor, caused a significant reduction of the TASK3 current (Veale *et al.*, 2007b). More recently, Vu *et al.* (2015) described a significant neuromodulatory role of TASK3 following histaminergic input in the basal forebrain, regulating changes in our arousal state, conscious awareness and maintenance of wakefulness (Vu *et al.*, 2015).

Histamine (H1) receptors belong to the rhodopsin-like GPCRs, which like M3 receptors, couple through G_q. Zhang *et al.* (2016) have shown that endogenously released neurotensin (NT) increased the excitability of the dentate gyrus granule cells via $G\alpha_q$-coupled inhibition of TASK3, which facilitates the induction of long-term potentiation (LTP). In co-immunoprecipitation studies, they showed that NT was able to inhibit TASK3 channels co-expressed with NT receptors (NTS1) via a direct interaction of $G\alpha_{q/11}$ with TASK3. Gastrointestinal tract NT has been implicated in modulation of a variety of physiological functions including pain, temperature, blood pressure, learning, memory and neurological diseases such as schizophrenia and Parkinson's disease. Similarly to histamine, NT has also been shown to have acute effects on sleep-wake regulation and interacts closely with the dopaminergic system (Mustain *et al.*, 2011). There is also evidence to suggest that NT and NTS1 receptors may be a component of a pathway involved in both sleep and mood disorders (Fitzpatrick *et al.*, 2012). High levels of NT have been detected in children diagnosed with Prader-Willi Syndrome, a condition with similarities to that of *KCNK9* Imprinting Syndrome (Butler *et al.*, 2015).

3.1.1 TASK3: Histamine, NT and Wakefulness

To stay awake, the brain requires the constant activity of multiple pathways including: aminergic (histamine, dopamine, noradrenaline, acetylcholine), peptidergic (hypocretin, orexin, cocaine- and amphetamine-regulated transcript peptide (CART)) and certain glutamatergic and GABAergic pathways (Yu *et al.*, 2018). These arousal pathways ascend through the paramedian region of the mid brain and divide into dorsal and ventral pathways. The dorsal pathway innervates the thalamus where it processes signals associated with sensation, motor responses and cognition. The larger ventral pathway stimulates the hypothalamus, basal forebrain and the cortex (Scammell *et al.*, 2017). Interestingly, patients sustaining severe injury to the dorsal regions tend to remain awake but in a vegetative state (Plum and Posner, 1972), which contrasts with injuries occurring within ventral pathway regions whereby patients display symptoms of low arousal and sleep more than average (Fuller *et al.*, 2011). Together this suggests that both the dorsal and ventral pathways are required for functional wakefulness with dorsal pathways supporting the *'content of consciousness'* through regulation of thalamocortical signalling and ventral pathways dictating the *'behavioural state'* of wakefulness (Scammell *et al.*, 2017).

TASK channels are widely expressed throughout the CNS (Talley *et al.*, 2001b) and as such, activation of TASK3 channels by neurotransmitters or volatile anaesthetics (i.e. halothane), causes neural hyperpolarisation and subsequent changes to neuromodulatory activity. TASK3 channels expressed on basal forebrain cholinergic neurons (BFCN) have been shown to modulate the electrocortical signatures of arousal following a histaminergic input (Vu *et al.*, 2015). Histamine is a neurotransmitter which modulates specific aspects of wakefulness like motivation and cognition (Haas and Panula, 2003). Histaminergic cell bodies originate purely within the tuberomammillary nucleus (TMN) and project extensively throughout the neocortex and hippocampus where they innervate the brain and promote wakefulness (Figure 39) (Haas and Panula, 2003, Yu *et al.*, 2018). Under normal physiological settings, histamine acts directly upon H1 receptors (Panula *et al.*, 2015), coupled with $G\alpha q_{/11}$, expressed upon BFCN to inhibit TASK3 channels, causing neuronal depolarisation and increased high frequency electroencephalogram (EEG) oscillations associated with wakefulness (Steinberg *et al.*, 2015). It was demonstrated that arousal states increased following the micro perfusion of histamine into the basal forebrain as seen by heightened EEG oscillatory activity during non-REM sleep, of which mice spent less time in, and more time in a quiet wakefulness (Vu *et al.*, 2015). In contrast, the effect of the micro perfusion in TASK3 KO mice was significantly less however, the histamine-induced arousal was not abolished suggesting that there are other mechanisms present supporting the histamine pathways (Vu *et al.*, 2015). The activity of TASK3 channels in the BFCN following histamine activation appears to rely critically upon with $G\alpha_{q/11}$ for channel inhibition (Broicher *et al.*, 2008).

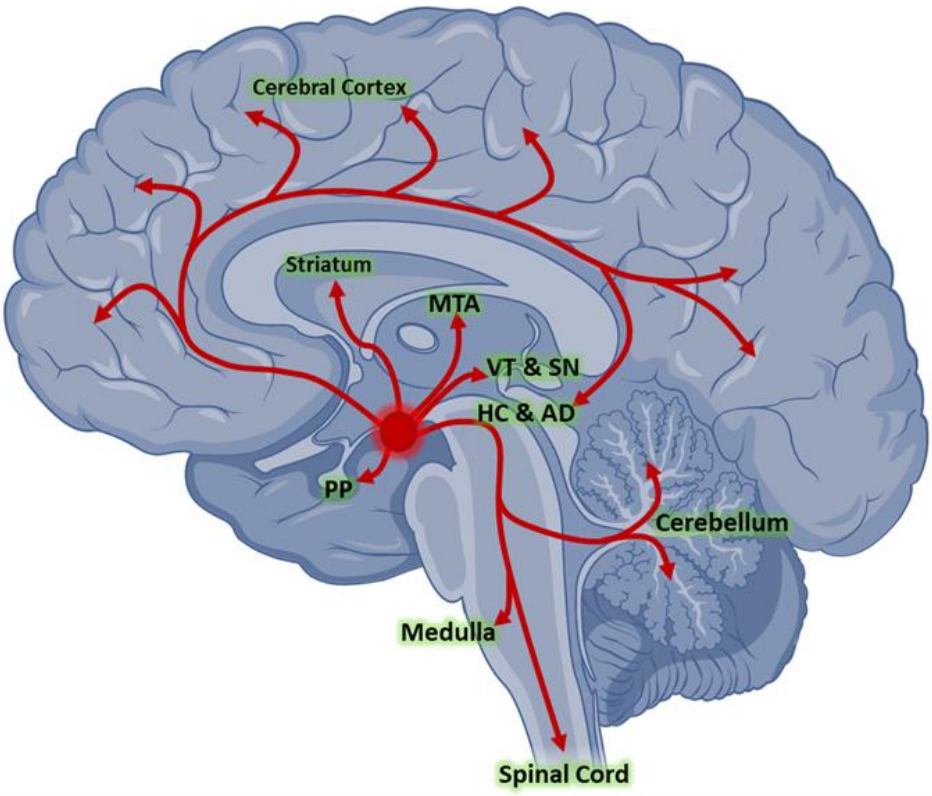

Figure 39 Histaminergic pathways originate from the tuberomammillary nucleus (red centre) and extensively innervate many areas of the brain.

PP = Posterior pituitary gland; MTA = midline thalamic areas; VT = ventral tegmentum; ST = substantia nigra; HC = hippocampus and AD = amygdala. Adapted from HAAS et al., (2003).

Neurotensin (NT) is a 13 amino acid neuromodulatory peptide which is expressed throughout the CNS where it acts through a diverse range of intracellular cascades to enhance or depress neuronal activity (Tschumi and Beckstead, 2019). Extensive expression of NT within dentate gyrus region of the hippocampus, alongside key receptors NTS1 and NTS2 (Quirion *et al.*, 1987, Boudin *et al.*, 2000), signifies a possible role of the neuropeptide in learning and memory processing and supporting wider cognitive functions (Azmi *et al.*, 2006, Tirado-Santiago *et al.*, 2006, Ohinata *et al.*, 2007, Yamauchi *et al.*, 2007, Li *et al.*, 2011, Laszlo *et al.*, 2010, Xiao *et al.*, 2009) although the molecular mechanisms underlying these activities remain undefined. Predominantly acting through GPCRs: NTS1 and NTS2 coupled to G_q proteins (Watson *et al.*, 1992), work carried out by Zhang *et al.* (2016) determined that the enhancement of action potential firing frequency induced by NT was independent of PLC, intracellular Ca^{2+} and PKC and rather a function of direct action of $G\alpha_{q/11}$ binding at the channel.

Following the discovery of the TASK3_G236R mutation associated with *KCNK9* imprinting syndrome (Barel *et al.*, 2008), one of the striking discoveries was that the channel no longer appears to be sensitive to inhibition following activation of similar GPCR, the muscarinic (M3) receptor (Veale *et al.*, 2014). Interestingly, low arousal states have been reported in patients expressing the TASK3_G236R mutation (Graham *et al.*, 2016). In addition, identification of a role for NT modulation of TASK3 via GPCR regulation in the dentate gyrus may offer an insight into the cognitive abnormalities which similarly arise in *KCNK9* Imprinting syndrome (Graham *et al.*, 2016) should NTS1 regulation of the TASK3_G236R variant be examined.

3.2 Aims and Objectives

Previously it was shown that WT-TASK3 is regulated by GPCRs acting through $G\alpha_q$ and that this is, at least in part, likely through a direct action of the G-protein on the channel (Veale *et al.*, 2007b, Zhang *et al.*, 2016). It was also shown that this regulation is lost from the *KCNK9* Imprinting Syndrome mutant (G236R) channel (Veale *et al.*, 2014). In this study, the mechanism by which the inhibitory effect of the activated G-protein occurs was examined in more detail. Electrophysiological experiments found that WT channels expressed with an activated G-protein resulted in a subsequent reduction in current levels. I aimed to determine using confocal imaging techniques if the observed reduction in current is a consequence of internalisation of the channel from the plasma membrane or a consequence of physiological changes to the channel itself.

Additionally, for the first time the effects of activated G-proteins on the G236R mutated channel were examined to determine whether the attenuated regulatory effect of the activated GPCRs is replicated by activated G-proteins and if there are any changes in expression of the channel at the membrane which mirrors the increase in current recorded, when GPCRs are present. A combination of confocal microscopy and electrophysiological methods were used.

Two forms of activated G proteins, $G\alpha_q$ and $G\alpha_{11}$, both of which have been found to have a similar inhibitory effect on TASK3 channels were studied.

3.3 Methods

3.3.1 Molecular Biology

The molecular biology in this chapter was carried out as described in section 2.3.1. Both human $G\alpha_q$ and $G\alpha_{q/11}$ plasmid DNA were bought from Origene (Rockville, USA).

3.3.2 Cell culture

The cell culture in this chapter was carried out as described in section 2.3.2.

3.3.3 Transfection

The transfections carried out in this chapter are as described in section 2.3.3.

3.3.4 Plasma Membrane Staining, Slide Preparation and Viewing

Cell membranes were stained as described in section 2.3.4. Slides were prepared and imaged as described in sections 2.3.7 – 2.3.11.

3.3.5 Whole-Cell Patch-Clamp

For whole-cell patch-clamp methodology, see '*materials and methods'* in Veale *et al.* (2014). Solutions listed in Appendix 3.4

3.4 Results

3.4.1 Reduced current of WT-TASK3 channels when co-expressed with activated G-proteins is not a consequence of channel internalisation

Cellular localisation of GFP-tagged WT-TASK3 transiently transfected in tsA201 cells was examined using confocal microscopy. GFP fluorescence was measured at the plasma membrane of cells transiently transfected with WT-TASK3_GFP and either activated $G\alpha_q$ or activated $G\alpha_{11}$. Control images were collected as displayed in Figure 40, [Ai-iii], [Bi-iii] and [Ci-iii]. Experimental procedure was as described in section 2.3.4 and 2.3.7 – 2.3.11. Co-expression of WT-TASK3 with $G\alpha_q$ [Di-iii] was compared to WT-TASK3 alone [Ci-Ciii]. Similarly, the same process was repeated for co-expression with $G\alpha_{11}$. [Ei-iii]. An ordinary one-way ANOVA significance test with an adhoc Tukey's multiple comparison comparing each situation with WT-TASK3_GFP was performed. Co-expression of either of the activated G-proteins had no significant effect ($P > 0.05$) on WT-TASK3_GFP plasma membrane expression with WT-TASK3_GFP producing a PCC (± SEM) of 0.52 ± 0.03 (n= 14, 95% CI: 0.46 – 0.57) compared to 0.56 ± 0.03 (n= 12, 95% CI: 0.50 – 0.62) and 0.63 ± 0.04 (n= 10, 95% CI: 0.55 – 0.71) for $G\alpha_q$ and $G\alpha_{11}$, respectively (Figure 41). This suggests that the reduced current recorded through WT-TASK3 when co-expressed with an activated G_q protein is not due to internalisation or recycling of the channel but likely due to a gating mechanism.

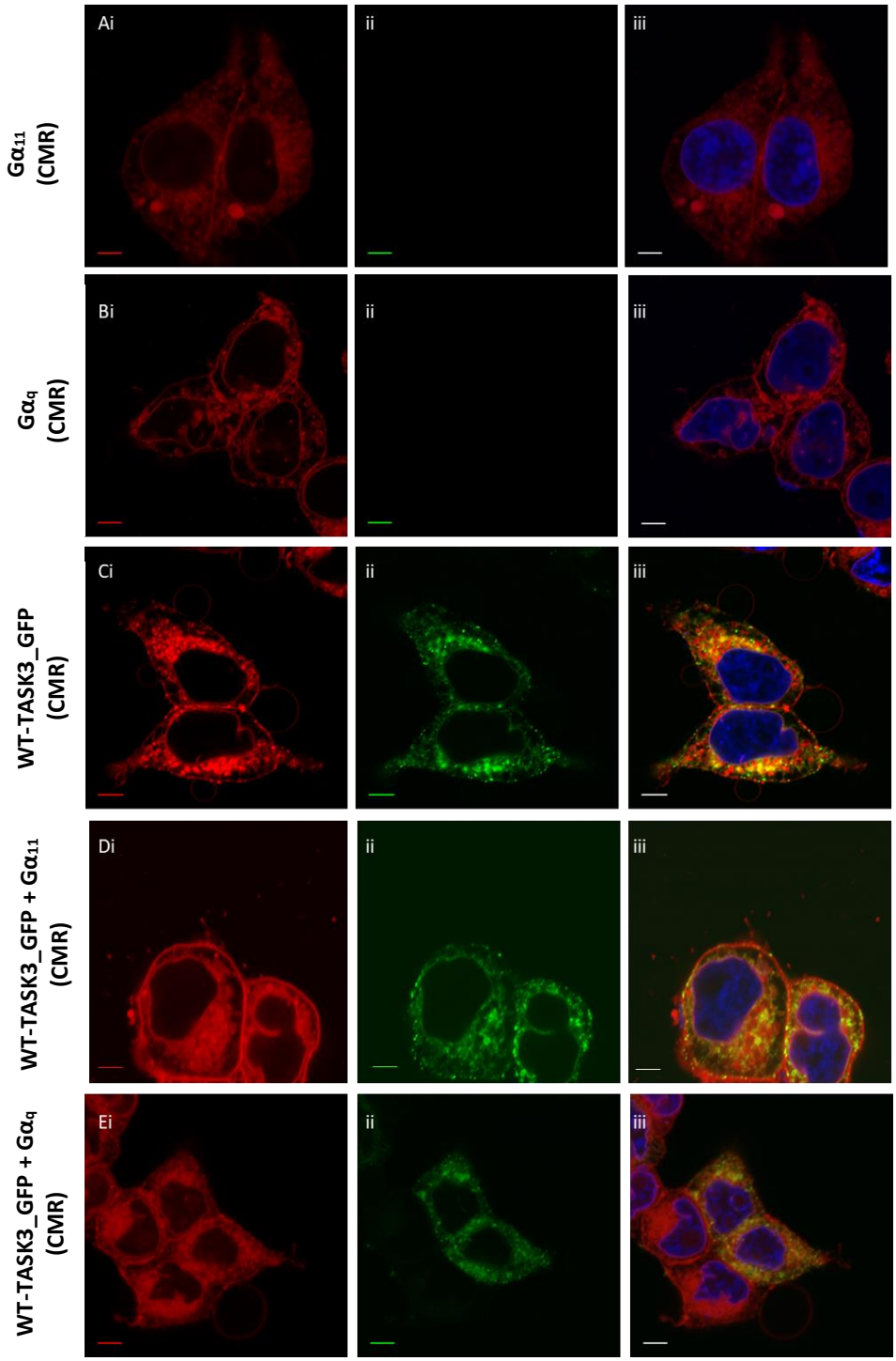

Figure 40 Plasma membrane localisation of WT-TASK3 is not altered by inhibitory activated G-proteins

A photomicrograph investigating the effect of $G\alpha_q$ and $G\alpha_{11}$ co-expression on plasma membrane localisation of GFP labelled TASK3. Confocal images [Ai-iii] represent tsA201 cells transfected with $G\alpha_{11}$. [Ai] displays the red stained plasma membrane; [Aii] the same cells in the green channel with no green autofluorescence and [Aiii] is the overlap of [Ai] and [Aii]; images [Bi-iii] represent tsA201 cells transfected with $G\alpha_q$. [Ci-iii] represent tsA201 cells transfected with GFP-tagged WT-TASK3; [Di-iii] represent tsA201 cells co-transfected with GFP-tagged WT-TASK3 and $G\alpha_{11}$; [Ei-iii] represent tsA201 cells co-transfected with GFP-tagged WT-TASK3 and $G\alpha_q$ All scale bars are calibrated to 5 µM.

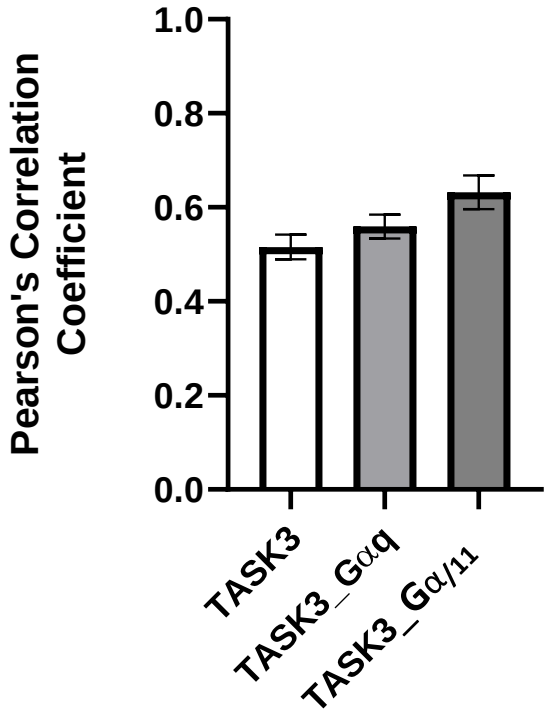

Figure 41 PCC quantification of plasma membrane expression of WT-TASK3 co-expressed with activated G-protein, $G\alpha_{11}$ or $G\alpha_q$

A histogram displaying the PCC quantification of plasma membrane colocalisation following co-transfection of $G\alpha_{11}$ or $G\alpha_q$. For both $G\alpha_q$ and $G\alpha_{11}$, no significant difference ($p > 0.05$) was observed in plasma membrane expression of TASK3, when compared to channel expression in the absence of G-protein expression.

3.4.2 TASK3 G236R mutant channels are not inhibited by activated G-proteins

We then went on to examine the effect of activated G-proteins on the pathogenic variant channel, TASK3_G236R. Using patch-clamp electrophysiology, comparison of current density between human TASK3_G236R and TASK3_G236R co-expressed with $G\alpha_q$ in a 1:1 ratio, found the channel to be insensitive to the presence of $G\alpha_q$ (Figure 42). The average whole-cell current of TASK3_G236R measured as a difference between that seen in -40 mV and -80 mV, increased but was not significantly different ($P > 0.05$, unpaired t-test, 95% CI: -12 to +20) when co-expressing 500 ng of each cDNA [TASK3_G236R: 13 pA pF^{-1} (n=3, 95% CI: 3 to 3); TASK3_G236R + $G\alpha_q$: 17 pA pF^{-1} (n= 3, 95% CI: -6 to 40). Whilst current density between human TASK3 and TASK3 co-expressed with G-protein alpha q ($G\alpha_q$) in a 1:1 ratio, found the average whole-cell current of TASK3 to be significantly reduced ($P < 0.05$, unpaired t-test, 95% CI: -62 to -39) from 72 pA pF^{-1} (n= 9, 95% CI: 60 to 84) to 22 pA pF^{-1} (n= 11, 95% CI: 16 to 28) when co-expressing 500 ng of each cDNA.

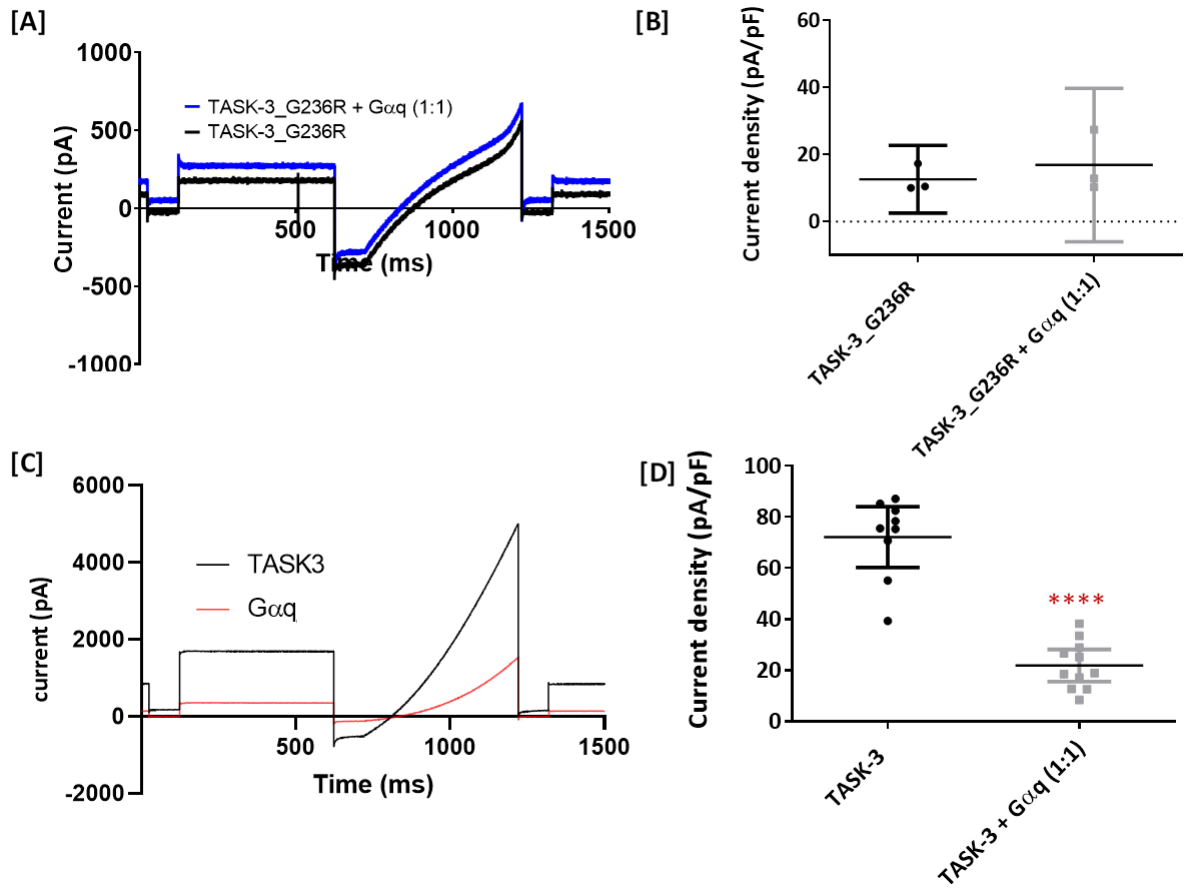

Figure 42 TASK3_G236R channels are not inhibited following co-expression of activated $G\alpha_q$.

[A] Averaged raw data traces of TASK3_G236R channels (black line) and TASK3_G236R + $G\alpha_q$ (blue line). [B] Comparison of current density between human TASK3_G236R and TASK3_G236R co-expressed with $G\alpha_q$ in a 1:1 ratio. The average whole-cell current of TASK3_G236R measured as a difference between that seen at -40 mV and -80 mV. [C] Average raw data traces (n= 9) of WT-TASK3 channels (black line) and WT-TASK3 co-expressed with $G\alpha_q$ (red line) (n= 12) transiently expressed in tsA201 cells and recorded using a "step-ramp" voltage protocol. [D] Comparison of current density between human TASK3 and TASK3 co-expressed with $G\alpha_q$ in a 1:1 ratio. The average whole-cell current of TASK3 was measured as a difference between that seen at -40 mV and -80 mV. This work was carried out by Dr E L Veale.

3.4.3 Plasma membrane localisation of TASK3_G236R is affected by activated G-proteins

Cellular localisation of GFP-tagged TASK3_G236R transiently transfected in tsA201 cells was examined using confocal microscopy. GFP fluorescence was measured at the plasma membrane of cells transiently transfected with TASK3_G236R_GFP and either activated $G\alpha_q$ or activated $G\alpha_{11}$. Control images were collected as displayed in Figure 40, [Ai-iii], [Bi-iii] and [Ci-iii]. Experimental procedure was as described in section 2.3.4 and 2.3.7 – 2.3.11. Co-expression of TASK3_G236R with $G\alpha_q$ [Bi-iii] was compared to WT-TASK3 alone [Ai-iii]. Similarly, the same process was repeated for co-expression with $G\alpha_{11}$. [Ci-iii]. An ordinary one-way ANOVA significance test with an adhoc Tukey's multiple comparison comparing each situation with WT-TASK3_GFP was performed. Co-expression of activated $G\alpha_q$ had no significant effect ($P > 0.05$) on TASK3_G236R_GFP plasma membrane expression when compared to TASK3_G236R_GFP producing PCC (± SEM) values of 0.44 ± 0.03 (n= 16, 95% CI: 0.37 – 0.51) compared to 0.32 ± 0.03 (n= 11, 95% CI: 0.25 – 0.39) respectively (Figure 43). Interestingly, co-expression of activated $G\alpha_{11}$ had a significant effect ($P > 0.001$) on TASK3_G236R_GFP plasma membrane expression, with PCC values of 0.54 ± 0.03 (n= 10, 95% CI: 0.47 – 0.60). These data suggest that whilst GPCR regulation of current by TASK3_G236R channels is completely abolished, direct G-protein interaction with these mutated channels cannot be ruled out.

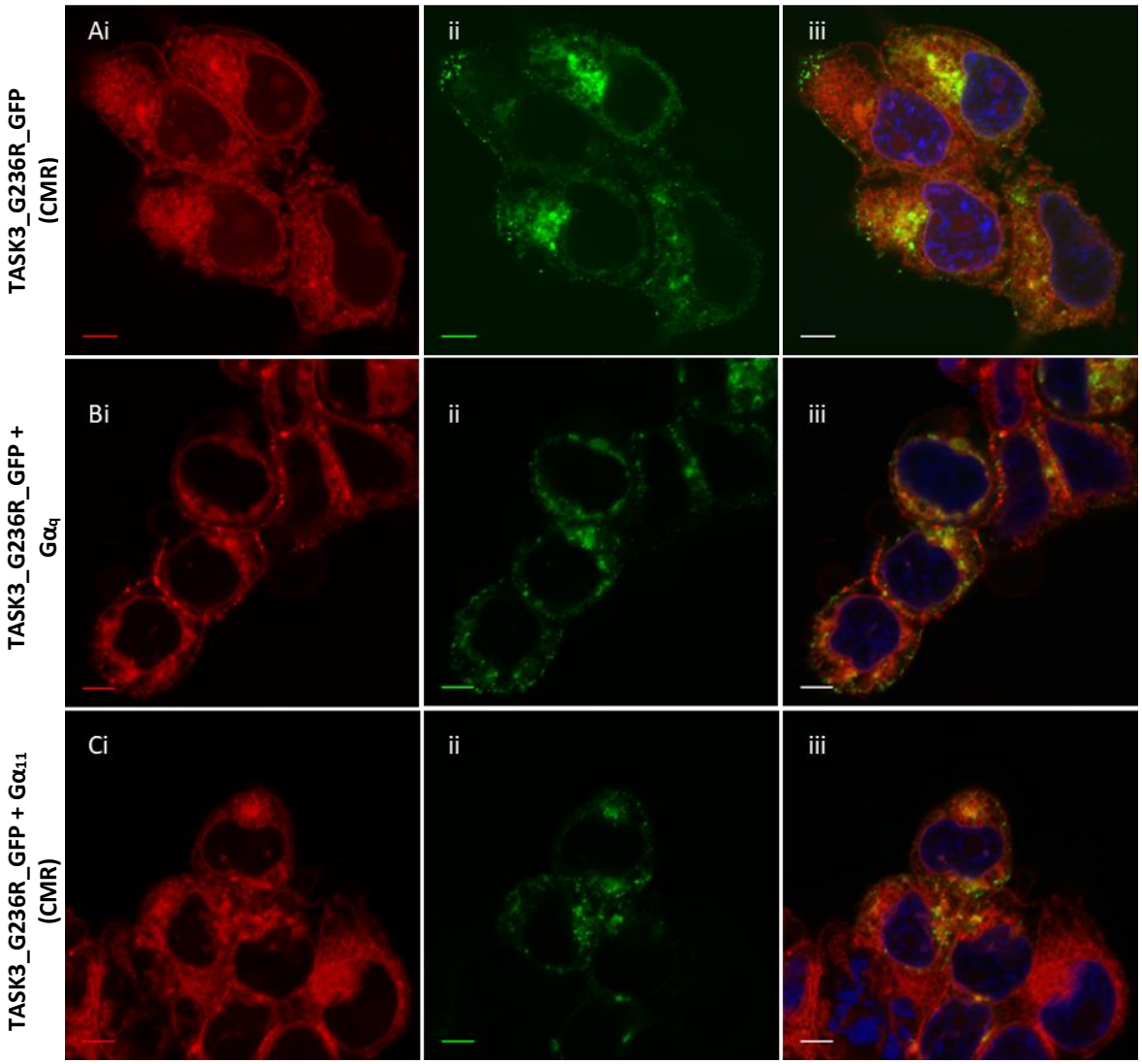

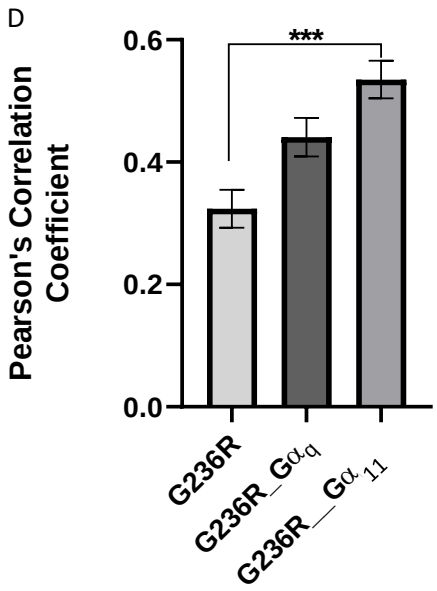

Figure 43 Plasma membrane localisation of TASK3_G236R is altered by inhibitory activated G-proteins

A photomicrograph investigating the effect of $G\alpha_q$ and $G\alpha_{11}$ co-expression on plasma membrane localisation of GFP labelled TASK3_G236R. Confocal images [Ai-iii] represent tsA201 cells transfected with TASK3_G236R_GFP. [Bi-iii] represent tsA201 cells c0-transfected with GFP-tagged TASK3_G236R and $G\alpha_q$. [Ci-iii] represent tsA201 cells co-transfected with GFP-tagged TASK3_G236R and $G\alpha_{11}$. [D] A histogram displaying the PCC quantification of plasma membrane colocalisation following co-transfection of $G\alpha_{11}$ or $G\alpha_q$. A significant difference ($p > 0.001$) was observed in plasma membrane expression of TASK3_G236R when co-expressed with $G\alpha_{11}$ when compared to channel expression in the absence of G-protein expression or $G\alpha_q$.

3.5 Discussion

TASK3 channel activity can be regulated by hormones and transmitters acting through GPCRs coupled to G-proteins of the $G\alpha_{q/11}$ subclass (Chen *et al.*, 2006). Following activation of a GPCR, the channel is inhibited, increasing neuronal excitability and encourages the firing of APs (Fink *et al.*, 1996, Kim *et al.*, 2000, Czirják *et al.*, 2001, Chemin *et al.*, 2003, Mathie, 2007). There is a large body of data available which debates the mechanisms of channel inhibition following GPCR activation (see section 1.5.2) however, the latest findings suggest a role for the binding of the activated $G\alpha_{q/11}$ directly to the channel (Zhang *et al.*, 2016). In contrast to WT-TASK3 channels, the G236R mutant channels responsible for *KCNK9* Imprinting Syndrome, have been found to give rise to smaller functional outward currents that are insensitive to the activation of GPCRs (Veale *et al.*, 2014). In this study, it was found that the TASK3_G236R mutant channel is not inhibited following co-expression of activated $G\alpha_{q/11}$ (Figure 42), however it does increase the plasma membrane expression of the pathogenic channel only (Figure 43).

For GPCR-regulated inhibition, TASK channels critically rely upon the presence of six residues ($V^{243}LRFLT^{248}$) at the interface of the final transmembrane domain and the Ct. Not only is this motif crucial for $G\alpha_q$-mediated inhibition, it has also been implicated in regulation by volatile anaesthetics, neurotransmitters (Talley and Bayliss, 2002b) and pharmacological agents (Veale *et al.*, 2007a). The complex cascade which follows GPCR activation is a highly debated topic as discussed in section 1.5.2.3 however, more recent hypotheses lean toward the direct binding of $G\alpha_{q/11}$ to the intracellular Ct (Zhang *et al.*, 2016). This concept raises questions with regards to the function of the VLRFLT motif. Do these six amino acid residues function as a direct binding site for $G\alpha_{q/11}$ or are they crucial to the transduction of an intracellular signal to the channel gate? It is tempting to lean towards VLRFLT behaving as a transducer due to the wide range of modulatory molecules known to act on the channel (see Table 3, section 1.5.2) with their diverse structures which influence channel function through this mechanism. K2P family member, TREK1, contains a similar region at the same location which is key to regulatory aspects including pharmacological mediators, volatile anaesthetics as well as physiological factors such as mechanical stretch, acidification and GPCR-mediated inhibition (Honore, 2007, Veale *et al.*, 2007a). In this channel, the region plays a structural as well as a modulatory role as it supports the channel in the post-synaptic scaffold (Sandoz *et al.*, 2006).

Novel insights into the VLRFLT region have recently been provided following the publication of the TASK1 crystal structure (Rödström *et al.*, 2019). Until now, K2P channels differed from other potassium channels as they appeared to lack a gating mechanism below the SF, believing that the inner vestibule remained open to this point. A new gating structure, the "*X-gate*," has since been identified in the TASK1 crystal structure in which the VLRFMT portions (analogous to VLRFLT in TASK3) within the fourth transmembrane domain/Ct of each monomer interact as they cross-link in front of the intracellular vestibule entrance (Rödström *et al.*, 2019), taking up a closed conformation (Figure 44).

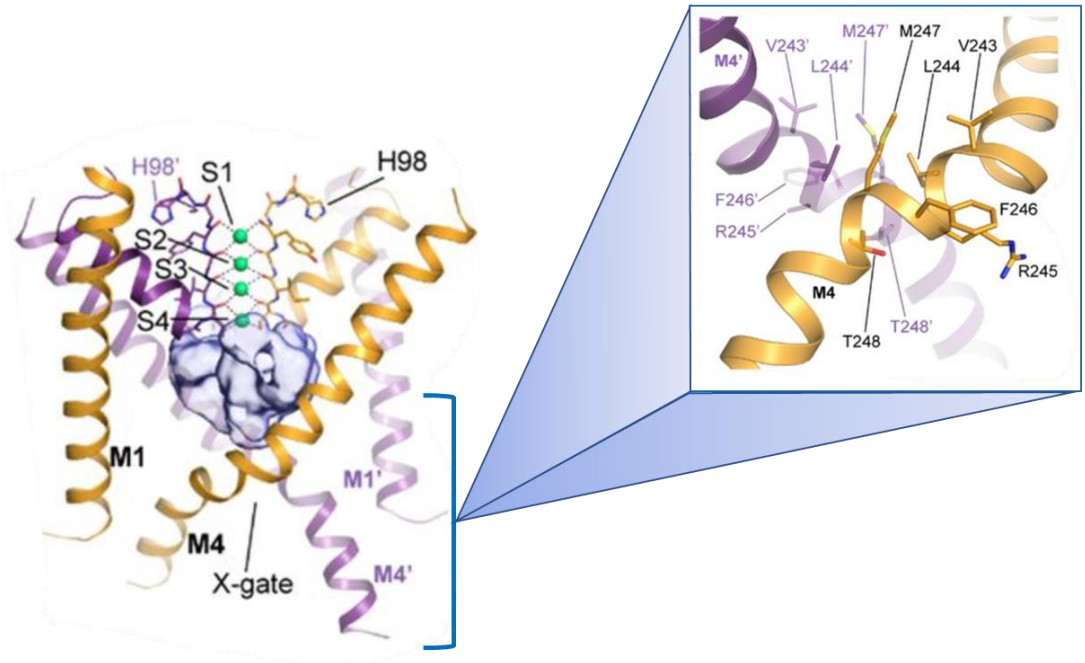

Figure 44 TASK1 crystal structure displays novel 'X-gate' beneath the SF.

View of the crossing TM4 helices from the membrane plane; (inset) Enlarged X-gate structure highlighting position of the VLRFMT residues. Adapted from Rödström et al. (2019).

The X-gate is stabilised by 'hinge' residues Leucine (Leu, L) 241 – Valine (Val, V) 242 and a 'latch' (Asn250) either side of the VLRFMT, creating the bends in TM4 which give it the characteristic 'X' shape. Alanine (Ala, A) scanning mutagenesis across Threonine (Thr, T) 230 – Thr248 (inclusive of the VLRFMT region) observed a 6-fold increase in outward current, with Leu244 at the centre of the X-gate creating the largest effect (Rödström *et al.*, 2019). Mutation of the equivalent residue in TASK3 similarly increased outward current suggesting that these residues are critical in supporting the closed state of the channel in both TASK1 and TASK3. Furthermore, mutations within the X-gate region reduced the sensitivity of the channel to volatile anaesthetics like sevoflurane, proving that the region has an active role in the channels response to activating agents (Rödström *et al.*, 2019). The

TASK3_G236R loss of function mutation directly precedes the hinge residue of the gating mechanism in TM4 and it has been suggested that the insertion of a large positive residue into the vestibule is likely to interfere with the ion conduction pathway (Rödström *et al.*, 2019). The effect of this mutation can be partly overcome by the A237T gain of function mutation (Ashmole *et al.*, 2009) or by application of the non-steroidal anti-inflammatory drug, flufenamic acid (FFA) (Veale *et al.*, 2014). The *Caenorhabditis elegans* protein SUP-9 is a K2P channel which shares a high degree of sequence similarity to TASK1 and TASK3 channel. Mutation of the analogous residue (A236T) in SUP-9 increased the open probability of the channel (Ashmole *et al.*, 2009, de la Cruz *et al.*, 2003). The human TASK1 crystal structure confirmed the existence a hydrogen bond between the carbonyl oxygen of Ala237 on TM4 and Asparagine (Asn, N)133 which disrupts the helical structure of TM4 and stabilises the helical bend created by the hinge residues (Ashmole *et al.*, 2009, Rödström *et al.*, 2019). It is possible that the introduction of Thr at this position prevents this interaction between TM2 and TM4, destabilising the helical bend and promoting the open conformation of the X-gate. Unfortunately, the A237T mutation was unable to overcome the loss of effect of GPCR regulation on the G236R mutated channel and remains inwardly rectifying (Veale *et al.*, 2014). Whilst the A237T mutation may improve K^+ permeability, it is unlikely to rescue G-protein regulation of the TASK3_G236R channel since it fixes the gate in an open position (Ashmole *et al.*, 2009), likely preventing the transduction of a cytoplasmic signal to the SF via TM4 (Bagriantsev *et al.*, 2011, Piechotta *et al.*, 2011). Indeed, presence of A237T in WT-TASK3 is similarly detrimental to the sensitivity of TASK3 channels to regulation by the muscarinic GPCR even in absence of the G236R mutation (Veale *et al.*, 2014). Although it is clear that X-gate is critical to the regulation of TASK channels, the exact function of the VLRF(M/L)T sequence remains unclear. It is possible that the presence of the rigid G236R mutation preceding the hinge alters TM4 conformation in a way which hinders the exposure of the VLRF(M/L)T sequence, preventing potential binding of $G\alpha_q$; alternately, in absence of the A237T gain of function mutation, G236R fixes the X-gate in semi-open/closed state which allows the reduced flow of ions however, the presence of the positively charged arginine near the inner mouth of the channel likely drives inward-rectification rather than outward, as described for calcium-activated K^+ (SK) channels (Li and Aldrich, 2011).

The TASK channel subfamily contributes to the background current in neuronal populations throughout the CNS and are inhibited by $G\alpha_q$-coupled receptors including those for thyrotropin-releasing hormone, serotonin (5-HT), glutamate and acetylcholine (Mathie, 2007). Another such GPCR regulating TASK3 current includes the histamine (H1) receptor underlying wakefulness. Activation of $G\alpha_q$-coupled H1 receptors by the wake-active neurotransmitter histamine, have been shown to inhibit TASK3 channels and this underlies activation of cholinergic neurons by histamine in the basal forebrain (Figure 39) (Vu *et al.*, 2015). Symptoms of low arousal have been reported in patients expressing the

TASK3_G236R mutation (Graham *et al.*, 2016). Whole-cell patch clamp recordings obtained from recombinant TASK3 and TASK3_G236R channels co-expressed with H1 receptors, showed that current through WT-TASK3 channels was inhibited following direct application of histamine. Conversely, inhibition of TASK3_G236R channels following histamine application was significantly attenuated and indeed, a small activation current by histamine was observed. A similar finding was recorded when the TASK3_G236R channel was co-expressed with the $G\alpha_q$-coupled muscarinic (M3) receptor (Veale *et al.*, 2014). Together with the electrophysiological recordings presented in Figure 45, it was confirmed that the G236R mutant is insensitive to $G\alpha_q$-mediated inhibition.

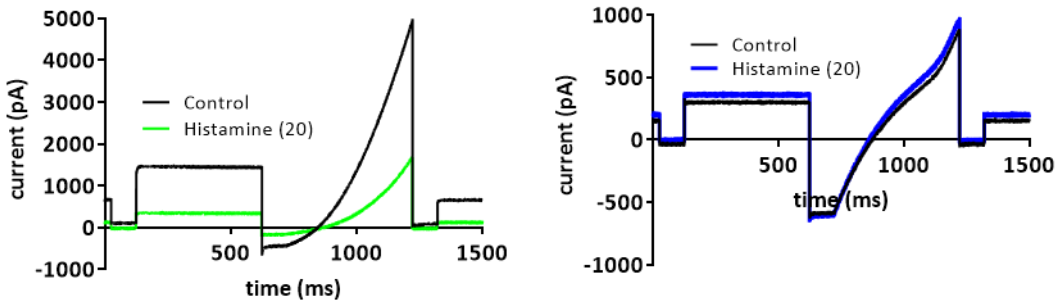

Figure 45 TASK3_G236R channels are no longer inhibited by activation of histamine (H1) receptors

[A] Averaged raw data traces of TASK3 channels co-expressed with H1 receptors was inhibited following activation of receptors by 20 μM of histamine using a step-ramp voltage protocol. [B] Inhibition of TASK3_G236R channels is significantly attenuated ($p < 0.01$) following application of histamine. Unpublished work carried out by Dr E L Veale.

G-proteins are commonly localised to the cytoplasmic face of the plasma membrane where they function as molecular switches (Wedegaertner, 2012), dynamically cycling between active and inactive states in the regulation of many intracellular signalling cascades (Preininger and Hamm, 2004, Dorsam and Gutkind, 2007). As described previously in Figure 10, following activation of the GPCR, GDP is released from the heterotrimeric G protein and phosphorylated at the intracellular face of the plasma membrane allowing the binding of GTP which drives the dissociation of the activated Gα protein from the Gβγ unit (Lambert, 2008). In order to remain bound to the membrane, G-proteins require multiple binding mechanisms to form a 'hydrophobic anchor' (Wedegaertner, 2012). The presence of single membrane binding signal, such as a covalently bound lipid, may offer weak affinity to the membrane alone however, the availability of multiple motifs or sequences may synergize to provide a high affinity, multivalent interaction, otherwise known as the 'two-signal hypothesis' or kinetic trapping (Dunphy and Linder, 1998, Hancock *et al.*, 1990, McLaughlin and Aderem, 1995,

Morales *et al.*, 1998, Resh, 1999, Wedegaertner, 2012). Curiously, an increase was observed in TASK3_G236R_GFP plasma membrane expression following co-expression with both constitutively active $G\alpha_q$ and $G\alpha_{q/11}$, although only the latter was significant ($p < 0.001$) (Figure 43). A similar trend was also detected with the WT-TASK3_GFP although this difference was not significant (Figure 41). Together with the loss of GPCR regulation following histamine and muscarinic activation, this would suggest that the G-protein remains able to interact with the channel directly but is no longer able to regulate the TASK3_G236R channel.

3.6 Conclusions and Further Study

Whilst the X-gate is intricately involved in the regulation of TASK channels, it is important to note that not all regulatory pathways converge and rely upon this region. The polymodal nature of TASK channels means it is likely to be regulated through alternate routes. For instance, application of EC zinc to a TASK3-VLRFLT deletion model results in an inhibition which is indistinguishable from WT-TASK3. Equally, pH sensitivity is shown to be altered in the deletion model yet the His98 proton sensor is present on the extracellular side of the SF (Veale *et al.*, 2007a). Therefore, alternate transduction mechanisms may be present unless it is later found that these two gating mechanisms are coupled.

It can be concluded that whilst less TASK3_G236R channels are expressed at the plasma membrane, this cannot explain all the effects of the mutation on the channel. The inhibition of these TASK3_G236R channels by H1 receptor activation is significantly attenuated despite a proportion of the channels continuing to be expressed. Co-expression of both WT-TASK3 and TASK3_G236R with activated G-proteins both appeared to increase expression of the channels at the plasma membrane, likely due to the hydrophobic anchor of the G-protein at the membrane. This suggests that the G-protein can still interact with the G236R channel but cannot regulate it. Attenuation of histamine inhibition may contribute to the low arousal state seen in patients with *KCNK9* Imprinting Syndrome however, it is now clear that therapeutic strategies which aim to increase TASK3_G236R channel expression at the membrane in this syndrome may fail to overcome all of the functional consequences of the mutation and may in fact be detrimental to the patient.

Therapeutic approaches should therefore focus upon improving channel function. Whilst genetic recovery of the G236R has been demonstrated following the co-expression of A237T, it was unable to reverse all the effects of the disease-causing mutant. Furthermore, genetic modifications by the likes of CRISPR-Cas9 gene therapies are still in infancy stages having only just entered human clinical trials phase. In absence of this therapy in practice, there remains precedents for overcoming the effects of

loss of function mutations using pharmacological manipulation with evidence of pharmacological application of the phospholipase inhibitor, ONO-RS-082, remedying the functional effects of the G203D mutation implicated in PAH (Ma *et al.*, 2013). Identification of the cytoplasmic X-gate has discovered a unique environment for molecular and pharmacological exploration. Whilst this novel gate is important for the control of channel activity, it remains unclear how the region is involved in the transduction of IC signal to functional response and the implications of the G236R mutation on this. Once functional mechanisms like these are determined, we can work towards identifying therapeutics which may at least soothe certain symptomatic effects such as low arousal in *KCNK9* Imprinting Syndrome.

Chapter 4:

Production and Purification of the TASK3 C-terminal Peptide

4.1 Introduction

The demystification of the human proteome offered novel mechanistic insights into function and disease however, the details in the 'how' remain highly sort after as structural determination remains the time-fast technical hurdle. Of the 24,000 genes humans possess, 19 – 20,000 are protein-encoding with 4,800 – 7,200 (20 – 30% of the total genome) encoding membrane proteins in the form of ion channels, receptors, transporters, and enzymes. Membrane proteins represent over half of all known drug targets (Babcock and Li, 2014). Therefore, the identification of structural points of interest will only work to enhance the development of more target-specific drugs, enhancing efficiency and reducing side-effects.

Unfortunately, the structural determination of membrane proteins is notoriously difficult. The first challenge being the removal of an integral membrane protein from the native environment. The cellular environment is complex. Firstly, the lipid membrane accounts for only 6 - 12% of the cytosolic volume, of which the plasma membrane represents only 2 - 5% (Rawlings, 2016). Therefore, the remaining 82% of cell weight is comprised of a highly specialised biochemical environment which stabilises the cell. Secondly, a plasma membrane protein exists in three different physiological environments at any one time: extracellular – intramembrane – intracellular, which equates to further considerations regarding pH and macromolecular organisation amongst others. Moreover, experimental requirements present yet a further problem, with many techniques such as NMR and X-ray crystallography requiring large quantities of pure protein which is expensive in terms of time and resources. Combined, these problems make the validation of topological and functional predictions very difficult and so remain the focus of many labs today.

K2P channel proteins are no exception. Since their first discovery, it took almost 20 years for the first two K2P crystal structures (TRAAK and TWIK-1) to be deposited into the PDB in 2012 (Brohawn *et al.*, 2012, Miller and Long, 2012) and a wait of almost 25 years for a crystal structure of a member of the highly studied TASK family, TASK1 to be published (Rödström *et al.*, 2019). Unfortunately, these structures are incomplete and do not contain information regarding the IC terminal regions, where much of the channels regulatory activity occurs, presenting only the transmembrane portions and the extracellular helical cap. It is common to remove soluble termini prior to crystallization as they are often intrinsically disordered and flexible which is detrimental to the formation of well-diffracting crystals for structural studies (Bertheleme *et al.*, 2013).

As discussed in section 1.5, TASK3 may be regulated by anaesthetic activation (Talley and Bayliss, 2002b), methanandamide inhibition (Veale *et al.*, 2007a), as well as hormones and transmitters which are all suspected to act through the intracellular Ct via GPCR activation of $G\alpha_{q/11}$ (Mathie, 2007). It was originally believed that TASK channels were activated by PIP_2 and inhibited by GPCR-induced PIP_2 depletion as was the case for K_V and K_{IR} channels (Czirják *et al.*, 2001, Chemin *et al.*, 2003, Lopes *et al.*, 2005) however, the confidence in these hypotheses was shaken when it was suggested that $G\alpha_{q/11}$ instead binds directly to the channel (Chen *et al.*, 2006, Veale *et al.*, 2007b, Zhang *et al.*, 2016). This led to a debate regarding the required necessity of PLC and PIP_2 in the inhibition of TASK until the application of DAG (a downstream product of $G\alpha_{q/11}$ activation and PLC) to DAG-depleted inside-out excised patches still resulted in the inhibition of TASK channels (Wilke *et al.*, 2014), thus maintaining their relevance to inhibitory mechanisms.

The presence of 6 amino acids 'VLRFLT' in the extreme proximal portion of the Ct has proven to be essential for modulation of channel activity (Wilke *et al.*, 2014, Veale *et al.*, 2007a, Talley and Bayliss, 2002b) with deletion abolishing halothane-induced activation and GPCR-inhibition and mutations to this motif serving to diminish these effects (Talley and Bayliss, 2002b). Furthermore, deletion of the VLRFLT motif has been shown to alter the pH sensitivity of the channel. Considering the locations of the motif in the IC Ct domain and the EC His98 proton sensor, this suggests that alterations to internal gating mechanisms are coupled to EC modulation. Such mechanical coupling has been observed in *Drosophila KCNK0* channels in which phorbol ester-mediated regulation of IC pathways influences EC modulation by Zinc (Zilberberg *et al.*, 2001). Interestingly, the deletion of the VLRFLT motif had no effect on zinc inhibition of TASK3 channels and so it can be concluded that this motif does not underpin all the regulatory pathways of this channel (Veale *et al.*, 2007a).

The VLRF(L/M)T (TASK1/TASK3) motif has recently been implicated in the formation of the novel 'X-gate' which lies on the cytosolic side of the SF (Rödström *et al.*, 2019). Until now, unlike most potassium channels, K2P channels lacked a lower gate on the IC side of the SF. The TASK1 crystal structure revealed a lower gate formed by the interaction of the VLRFMT domains within the Ct of each monomer, crossing over to form the 'X'-like structure. As discussed previously in section 3.5, mutations occurring within and around this motif drastically effect the open probability of the channel and reduce channel's sensitivity to volatile anaesthetics (Rödström *et al.*, 2019). Loss of function variants of TASK channels are associated with diseases like PAH (Ma *et al.*, 2013, Navas *et al.*, 2016) and *KCNK9* Imprinting syndrome (Barel *et al.*, 2008, Veale *et al.*, 2014). Such variations cause mutations which occur around the X-gate leading to pathologic reductions in outward current and an inability to respond to GPCR regulation. Whilst this region is clearly significant to channel function, it is unclear whether the VLRFLT (in the case of TASK3) motif participates as a transducer of signal to the

gate or, as a direct binding site of modulatory molecules. Due to the diverse range of modulatory molecules known to induce an effect on the channel and the wide range of channels these molecules can act upon, the former is most likely (Veale *et al.*, 2007a). In support of this, work carried out by Andres-Enguix *et al.* (2007) found that the *Lymnaea* orthologue of hTASK1 (LyTASK) was also highly responsive to activation by general anaesthetics with additional stereoselectivity. Mutating the six analogous amino residues of LyTASK to that of hTASK1 resulted in anaesthetic sensitivity reflective of hTASK1 yet, the stereoselectivity remained. This supports the idea that the VLRF(L/M)T residues are critical to sensitivity but are unlikely to function as a binding site (Veale *et al.*, 2007a).

4.2 Aim and Objectives

The aim of this chapter was to produce and purify the hTASK3 Ct peptide inclusive of the VLRFLT motif in order to investigate its functional capacity. The overall objective of this chapter was to use recombinant protein expression methods to produce a functionally active and conformationally correct hTASK3 Ct peptide to test the significance of the VLRFLT motif in protein-protein interactions in the following chapter. The first objective was to identify optimal expression conditions of the BL21 (DE3) *Escherichia* coli (*E*.coli) bacteria by varying the temperature and time of the induction phase until the highest concentration of protein was achieved. The second objective was to effectively purify and store the protein in a way that it remains stable in solution using a variety of chromatographic and electrophoretic techniques. Finally, the third objective used a combination of dynamic light scattering and circular dichroism to confirm that the protein existed homogenously in solution in a conformationally correct state.

4.3 Methods

4.3.1 Transformation

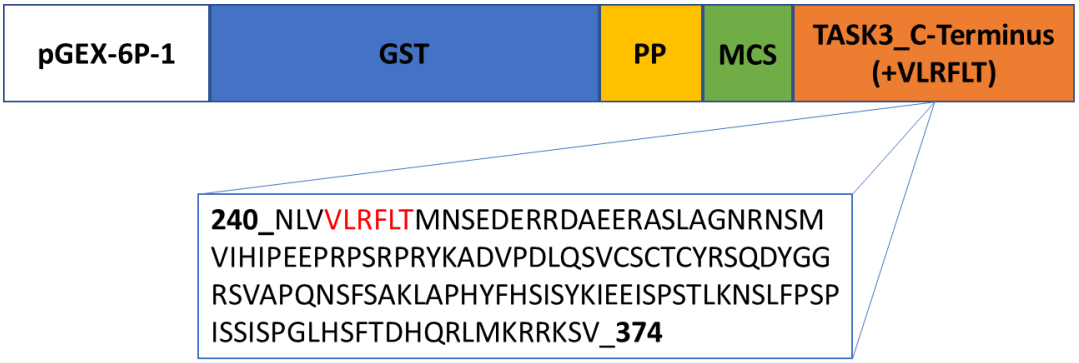

Figure 46 Schematic displaying the TASK3_C-Terminus (+VLRFLT) construct design

The peptide sequence is subcloned within the multiple cloning site (MCS) and fused to a glutathione-S-transferase (GST) tag. The pGEX-6P-1 vector contains a cleavage site for Precision Protease ™ (PP) for specific removal of the GST tag following purification.

The TASK3_C-terminus (including VLRFLT) insert (AA240–374) was cloned into the multiple cloning site (MCS) of the pGEX-6P-1 vector (Genscript) (Figure 46) with ampicillin (AMP) resistance. The plasmid was transformed in competent BL21 (DE3) *E*.coli under control of the isopropyl-β-D-1 thiogalactopyranoside (IPTG)-inducible tac-promoter, engineered alongside a *lac* repressor protein that binds the DNA operator sequence and prevents access of RNA polymerase to the promotor site. IPTG resembles the galactose sugar structure and is added to the solution when the conditions are correct for protein expression as it binds to the *lac* repressor protein causing a conformational change which reduces its binding affinity for DNA. This feature allows for controlled expression as RNA polymerase once again has access to the promoter site in order to transcribe the target gene. PGEX6P-1 aids high-level expression of fusion proteins however, in suboptimal conditions basal levels of expression from a lac promoter and the tac promoter may interfere with the isolation of clones containing the insert in the proper orientation. An outcome which may persist if the insert is toxic to the host. Basal-level expression, from the *lac* promoter was minimised via the incorporation of the catabolite glucose into the SOC growth medium (Appendix 3.2).

Competent BL21 (DE3) (Novagen, EMD Millipore) (~100 µL) were removed from -80°C and defrosted on ice. The cell aliquot was transferred to a 15 mL falcon. Plasmid stock concentration was 50 ng/µL. A working concentration of 100 ng of TASK3_(+VLRFLT) plasmid was added to cells and mixed prior to incubation on ice for 30 minutes (mins). Cells underwent heat-shock in a bath pre-warmed to 42°C for 37 seconds (sec). The falcon tube was briefly returned to ice for 2 mins and recovered with 600 µL of

LB/SOC media. Cells were incubated for 1 hour (hr) at 37°C/220 rates per mins (rpm). An ampicillin (AMP) agar plate was equilibrated to room temperature (RT). Following incubation, cells were centrifuged at 4000 rpm/10 mins/RT. Having discarded 400 µl of the supernatant (SN), the pellet was resuspended in the remaining SN and 200 µL spread onto the AMP agar plate which was left to set at RT for approximately 20 mins before being transferred to 37°C overnight (ON).

4.3.2 Starter Culture

The following morning, the plate was checked for single colonies prior to being placed at 4°C until late afternoon in preparation of the small ON culture. For the cultures, 10g of LB Broth (Sigma, USA) was dissolved in 500 mL in double-distilled water (ddH_2O). The media was sterilised using a Stericup and Steritop (0.22 µM) Vacuum driven Sterile Filter™ (Merckmillipore, USA). AMP (stock concentration: 1000 µg/mL) was removed from -20°C and the plate from 4°C and allowed to equilibrate to RT. Into each of two 14 mL propylene, round-bottomed culture falcons (Falcon), 5 mL of LB broth was added followed by AMP to a final dilution of 1:1000. A -single colony was transferred into each of the culture falcons and placed at 37°C/220 rpm/ON.

4.3.3 Induction

AMP was removed from -20°C and the small cultures removed from the incubator. The Nanodrop™ 2000C spectrophotometer was used to measure optical density (OD) of the starter cultures. Into one cuvette 600 µL of LB broth was added, serving as a blank. Into two other cuvettes, 540 µL of LB broth and 60 µL of the respective starter culture was added to obtain a 10x dilution (OD >1 falls outside of the linear range of detection). OD was measured, ensuring to blank first. IPTG induction requires a starting OD of 0.1 and so it is necessary to determine the appropriate dilution factor. To 100 mL LB in a 500 mL conical, 100 µL AMP and the appropriate volume of starter culture was added. Growth rate of the culture was checked every hour (approximately 2 hrs) until a desired induction OD of 0.6-0.8 (exponential growth phase) was reached. IPTG was added to the culture at a final concentration of 1 mM and placed at 30°C/220 rpm. Cells were harvested 3 hrs post-induction, as determined to be the optimal conditions. The culture was transferred to two 50 mL falcons and spun down in a pre-cooled centrifuge at 4°C/4000 rpm/20 mins. The SN was discarded, and the cell pellet frozen ON at -20°C or until ready for lysis.

4.3.4 Solubilisation

Cell pellets were defrosted on ice for 30 mins. Working on ice, 30 mL of 1X PBS solution was added to one pellet and pipetted to dissolve. This solution was transferred to the other pellet and pipetted once again to dissolve. Cells were lysed using sonication: 5-min experimental time, 30 sec pulses on/off at 80% amplification. Following sonication, a 30 µL ('total protein') sample was collected for gel analysis. Initially, four different solubilisation buffers were trialled: 8M Urea, 6M Guanidinium (GuHCl), 1M Urea or 1M GuHCl. Into four labelled Eppendorf tubes, 1 mL of sonicated solution was added to each. In a pre-cooled centrifuge, samples were spun at 4°C/13500 rpm (maximum)/10 mins. From one of the centrifuged samples, 30 µL of SN was removed and placed in a new Eppendorf tube labelled: PBS. All remaining SN was removed from cell pellets and placed in a falcon tube. Expression tests showed the protein to be insoluble in phosphate-buffered saline (PBS), the protein was suspected to be contained within the cell pellet. Each pellet was resuspended in 1 mL of the respective solubilisation conditions prior to centrifugation at 4°C/13500 rpm/10 mins. Resulting SN was transferred to freshly labelled Eppendorf tubes and stored on ice.

4.3.5 Guanidinium (GuHCl) Precipitation

To avoid the precipitation of GuHCl in presence of sodium dodecyl sulphate (SDS) and interference on the gel, 25 µL of each sample SN was collected and transferred to labelled Eppendorfs prior to addition of 225 µL ice cold ethanol. These samples were vortexed and incubated at -80°C for 10 mins followed by centrifugation at 4°C/13500 rpm/5 mins. The SN was discarded, the pellet suspended and mixed thoroughly in 250 µL ice cold ethanol to remove remaining traces of GuHCl. Samples were spun at 4°C/13'500 rpm/5 mins before SN was removed and the pellet air dried prior to resuspension in 25 µL PBS.

4.3.6 Sodium Dodecyl Sulphate Polyacrylamide Gel Electrophoresis (SDS-PAGE)

To each 25 µL of sample following GuHCl precipitation, 25 µL of SDS sample Buffer (2X) was added and inverted to mix. Samples were boiled for 5 min (100°C). A 12%, 15 well precast gel (BioRad™) was loaded into a cassette and tank before the central reservoir was filled with running buffer. Into each well, 13 µL of each sample (5 µL of the Amersham Blue™ Mwt marker (BioRad™)) was loaded whilst remaining wells were filled with sample buffer. The samples were stacked at a voltage (V) of 120 until linear prior to increasing voltage to 170 V until the gel was complete (approximately 40 mins). On

completion, the gel was removed and submerged in staining solution on a rocking table for 15 mins before transfer into de-staining solution for 15 mins. De-staining solution was refreshed and left on rocking table ON for development.

4.3.7 DNA Precipitation

The samples were further purified via precipitation of contaminant DNA. From a 10% stock Polyethyleneimine (PEI) solution, PEI was added to the protein solution at a final concentration of 0.2%. Care was taken to add PEI in small increments with gentle stirring between additions. The solution was left on the bench for approximately 20 mins at RT. Following the rest period, the sample was centrifuged at RT for 1 hour/20000 rpm and the SN collected.

4.3.8 Protein Precipitation

Ammonium Persulfate (APS) (228.18 g/mol) was added to a total of 65% solution saturation. This was calculated using software provided by Encorbio (http://www.encorbio.com/protocols/AM-SO4.htm). APS was crushed to remove crystals. APS was added gradually at RT. Solution was stirred for a minimum of 1 hr however, best results were obtained following an ON-stirring period, or until completely dissolved. The solution was split evenly into two centrifuge vials and filled with ddH_2O to aid pellet formation. Samples were centrifuged at 4°C/17000 rpm/3 mins. The pellet at this stage is extremely delicate so SN was immediately discarded, and the pellet kept on ice. Next, one pellet was resuspended in 5 mL of 8M urea solubilisation buffer, transferred to the other pellet and again resuspended. Using a 0.22 µM filter syringe the sample was filtered, and protein concentration determined using 2 µL of sample on the Nanodrop™. The Nanodrop™ (baseline wavelength nano meter (nm) correction: 340 nm) provides protein concentration (A280) in mg/mL with an A260:280 ratio value. The ultraviolet (UV) 260:280 ratio signifies level of deoxyribose nucleic acid (DNA) contamination in the sample; a reading of <1.0 is considered acceptable. Protein peaks maybe visible at both 230 nm/280 nm whilst DNA absorbs at 260 nm. All the collected protein was diluted in an arginine-based refolding buffer to obtain an approximate concentration of 0.1 mg/mL and left ON at 4°C.

4.3.9 Glutathione-S-Transferase Column

A Glutathione-S-Transferase (GST) column was attached to the chromatography system and the column/sample pump washed through with PBS. The Column was set at a perfusion rate of 2 mL/min. The refolded sample was re-filtered using a 22 µM syringe filter. The column was equilibrated for approximately 5 X maximum volume (25 mL) or until all parameters remained constant. The sample was injected, flow-through (FT) collected and the column washed with PBS following complete loading. Elution buffer (reduced glutathione – Appendix 3.3) was then applied, and appropriate samples collected.

4.3.10 Size Exclusion Chromatography

Size exclusion chromatography (SEC) was carried out using an AKTA Purifier 100 HiLoad 16/60 Superdex 75 Prepgrade (PG) (120 mL) column with a maximum detection weight of 75 kilodalton (kDa) and 4 mL fraction volume. Rate of elution was compared to a set of standards with known Mwt and elution rates for reference.

4.3.11 Strong-Q Anion Exchange Chromatography

Two sample buffers were prepared for the Strong Q-column anion exchange chromatography (QC):

Buffer A (500 mL): 25 mM HEPES/70 mM NaCl (pH 10)	Buffer B (500 mL): 25 mM HEPES/1 M NaCl (pH 10)
12.5 mL HEPES 7 mL NaCl (5 M) 2.2 mL NaOH (4 M)	12.5 mL HEPES 100 mL NaCl (5 M) 2.2 mL NaOH (4 M)

The anion QC was washed and equilibrated first with three column volumes (60 mL) of a combination of sample buffers (A and B) prior to column activation with sample buffer A for 3 column volumes. Once the sample had finished loading, the column was briefly washed with sample buffer A, before a sample B concentration gradient to 100% was executed.

4.3.12 Dynamic Light Scattering

Size of protein (aggregates) was estimated using the DynaPro – Nanonstar (WYATT) at 25°C. In 10 µl, sample was diluted 1:20 in 4-(2-hydroxyethyl)-1-piperazineethanesulfonic acid (HEPES) buffer ranging in pH from 10 to pH 6 or PBS.

4.3.13 Circular Dichroism

Conventional circular dichroism (CD) spectra were measured on a Chiracscan (v.4.2.15) spectrometer calibrated with HEPES buffer. Measurements were collected under the following parameters: 1 mm path length cell, 1 nm increments, 0.5 second integration time and a 0.5nm bandwidth at 4°C. Spectra were measured in the wavelength range of 260 to 190 nm.

4.4 Results

4.4.1 Protein is Solubilised only by 8 M Urea

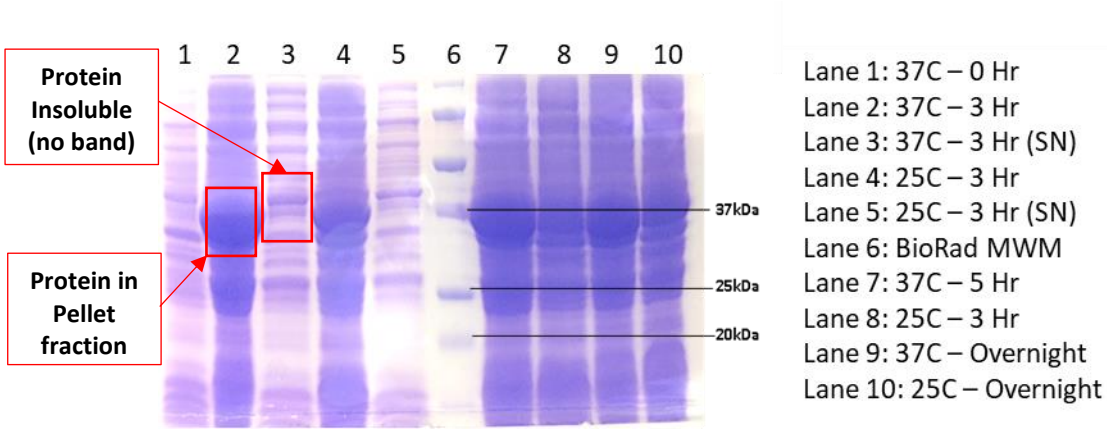

Figure 47 The TASK3 peptide is most efficiently expressed at 3-5 hours post induction at 37°C

An SDS-PAGE gel demonstrating the different induction conditions trialled for the expression of (+VLRFLT) TASK3 in BL21 E. coli. Lane 1 shows no prominent expression at approximately 43 kDa immediately after induction. Lane 2 shows significantly more expression at 43 kDa, after 3 hours incubation at 37°C after induction. The protein is not soluble, confirmed by lack of protein band in the supernatant fraction (lane 3). Lanes 4 and 5 show a similar expression rate following a 3-hour incubation at 25°C however protein remains equally insoluble. At 5-hours in 37°C (lane 7) not much more protein is expressed compared to 3-hours in lane 2. The conditions observed in lanes 8 – 10 were equal or less.

Initial expression tests showed that protein expression was highest 3 – 5 hours post induction at 37°C, although the product did not appear to be soluble (in PBS) as seen by the absence of bands at predicted molecular weight of 43 kDa in the supernatant (SN) fractions in Figure 47. Following recombinant expression, *in vitro* denaturation & refolding of the protein was carried out in attempt to resolubilise. Chaotropic denaturants: urea and GuHCl, were used in attempt to partially unfold the peptide by disrupting the hydrogen bonding network between water molecules to reduce the stability of the protein's native state by weakening the hydrophobic effect. The protein remained insoluble in 1M urea/GuHCl and precipitated out of solution as can be seen by the lack of bands in lanes 5 and 6 of Figure 48. Whilst the protein is marginally solubilised in 6M GuHCl (lane 10), solubilisation occurs most efficiently in 8M urea as evidenced by the prominent band at approximately 43 kDa in lane 8. Under such conditions most, if not all, proteins denature and require a refolding phase to be included in protein production.

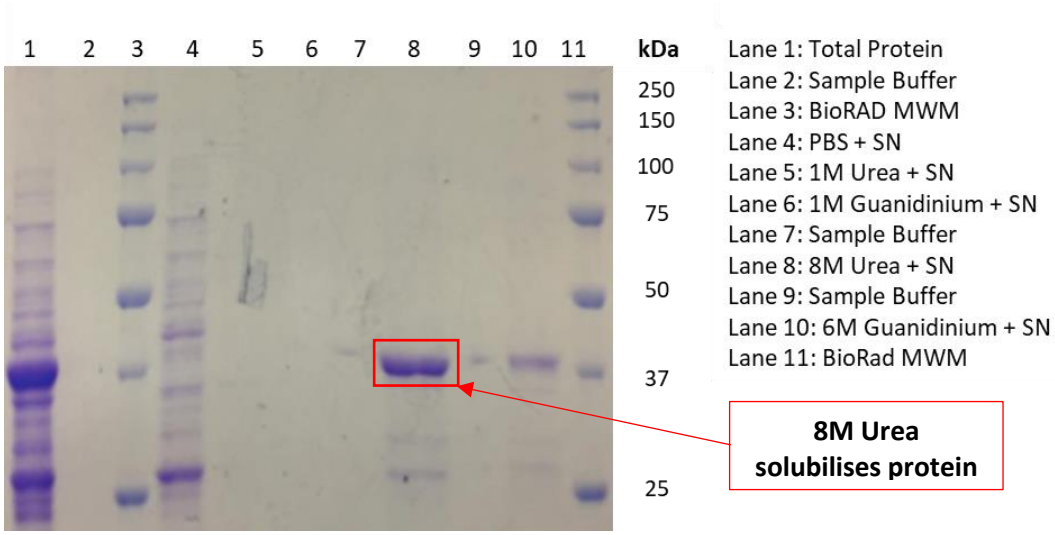

Figure 48 The TASK3 peptide is most efficiently solubilised in 8M urea

An SDS-PAGE of the trialled solubilisation conditions, specifically chaotropic agent's urea and GuHCl at varying concentrations. Lane 1: total protein sample collected after bacterial sonication. Lane 3: molecular weight marker (MWM). Lane 4 shows no prominent protein band at approx. 43 kDa in PBS suggesting that the peptide is insoluble in PBS. Lanes 5 and 6 shows that peptide is equally insoluble in 1M urea and GuHCl respectively by lack of band. Protein is most successfully solubilised in 8M (lane 8) which is clearly more intense than solubilisation in 6M GuHCl (lane 10). MWM is in kDa (lane 11).

4.4.2 GST Tag Cleavage upon Exposure to PBS

To purify the protein, it was loaded onto a GST column utilising the GST-tag present in the pGEX-6P-1 vector (Figure 49). Following first application of elution buffer (10 mM reduced glutathione), no significant elution peak was observed and DNA contamination (260 nm absorbance) was apparent despite previous Nanodrop™ confirmation of no contamination. This suggested an error in the refolding phase despite visible absence of protein precipitation in solution prior to the column. It was suspected that the protein remained bound to the column. To investigate the latter, flow rate was decreased to 0.5 mL/min to increase binding time, and concentrations of tris(hydroxymethyl)aminomethane hydrochloride (TRIS-HCl) and reduced glutathione in the elution buffer were increased to 150 mM and 30 mM respectively. The pH of the elution buffer was adjusted with the addition of TRIS-Base® as opposed to salt (NaOH) to prevent interference. Elution was repeated with the revised buffer resulting in a diffuse peak Figure 49, with low 280 nm absorption despite a high protein concentration observed prior to the refolding process. Post-refolding Nanodrop carried out on the collected A3 fraction (blanked against the new elution buffer) confirmed no DNA contamination as evidenced by lack of a 260 nm absorption peak but is instead likely a case of glutathione absorbance. Whilst protein concentration at this stage appeared low (400 µg/mL), it was

consistent with the small bacterial culture it was derived from (100 mL). SDS-PAGE Gel was carried out to determine the origin of the peak.

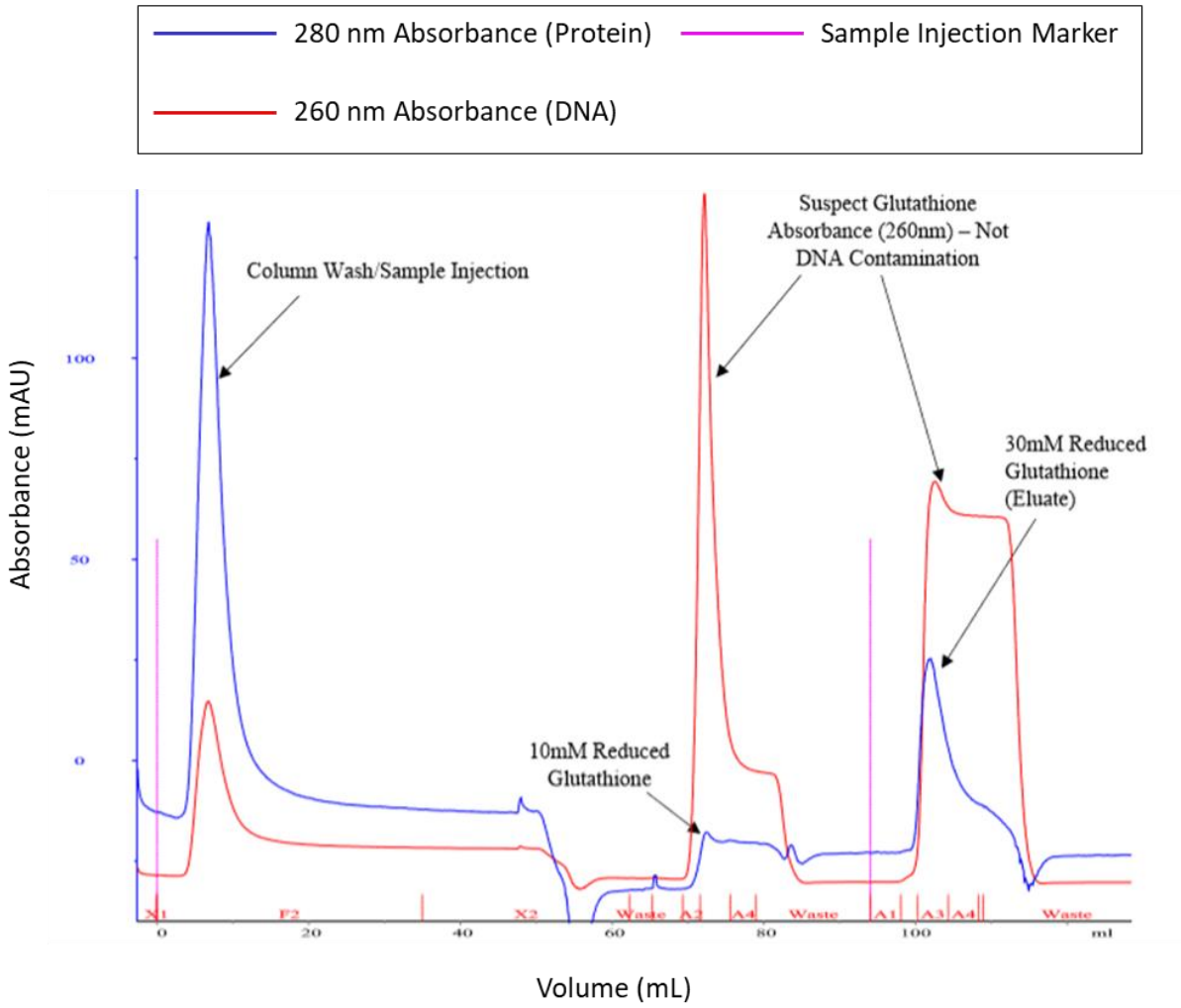

Figure 49 The GST column used for peptide purification was unable to elute the protein following application of 10mM reduced glutathione

The product was only eluted upon application of 30 mM reduced glutathione as observed in the second significant blue peak. Blue trace: UV 280 nm, wavelength at which protein absorbs; red trace: UV 260 nm, wavelength at which DNA is absorbed. Elution with 10 mM reduced glutathione was unsuccessful. Repetition of elution using a 30 mM reduced glutathione. Fraction A3 following elution by 30 mM reduced glutathione was collected.

In Figure 50, GST-tagged protein remained in the flow through (FT) in lane 3, whilst the protein appears to have been cleaved during chromatography as identified by a GST band present at 28 kDa and the absence of free TASK3 at 15 kDa in lane 4 (Figure 50). It was suspected that the TASK3 portion had ran from the gel or precipitated into the column upon cleavage of the GST fragment which transfers solubility. Alternately, the entire sample may have been in the FT and there may be excess free-GST

within the column left from a previous experiment. Regardless, the lack of binding to the column could be due to poor refolding of the GST itself or structural interference of the TASK3 protein with the GST binding motif.

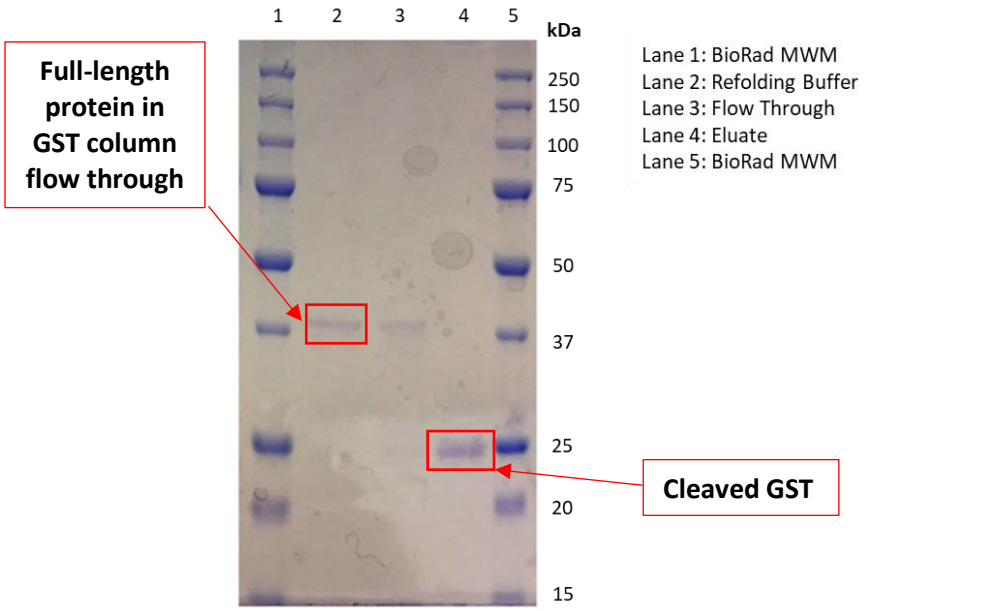

Figure 50 An SDS-PAGE gel analysing the GST column flow through and eluate suggests the peptide is cleaved upon exposure to PBS (pH 7.0)

Lanes 2 and 3 show that the GST-tagged peptide remains in the flow through as well as the eluate, evidenced by the bands at 38 kDa. Lane 4 shows the eluate (fraction A3 from figure 45) contains cleaved protein in the form of free-GST suggesting free-TASK3 has either precipitated into the column or has run from gel. Mwt marker is in kDa (lane 1 and 5).

Size exclusion chromatography (SEC) was carried out using an AKTA Purifier 100 HiLoad 16/60 Superdex 75 Prepgrade (PG) (120 mL) column with a maximum detection weight of 75 kDa and 4 mL fraction volume. SEC is a chromatographic method used to separate molecules in solution by size. Larger proteins are excluded from gel matrix as they have less volume to traverse and elute sooner; whilst smaller proteins are permitted to enter the gel matrix and with more volume to traverse, they elute later. Rate of elution is compared to a set of standards with known Mwt and elution rates for reference. SEC was first carried out on the GST column (un-concentrated) FT using a Superdex 75 10/300 GL column (Appendix 2.1) as this appeared to contain the full length protein as seen in lane 3 (Figure 50). Elution rate of Ovalbumin (43kDa) (approx. 11 mL) was used as a reference for the elution of TASK3. Whilst a peak was present at the suspected elution point (Appendix 2.1), the protein concentration of the FT peaks was low (A280: 0.124 mg/mL; 280:260 of 1.5) so the sample was concentrated, and SEC repeated to amplify the signal. The FT sample was concentrated using a Sartorius Viva Spin 20 concentrator by centrifugation at 4°C/3700 rpm for approximately 3 hrs (checked every hr until a volume of 3 - 5 mL was obtained). Nanodrop™ reading of the concentrated

FT determined protein concentration to be 3.27 mg/mL (280:260 of 1.25). The large (4 mL) loop was attached to the HiLoad 16/60 Superdex 75pg column and 2 mL of sample injected at a flow rate of 0.6 mL/min; fraction size collected was set to 3 mL (Figure 51).

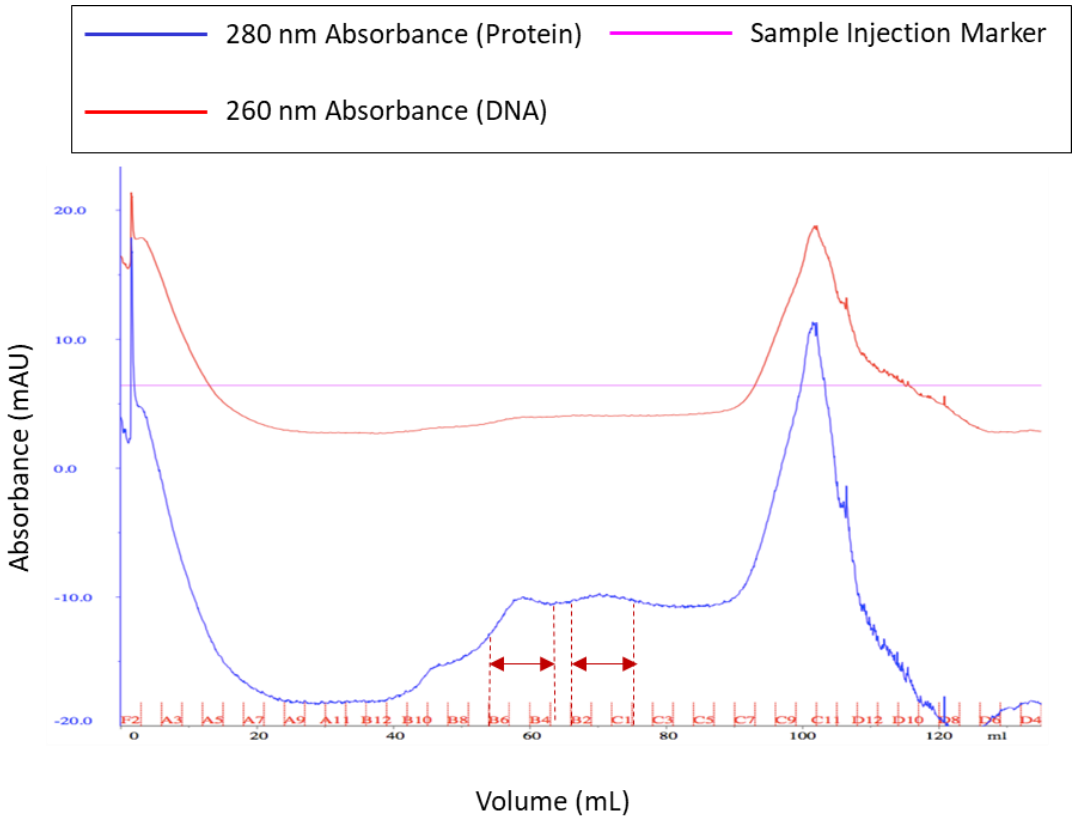

Figure 51 Following concentration of the GST column flow through collected in Figure 17, the SEC graph suggests the peptide has denatured in solution

Two minor broad peaks (red arrows) were observed around the estimated elution volume for this column (60 mL). Fractions B6B5B4 and B2B1C1 (see red fractions on X-axis) were collected to run on a gel. The large 280 nm (blue)/260 nm (red) absorption peaks at 100 mL suggests the protein has degraded/precipitated out of solution.

The chromatographic separation and calibration curve for the standard protein on the HiLoad 16/60 Superdex 75 pg column inferred that TASK3 protein was expected to elute at approximately 60 mL. The SEC graph of the concentrated GST flow through (Figure 51) displays two minor peaks around this volume (see fractions: B6-B4/B2-C1). Whilst it is likely that these fractions may contain the protein, the high 260 nm absorbance suggests DNA contamination through binding to the protein. Observation of a peak later than 100 mL was unexpected since it minimally coincides with Aprotonin (Mwt: 6.5 kDa), yet the Sartorius viva spin 20 concentrator has molecular cut-off of 5 kDa. Taken together, seemed the protein had degraded. Regardless, fractions: B6B5B4 and B2B1C1 were pooled and concentrated using the 6 mL volume Sartorius concentrator and centrifuged at 4°C/3700 rpm for approximately 3 hrs until a volume of 1 mL was obtained. Nanodrop™ confirmed fractions B6B5B4

had a final concentration of 0.432 mg/mL (280:260 of 0.66) and fractions B2B1C1 a concentration of 0.219 mg/mL (280:260 of 0.71) following concentration. Samples of each were loaded onto a gel for SDS-PAGE (Figure 52).

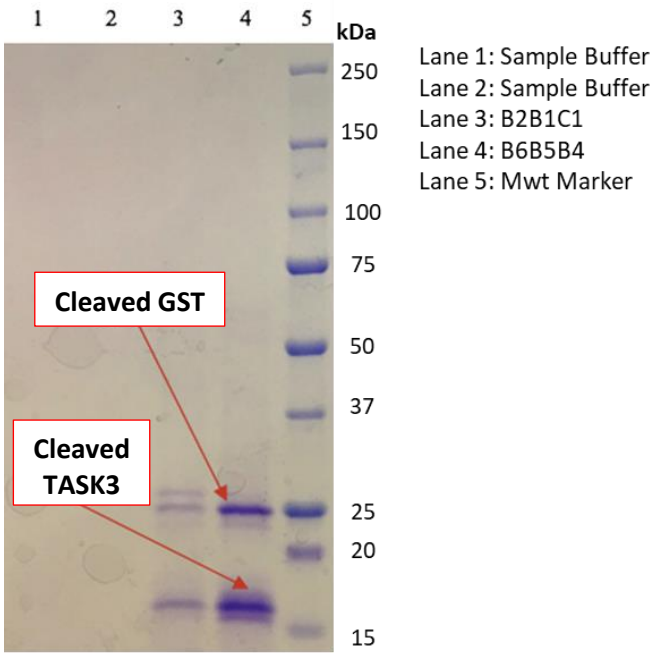

Figure 52 SDS-PAGE confirms protein is cleaved during the GST column purification stage

Lanes 1 and 2 are empty. The B6B5B4 and B2B1C1 elutions collected from the previous SEC of the concentrated GST-column flow through shows that the protein is cleaved as demonstrated by bands present in lanes 3 and 4 at 25kDa and 15kDa indicative of free-GST and TASK3 respectively. Mwt marker is in kDa.

The B6B5B4 fraction collected from the SEC at the correct volume clearly contained both cleaved protein and GST as seen in lane 4 (Figure 52). The protein was whole following refolding but was cleaved during GST column purification.

It is sometimes the case that high-level expression of foreign fusion proteins in *E*. coli may result in the formation of insoluble inclusion bodies that consist of aggregated proteins in complex with ribonucleic acid (RNA). This interferes with the ability of detergents to solubilise proteins.

In attempt to improve the solubility of the GST-tag, a new transformation was carried out with the following adjustments as suggested in literature (Saluta and Bell, 1998):

- Growth temperature reduced from 37°C to 20°C
- Reduced induction period from 3 hours to 1.5 hours (O_D: 0.6)

- Inducing at a higher cell density (O_D: 2.0) for a shorter period
- Increasing culture aeration (minimum of 1:5 volume)
- Rat lysate buffer as suggested by (Zuzarte *et al.*, 2009)

Two 50 mL cultures and one 500 mL culture were produced from three 5 mL starter cultures and grown ON at 37°C. Each 50 mL culture was induced with 1mM IPTG at 20°C for a period of 1.5 hrs, except one had a starting O_D of 0.6 and the other an O_D of 2.0.

The protein remained insoluble in PBS as evidenced by lack of bands in the SN samples (lanes 5 and 7) in Figure 53, despite altering expression conditions. Protein also remained insoluble in Triton-X-100 buffer and expression was strongest with induction carried out at 37°C for 3 hrs. The next expression test moved forward using the pellet obtained from the Triton-X-100, 500 mL culture since the protein was absent in the SN and was denatured in 8M urea as before. At this stage, two different refolding buffers were trialled: an arginine-based buffer versus PBS overnight.

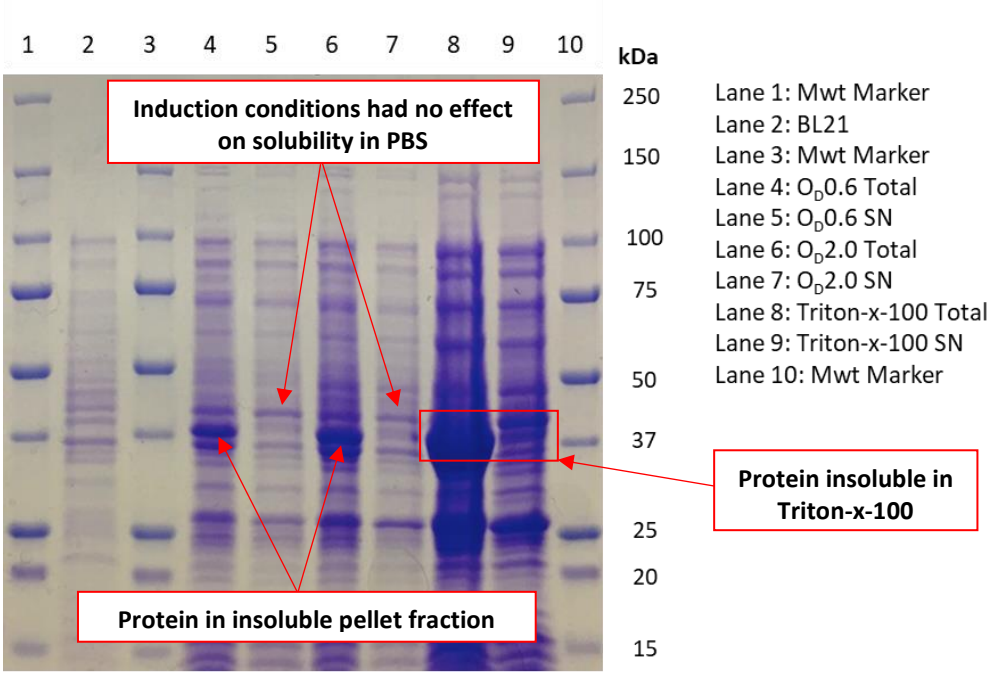

Figure 53 SDS-PAGE following a new peptide expression test in attempt to increase solubility of the GST tag confirms the protein remains insoluble in PBS and Triton-X-100

Lane 2: Pre-induction starter culture. Adjusting induction conditions had no effect on protein solubility in PBS as seen by the lack of bands at 43 kDa in lanes 5 and 7 as the protein remains in the insoluble pellet fraction in lanes 4 and 6. Protein is equally insoluble in Triton-X-100 solution in lanes 8 and 9. Expression remains strongest at 3 hrs/37°C/OD: 0.6-0.8. Mwt marker is in kDa (lanes 1, 3 and 10)

To avoid the use of a GST column for purification and subsequent protein cleavage, the protein was dialysed to remove traces of arginine from the refolding buffer prior to attempting Q-column (QC) exchange chromatography. Since the protein is currently at a pH above the isoelectric point (PI), it would bind to a positively charged anion exchanger and therefore, a Q-strong anion exchanger was used. The initial salt concentration of the protein solution was 200 mM, whilst total salt concentration of sample buffer B was 1M [NaCl]. The protein eluted at approximately 82% of sample B. Due to a lag caused by system dead space, it was more appropriate to refer to conductivity, which suggested that protein was truly eluted at approximately 400 mM NaCl (Figure 54). Fractions A12-B12 were collected for SEC and fractions B10-9, B8 and B7-6 were also collected for gel peak identification.

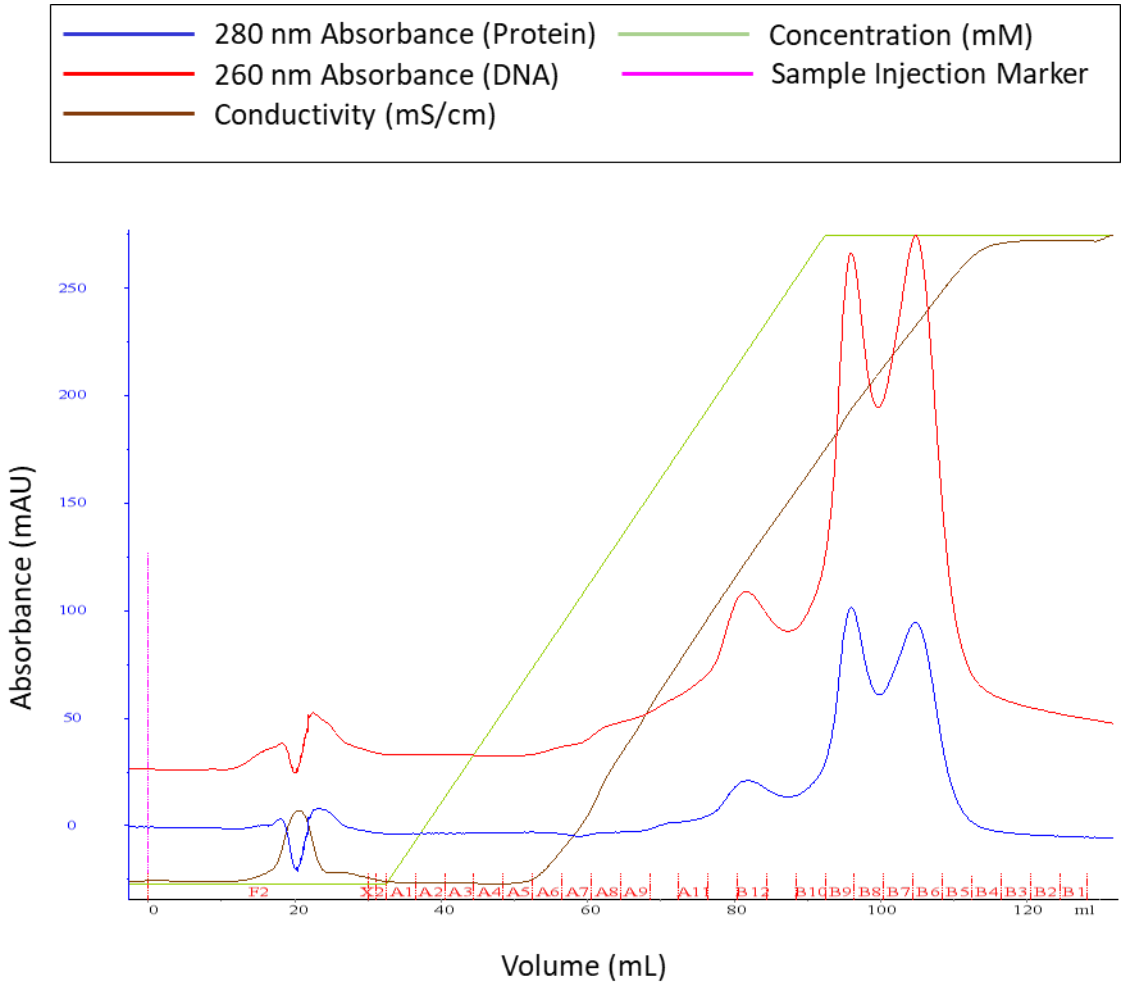

Figure 54 To avoid the use of a GST column, Strong QC Exchange Chromatography was carried out on the refolded protein following denaturation by 8M Urea

The protein began to elute at approximately 80% of sample B application (green trace) however in the event of lag caused by system dead space, conductivity (milli-siemens (mS)) (brown trace) is referred to for elution. Protein eluted at approximately 400 mM NaCl. Fractions A12-B12 were collected for analysis. The blue trace: 280 nm absorption and red: 260 nm absorption

The below gel (Figure 55) suggests that despite some cleavage, as displayed faintly by bands at 28 kDa in lane 6, stable, full-length protein at the correct Mwt was also present however, the product was very dilute. For this reason, eluates A12-B12 were concentrated to 1 mL prior to application on SEC for confirmation and GST column for investigation of binding capacity. A 500 µL sample was loaded onto both. Fractions B10-9, B8 and B7-6 produced no protein bands, suggesting that the later peaks on the GST column were just noise.

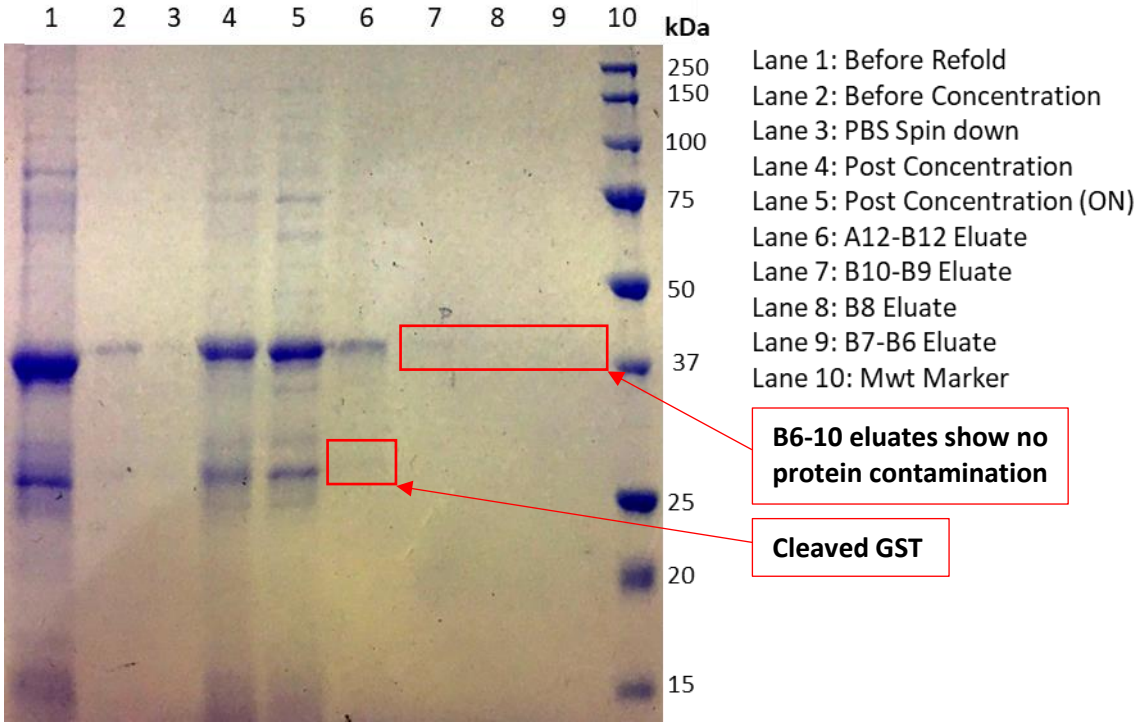

Figure 55 Following QC in HEPES buffer, the TASK3 peptide appears whole and reasonably pure

The gel shows that protein is whole at the expected Mwt in lane 1 following denaturation and prior to refolding. Following refolding, the sample required concentrating prior to application on the QC (see weak band in lane 2). Lane 3 highlights the unsuitability of PBS for the refolding phase supporting the solubilisation of the peptide as the lack of band points towards the precipitation of the protein. Following the arginine refold and concentration, the protein band in lane 4 at 38 kDa is more apparent; whilst some GST cleavage is apparent, the quantity of whole protein remaining is increased. The protein remained stable ON in the arginine refold buffer in lane 5. Lane 6 Fraction A12-B12 collected from QC required concentrating prior to SEC analysis. Fractions B10-B6 in lanes 7-9 were collected from the QC to confirm the late signal was noise and not TASK3 degradation proved correct as no protein is visible. Mwt marker is in kDa (lane 10).

The A12-B12 concentrate was loaded onto SEC for analysis (Figure 56). Fractions A8-10 were thought most likely to contain the protein however the peak arrived too early at volume 8.5 mL, indicative of a Mwt of approximately 75 kDa and suggestive of dimerization. Alternately, it may be an aggregate of cleaved protein. Regardless, eluate fraction A9 was collected for gel confirmation. The noise at the end of the graph are the result of system pressure fluctuations and may be ignored.

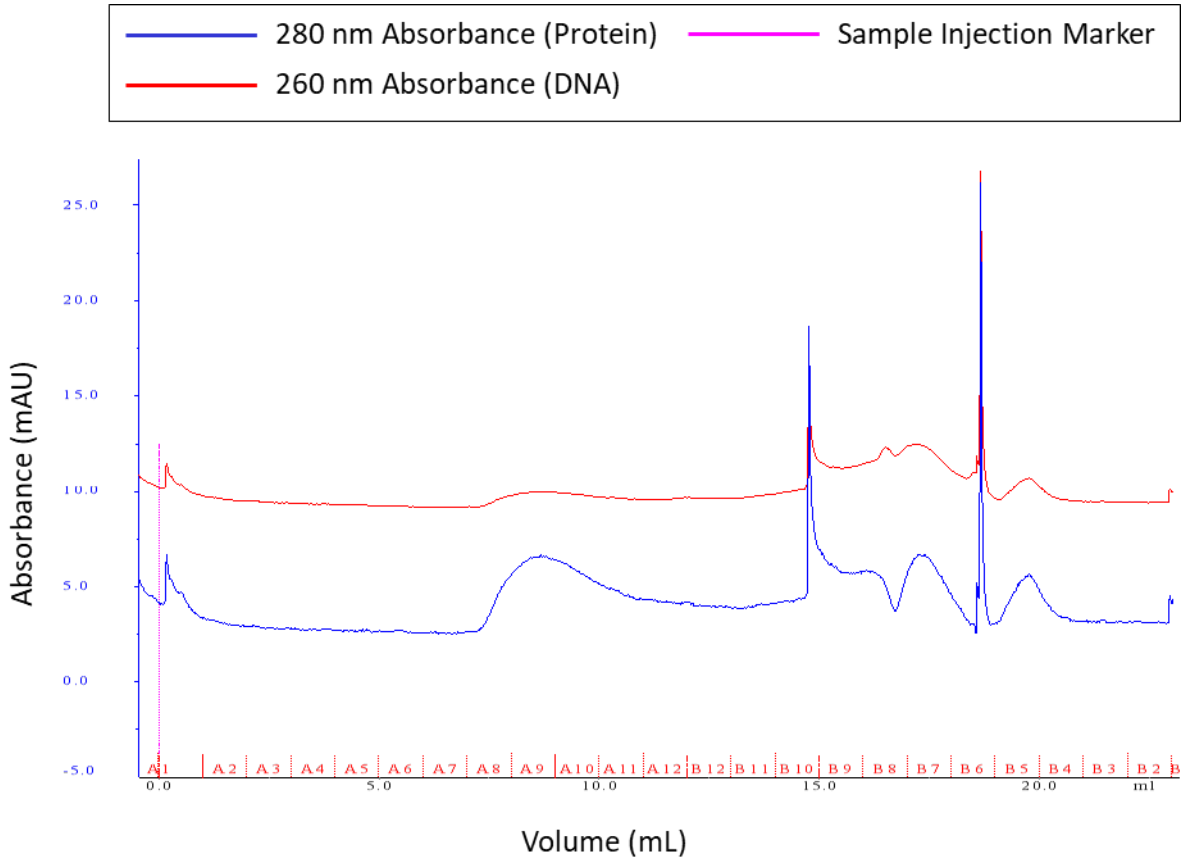

Figure 56 SEC analysis of the A12/B12 fraction from the QC column suggests dimerization

The peptide eluted earlier than expected (8.5 mL rather than the ovalbumin reference volume of 11 mL) but as a single peak however it may be an aggregate of cleaved protein. Fraction A9 was suspected to hold the peptide and collected for gel analysis.

For the GST-column, the QC A12-B12 concentrate was diluted in 50 mL PBS to achieve a final concentration of 0.1 mg/mL. At first the sample appears highly contaminated as suggested by the exceeding 260 nm absorbance in Figure 57. However, as confirmed by the Nanodrop™, this is due to absorbance by glutathione. Fractions A5-A6 contain the eluted protein and were collected for SDS-PAGE determination.

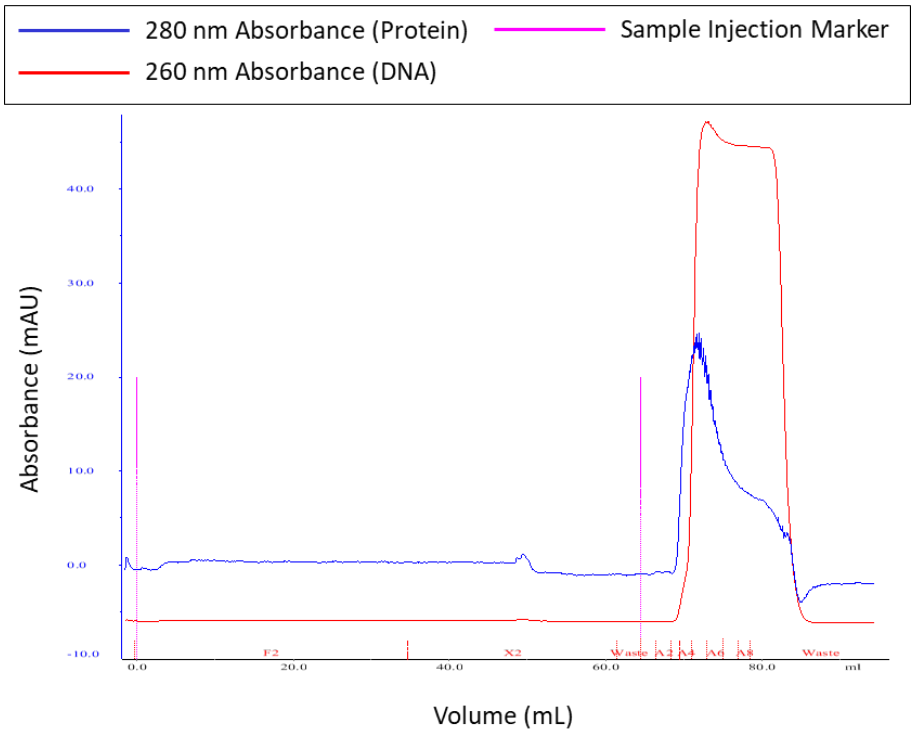

Figure 57 Application of whole protein purified on QC to the GST column, diluted in PBS saw no protein in the flow through and eluate fractions A5-A6 were collected for gel analysis

The exceedingly high 260 nm absorbance (red trace) would suggest contamination however Nanodrop™ analysis confirmed this to be absorbance by glutathione. Eluate fractions: A4-6 and A9 were collected for gel analysis.

From the gel in Figure 58, it appears that the GST is cleaved either upon exposure to PBS or during dissolution in a buffer of pH 7.0 having been previously stored in HEPES at pH 10 post QC purification. Following refolding, TASK3 is predominantly whole with minor cleavage observed in lanes 2 and 3 (Figure 58). Protein was diluted in PBS in preparation for GST column purification, lane 4. The absence of a band in lane 4 could be that the sample was too dilute or more likely, hints at the precipitation of TASK3 upon exposure to PBS. Following GST purification, Lanes 5, 6 and 7 show only the GST-tag present at 25 kDa and the absence of protein entirely – further supporting precipitation prior to GST purification. The peak present on the GST column is likely GST alone. It was decided to repeat the GST column but in the presence of pH 10 HEPES as opposed to PBS (pH 7.0).

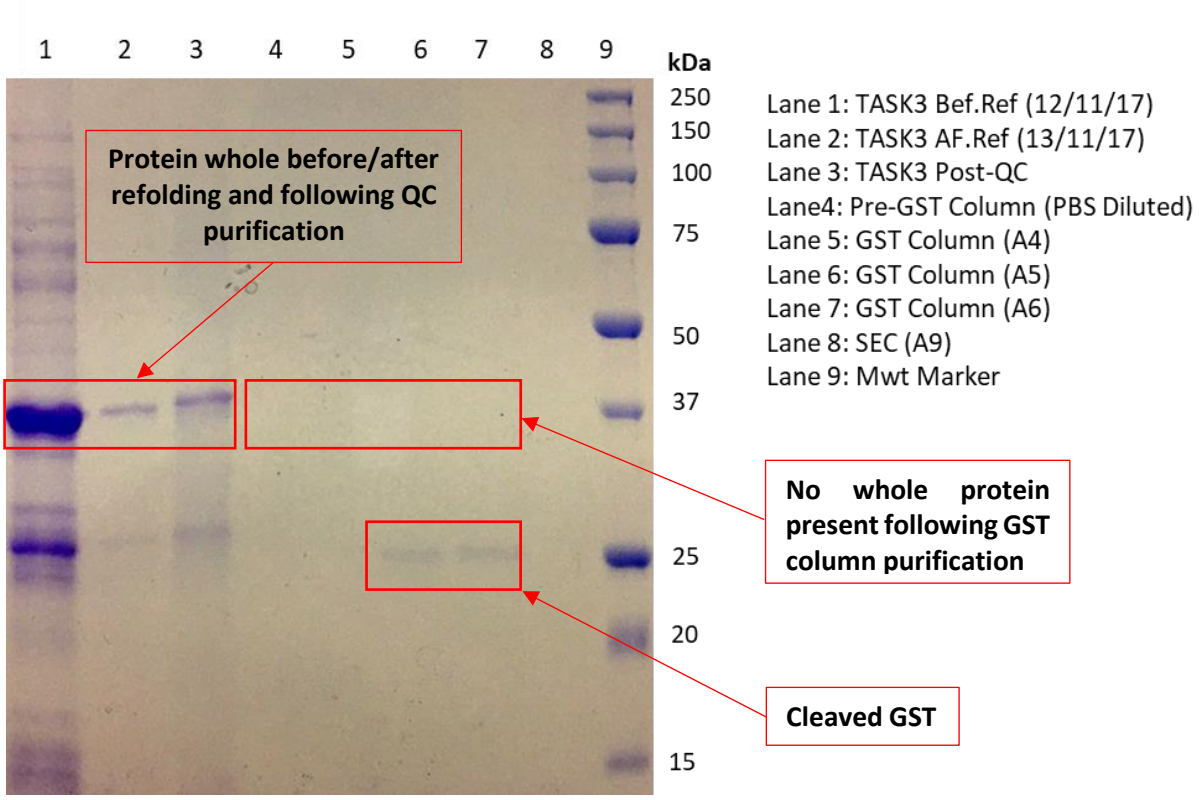

Figure 58 GST is either cleaved upon exposure to PBS or during the transfer into pH 7 buffer having been stored in HEPES pH 10 following QC purification

TASK3 remains relatively whole during refolding and QC purification in lanes 1 – 3 however, following application the GST column (lane 4) no protein is apparent. It is possible that the protein sample was too dilute but it is more likely that the TASK3 precipitated out of solution following exposure to PBS as suggested previously. Following GST column purification, eluates A4 – A9 (lanes 5 – 8) vaguely show only the presence of free-GST at 25 kDa and no TASK3, further supporting precipitation. Mwt is in kDa (lane 9).

4.4.3 The TASK3 Peptide is Stable in HEPES Buffer (pH 10)

Considering these findings, it raised the question: is the peptide sensitive to the PBS buffer itself or is it a matter of pH? It appeared that once the protein is introduced to PBS (pH 7.0), it undergoes cleavage. However, stored in the HEPES buffer (pH 10) for the strong QC exchange, the protein remains whole. Was it HEPES or was it the change from pH 10 to pH 7.0?

Following a new QC in which the protein appeared whole (Appendix 2.2), the GST column was repeated in both pH 10 & pH 7 HEPES. Figure 58 showed the minor presence of cleaved GST therefore, on the following GST readouts (Figure 59), the presence of protein in the FT was thought to be free protein. The second peak following elution was suspected to be a combination of free-GST and GST-tagged TASK3.

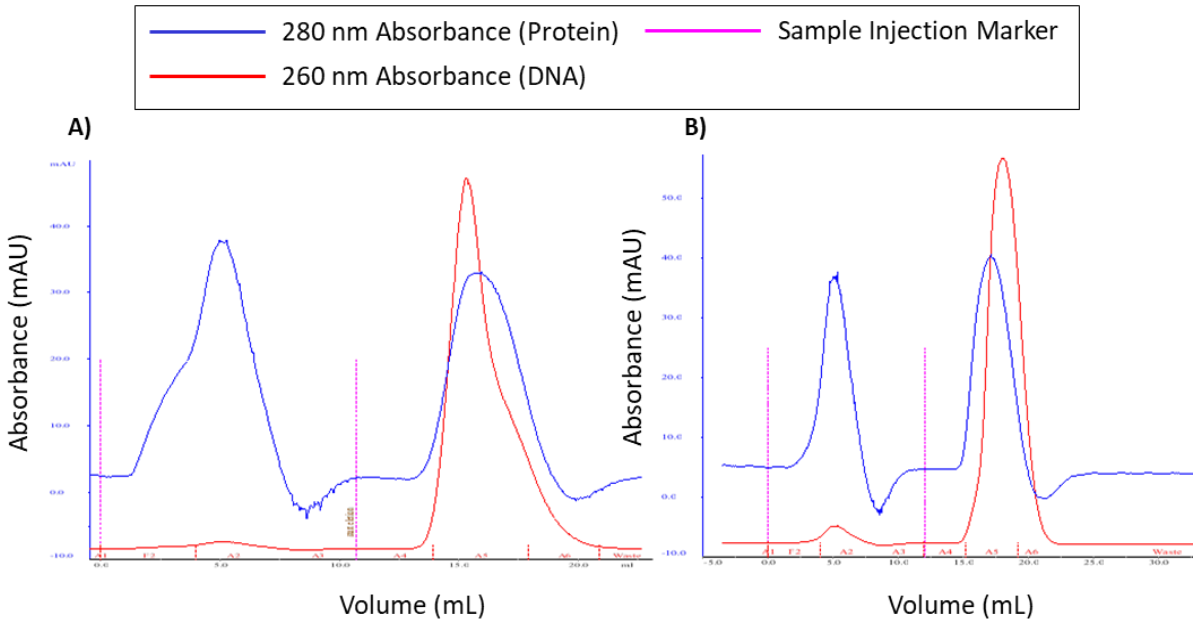

Figure 59 Comparison of GST columns carried out in (A) HEPES pH 10 and (B) HEPES pH7 confirm GST cleavage occurs as a result of exposure to PBS and not as a function of pH

Whole protein collected from the QC and applied to the GST column in either HEPES pH 10 or pH 7 generated graphs display peaks (UV 280 nm, blue trace) occurring at similar positions and intensities (mAU). The first peak is the flow through and expected to contain free protein whilst the second peak is the elution, expected to contain a combination of free GST and some GST-tagged TASK3 if cleavage is indeed a function of PBS exposure. For gel analysis, HEPES pH 10 (A), flow through fractions A2 and the 'peak shoulder' A1 were collected alongside eluate fraction A5. From HEPES pH 7, the flow through fraction A2 and eluate fraction A5 were collected.

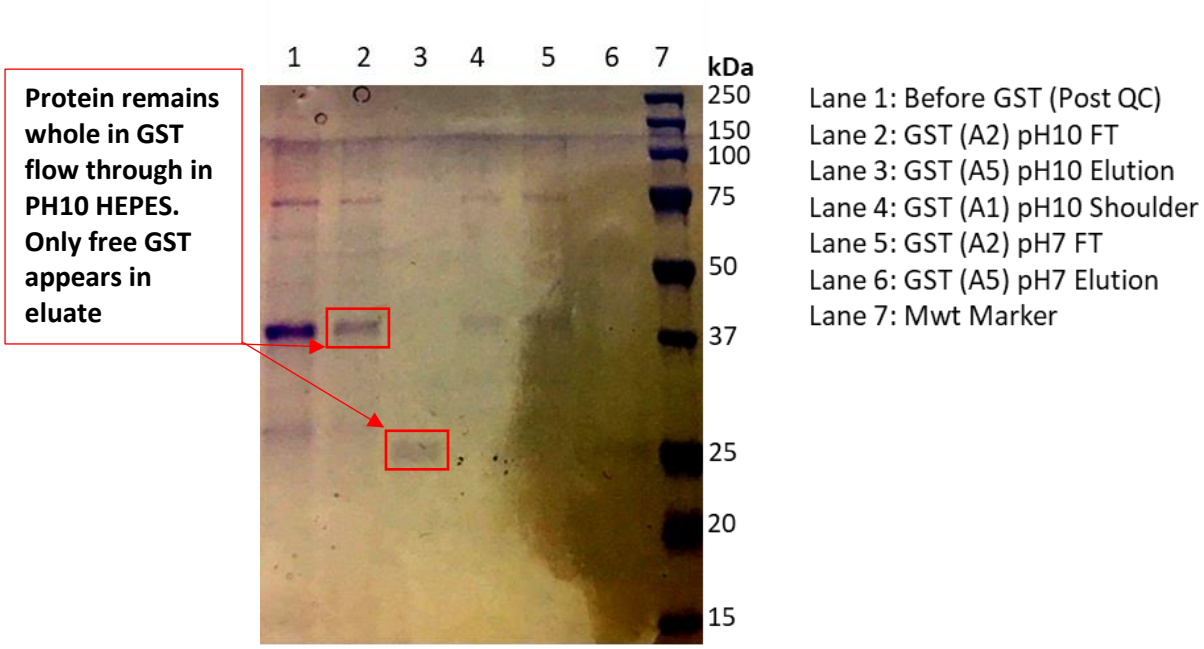

Figure 60 The peptide remains whole in pH 10 HEPES flow through however the GST is dysfunctional for purification purposes

To confirm, the protein was in a whole state following the QC and prior to the GST column (lane 1). In pH 10 HEPES, full protein is visible in the flow through (lanes 2 and 4) however, only free GST remains following elution (lane 3). There appears to be significantly less whole protein in the HEPES pH 7 samples however, lanes 5 – 6 display a similar flow through and elution product as pH 10. Mwt marker is in kDa (lane 7).

Comparison of the GST columns carried out in HEPES (pH 10) versus HEPES (pH 7) showed peaks occurring at similar positions and intensities (milli-absorbance units (mAU)), implying that it is not the pH of the buffer dictating protein cleavage but is rather the exposure to PBS buffer itself. Whilst the protein was still detected in the GST column FT, it remained predominantly uncleaved at pH 10 as seen in lane 2 (Figure 60).

To further confirm the incompatibility between the protein and PBS as a storage buffer, the samples B2B1C1 and B6B5B4, collected from the FT of the GST column/SEC in Figure 49 and Figure 51 respectively, were defrosted having been stored at -80°C as they contained cleaved TASK3. Upon defrosting on ice, protein precipitation was immediately apparent as evidenced by the turbidity of the solution. The samples were briefly centrifuged at maximum rpm with pre-/post-spin samples taken for loading onto a gel prior to GST column application. Following the reaffirmation of the unsuitability of PBS, it was hopeful that a GST column may further purify the cleaved protein in the flow through when the running buffer was switched to HEPES (pH 10). Initially the GST graph in Figure 61 seems exceedingly noisy however, it was likely the presence of an air bubble in the system. To confirm this was the case, fraction A4 was collected for a UV check when the reading was at what appeared to be baseline. FT fraction A2 was collected as was the fraction A9 eluate.

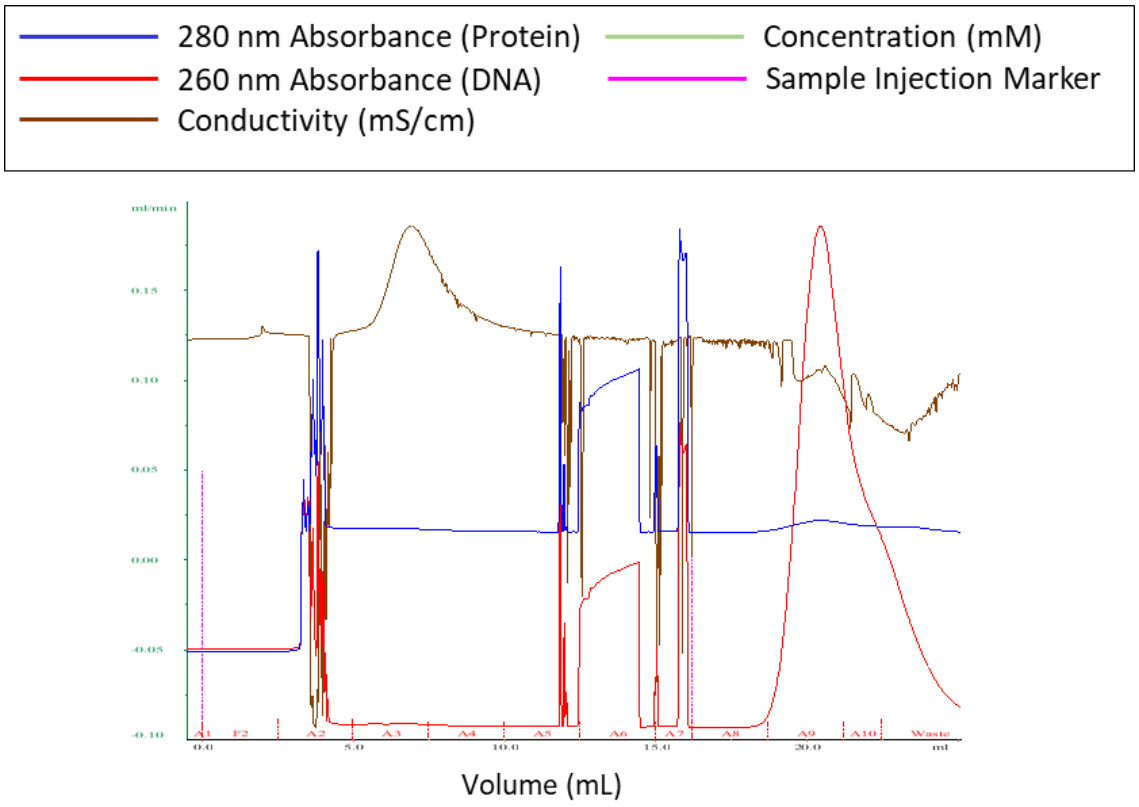

Figure 61 Frozen flow through samples (in PBS) of previous GST column shown to contain free TASK3 were reloaded onto a GST column in HEPES pH 10 in attempt to purify the free protein

Flow through samples B2B1C1 and B6B5B4 collected from the size exclusion chromatography following a GST column (Figure 19 and Figure 17 respectively) were pooled and stored in PBS at -80°C as they were observed to contain free-TASK3 (Figure 20). Following defrost, there was a clear precipitate. Samples were collected pre- and post- spin down for gel analysis prior to loading onto the GST column in HEPES pH 10 to purify cleaved protein. The trace is initially noisy due to an air bubble in the system. Flow through fraction A2 and eluate fraction A9 were collected for gel analysis.

It was confirmed using the Nanodrop™ on fraction A4 that the noise observed on the graph was indeed air as it contained a protein concentration of 0.0 mg/mL (280:260 of 0.07). Alternately the first peak observed in the FT (A2) contained 0.021 mg/mL whilst the eluate had a protein concentration of 0.118 mg/mL with A260/280 ratios of 1.91 and 9.06 respectively. With such low protein concentrations observed combined with drastic RNA/DNA contamination depicted by the A260/280 (>1.0), a gel was carried out (Figure 62).

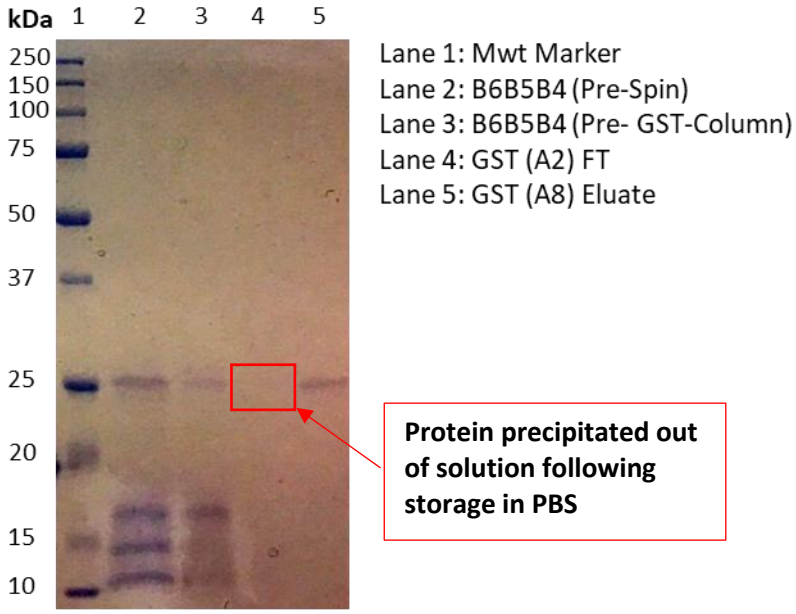

Figure 62 No free-TASK3 remained in solution following PBS storage at -80°C

A sample of the turbid protein solution following defrosting was collected prior to centrifugation, lane 2, contains both free-GST (25 kDa) and TASK3 (15 kDa). Following spin down (lane 3) a significant reduction in band intensity and therefore protein is observed. As such, no protein is visible in the GST column A2 flow through (figure 30) in lane 4 and only free-GST in the A9 eluate as TASK3 no longer remained in solution. Mwt marker is in kDa (lane 1).

It is apparent from the gel that following centrifugation, protein concentration has declined significantly as can be seen by a reduction in band intensity between lanes 2 and 3 respectively (Figure 62) at both 25 kDa but more so at 15 kDa where the TASK3 band is now non-existent. It is therefore not surprising that no bands are seen in the FT (lane 4) as the protein appears to have precipitated out of solution. Only residual GST can be seen in the eluate as expected. It was thus decided that a new preparation would be carried out, maintaining the protein in HEPES where possible with an additional pH scout using dynamic light scattering (DLS) to investigate the effect of HEPES pH on protein polydispersity/homogeneity. To investigate the effect of the 6 amino acid (VLRFLT) motif on solubility, a second construct in which the motif was deleted was also transformed (Figure 63).

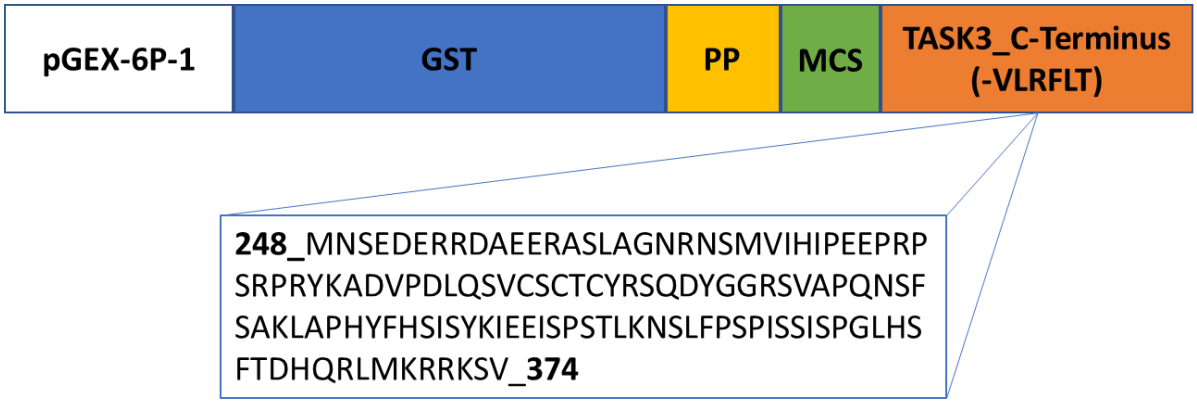

Figure 63 Schematic displaying the TASK3_C-Terminus (-VLRFLT) construct with the pGEX-6P-1 vector

The peptide sequence (in which the VLRFLT motif has been deleted) was subcloned within the multiple cloning site (MCS) and fused to a glutathione-S-transferase (GST) tag. The pGEX-6P-1 vector contains a cleavage site for Precision Protease ™ (PP) for specific removal of the GST tag following purification.

Following expression, it is clear from lanes 3 and 4 in Figure 64, that the new construct containing the motif deletion (-VLRFLT) is equally insoluble in PBS buffer as it cannot be seen in the SN portion, and that expression closely imitates that of the +VLRFLT construct. Therefore, the 6 amino acid motif is not the cause of peptide insolubility. This protein also remains stable at the correct Mwt following the QC in HEPES buffer pH 10. For the purpose of this study, work progressed with the TASK3_(+VLRFLT) construct only.

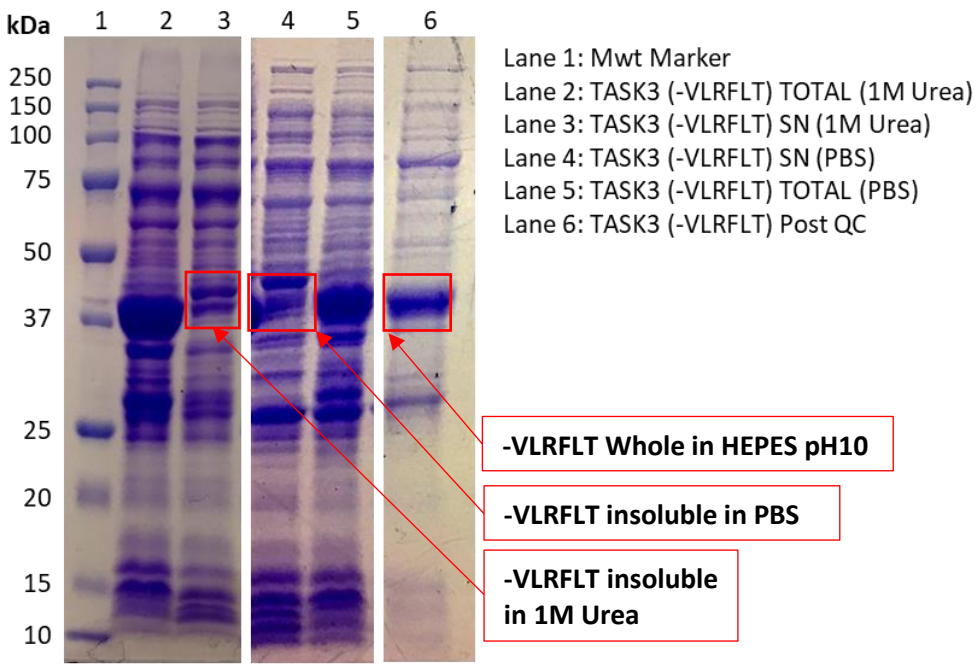

Figure 64 The TASK3 peptide expressed without the VLRFLT motif is equally insoluble

TASK3 with the VLRFLT motif deletion is equally insoluble in PBS as shown by lack of band at 43 kDa in the supernatant in lane 4. The protein remains insoluble in 1M urea (lane 3) and will require 8M urea solubilisation and refolding like its (+VLRFLT) counterpart. Following QC purification of the deletion construct in HEPES pH 10, the protein remains whole (lane 6) at the correct molecular weight. Mwt marker is in kDa (lane 1).

To determine the effect of HEPES buffer pH on the protein polydispersity index (PDI), a pH scout was carried out in which protein, following QC separation, was diluted 1:20 in HEPES buffer ranging in pH (6, 7, 8 and 10) and in PBS as a control. The data can be seen below in Table 7. The protein is most predominantly retained in a monomeric state at pH6.0 in a salt concentration that has been reduced from 200 mM to 70 mM, which is more convenient both physiologically and experimentally as the likes of nuclear magnetic resonance (NMR) are carried out at this pH. In DLS, it is only possible to make a generalised assumption with regards to protein species size, i.e. whether the protein is present as monomer (small), dimer/trimer (medium) or polymer/aggregate (large) species.

Table 7 DLS investigation of the effect of HEPES pH on homogeneity/aggregation of the protein
TASK3_(+VLRFLT) is aggregated in solution as indicated by the significantly higher Mwt and % mass

		Diffusion Coefficient (Cm^2)	Radius (nm)	Diameter (nm)	% PD	PD (nm)	PDI	MWt (kDa)	% Intensity	% Mass
HEPES pH10	pH10-1									
	Peak1	3.52E-07	6.84	13.69	108.22	7.41	1.17	303.13	100	100
	pH10-2									
	Peak1	3.66E-07	6.57	13.15	20.36	1.34	0.04	275.95	18.95	95
	Peak2	7.69E-08	31.32	62.65	31.64	9.91	0.1	10646.1	81.05	4.99
	pH10-3									
	Peak1	3.71E-07	6.49	12.98	25.26	1.64	0.06	267.92	17.85	94.79
	Peak2	7.46E-08	32.28	64.56	37.17	12	0.14	11421.1	82.15	5.2143
HEPES pH8	pH8-1									
	Peak1	3.86E-07	6.24	12.48	5.25	0.33	0.002	244.1	5.06	79.11
	Peak2	7.57E-08	31.81	63.63	21.77	6.93	0.05	11041.3	59.83	8.78
	Peak3	1.13E-08	213.09	426.18	16.55	35.26	0.03	945237	35.12	12.11
	pH8-2									
	Peak1	3.71E-06	0.65	1.3	15.37	0.1	0.02	1.23	0.13	93.59
	Peak2	7.16E-07	3.36	6.73	35.3	1.19	0.12	57.45	0.949	3.75
	Peak3	1.37E-07	17.53	35.07	78.52	13.77	0.62	2739.03	74.27	1.74
	Peak4	1.88E-08	128.29	256.59	13.63	17.49	0.02	288370	8.68	0.14
	Peak5	3.20E-09	753.08	1506.16	36.86	277.55	0.14	18130600	15.97	0.78
	pH8-3									
	Peak1	3.90E-07	6.17	12.34	19.9	1.04	0.03	238.03	4.91	79.64
	Peak2	7.68E-08	31.39	62.77	34.93	10.96	0.12	10695.7	72.19	11.5
	Peak3	1.62E-08	148.51	297.017	11.74	17.44	0.01	406108	9.88	2.81
	Peak4	1.04E-08	231.19	462.38	10.63	24.57	0.01	1143920	13.02	6.05
HEPES pH7	pH7-1									
	Peak1	2.95E-07	8.16	16.32	9.39	0.77	0.01	457.31	3.94	78.07
	Peak2	5.59E-08	43.09	86.19	24.99	10.77	0.06	22460.2	96.06	21.93
	pH7-2									
	Peak1	4.10E-07	5.88	11.75	13.93	0.82	0.02	212.11	1.83	81.95
	Peak2	4.75E-08	50.76	101.51	38.68	19.63	0.15	32936.1	98.17	18.046
	pH7-3									
	Peak1	4.29E-07	5.62	11.23	15.06	0.85	0.02	190.903	1.63	81.03
	Peak2	4.89E-08	49.26	98.52	37.32	18.38	0.14	30709.5	90.76	16.28
	Peak3	2.26E-08	106.77	213.55	0	0	0	187665	7.61	2.69
HEPES pH6	pH6-1									
	Peak1	2.38E-08	101.09	202.184	9.69	9.8	0.01	165126	100	100
	pH6-2									
	Peak1	2.77E-06	0.87	1.74	9.87	0.09	0.01	2.44	0.47	99.08
	Peak2	1.87E-08	129.02	258.05	18.64	24.05	0.03	292227	82.93	0.64
	Peak3	9.49E-09	253.88	507.77	22.8	57.89	0.05	1424110	16.6	0.28
	pH6-3									
	Peak1	2.34E-06	1.029	2.06	11.9	0.12	0.01	3.60138	1.03	99.2
	Peak2	1.81E-08	132.82	265.64	16.44	21.84	0.02	312750	75.46	0.51
	Peak3	9.84E-09	244.97	489.94	18.07	44.25	0.03	1309830	23.51	0.29
	pH6-4									
	Peak1	3.31E-06	0.73	1.45	0	0	0	1.6	0.29	98.39
	Peak2	4.35E-07	5.54	11.09	11.76	0.65	0.01	185.18	0.7	0.52
	Peak3	1.75E-08	137.71	275.42	15.36	21.15	0.02	340344	99.01	1.1
	pH6-2.1									
	Peak1	4.20E-06	0.57	1.15	1.13E-14	6.51E-17	1.29E-32	0.917173	0.12	98.31
	Peak2	4.29E-07	5.62	11.23	11.49	0.65	0.01	190.83	0.7	0.6
	Peak3	1.91E-08	126.47	252.93	12.26	15.5	0.02	278847	99.19	1.1
	pH6-2.2									
	Peak1	2.27E-06	1.06	2.12	11.6	0.12	0.01	3.86	0.24	96.02
	Peak2	1.79E-08	134.48	268.96	14.17	19.06	0.02	321972	83.18	2.97
	Peak3	1.07E-08	225.55	451.1	8.8	19.85	0.01	1079700	16.58	1.01
PBS pH7	PBS-1									
	Peak1	2.87E-07	8.39	16.77	11.07	0.93	0.01	487.82	4.49	67.95
	Peak2	5.35E-08	45.05	90.09	17.55	7.9	0.03	24912.3	90.24	15.64
	Peak3	2.44E-09	986.03	1972.06	11.59	114.24	0.01	34062900	5.26	16.41
	PBS-2									
	Peak1	3.90E-07	6.17	12.34	0	0	0	237.964	1.06	65.13
	Peak2	4.58E-08	52.58	105.15	32.48	17.08	0.11	35766.4	87.13	21.66
	Peak3	1.99E-08	121.11	242.21	11.82	14.32	0.01	251987	10.3	9.01
	Peak4	4.19E-09	574.97	1149.93	18.01	103.55	0.03	9642460	1.51	4.2
	PBS-3									
	Peak1	7.26E-07	3.32	6.63	11.73	0.39	0.01	55.66	0.42	76.78
	Peak2	5.22E-08	46.18	92.36	28.42	13.12	0.08	26404.4	54.92	7.21
	Peak3	1.93E-08	124.9	249.8	16.55	20.68	0.03	270840	44.66	16.01

Briefly, DLS functions via the shining of a monochromatic light source in a Brownian motion into a solution containing moving particles such as protein. This results in a Doppler shift that alters the wavelength in a way which corresponds to the size of the particle. Unfortunately, such multimodal approaches are skewed towards larger species. As soon as protein is removed from ice it will eventually begin to aggregate. The presence of large aggregates even at a low mass population alters the mean hydrodynamic size. This will have an adverse effect on the accuracy of data associated with smaller molecules in the same solution as the larger species effectively obscure the scattering of smaller species. This makes it difficult to differentiate between monomers, oligomers and aggregates, leading to a potentially inaccurate assumption that a very monomeric solution with a low mass population of aggregate may resemble a solution with a very high mass population of large aggregates.

In this instance, the focus was upon the predicted Mwt and percentage (%) mass. Ideally, a high % mass of low Mwt would indicate a homogenous monomeric solution. On average at pH 6, 98.19% of the solution peaks consisted of protein with an average predicted Mwt of 2.48 kDa. Furthermore, literature dictates a % polydispersity (Pd) <20% is considered monodisperse (Stetefeld *et al.*, 2016). At pH 6 the average %Pd (considering all peaks) of 12.05% suggests the solution is monodisperse, containing particles of uniform size that are stable as they did not appear to degrade and aggregate over experimental time. In comparison, the PBS sample carried out with the same DF and protein batch, saw an average of 69.87% of the prominent solution peaks contained protein of an average Mwt of 260.48 kDA. With an average %Pd of 15% you could argue that the solution is monodisperse but in combination with the previous gels, it is most likely only cleaved GST present that is predominantly aggregated in solution. Similar results were obtained in pH 7.

Despite all previous gels describing a protein that was stable at pH 10, the DLS results would suggest otherwise. With an average mass of 96.6% containing protein with an average Mwt of 282.3 kDa and a %Pd of 44.49 it is easy to suggest that in reality, pH 10 HEPES buffer is less stabilising than HEPES at pH7 however, a Mwt of 282.3 kDa is still considered small and may potentially represent dimer, trimer or oligomer conformation.

Circular dichroism (CD) was used to determine whether the recombinant protein is folded or unfolded. Whilst it may not provide the residue specific information that can be extracted from X-ray crystallography or NMR data, it requires <20 µg of protein to estimate the secondary structural composition. The data in Figure 65 (top left) is reported in units of 'ΔE.' Briefly, CD functions via an unequal absorption of left-/right-handed orientated circularly polarised UV light. This light has both time-dependent electric and magnetic fields associated with it. By passing through various prisms/filters, light becomes polarised and its electric field vector will oscillate sinusoidally in a single

plane. Unlike linearly polarised light, rather than oscillating in a single direction, circularly polarised light has an electric field vector which maintains its magnitude but begins to rotate. The result is two vectors of equal length, one of which is rotating clockwise (ER) and the other, in an anti-clockwise (EL) direction. An asymmetric molecule such as a protein will absorb right and left-handed circularly polarised light to different extents thus requiring separate indices of refraction. Therefore, in reporting units as [ΔE] (M-1cm-1), it is describing the difference in ER and EL absorbance by the molecule in question. Amides of the polypeptide backbone contain chromophores which are aligned in arrays, allowing their optical transitions to split or be shifted into multiple characteristic transitions, or 'spectra.'

Using a CD analysis programme such as 'CAPITO' exposes the data to various algorithms including the likes of multilinear regression, singular value decomposition, ridge regression, principal component factor analysis, convex constraint analysis, neural-based network analysis and the self-consistent method (Wiedemann *et al.*, 2013). Such calculations refine the CD output into displays of α-helical proteins which display negative bands at 222 nm, 208 nm and positive bands at 193 nm; alternately, antiparallel β-pleated sheets produce CD spectra with negative bands 218 nm and positive bands at 195 nm.

According to the plot comparison of spectral values at λ=200 nm vs λ =222 nm (Figure 65, top left), the CAPITO software predicts (+VLRFLT)TASK3 to be folded when compared to the Far-UV CD spectra of entries within the 'Protein Circular Dichroism Data Bank' (PCDDB). Whilst CD curve of TASK3 itself (top left, upper panel) appears slightly noisy, it vaguely depicts the presence of α-helices (7%) with positive and negative absorbance peaks at approximately 198 nm and 220 nm respectively; β-sheet (41%) positive/negative absorption at 218 nm and 195 nm respectively and 52% irregular conformation. As the TASK3 fragment expressed here is suspected to contain a flexible tail region, it is not unsurprising that the protein contains a relatively high proportion of irregular structure. Equally a small proportion of α-helices is to be expected as the VLRFLT motif is superficially embedded in the intracellular side of the membrane as it is in the extreme portion of the transmembrane domain 4. Regardless, the value of 7% is too low when you consider that the Schistosoma japonicum GST class-mu included in the PGEX-6P-1 vector has 47% of its structure attributed to α-helices. This raises several questions in the realms of sample purity and folding. Considering the purity observed in previous gels, it is more feasible the high salt concentration (200 μM) and the presence of arginine may interfere with the spectra.

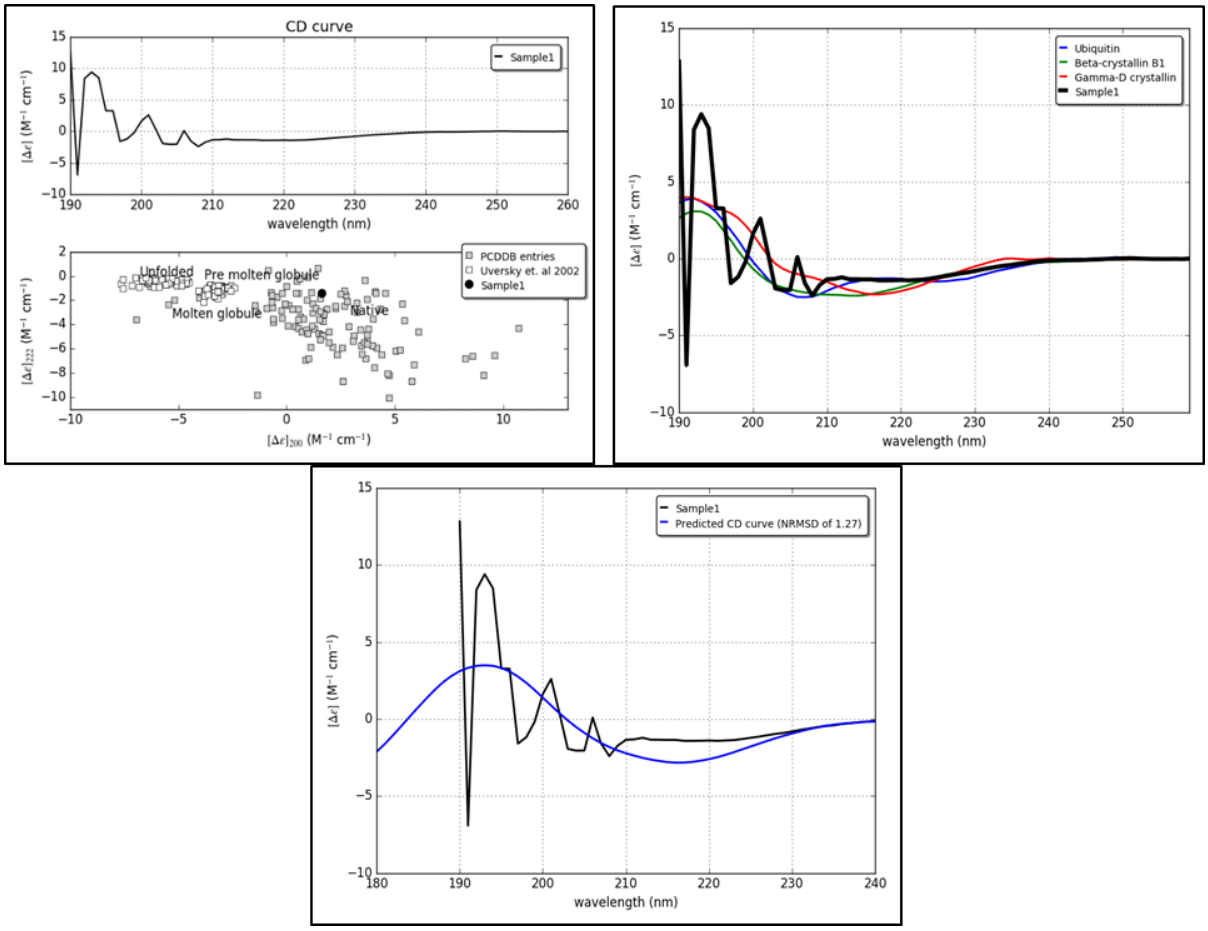

Figure 65 CD spectra of the peptide with the VLRFLT motif contains regions of α-helices and β-pleated sheets but is predominantly irregular in structure in line with its flexible Ct nature

Upper left: Smoothed Far-UV CD spectra of (+VLRFLT) TASK3, lower panel: a plot comparison of spectral values at λ= 200 versus λ= 222 nm to predict folding state against CAPITO reference data bank. Upper right: Recorded (+VLRFLT) TASK3 CD overlaid with CD spectra of 'similar' proteins based upon lowest area difference (Δa): black (TASK3), blue (ubiquitin), green, (β-crystallin B1) and red (γ-D crystallin). Bottom: Predicted CD curve via basis spectra (NRMSD: 0.93).

4.4.4 GST-TAG: Dysfunctional but Necessary

In order to determine whether it is the GST that is correctly folded alone with an unfolded TASK3 or correct folding of the entire protein, it was necessary to plan a new CD experiment involving protein in which the GST had been enzymatically cleaved whilst reducing the concentration of salt in the buffer. In Figure 66, there appeared to have been some minor cleavage achieved as evidenced by very faint GST bands at 28 kDa as seen in lanes 5 and 6 with the 'strongest' TASK3 band vaguely apparent at 15kDa following O/N cleavage. This suggested that cleavage is possible however, the process required optimisation.

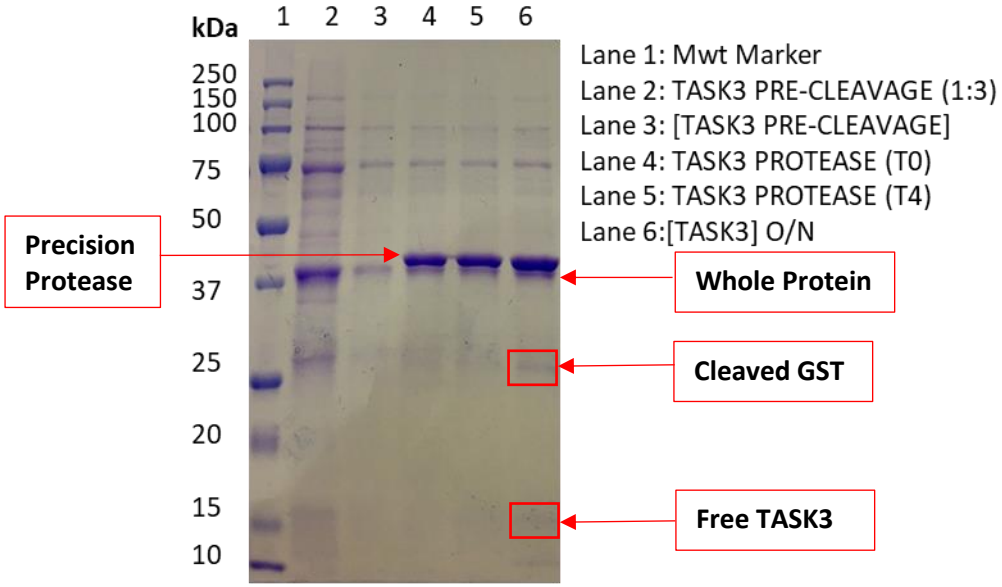

Figure 66: SDS-PAGE showing GST cleavage by PreScission protease was 'most' efficient following overnight incubation

In lane 2 the protein is present in a full state prior to enzymatic cleavage. Lanes 3 – 6 show different incubation time points of the +VLRFLT peptide with the Prescission protease enzyme. Very faint bands of free protein can be seen around 25 kDa and 15 kDa in lane 6 following overnight incubation however this requires optimising as the majority remains in full state (43 kDa).

An APS flash refold test in HEPES buffer of various pH resulted in the immediate precipitation of protein out of solution. This was visible by the instantaneous turbidity of the solution and is supported by the lack of bands in lanes 2 – 6, Figure 67. To cross-check the DLS data that suggested the use of pH 6 HEPES buffer kept the protein in a stable monomeric state, the concentration of the pH 6 flash refold was checked before and after centrifugation. If the protein had precipitated out of solution, the concentration would be reduced following spin down as the precipitated protein will pellet. True enough, the concentration reduced from 0.184 mg/mL to 0.128 mg/mL; whilst not a significant reduction, it is important to consider the small size of this sample.

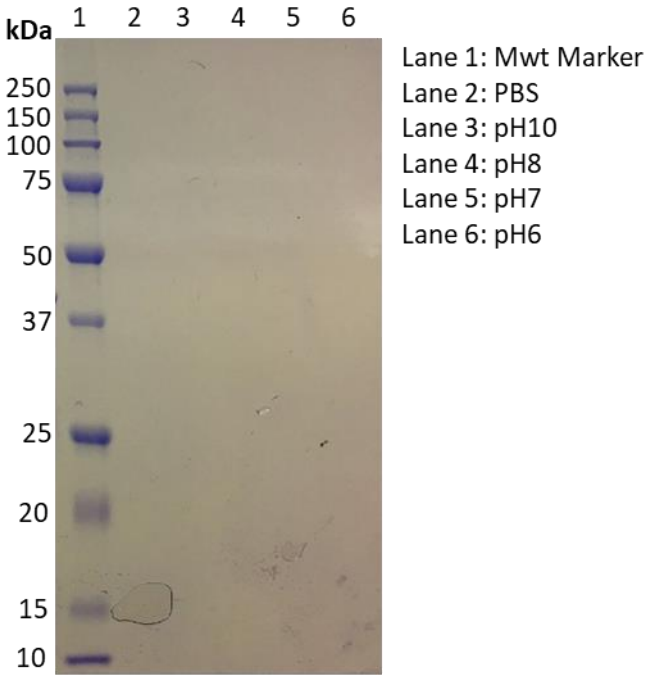

Figure 67 A flash refold test following APS protein extraction in HEPES buffer of varying pH resulted in immediate precipitation

The absence of any protein in lanes 2 – 6 show that the use of HEPES buffer as a direct refolding agent is unsuitable regardless of pH. Mwt marker is in kDa (lane 1).

Both constructs eluted at approximately the same conductivity (concentration of buffer B) as to be expected as there is only a difference of 6 amino acids between the two (Figure 68). Equally, a reduced protein absorbance observed from the new construct was unsurprising as it was produced from a smaller batch volume. In both instances, there appears to be limited DNA contamination as evidenced by a much smaller red 260 nm absorbance when compared to the fuchsia 230 nm absorbance.

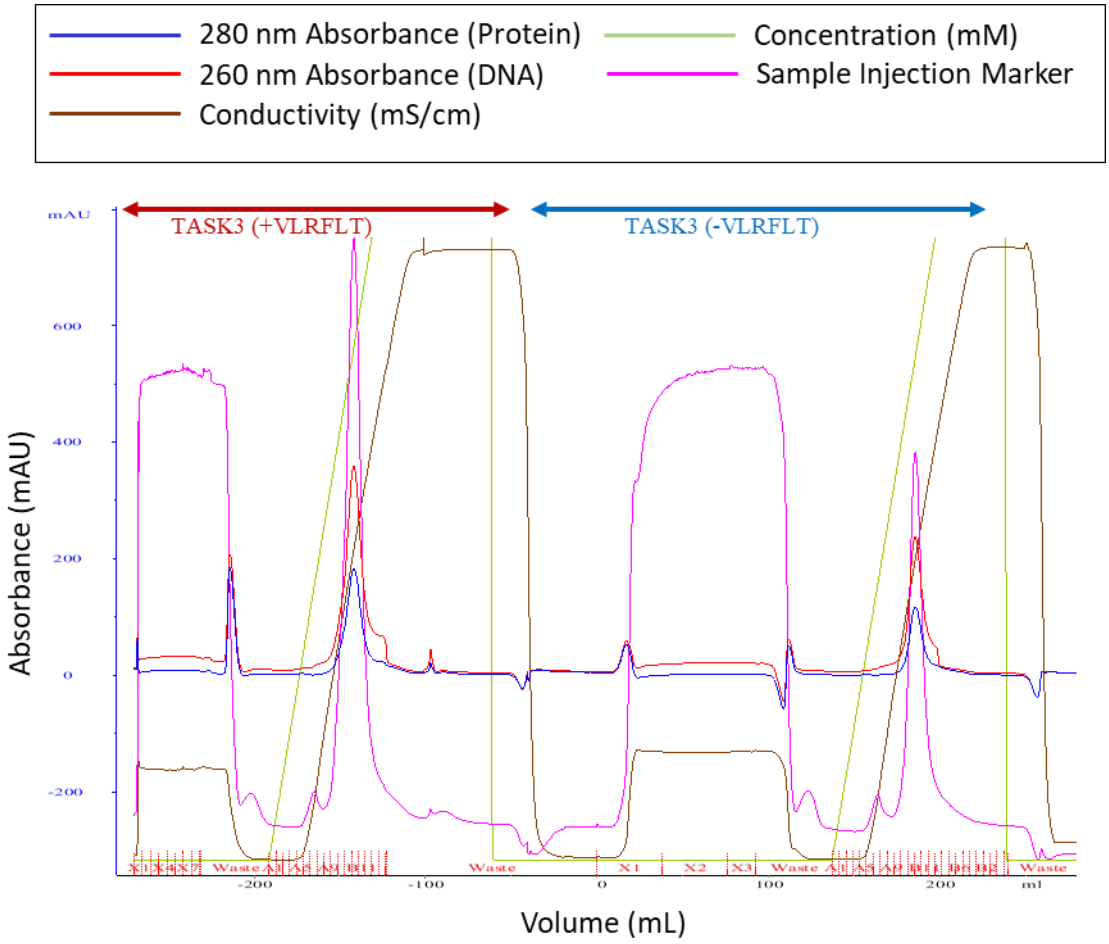

Figure 68 QC of product from a new expression including readings for the (+VLRFLT) TASK3 (Left) and (-VLRFLT) TASK3 (Right)

The +VLRFLT construct was eluted at approximately 50 mL of buffer B with a conductivity of 43.065 mS/cm with a 280 nm UV reading of 183.71 mAU and fractions A10 – B11 were collected and pooled. The -VLRFLT construct was eluted at approximately 40 mL of buffer B with a conductivity of 41.242 mS/cm with a 280 nm UV reading of 117.749 mAU and fractions B10 and B11 were collected and pooled. The -VLRFLT shows reduced protein absorbance (blue 280 nm trace) as it was produced from smaller culture batch.

The initial SEC carried out on the +VLRFLT construct purified from the previous QC (Figure 69, left) carried out at pH 10 appeared to be too dilute with a concentration of 0.419 mg/mL (A260:280 of 0.98) as shown below by the minimal 280 nm absorbance despite being at the correct elution volume. Therefore, the sample was concentrated and rechecked on the Nanodrop™. The final concentration was 0.659 mg/mL (A260:280 of 0.71). Following this result, the -VLRFLT construct was concentrated immediately prior to SEC and had a concentration of 0.25 mg/mL (A260:280 of 0.76). The pH 10 sample is pure producing a single peak region with a protein absorption of 146.305 mAU (Figure 69, right). The peak occurs at an earlier volume than expected, corresponding to a Mwt of 70 kDA. It is unlikely that this is the result of aggregation, rather indicating the presence of dimers as the peak is narrow and tall. Lane 3 of the gel in Figure 71 confirms the protein is uncleaved.

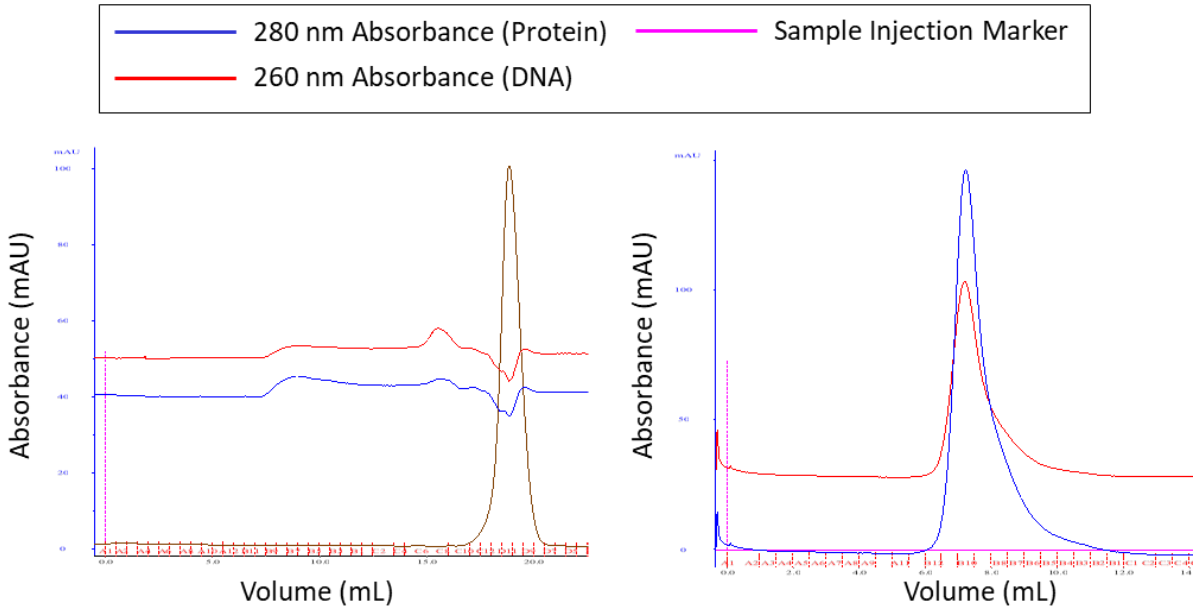

Figure 69 SEC of +VLRFLT construct purified in the previous Q-column

(Figure 66, fractions A10 – B11) ***(A)*** *Chromatograph depicts a peak at a slightly early position but was too dilute as seen by the low 280 nm (blue) absorbance.* ***(B)*** *Chromatograph is the same protein following concentration. The sample is pure in HEPES pH 10, producing a single peak with a protein absorption of 146.305 mAU. Fraction B10 was collected*

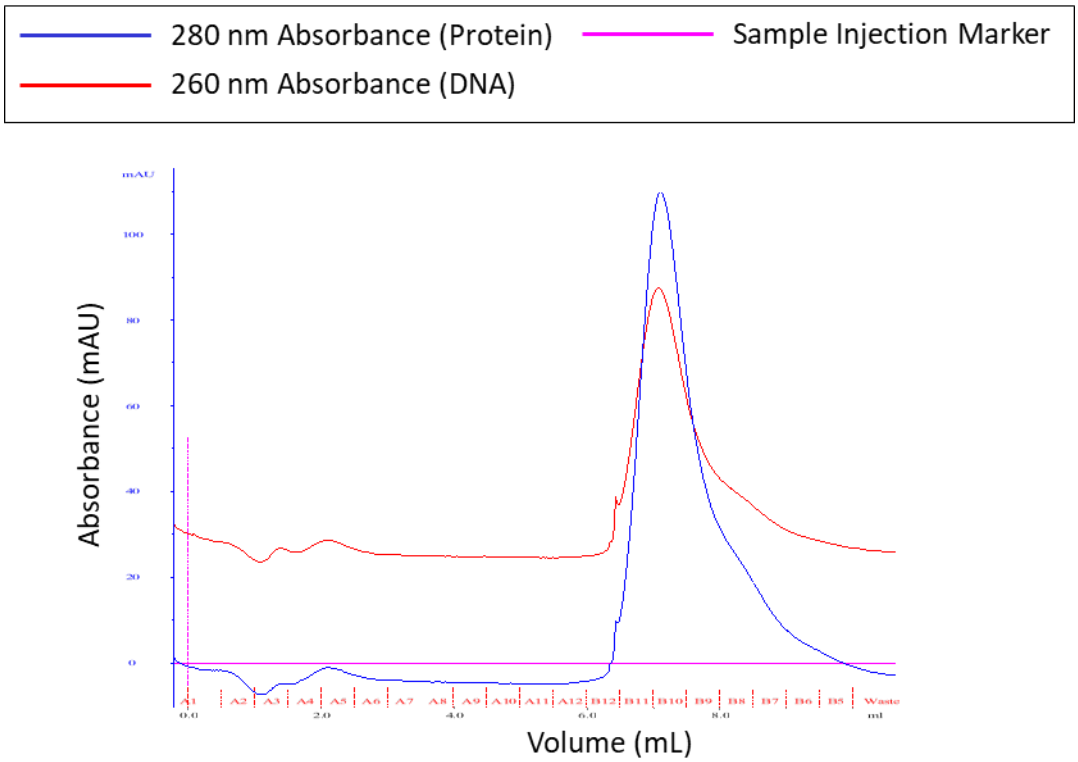

Figure 70 : SEC of -VLRFLT construct in HEPES pH 10 is pure

With a peak 280 nm absorption (blue trace) of 109.823 mAU. Fraction B10 was collected as suspected to contain most of the protein however, the B8 fraction which contain a small shoulder on the peak was collected for gel analysis.

The SEC profile of the -VLRFLT construct (Figure 70) closely resembles that of the +VLRFLT construct at the same pH (pH 10) (Figure 69, right). The 280 nm peak has an absorption value of 109.823 mAU and appeared earlier expected, again, most likely due to the presence of dimers in solution. Fraction B10 was collected as it contains the majority of the eluted protein however, there is also a small shoulder on the peak descent and so fraction B8 was collected to investigate on the gel in Figure 71. From lanes 1 and 2, bands at the correct Mwt show the protein remains whole.

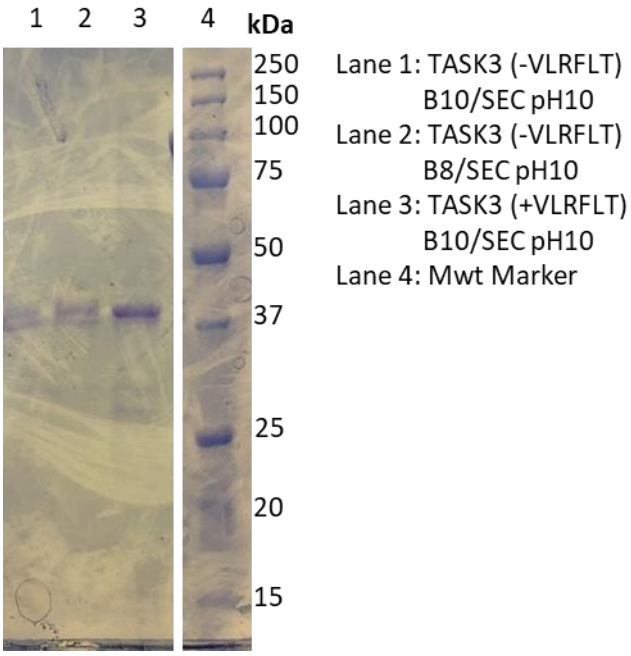

Figure 71 SDS-PAGE confirms that both the -VLRFLT and +VLRFLT (B8/B10 and B10 fractions respectively) were pure and in whole conformation as depicted by a single band at 43 kDa in lanes 1 – 3. Mwt marker is in kDa (lane 4).

This is also true for the (+VLRFLT)_TASK3 construct at pH 8 (Figure 72B) which depicts an early (7.3 mL), narrow peak with minimal DNA contamination however, there was a considerably smaller 280 nm UV absorbance of 84.601 mAU – this suggests that the protein may have precipitated into the column. Contradicting the previous DLS results, SEC carried out in pH 6 HEPES buffer with the (+VLRFLT)_TASK3 construct, depicts severe protein precipitation with a 280 nm absorbance of 55.609 mAU, post-concentration (Figure 72A) when compared to 146.305 mAU of the pH 10 SEC sample (Figure 70). With a considerably higher 260 nm absorbance level, the presence of more than one broad peak and an elution volume that remains too early. Following concentration, fraction B9 contained the highest protein concentration, as determined by the Nanodrop™ to be 0.037 mg/mL.

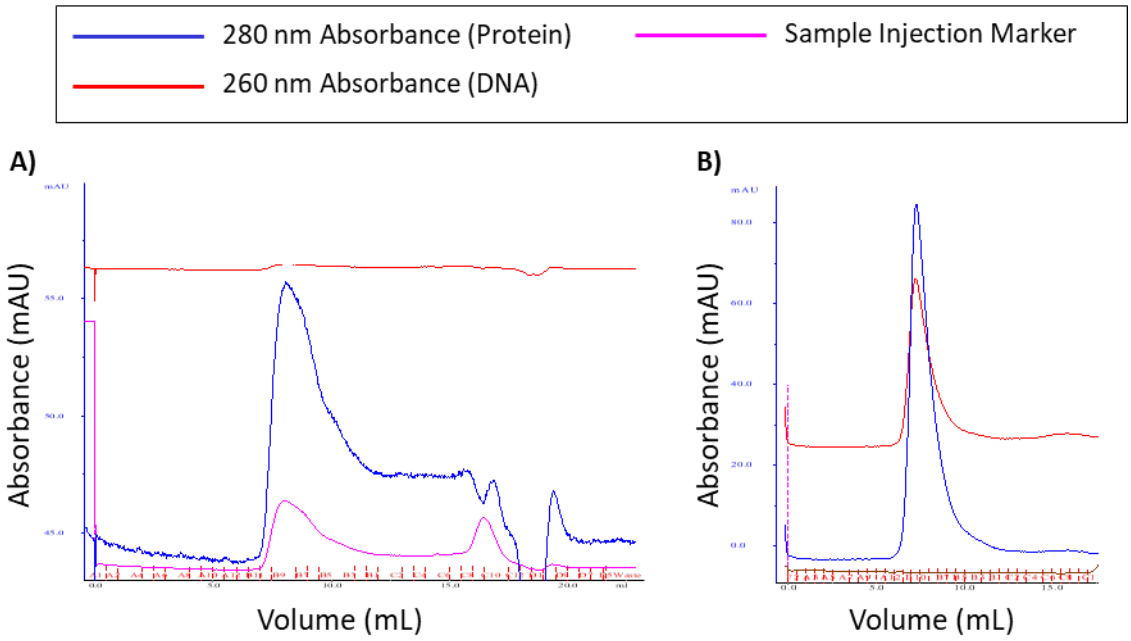

Figure 72 Up to 95% purified when carried out at more physiologically feasible pH

Purification in pH 10 HEPES buffer, was repeated at pH 6 (A) and pH8 (B) in attempt to achieve a more biologically feasible pH condition. A) Repetition of the SEC in pH 6 resulted in severe protein precipitation as the 280 nm absorbance (blue) drops to 55.608 mAU compared to 146.305 mAU recorded in pH 10 purification. The presence of a broad peak and increased 260 nm absorbance (red) suggests DNA contamination and likely aggregation. Fraction B9 was collected for gel analysis. B) A single narrow peak like that observed in pH 10 (figure 36) eluted earlier than the reference at approx. 70 kDa suggestive of dimerization however, 280 nm absorbance was significantly less at pH 8 (84.601 mAU) compared to pH 10 (146.305 mAU). Suspected to be precipitating into the column. Fraction B8 was collected for gel analysis.

Following these results, it was clear that the pH 6 HEPES buffer was an unsuitable solution for TASK3 purification and storage. With very similar outputs, it was decided to repeat the process from the QC purification in pH 10 (required for anion exchange) prior to repetition of SEC using the HiLoad Superdex® 75 pg column at pH 10 and pH 8.

From a new 2 L preparation of the TASK3_(+VLRFLT), the QC (Figure 73) exhibits protein elution with a reduced conductivity (34.961 mS/cm) when compared to the previous anion exchange (43.065 mS/cm). The profile has shifted considerably to the left, with the peak maxima occurring at 66.698 mL. This is most likely due to the increased size of the bacterial media used in this production. Nevertheless, the peak has a reasonable width considering a protein concentration of 6 mg/mL was achieved in this preparation.

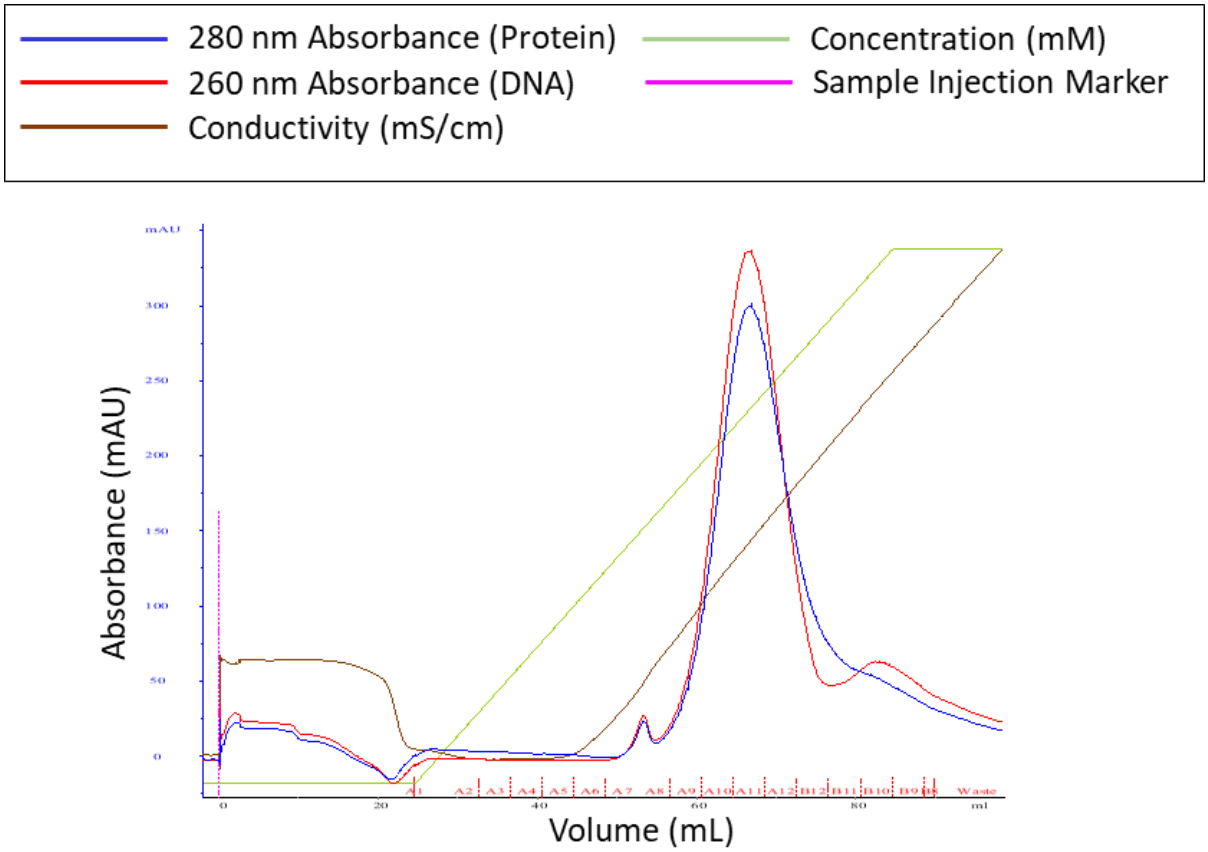

Figure 73 QC from a new 2L preparation of + VLRFLT TASK3.

The protein elution conductivity (brown trace) has shifted left and is reduced (34.961 mS/cm) when compared to previous anion exchanges (approx. 43.065 mS/cm). This is due to the increased size of bacterial culture used in this preparation. Samples A11 – B11 were collected and pooled for SEC analysis.

Figure 74 displays stark differences between protein elution and buffer pH. Despite the equal loading of protein, the very broad pH 8 peak (Figure 74B) displays a maximum mAU of 50, approximately half of that displayed in the pH 10 buffer (Figure 74A). This confirms the previous suspicion that protein in the pH8 buffer is precipitating into the column. A following Nanodrop™ indeed confirms the presence of little-to-no protein present in fraction A12 of the pH8 SEC (Figure 75, lane 1), with a total concentration of 0.304 mg/mL (A260:280 of 0.72) compared to that of the pH 10 SEC in which fractions A11-B11 had a concentration of 1.332 mg/mL (A260:280 of 0.61) (Figure 75, lane 2).

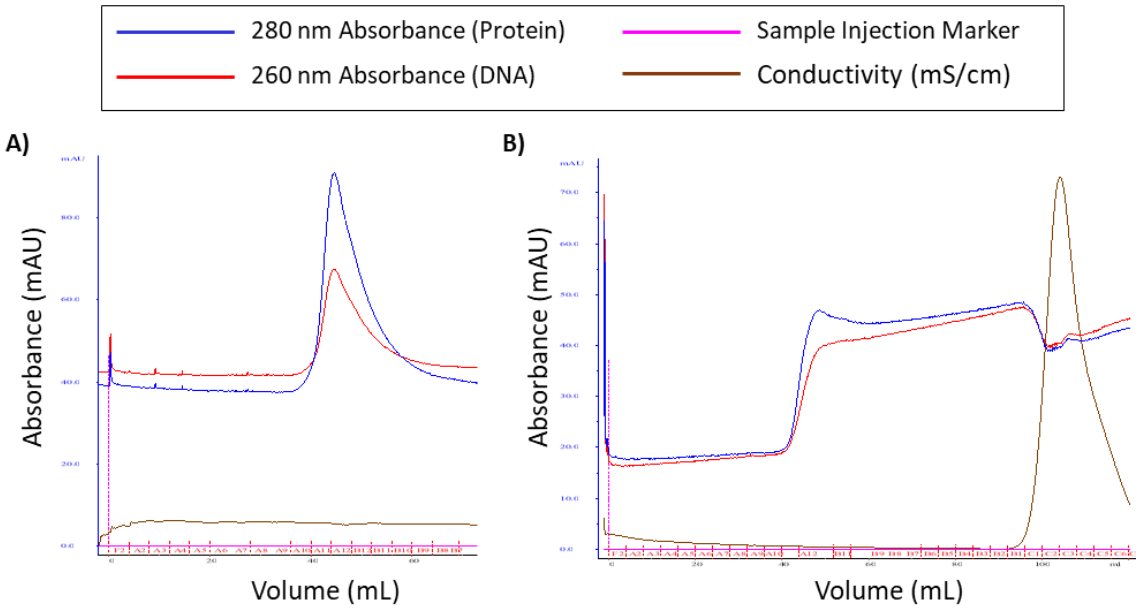

Figure 74 Comparing SEC traces of pH8 and pH 10 confirms pH8 HEPES produces 77% less produce as TASK3 is confirmed to precipitate into the column

A) SEC of +VLRFLT TASK3 in pH 10 HEPES produces a single peak at the correct elution volume with an 280nm absorbance (blue trace) of 90 mAU. Fractions A11 to B11 were collected for gel analysis. B) SEC of +VLRFLT TASK3 in pH 8 HEPES produces a broad peak with a maximum 280 nm absorbance of 50 mAU, fractions A11 and A12 were collected for gel analysis.

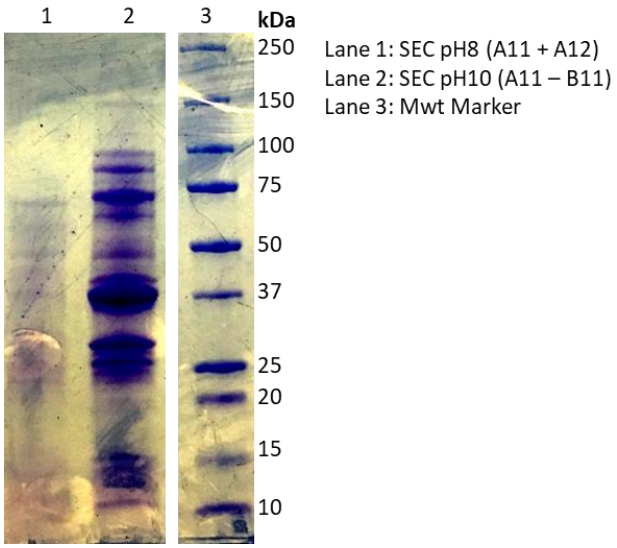

Figure 75 Peptide precipitates out of solution following SEC in HEPES pH 8

SEC of +VLRFLT TASK3 in pH 8 HEPES produced a broad peak in the previous SEC of which fractions A11 and A12 were collected. Lane 1 shows that the reduction in protein elution is due to the precipitation of protein seen by the lack of band at 43 kDa. SEC of +VLRFLT TASK3 in pH 10 HEPES produced a single peak at the correct elution volume and fractions A11 to B11 were collected. Despite the presence of free GST and TASK3 at 25 kDa and 15 kDa, significantly more of the whole protein is apparent at 37 kDa in lane 2.

4.4.5 Production and Purification of PreScission Protease™

Fractions A4 and A5 in Figure 76 containing the newly expressed PreScission protease were collected, pooled, concentrated and dialysed ON at 4°C to remove residual glutathione present in the elution buffer used for the GST-column. The Nanodrop confirmed a final concentration of 5.387 mg/mL (A260:280 of 0.84) and confirmed on a gel, lanes 4 and 5 (Figure 77).

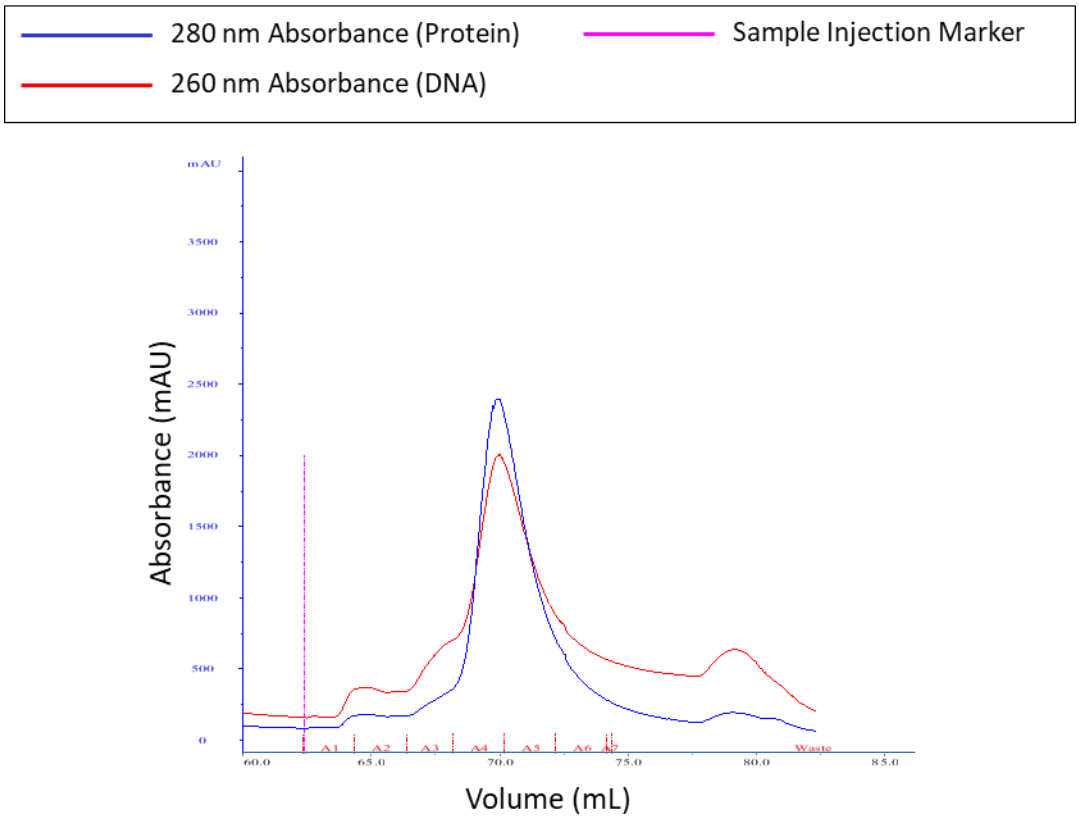

Figure 76 Newly expressed PreScission protease is successfully purified on the GST column with a 280nm absorbance (blue) of 280 mAU

Fractions A4 and A5 were collected and pooled for gel analysis. Nanodrop confirmed a total of 5.387 mg/mL.

The new protease was added to (+VLRFLT) TASK3 at a ratio of 1:5 (i.e. 450µl TASK3 with concentration of 0.2 mg/mL and 50µl cleavage buffer (10X): 90µg total protein in a 1:5 dilution gives a DF of 18. Divide this by the concentration of the protease (5.387 mg/mL) gives the volume of protease to add: 3.34µl). A positive control for protease, amylose protein, was also included. Samples were collected at time points: 1 hour, 4 hours and ON for a gel.

The protease has a Mwt of 46 kDa. The expressed protein in lane 1 (Figure 77) is at the correct Mwt and is soluble as seen by a band in the SN in lane 2. A small proportion is seen in the GST-column FT but this is likely due to saturation of the column as the protein was highly concentrated. Eluate fractions A4 and A5 seen in lanes 4 and 5 respectively show broad bands of high protein concentration at the correct Mwt. A positive control was included in the form of amylose protein in lane 6 to test the functionality of the protease. It is evident that the protease is effective in cleavage even after 1 hour as seen in lane 7, a band is present at the correct Mwt of 46 kDa for the protease and the cleaved product is present at 12 kDa. TASK3 in lane 8 is the negative control in absence of protease (pre-digestion). One hr following digestion, there is no cleavage as shown by the unchanged TASK3 band in lane 9. After 3.5 hrs and ON (lane 10 and 11 respectively), there are extremely faint bands present depicting free-GST (28 kDa) and TASK3 (15 kDa) although this required optimisation.

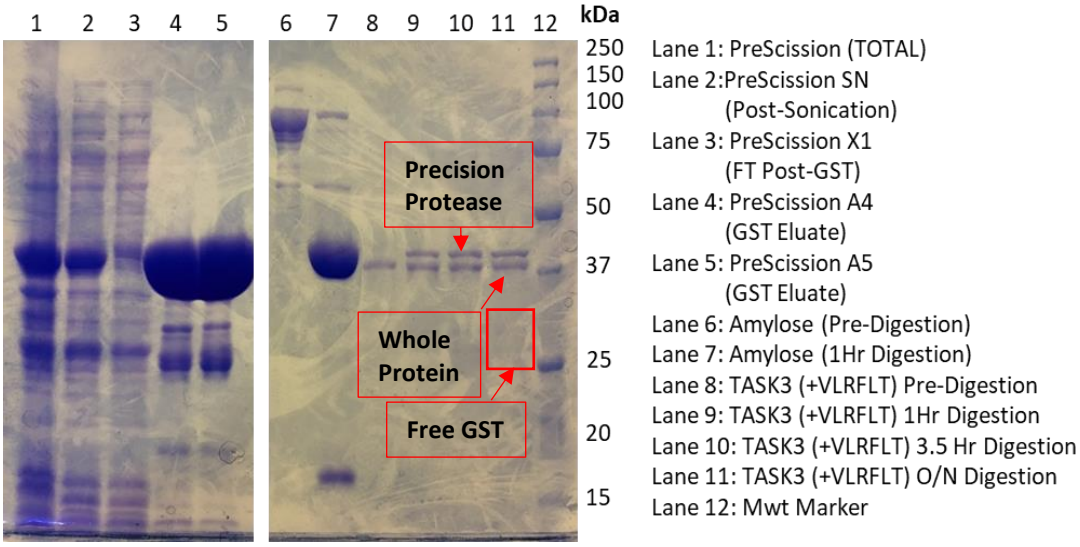

Figure 77 The Precission protease was successfully eluted on the GST column and effective at cleaving GST from the amylose control sample and TASK3 (+VLRFLT) but requires optimisation

Lane 2 shows that the PreScission protease in soluble in solution as observed by a band at approx. 46 kDa. The protein was successfully purified on the GST column as there is no protein present in the column flow through (lane 3) but is successfully eluted in the A4 and A5 fractions collected in lanes 4 and 5. Lanes 6 and 7 contain the gst-tagged amylose control pre-digestion (lane 6) and after one hour incubation (lane 7) in which two clear bands are present with the cleaved product at 12 kDa. Cleavage of the GST-tag from TASK3 (+VLRFLT) was attempted in different conditions. Lane 8 contains the whole peptide as a single band at 43 kDa pre-digestion. After one hour (lane 9), 3.5 hours (lane 10) and overnight (lane 11) there was only very faint presence of free-GST however the protein remains predominantly whole and requires optimisation. Mwt marker is in kDa (lane 12).

To improve the efficiency of the cleavage, protein concentration was increased, and the ratio increased from 1:5 to 1:2; the cleavage buffer was also revised and can be seen in Appendix 3.3. In particular, the concentration of EDTA and Triton-X-100 were increased. Product literature states that PreScission protease has an active range of pH 6 – pH 8. It is apparent from lane 1 in Figure 78 that TASK3 in pH 8 the protease was unable to cleave the protein. Considering the previous results surrounding pH 8, this not a dysfunction of the protease, more likely the denatured protein blocking enzyme active site. This is a reasonably confident conclusion to draw since lane 2 shows the ability of the protease to cleave TASK3 at pH 10 (Figure 78). Whilst there is still a considerable amount of total protein present at 45 Kda however, there is considerably more free-GST and TASK3 present when compared to that in Figure 77 (lanes 9 – 11).

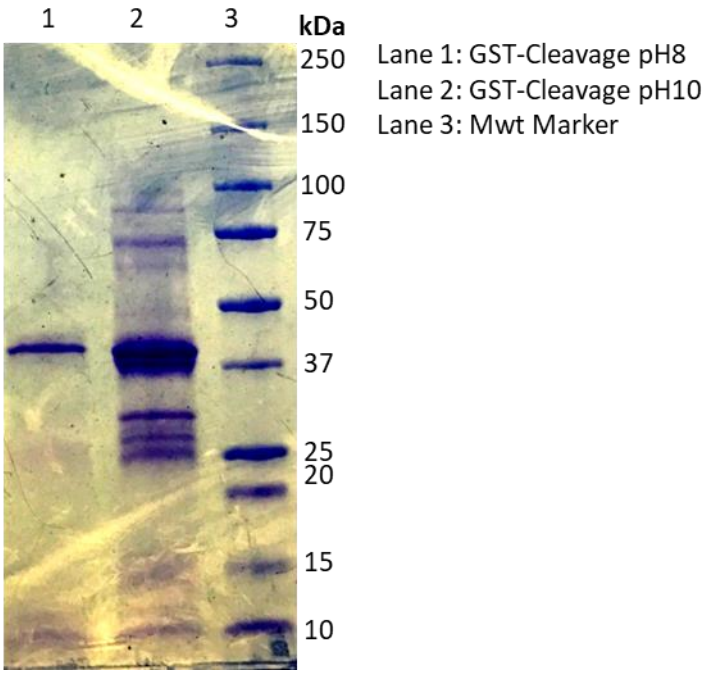

Figure 78 Despite adjustment of the conditions, PreScission protease cleavage remains inefficient

At pH 8, no protein remains as the peptide has precipitated leaving only the protease itself in lane 1. Cleavage is slightly more successful in pH 10 conditions with evidence of free protein at 25 kDa and 15 kDa however, it remains mostly whole (lane 2). Mwt marker is in kDa (lane 3).

Following this cleavage test, the remaining (+VLRFLT) _TASK3 was cleaved under the newly optimised conditions prior to loading onto a GST-column to separate the free-TASK3 from the cleaved GST. The GST column below in Figure 79 has an interesting profile, most likely caused by trapped air in the system. The FT peak contained within fraction A3 was intended to contain free-TASK3 should cleavage have been successful, with a second peak observed in the eluate containing free-GST. It is curious that this peak is equal but opposite in the UV 280 nm with apparent high DNA contamination suggestive of protein degradation. However, when fraction A7 was run on the Nanodrop™, there appeared to be no 260 nm absorbance at all, with clean peaks at both 230 nm and 280 nm with a protein concentration of 1.461 mg/mL (A260:280 of 0.37). This points towards a mechanical error in the system as opposed to a poor sample. To confirm the nature of the protein present within each peak, SDS-PAGE was carried out, see Figure 80.

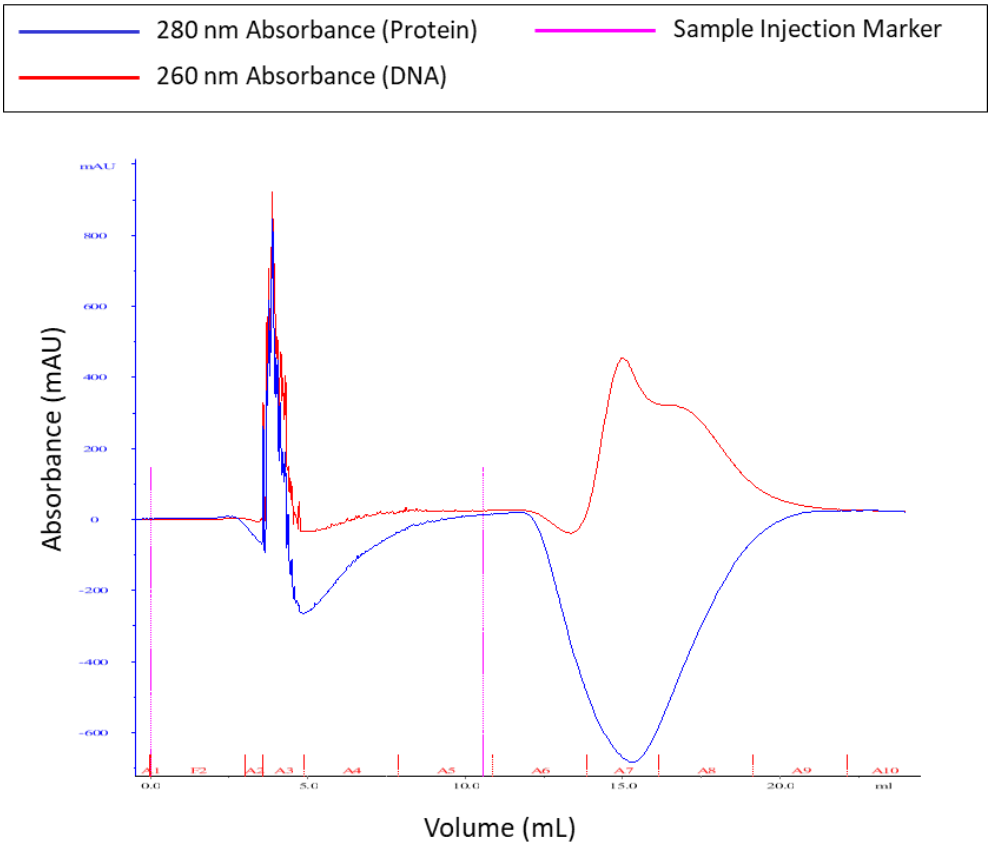

Figure 79 GST column was unable to separate free protein in pH 10 from the cleaved GST

Free-TASK3 was expected to be found in the flow through however the 280 nm adsorption (blue) was very noisy, likely due to air in the system. Fraction A3 was collected for gel analysis. Very little protein appeared to elute following application of reduced glutathione however, A7 was collected for gel analysis regardless.

In Figure 80, a TASK3 pre-cleavage sample was included to ensure the protein was whole to begin with and that there had been no extensive degradation prior to cleavage, lane 1. Despite seeing significant improvement in cleavage following the alteration of the cleavage conditions (Figure 78), there is still a considerable amount of whole protein immediately post-digestion as can be seen by a band alongside that of protease itself in Lane 2. Lane 3 confirms that without undergoing cleavage, the GST-TASK3 remains unable to bind the column. This is possibly due to the denaturing of GST itself at pH 10 which the TASK3 requires to remain solubilised and stable. Equally it could be that, should the peptide have the flexible-tail-like properties it is suspected to have, it may be obstructing the binding sites of GST that are required for column adherence. Unfortunately, there was little-to-no free-TASK visible within the FT. It could be that cleavage was so inefficient and that there may be some TASK3 present but is too dilute and falls below the sensitivity of SDS-PAGE. The only protein present within the GST-eluate fraction appears to be the protease at 46 kDa at a reduced concentration, this is likely due to some being retained within the column.

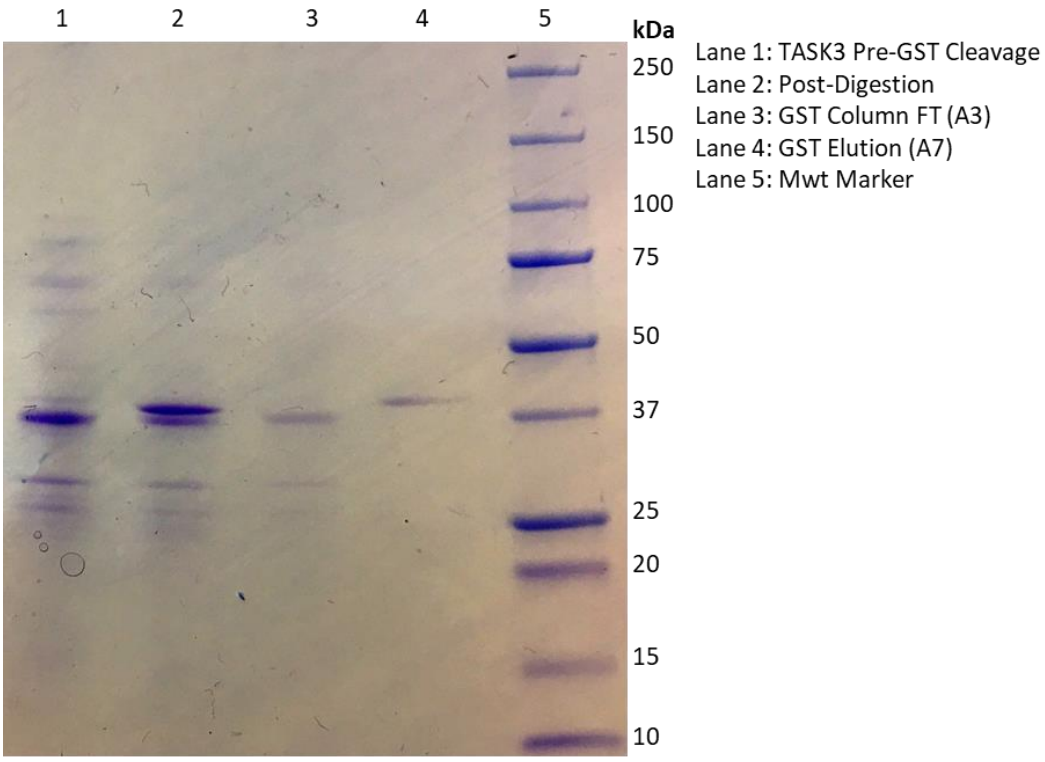

Figure 80: SDS-PAGE of GST column attempted to purify free-TASK3 was unsuccessful as protein remained whole

Lane 1 shows TASK3 (+VLRFLT) prior to cleavage. Lane 2 shows TASK3 following a 3 hr incubation with the protease in pH 10 conditions. Both the protease and the whole protein remain present as two separate bands. The whole protein appears uncleaved in the flow through (lane 3) with only the protease left in the eluate (lane 4). Mwt marker is in kDa (lane 5).

To confirm whether this process of cleavage had any effect on protein secondary structure, the CD experiment discussed above was repeated using the FT protein from the above GST column. The plan initially was to repeat the CD using cleaved protein to determine whether it was in fact the TASK3 that was folded and not just the GST portion alone. However, it is difficult to draw a solid conclusion from the CD data at this stage as free-TASK3 was not clearly visible on the gel in Figure 80. There is a clear reduction in concentration of whole protein between lanes 2 and 3 which would imply some protein has been successfully cleaved and therefore CD was attempted due to its high sensitivity.

It is clear that this process has a significant effect on protein secondary structure as can be seen via the difference in profiles in Figure 81 and Figure 65. Since the sample is not homogenous, some noise was to be expected. Prior to GST-cleavage, the protein clearly displays folded regions of α-helices, β-pleated sheet and the irregular domains suspected of a cytosolic tail, all of which are comparative to other reference proteins stored within the PCDDB.

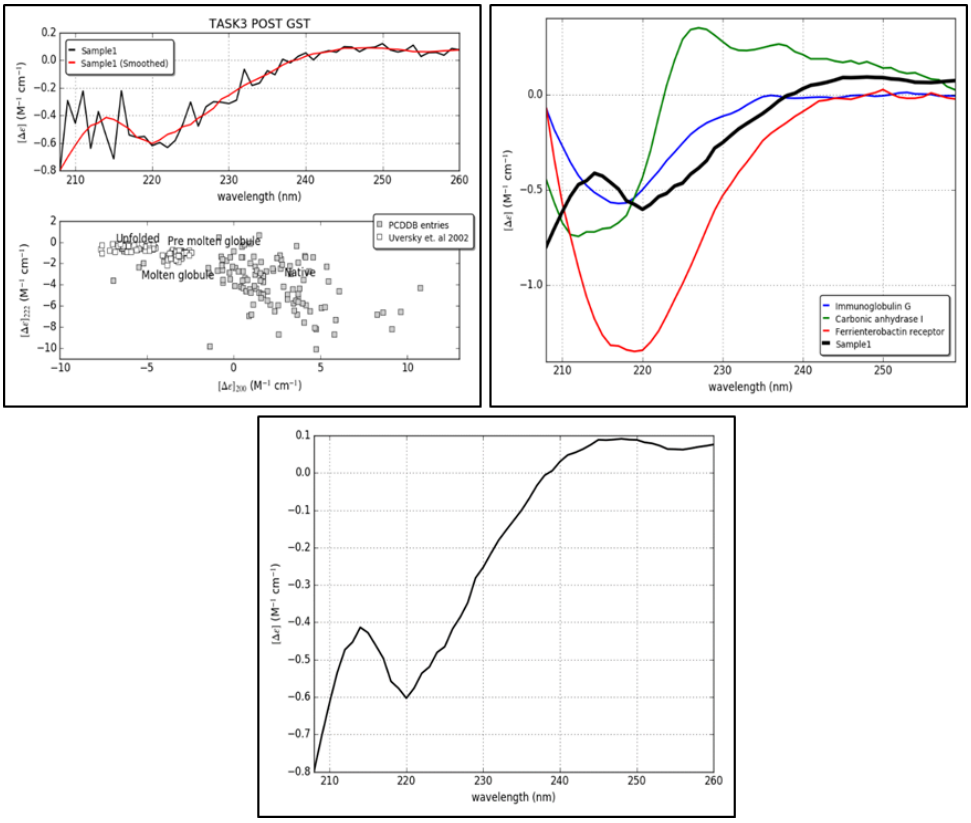

Figure 81 CD investigation of effect of GST cleavage on 'free' TASK3 secondary structure. Presence of GST is essential for retaining secondary structure of TASK3 (+VLRFLT)

(Upper left) Upper panel: Smoothed Far-UV CD spectra of (+VLRFLT) TASK3, lower panel: a plot comparison of spectral values at λ= 200 versus λ= 222nm to predict folding state against CAPITO reference data bank (Top Left). Recorded (+VLRFLT) TASK3 CD overlaid with CD spectra of 'similar' proteins based upon lowest area difference (Δa): black (TASK3), blue (ubiquitin), green, (β-crystallin B1) and red (γ-D crystallin) (Top Right). Predicted CD curve via basis spectra.

4.5 Discussion

The cytosolic carboxyl domain of TASK3 has been implicated in GPCR regulation (Fink *et al.*, 1996, Kim *et al.*, 2000, Czirják *et al.*, 2001, Chemin *et al.*, 2003). A hydrophobic motif consisting of 6 amino acids [VLRFLT] found in the extreme proximal region of the Ct, is crucial for GPCR regulation (Talley and Bayliss, 2002b). In the absence of this motif, the effects of anaesthetic activation, methanandamide inhibition and GPCR mediated regulation are lost (Talley and Bayliss, 2002b, Veale *et al.*, 2007a) in such a way that mimics the loss of GPCR regulation causative of *KCNK9* Imprinting Syndrome (Veale *et al.*, 2014). It is unclear whether this motif behaves as a direct binding site for regulatory molecules or is essential for intracellular signal transduction to the SF gating mechanisms. To address the role of the VLRFLT motif as a potential binding site in the following chapter, it was necessary to produce the Ct of TASK3 inclusive of the VLRFLT motif which has not been achieved before.

In the absence of crystal structures, homology models were previously relied upon to determine proximity of amino acids in suspected bond formations and provide insight into potential mechanisms. Homology models of TASK3 (Veale *et al.*, 2014), based upon the crystal structure of TRAAK (Brohawn *et al.*, 2012), elucidated upon the transmembrane portions of the channel however, structure in-relation-to function of the Ct remains unknown due to its lack of apparent tertiary arrangement and prominent irregularity, even following publication of the TASK1 crystal structure (Rödström *et al.*, 2019). It has become standard practice in recombinant protein expression for structural analysis to remove flexible amino acid sequences as it is the more rigid, stable proteins that are likely to crystallise (Long *et al.*, 2005, Long *et al.*, 2007, Tao *et al.*, 2009, Brohawn *et al.*, 2012, Miller and Long, 2012). Removal of the N- or Ct serves to reduce conformational heterogeneity and enhance the formation of ordered crystal lattices (He *et al.*, 2014, Holcomb *et al.*, 2017). Indeed, using the Karplus and Schulz flexibility prediction tool (Karplus and Schulz, 1985), it is clear in Figure 82 that the transmembrane portions of the channel are significantly more rigid than the regions of the Ct. Through recombinant expression of the GST-TASK3(+VLRFLT) peptide alone, the Ct is stripped of any possible interactions it may have when present in the cell. Removal of local stability may cause the peptide to partially unfold, in turn exposing non-polar regions and residues, reducing solubility and making aggregation more likely (Hwang and Park, 2008).

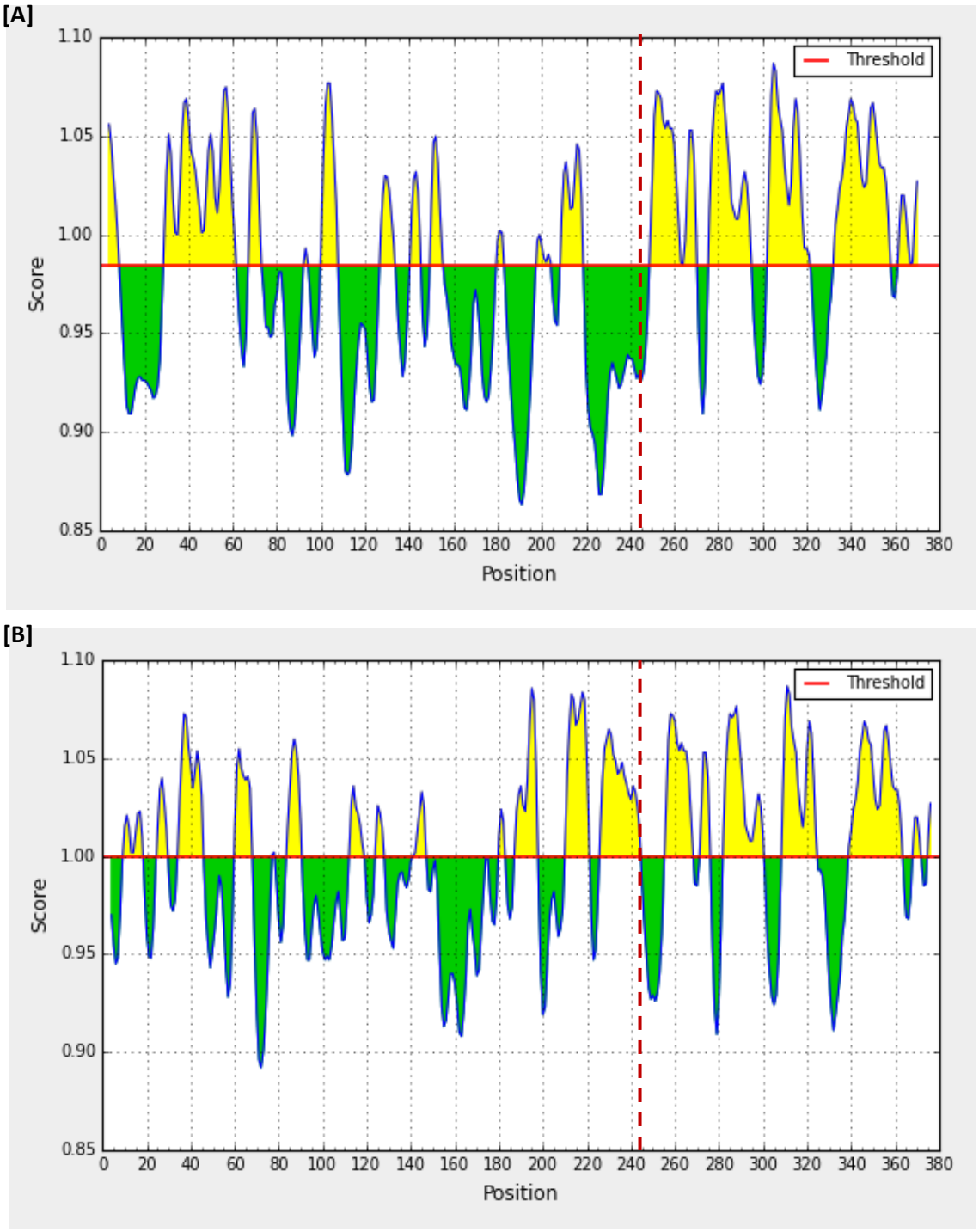

Figure 82 Karplus and Schulz flexibility predictions

The x-axis represents residue position and y-axis, the flexibility score. The threshold is 1.0. Flexible regions are yellow (above threshold) and rigid regions are green (below threshold). Area to the right of the red dashed line represents the TASK3 C-terminal portion (+VLRFLT); area to the left of the red dashed line [A] WT TASK3 and [B] is the GST portion.

The introduction of *'intrinsic disorder'* has recently emerged as a concept used to describe functional proteins lacking a clear tertiary arrangement (Tompa, 2009, Dunker *et al.*, 2001, Deiana *et al.*, 2019). Whether present as an intrinsically disordered protein (IDP) as a whole or a structured protein containing intrinsically disordered regions (IDPRs), rapid identification of these structures continue to challenge the traditional sequence-structure-function paradigm (Schlessinger *et al.*, 2011, Babu, 2016, Deiana *et al.*, 2019) in health and disease (Uversky *et al.*, 2014). According to this criterion, and as stated by the classical *lock-and-key* mechanism (Fischer, 1894), molecular interactions require complimentary binding surfaces. It is now realised however, that the presence of functionally active disordered domains participate in the formation of stable complexes through *induced-fit* interactions (Borgia *et al.*, 2018, Arai, 2018), serving to expand the repertoire of possible protein interactions (van der Lee *et al.*, 2014).

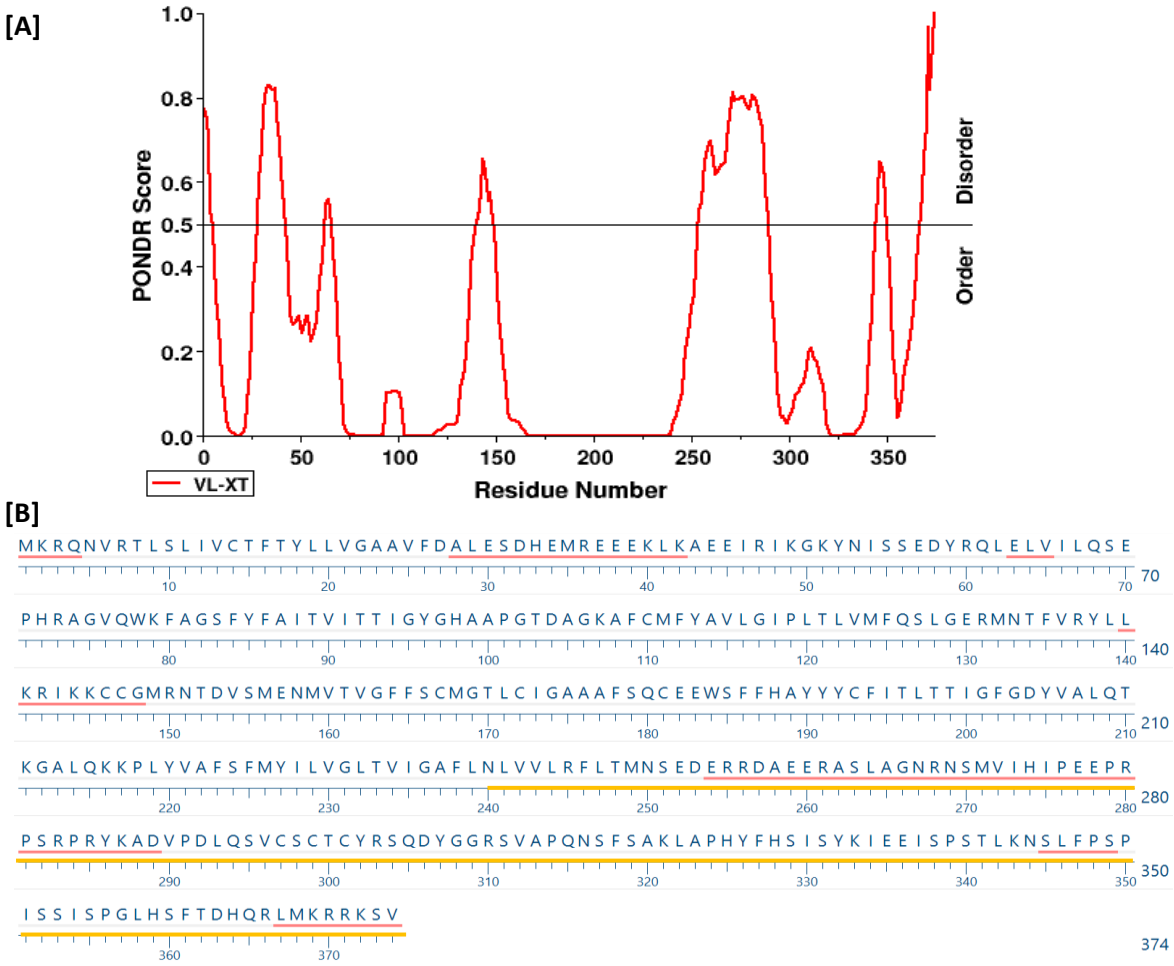

Figure 83 Prediction of naturally disordered regions

[A] The PONDR® VL-XT online algorithm was used to predict disordered regions with the full TASK3 protein. Outputs are measured between 0 and 1 before smoothing with a window of 9 amino acids. A residue score ≥ 0.5 is considered disordered. [B] The TASK3 sequence and ruler. Red underline highlights sequences of disorder promoting residues; yellow underline highlights the Ct domain.

IDPRs are characterised as containing <30% of disordered residues with at least one terminal segment (Nt/Ct) containing a region longer than 30 consecutive disordered residues or, a segment longer than 40 disordered residues at a location distinct from the terminal regions (Deiana *et al.*, 2019). Frequently found within the cytoplasmic domain of transmembrane proteins (Dosztanyi *et al.*, 2006, Iakoucheva *et al.*, 2002, Bürgi *et al.*, 2016), it is suspected that these regions play a possible role in the recruitment of regulatory molecules due to the often close proximity to phosphorylation sites (Iakoucheva *et al.*, 2004). Sequence analysis of the TASK3 protein identified a long stretch of disorder promoting residues closely following the VLRFLT motif (Figure 83) and preceding the phosphorylated residues critical for channel trafficking following 14-3-3 and COPI binding (Kilisch *et al.*, 2016). IDPRs are also suspected to play a major functional role in their ability to undergo folding upon contact with a phospholipid membrane or binding partner as part of a signalling pathway (Davidson *et al.*, 1998, Weinreb *et al.*, 1996, Sugase *et al.*, 2007, Bürgi *et al.*, 2016), similarly to that described in TREK1 regulation (Sandoz *et al.*, 2011).

Like TASK3 GPCR inhibition depends upon the VLRFLT motif, inhibition of TREK1 channels by a wide range of neurotransmitters, hormones, and pharmacological mediators all converge upon a glutamate residue (E306) within the cytosolic Ct, following stimulation from GPCRs coupled to G_q and G_s proteins (Honoré *et al.*, 2002). Whilst the mechanisms by which TREK1 is regulated by G_q-coupled receptors remains unclear, Sandoz *et al.* (2011) identified that GPCR inhibition of TREK1 occurs through the direct association and dissociation of the Ct with the plasma membrane. With inhibition associated with the dissociation from the membrane and vice versa with channel activity. This function appeared to be independent of PKC, rather depending on the hydrolysis of PIP_2 into DAG and IP3 but not when PIP_2 is converted to PIP via the Ciona intestinali voltage sensing phosphatase or rapamycin system which rapidly transports phosphoinositide 5-phosphatase enzymes to the membrane in order to break down PIP_2 to PIP. This suggests that the TREK1 Ct interacts non-specifically via electrostatic interactions to phosphoinositides generally rather than specifically binding to PIP_2 alone. This is not specific to TREK1 and resembles that of other K_{IR} channels including GIRK (KIR.X), ROMK1 (KIR1.1) and K_{ATP}. Such mechanisms are not restricted to potassium channels. The transient receptor potential ankyrin 1 channel (TRPA1) is a non-selective cation channel relying upon certain domains within the cytosolic Ct which are critical to channel activity in response to temperature, osmolarity, chemical compound, pH and many more (Witschas *et al.*, 2015).

Whilst it is established that basic residues in the TREK1 Ct electrostatically interacts with negatively charged head groups on the inner leaflet of the lipid bilayer resulting in a conformational change from a largely irregular random coil structure to β-pleated sheets (Sandoz *et al.*, 2011), the mechanisms involved in IDPRs binding to signalling molecules is unclear. There are currently two proposed mechanisms: 1) the induced fit, in which the IDPR folds in a way that is specific to the ligand binding, or 2) IDPRs dynamically adopt several conformations allowing a ligand to bind to a specific subpopulation of conformations, otherwise known as '*conformational selection'* (Gianni *et al.*, 2014, Vuzman and Levy, 2010, Bürgi *et al.*, 2016). The latter mechanism may explain how the plethora of structurally diverse modulatory molecules act upon TASK3 channels and supports the role of the VLRFLT as a transduction motif rather than a binding site (Veale *et al.*, 2007a), since the large disordered region immediately follows.

The biophysical analysis of peptide fragments in this instance is subject to a considerable degree of uncertainty since the behaviour of the fragment alone may differ from that of the full-length protein. Previous studies have shown that proteins containing >30% of disordered residues have an increased propensity to undergo proteolytic degradation (Gsponer *et al.*, 2008), likely due to the lack of tertiary arrangement (Deiana *et al.*, 2019). The GST-TASK3 peptide produced here displayed a disordered residue content of 43.4%. Whilst the protein was not cleaved during expression, it was readily cleaved throughout the purification stages and remained insoluble under normal physiological conditions.

Following successes of Zuzarte *et al.* (2009) in the production of a soluble TASK3 Ct (not inclusive of the VLRFLT, amino acid (AA) 249-374), this investigation mirrored their expression using PGEX vectors, with added inclusion of the VLRFLT motif. BL21 (DE3) *E. coli* were selected as the expression host of choice due to the documented ease of use, availability, high growth and production rates (Hammarström *et al.*, 2002), and to remain in line with the Zuzarte *et al.* (2009) method. The disadvantages of this expression system lie in the loss of post-translational modifications and production commonly in the form of inclusion bodies (Baneyx, 1999). The pGEX-6P-1 vector was therefore utilised as it included the GST fusion tag to support solubility and folding of the peptide. GST is commonly utilised as fusion partner for single-step purification (Smith and Johnson, 1988), owed to its binding with high-affinity to solid-state chromatography resins coupled with glutathione and elution in mild and non-denaturing conditions following the addition of reduced glutathione. GST fusion tag expression on the Nt has also been shown to stabilise protein folding and promote expression as a soluble protein rather than in inclusion bodies (Harper and Speicher, 2011) due to its hydrophilic surface. Despite its often-successful application, GST fusion proteins are susceptible to proteolytic degradation and inconsistent solubility, having severe effects on peptide production (Li, 2011).

Comparing isoelectric point (pI) of the fragment containing the motif (135 AA) against that of Zuzarte *et al.* (2009) (126 AA), resulted in only a 0.2 difference in overall net charge, becoming slightly more positive, yet (+VLRFLT) and (-VLRFLT) TASK3 constructs were found to be equally insoluble (see Figure 47 and Figure 64 respectively). This implied that the presence of the hydrophobic motif had no effect on protein stability in solution as hypothesised due to residence within the IC membrane. It also suggested that the presence of the hydrophobic VLRFLT motif alone was not the reason for insolubility. Despite being polar in nature the peptide remained insoluble in physiological conditions. This phenomenon is not unheard of in the production of IDPs (Graether, 2019) which have a propensity to form protein-protein interactions due to their ease of hydrogen bond formation and the availability of charged residues that readily contribute to electrostatic interactions (Linding *et al.*, 2004). Together, these factors make the aggregation of the peptide almost inevitable. Considering this, application of the mild chaotrope GuHCl was first attempted since this resolubilisation agent induces the least protein modifications and would not interfere with affinity purification, although requiring removal prior to SDS-PAGE analysis to prevent precipitation. Unfortunately, this agent and urea were unable to effectively solubilise protein at moderate concentrations, with the application of 8M urea most successful but the sample required refolding. Another disadvantage of this approach is the potential for covalent modification as concentrated urea solutions can accumulate isocyanate ions over time, leading to the carbamylation of amino groups (Hwang *et al.*, 2014). This was avoided as much as possible by the production of fresh solution each trial.

Unlike many ordered proteins, proteins containing regions of intrinsic disorder display often inexplicable resilience when exposed to harsh conditions like extreme temperatures and pH (Uversky, 2017, Lee *et al.*, 2019), maintaining functionality or rapidly regaining it when returned to physiological conditions (Uversky, 2013, Uversky, 2016). Unexpectedly, the GST-TASK3 peptide was stable and whole in a monomeric conformation only in HEPES (pH 10) solution and not PBS (pH 7); with exposure to the latter resulting in cleavage of the GST tag and precipitation, thus of no use for purification via the GST column. Furthermore, enzymatic cleavage of GST from the peptide in HEPES buffer resulted in a loss of structure. The protein was first exposed to this high pH during the utilisation of the strong anion exchange column. The peptide exhibited a predicted pI of 9.3. As the protein appeared unstable in buffers such as TRIS at a pH below the pI, anion exchange purification was used. In a buffered solution of a pH > pI, the peptide becomes negatively charged allowing binding to the positively charged functional groups of the anion exchange resin. HEPES buffer is a zwitterionic sulfonic acid buffering agent used in the standard ion exchange protocol due to its capacity to maintain physiological pH despite fluctuations in environmental CO_2. HEPES buffer was used at pH 10 in order to exceed the protein pI despite HEPES maintaining a pH buffering capacity of 6.8 – 8.2 (Good *et al.*,

1966). Although alternative buffers such as diethylamine are more equipped to this alkaline condition (Fekete *et al.*, 2015), HEPES has been successfully used in anion exchange chromatography at a pH which exceeds this capacity elsewhere in literature in the purification of proteins (Tamaskovic *et al.*, 2012).

In absence of knowledge of the buffers used by Zuzarte *et al.* (2009) in the production of the TASK3 Ct without the VLRFLT motif included, it remains unclear as to why the Ct peptide produced in this study was insoluble. With deletion of the motif failing to save the solubility of the peptide, this study found the technique impossible to replicate.

4.5.1 Limitations

The findings of this study must be seen with consideration of the limitations. Due to the difficulties experienced in protein production and purification, time limitations meant that we were unable to alternate expression approaches or undertake extensive optimisation. Whilst the protein is currently stable in HEPES at pH 10, this buffer may not be the most suitable with regards to the strong anion exchange chromatography or from a physiological perspective. Given more time it would be useful to experiment with alternate fusion tags which may be better equipped to solubilise and purify the protein at a physiological pH such as the SUMO tag (Marblestone *et al.*, 2006). Optimisation of this phase could eventually lead to a more homogenous product which would provide better insight into the structural features following CD or even NMR spectroscopy.

4.6 Conclusions

The Ct peptide produced in this chapter displayed significantly different physicochemical properties with regards to pI and stability in solution. Expression of this peptide in an environment lacking the possible electrostatic interactions provided by the phospholipid bilayer may be equally detrimental to the solubility of the peptide. Nevertheless, the GST-TASK3(+VLRFLT) peptide remains stable in HEPES buffer at pH 10 despite the GST fusion tag appearing to be dysfunctional. Both the CD data presented herein and sequence analysis point toward the peptide being intrinsically disordered in nature. Since intrinsically disordered proteins display high resilience in extreme conditions such as the highly basic environment described here, it is hopeful that the peptide remains stable enough for binding characterisation studies of the VLRLFLT motif in the following chapter.

Chapter 5:

Functional Characterisation of the TASK3 VLRFLT Motif

5.1 Introduction

Like TREK1, channel inhibition of TASK3 following GPCR regulation has been shown to occur mostly independently of PKC, unable to entirely abolish TASK3 current in certain conditions, with some evidence supporting a counteractive performance of PKC, targeting threonine 341 (Thr341) within the Ct to prevent prolonged inhibition and support reactivation of the channel (Veale *et al.*, 2007b). However, differing from TREK1, it has also been suggested that inhibition of TASK3 occurs independently of $G\alpha_{q/11}$ mediated activation of PLC and PIP_2 (Chen *et al.*, 2006, Zhang *et al.*, 2016). In the event of GPCR stimulation, it is suspected that insertion of PIP_2 into the inner leaflet allows non-specific electrostatic interactions of the TREK1 Ct and, whilst the channel remains 'gated,' it is now activatable following stimulation by depolarisation, membrane stretch or IC acidification. It is only when the negative charge of the E306 residue is masked either via protonation in acidic conditions where the channel remains open in a typical 'leak' state or through mutations such as E306A which retains the pore in a 'locked' open position. Considering this, how could a similar affect be achieved following the direct binding of $G\alpha_{q/11}$ to the Ct domain of TASK3 without PIP_2 or PKC activity? Direct inhibition of channel activity by $G\alpha_{q/11}$ has been previously described in the cold-activated TRPM8 ion channel following histaminergic input (Zhang *et al.*, 2012, Zhang, 2019).

Unlike conventional signalling cascades, $G\alpha_q$ was reported to cause channel inhibition independently of PLC and PKC activity, as well PIP_2 hydrolysis by forming a complex with the channel and was dependent upon the presence of a VLRFLT motif (Talley and Bayliss, 2002a). Instead, it was proposed that direct binding of inactivated $G\alpha_{q/11}$ in a constitutive complex undergoes a conformational change following GPCR activation causing a 'rapid and direct trans-inhibition' (Zhang *et al.*, 2012). It would be tempting to speculate that considering PIP_2 independence, following GPCR activation, should the $G\alpha_{q/11}$ already be complexed with the TASK3 Ct, $G\alpha_{q/11}$ could be activated faster than the conventional PLC pathway can be initiated. This would negate the requirement for PIP_2 depletion. Couple this with a potentially high affinity of TASK3 for PIP_2, may also address theories surrounding PIP_2 depletion, should the channel be fully occupied by PIP_2 even in the event of depletion as a result of PLC activation (Gamper and Shapiro, 2007, Suh and Hille, 2008). Such a theory is supported by the work carried out by Zhang *et al.* (2016), demonstrating the co-precipitation of TASK3 with $G\alpha_{q/11}$ following neurotensinergic excitation of NTS1. Model structures of the heterotrimeric $G\alpha\beta\gamma$ hint at the presence of a switch III loop extending out from the protein surface to bind to proteins such as the TRPM8 channel however, this binding site differs from that which interacts with PLC. Therefore, their separate binding domains which permit mutual and independent regulation by $G\alpha_{q/11}$ may potentially offer an explanation of the minor effects of PLC and PIP_2 reported by some groups (Zhang *et al.*, 2012).

5.2 Aims and Objectives

The most recent literature suggests that WT-TASK channels are regulated by the direct binding of activated $G\alpha_{q/11}$ to the Ct following activation of GPCRs by external agonists (Zhang *et al.*, 2016). This regulation is also reported to be dependent on the presence of the VLRFLT motif at the extreme proximal end of the Ct. To date, it has not yet been confirmed whether these 6 amino acids serve as a binding site or a transducer of the intracellular signal to the selectivity filter gating mechanisms. The aim of this study was firstly to determine whether a constitutively active $G\alpha_{q/11}$ analogue, GAQ/11, binds directly to the channel and secondly, to characterise the affinity of binding events should they take place. The objective of this chapter was to investigate the binding properties of the hTASK3 Ct peptide inclusive of the VLRFLT motif produced in Chapter 4, and conclusively confirm the direct binding of $G\alpha_{q/11}$ to the channel. Using synchrotron radiation circular dichroism, this chapter provides insight into conformational changes occurring at a secondary structure level upon binding of GAQ/11 to the TASK3_(+VLRFLT) Ct peptide.

5.3 Methods

5.3.1 Protein Production and Purification

The TASK3_(+VLRFLT) and TASK3_(-VLRFLT) peptide were produced and purified as described in Chapter 4.

5.3.2 Synchrotron Radiation Circular Dichroism (SRCD)

SRCD spectra were measured on beam Line B23 at the Diamond Light Source Ltd (Didcot., UK). The instrument was calibrated with HEPES buffer. SRCD measurements were collected under the following instrument parameters: a 10 mm path length cell, 1 nm increments, 1 second integration time and a 1nm bandwidth at approximately 24.6°C. Spectra were measured over the wavelength range of 260 to 185 nm, however below 210 nm the spectra were too noisy to include below (likely due to high salt concentration of the buffer), therefore only the far-UV spectral region (210 - 260 nm) are shown. Each wavelength represents 4 replicates and the error bars on the graph represent standard deviation.

Samples were used at a concentration of 0.22 μM in 25 mM HEPES/70 mM NaCl at pH 10 (Appendix 3.3). Sample controls can be seen in the table below:

Sample	
GST-TASK3_(+VLRFLT) (43 kDa)	Protein produced in Chapter 4
Glutathione-*S*- Transferase Tag (26.98 kDa) Purified Protein	OriGene (Rockville, USA)
14-3-3 α/β (29 kDa) Purified Protein	Merck (Darmstadt, Germany)
GAQ/11 (41.9 kDa) Purified Protein	OriGene (Rockville, USA)

5.4 Results

5.4.1 The 14-3-3 α/β positive control binds the TASK3 (+VLRFLT) peptide

SRCD spectroscopy was carried out to explore the interactions of the TASK3_VLRFLT peptide with the GAQ/11 protein. The 14-3-3 α/β adaptor protein was included in this study as a positive control known to bind the [RRKSV] motif expressed in the extreme distal portion of the TASK3 Ct (Zuzarte *et al.*, 2009). Through analysis of the spectra in the far-UV region (210 – 260 nm) it is not possible to identify conformational changes occurring at the secondary structure level with regards to the formation of α-helices *etc.* however, it can confirm overall changes in secondary structure as a result of interactions in equimolar combinations. In support of the binding of 14-3-3 α/β to the TASK3 Ct which is reported in literature to be critical for the forward traffic of the channel to the membrane, distinct differences were observed between the calculated (red dotted line) and observed (solid blue line) values in the SRCD spectra for the TASK3_(+VLRFLT) peptide and 14-3-3 α/β (Figure 84). When titrated together, both the 14-3-3 (green line) and TASK3 (black line) spectra appear to change significantly when compared to the proteins in isolation. This suggests that despite existence in pH 10 conditions, the TASK3 peptide remains conformationally correct and able to bind with a known binding partner.

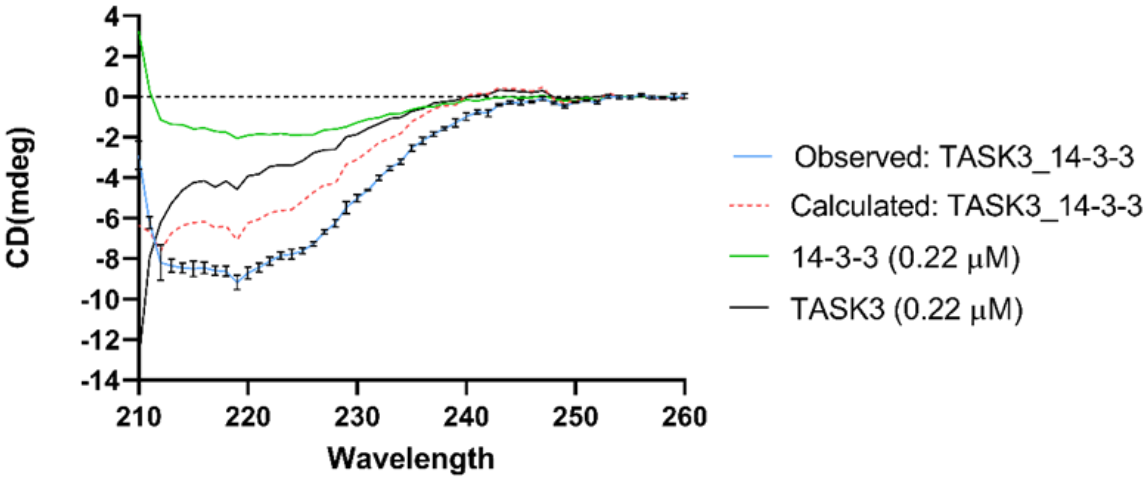

Figure 84 SRCD spectra of the TASK3 peptide in combination with 14-3-3 in equimolar conditions

Spectra of TASK3 (black) and 14-3-3 (green) were first collected in isolation for generation of calculated value (red dashed). Titration of the two proteins together produced an observed spectra (blue) that was significantly different from the calculated trace, confirming that the 14-3-3 does bind to the TASK3_(+VLRFLT). Error bars represent standard deviation (n= 4).

In Figure 84, the calculated trace was first obtained by collecting the SRCD spectra for both 14-3-3 (solid green line) and TASK3 (solid black line) were first collected in isolation. These two spectra were then added together to generate a calculated value (red dashed line) for the titration of the proteins. Following the titration of TASK3 and 14-3-3 together in solution at equimolar concentrations, the actual observed spectra (solid blue line) is not superimposed with the calculated value. Since there remains a clear difference between the observed spectra and the calculated spectra of the binding partners in isolation, it confirms that a significant binding event is occurring between the peptide and the 14-3-3 ligand has taken place.

To validate the effect of binding as a result of interaction with the Ct peptide rather than the associated Nt GST tag, purified recombinant GST protein was also assessed for binding with the purified partners. For Figure 85, the SRCD spectra for both GST and 14-3-3 were first collected in isolation. These two spectra were then added together to generate the calculated value (red dashed line). Following the titration of GST and 14-3-3 together in solution at equimolar concentrations, the observed spectra (solid blue line) is seen to completely overlap the calculated value. No difference between the observed spectra and the calculated spectra of the binding partners in isolation confirms that no binding between the tag and the ligand takes place and that the binding observed in Figure 84 is a result of 14-3-3 binding the peptide and not the tag and provides a suitable negative binding control for the following results.

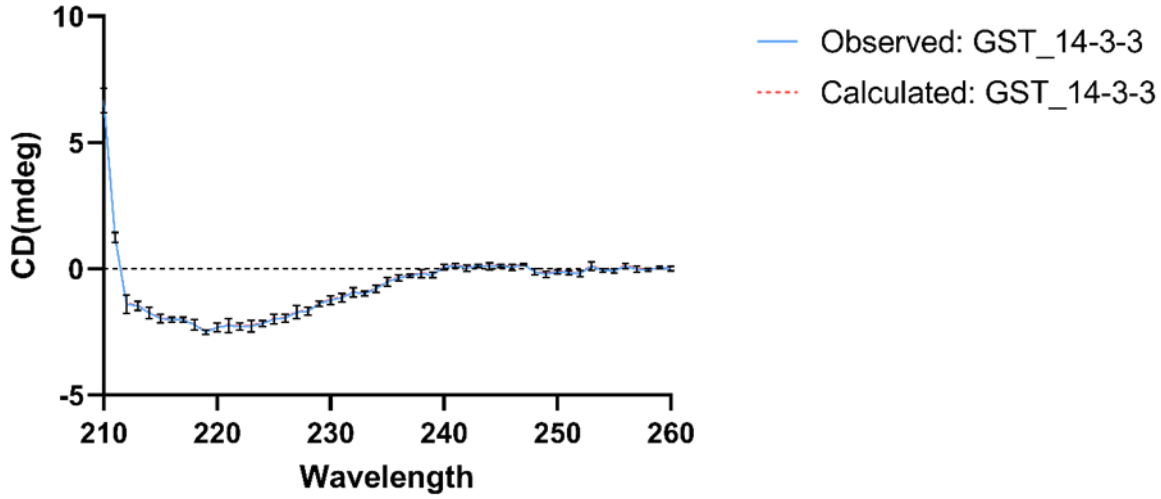

Figure 85 SRCD spectra of purified GST in combination with 14-3-3 α/β

The titration of purified GST tag with the 14-3-3 ligand together produced an observed spectra (blue) that was no different from the calculated trace (dotted red), confirming that the 14-3-3 does not bind to the GST tag. Error bars represent standard deviation (n= 4).

5.4.2 GAQ/11 directly interacts with the TASK3 (+VLRFLT) peptide

To validate the effect of GAQ/11 binding as a result of interaction with the peptide rather than the associated Nt GST tag, purified recombinant GST protein (orange line) was first assessed for binding with the purified GAQ/11 (green line). It can be seen in Figure 86, that there is a significant difference between the observed and calculated values obtained following the GST_ GAQ/11 titration, confirming the presence of non-specific binding between the tag and the GAQ/11 ligand. In this case, the difference between the calculated and observed values of the GST_GAQ/11 spectra were calculated and subtracted from the observed values of the TASK3_GAQ/11 spectra (Figure 87) to account for any binding of the GAQ/11 protein to the tag.

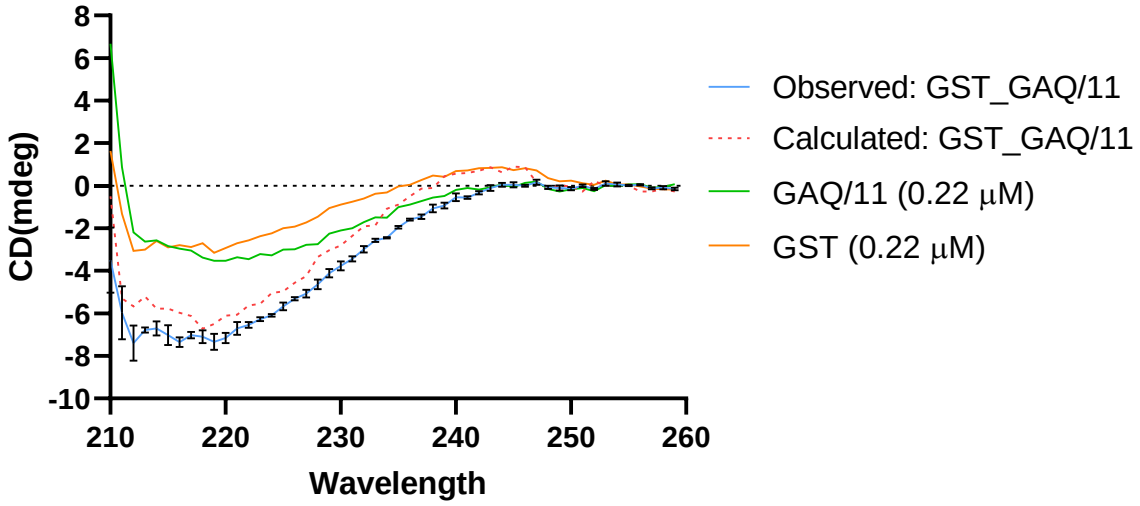

Figure 86 SRCD spectra of purified GST in combination with GAQ/11

Spectra of GST (orange) and GAQ/11 (green) were first collected in isolation for generation of calculated value (red dashed). Titration of the two proteins together produced an observed spectra (blue) that was significantly different from the calculated trace, confirming that the GAQ/11 does non-specifically bind to the GST tag. Error bars represent standard deviation (n= 4).

The structure of GAQ/11 consists of a combination of α-helices, β-sheets and turns (Kamato *et al.*, 2015). It appears that the spectra of GAQ/11 alone (green line) in Figure 87, that the protein has retained secondary structure following storage in pH 10 solution as the spectra resembles beta-sheet conformation by its positive value at 210 nm. Alternately, the TASK3_(VLRFLT) peptide (black line) appears to be predominantly irregular in structure however, the spectra unfortunately do not contain low wavelength regions (<200 nm), where signature spectrums for 'random coil' and 'unfolded' and denatured regions reside and are therefore unable to make predictions regarding structure from this data.

Fortunately, the GST_14-3-3 and TASK3_(+VLRFLT) Ct_14-3-3 interactions depicted in Figure 85 and Figure 84 offer both negative and positive controls respectively. It can therefore be said with a great certainty that upon the titration of the protein and the peptide, and subtraction of the GAQ/11 interaction with the GST tag, as quantitatively it appears that a complex is formed since the calculated (red dotted line) and observed spectra (blue solid line) continue to remain significantly different, an observation supported by the small, non-overlapping error bars. Whilst the difference is very clear at wavelengths between 210 and 225 nm, the difference appears much smaller at ~235 nm. Although inferential statistical analyses are not routinely conducted for SRCD, to demonstrate the magnitude of suspected binding, an unpaired students t-test was carried out on the smallest (230 nm) and largest (215 nm) differences between observed and calculated spectra in Figure 87 to confirm significance. The smallest absolute difference between the calculated and observed spectra was 0.5576 ± 0.1061 (unpaired student's t-test, $p < 0.01$) when compared to the largest absolute difference, 1.37 ± 0.4761 (unpaired student's t-test, $p < 0.05$), confirming that the binding remains significant.

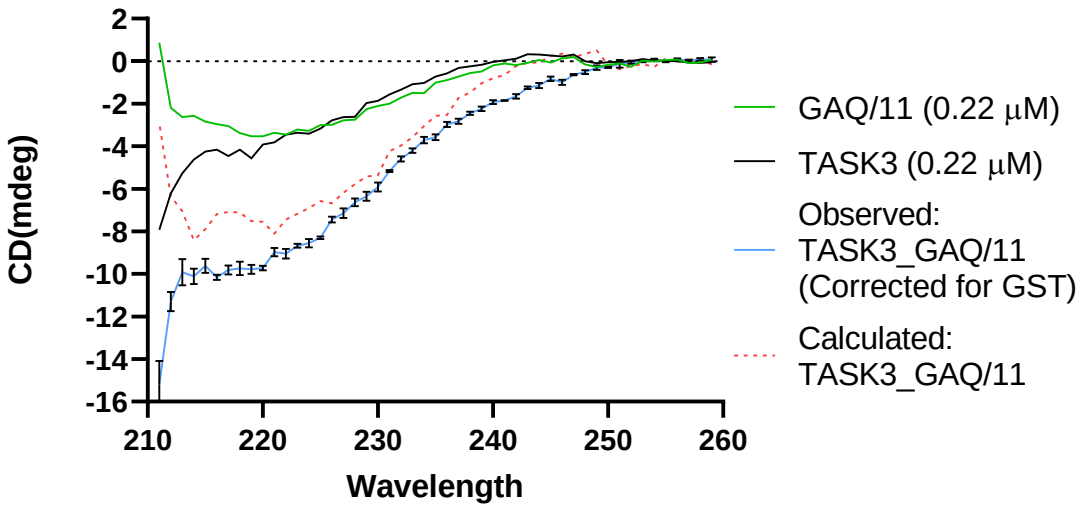

Figure 87 SRCD spectra of the TASK3 peptide in combination with GAQ/11 in equimolar conditions

Following confirmed binding of GAQ/11 to GST, the effect of this binding was subtracted, and any difference observed above is the direct result of GAQ/11 (green line) binding to the TASK3 peptide (black line) and not the tag. Differences between the observed (blue line) and calculated (red dotted line) values for the TASK3_GAQ/11 interaction confirms a conformational change in secondary structure associated with a binding event. Error bars represent standard deviation (n= 4).

5.5 Discussion

Activation of $G\alpha_{q/11}$-coupled receptors by neurotransmitters, hormones and pharmacological agonists inhibit TASK3 channels, causing depolarisation and increasing excitability of the membrane. Unlike conventional GPCR regulation, inhibition of TASK3 channels continues independently of PIP_2 and PKC actions (Wilke *et al.*, 2014, Zhang *et al.*, 2016) and instead the direct interaction of $G\alpha_{q/11}$ with the channel rather than the downstream signals has been observed (Zhang *et al.*, 2016, Chen *et al.*, 2006). A similar model of channel inhibition was previously reported by Wilke *et al.* (2014) who argued for the role of the direct binding of resident membrane messenger DAG to the channel, inducing channel inhibition following GPCR activation of PLC. However, other groups have determined GPCR regulation of TASK3 to occur independently of this action (Zhang *et al.*, 2016). It is becoming increasingly evident that there is no single pathway involved in the GPCR regulation of TASK3 channels (Mathie, 2007), with all of those mentioned above likely to contribute to channel regulation. The data presented in this chapter primarily supports the direct interaction of $G\alpha_{q/11}$ with the channel.

SRCD was used to identify possible changes in secondary structure content accompanying the formation of a complex between the TASK3_(+VLRFLT) peptide and the $G\alpha_{q/11}$ analogue. Direct interaction of TASK channels with 14-3-3 α/β proteins has previously been detected in yeast-two-hybrid screens and co-immunoprecipitation studies (O'Kelly *et al.*, 2002, Rajan *et al.*, 2002, Shikano *et al.*, 2005). This interaction is identified to occur at the [xRRKS^{P}V] motif at the extreme distal portion of the TASK Ct and is critical for forward traffic from the ER (Zuzarte *et al.*, 2009). As such, 14-3-3 α/β was included as a positive control for its known binding activities however, this interaction has not before been observed using CD technology. The SRCD data in Figure 85 initially confirms that the GST tag expressed on the TASK3 Ct peptide does not interact with the 14-3-3 α/β at all, as evidenced by the complete overlap of the GST and 14-3-3 α/β traces. This data set therefore serves as an important negative control for any binding activity. Upon titration of 14-3-3 α/β with the TASK3_(VLRFLT), the peptide continued to interact with the protein binding partner, as can be observed by the clear lack of overlap in Figure 84. Not only does this finding serve as a positive control for peptide-protein interaction, it shows that the peptide is likely to remain conformationally correct and functional despite having been expressed in non-physiological conditions. Whilst it is apparent that direct interaction of the 14-3-3 protein with TASK channels is critical in the regulation of channel expression (Zuzarte *et al.*, 2009), the mechanism of binding and the subsequent transduction remains unclear. The mammalian 14-3-3 proteins are suspected to contain an interactome consisting of >200 proteins (Mackintosh, 2004), many of which are known to be ion channels other than TASK3. Therefore, it is unlikely that each of these target proteins contain a conserved binding site for a protein which is a

notably rigid dimeric structure (Yaffe, 2002, Obsil *et al.*, 2001, Rittinger *et al.*, 1999). The binding of 14-3-3 to its target protein has been shown to induce a conformational change and/or constrain the protein in a particular conformational arrangement leading to a plethora of functional outcomes including: promotion of substrate binding, stabilisation of transition states, enhancing post-translational modifications (Yaffe, 2002) or, in the case of TASK1 and TASK3, facilitation of channel localisation by masking the retention signal (Zuzarte *et al.*, 2009). Such an interaction supports the theory surrounding the presence of IDPRs within the TASK3 Ct which undergo induced-fit or conformational selection interactions as discussed previously in section 4.5. SRCD spectroscopy techniques were originally employed to investigate the changes in secondary structure following protein-peptide interactions at wavelengths lower than the detection limit of conventional CD. Unfortunately, the high salt concentration of the HEPES buffer used in these experiments made the identification of specific changes at the secondary level impossible since the spectra were too noisy at wavelengths <210 nm. Therefore, predictions cannot be made regarding the degree of order or structure of the peptide/complex because these features are typically found in the range of 180 – 200 nm (Wallace, 2009) and can only elucidate upon the presence of binding activity. However, SRCD displaying the direct 14-3-3 interaction with TASK3_(+VLRFLT) remains to be a novel finding.

Whilst the GST tag did not bind to 14-3-3 α/β, it did unexpectedly exert a small amount of interaction with GAQ/11 (Figure 86). After correcting for GST binding, the difference in overall secondary structure continued to be significantly different following titration when compared to the GAQ/11 and TASK3_(+VLRFLT) in isolation (Figure 87). This finding supports previous studies that utilised co-immunoprecipitation approaches that hinted toward the direct binding of $G\alpha_{q/11}$ with the TASK3 Ct (Chen *et al.*, 2006, Zhang *et al.*, 2016). The direct binding of $G\alpha_{q/11}$ with the termini of transmembrane ion channels following GPCR activation is not a novel phenomenon, having been previously described for Ca_V (Simen *et al.*, 2001), GIRK (Koike-Tani *et al.*, 2005) and more recently TRPM8 channels (Zhang, 2019). In the case of TRPM8, $G\alpha_{q/11}$ gates the channel through interactions with its Switch III domain. The exchange of GTP to GDP following GPCR activation causes major conformational changes to $G\alpha_{q/11}$, engaging the negatively charged switch III loop for interaction (Waldo *et al.*, 2010, Zhang, 2019). $G\alpha_{q/11}$ may then electrostatically bind via its switch III loop to positively charged residues in the TRPM8 Nt whilst its α3 helix binds to the TRP domain in the proximal region of the Ct. Together, these two binding sites likely tether the G-protein to a site within the cytoplasmic cavity of TRPM8, causing allosteric inhibition (Zhang, 2019). Indeed, the recent discovery of a lower X-gate of TASK1 channels have been shown to 'trap' channel inhibitors within the vestibule, snaring inhibitors by the crossing of the individual subunit Ct at the VLRFLT motif (Rödström *et al.*, 2019). The VLRFLT motif is critical for the response following application of volatile anaesthetics (Patel *et al.*, 1999) and GPCR activation

(Talley and Bayliss, 2002a), with deletion of the VLRFLT motif abolishing channel inhibition (Veale *et al.*, 2007a) whilst truncation (removal of the phosphorylation sites at the extreme distal portion of the Ct) significantly reduces inhibition (Talley and Bayliss, 2002a). Since GPCR-mediated channel inhibition has been shown to continue unabated following PKC and PLC inactivation (Zhang *et al.*, 2016), it is unlikely that the TASK3 Ct functions as a molecular scaffold, bringing together $G\alpha_{q/11}$ and PKC in proximity. Neither is it likely that the binding of $G\alpha_{q/11}$ to the Ct activates local PKC to induce channel phosphorylation since 1) channel inhibition is not abolished following Ct truncation (Talley and Bayliss, 2002a) and 2) channel inhibition remains unaffected in absence of PLC conversion of PIP_2 to IP_3 and DAG (Zhang *et al.*, 2016) despite the direct application of DAG also proving to inhibit the channel (Wilke *et al.*, 2014).

As discussed previously in section 4.5, GPCR inhibition of TREK1 occurs through the direct association and dissociation of the Ct with the plasma membrane (Sandoz *et al.*, 2011). This function appeared to be independent of PKC but instead relied upon electrostatic interactions to phosphoinositides generally rather than specifically binding to PIP_2 alone (Sandoz *et al.*, 2011). Like the allosteric inhibition of TRPM8 following direct $G\alpha_{q/11}$ binding (Zhang, 2019), it is possible that $G\alpha_{q/11}$ requires the positively charged residues of the VLRFLT motif for the switch III loop interaction whilst the rigid α3 helix binds to an unknown site within the channel vestibule. Binding of $G\alpha_{q/11}$ in such a manner at the extreme proximal portion of the Ct may alter the conformational arrangement, in turn allosterically hindering the electrostatic interaction with the inner leaflet of the plasma membrane. It is possible that this could drive the dissociation of the Ct, resulting in channel inhibition. Indeed, the crystal structure of TASK1 has shown that the VLRFLT X-gate structure must be capable of undergoing significant conformational changes to accommodate for the presence of hydrated K^+ ions and channel inhibitors (Rödström *et al.*, 2019). Such conformational changes include the relaxation of the X-gate from an extended helix into a α-helical conformation, allowing the straightening of the TM4 domains as the channel takes on a more activated state (Rödström *et al.*, 2019). It has been suggested that the G236R loss of function mutation associated with *KCNK9* imprinting syndrome is caused by the insertion of a large, positively charged amino acid may prevent the conduction of ions through the pore (Veale *et al.*, 2014) however, the loss of GPCR regulation observed in this syndrome closely resembles that of the VLRFLT deletion studies (Veale *et al.*, 2007a). Since the binding of $G\alpha_{q/11}$ to TRPM8 requires two binding sites to stabilise the interaction (Zhang, 2019), it is not unreasonable to suggest that the G236R mutation may either be very close to the α3 helix binding site thus impeding access or, it may prove to be the binding site required to stabilise the $G\alpha_{q/11}$ interaction. Since my investigation consisted of the Ct peptide only, this may only be hypothesised.

5.5.1 Limitations and Future Work

In continuation of these findings, it would be appropriate to first repeat the SRCD investigation using the TASK3 peptide that does not contain the VLRFLT motif. This would finally confirm whether the motif functions as a binding site for $G\alpha_{q/11}$ or is required for the transduction of intracellular signals to the SF. Unfortunately, the time constraints of the PhD research programme prevented this study from being fully conducted at the Diamond Light Source (Didcot, Oxford).

Following confirmation of direct binding of $G\alpha_{q/11}$ to the peptide, it would be useful to identify the properties of this interaction using techniques such surface plasmon resonance. Such approaches would elucidate a selection of relevant parameters including reaffirmation of ligand binding, specificity, binding stoichiometry, kinetics (association/dissociation) and affinity. Due to the high salt content of the peptide storage buffer, SRCD was unable to specifically identify changes occurring at the secondary level following protein-peptide interactions. Due to the flexible nature of the Ct, the techniques usually used for structural investigation, such as X-ray crystallography and single-particle electron microscopy, are limited. A better approach would be to consider NMR spectroscopy, which can provide residue-specific information, or small-angle X-ray scattering to identify the changes in shape, especially when working with proteins containing IDPRs (Ambadipudi and Zweckstetter, 2016).

One of the key limitations of this study was that the production of the isolated peptide meant these findings could not be directly related to events occurring *in vivo* or *in vitro* and may only be used to hypothesise upon cellular mechanisms. In producing the peptide fragment alone, it was stripped of the naturally occurring interactions within the cellular environment which would likely destabilise the fragment in solution. During the period of this PhD programme, phospholipid bilayer nanodisc technology has advanced, providing an alternative approach to the studying of whole transmembrane proteins in membrane mimetics using styrene maleic acid rather than denaturing detergents (Bayburt and Sligar, 2010). These systems have been successfully implemented in purification and reconstitution of full-length transmembrane ion channels, which stabilise the structure and enable the application of conventional NMR technology for full structural resolution (Autzen *et al.*, 2018).

The modulation of TASK3 channels occurs in a complex interactome where it is possible that regulation manifests from multiple binding events. Such an observation alludes to the limitations of clinical benefits produced by mono-target therapies. Using technologies such as those mentioned above may serve to identify distinct binding epitopes/interactions which will aid in the development of novel multi-target drugs with a more favourable therapeutic profile.

5.6 Conclusions

This chapter provides evidence that the TASK3_(+VLRFLT) peptide produced in Chapter 4 is likely to be conformationally correct, as SRCD spectra confirms for the first time the direct interaction of the known binding partner: 14-3-3 α/β. Furthermore, the direct binding of $G\alpha_{q/11}$ to the peptide was also confirmed although it was not possible to identify whether the VLRFLT motif serves as a transduction region or a direct binding site. Whilst the study was unable to determine the specifics of the structural changes occurring at a secondary level following the binding of GAQ/11, it is possible due to the flexible nature and the presence of IDPRs, that the Ct fragment both *in vivo* and *in vitro* are likely to undergo induced-fit or conformational selection interactions upon binding of $G\alpha_{q/11}$.

Chapter 6:

Consolidation

This thesis set out to explore the regulation and function of TASK channels in disease, with focus upon variants associated with *KCNK9* Imprinting syndrome and PAH. The first part of this study sought to explore the cause of the reduced activity of TASK channel variants associated with disease as a function of impaired trafficking to the plasma membrane. Additionally, the investigation extended to the subcellular organelles to determine differences in expression of the mutant channels in the ER and mitochondria, and the possible implications in pathogenesis. The second part of the study surrounded the regulation of TASK3 channels following the activation of $G\alpha_q$-coupled receptors. Our lab has previously shown that GPCR-induced inhibition of TASK3_G236R channels was abolished (Veale *et al.*, 2014). For the first time, the effects of activated G-proteins on the G236R mutated channel were investigated to determine whether the regulatory effect could be replicated following the direct application of activated $G\alpha_q$ in absence of the receptor. It also aimed to determine whether any reduction in current was a consequence of internalisation of the channel from the plasma membrane or a consequence of physiological changes to the channel itself following co-expression with activated G-proteins. The final portion of this research focused upon the binding characteristics of the TASK3 Ct. Deletion of the VLRFLT motif from the proximal region of the TASK3 Ct has been shown to attenuate channel regulation by anaesthetics and GPCR activation, a functional consequence mirrored by the TASK3_G236R variant. In absence of a crystal structure containing this motif, determining its role as a signal transducer or a binding site remained to be resolved. For the first time, a TASK3 Ct peptide was produced that contained the VLRFLT motif, allowing for the characterisation of the binding activity of the Ct peptide.

6.1 Exploration of TASK channel trafficking and the functional consequences of pathological variants

Upon discovery of the TASK3_G236R mutation, it was originally concluded that the channel was non-functional, a finding that has since been disproved following confirmation of a current which is significantly reduced and predominantly inwardly rectifying when compared to the WT (Veale *et al.*, 2014). Similar manifestations were identified in novel TASK3 channel variants: Y205C and Y205Δ which also present with the *KCNK9* Imprinting syndrome phenotype. Likewise, the loss-of-function G106R and L214R mutations occurring in TASK1, have been implicated in an aggressive form of PAH (Navas *et al.*, 2016). Due to the constitutively active nature of TASK channels expressed at the plasma membrane surface, changes in the level of surface expression can directly alter current density and thus function (Mathie *et al.*, 2010). In Chapter 2, I show that the TASK3_G236R channel exhibits reduced expression at the plasma membrane. Considering the data confirmed that the channel

continues to be trafficked to the ER and mitochondrial compartments as efficiently as the WT, it suggests that the channel is rapidly recycled from the plasma membrane and recruited into alternate degradative pathways rather than displaying impaired trafficking ability. Regardless, a small proportion of the G236R variant continued to traffic to the plasma membrane however, GPCR-mediated inhibition of the channel remained significantly attenuated (Chapter 3). Whilst previous literature had shown that activated $G\alpha_q$ interacts directly with the WT channel (Zhang *et al.*, 2016), we confirm in Chapter 3 for the first time that the TASK3_G236R channel continues to interact with activated $G\alpha_q$ as the co-expression of TASK3_G236R with the activated G-protein enhanced the colocalisation of the mutant channel with the cell surface membrane although all regulatory activity is lost.

Unlike TASK3_G236R, the Y205C and Y205Δ variants were found to have no effect on channel trafficking to the plasma membrane and were indistinguishable from WT. Previous investigation into TASK3 trafficking had suggested that the channel required the 14-3-3 and COPI binding motifs within the Ct to drive antero- and retrograde transport (Zuzarte *et al.*, 2009). I found this not to be the case with the Y205 truncation and instead suggest that the channel either contains internal trafficking motifs which are exposed following the truncation of the protein or, that the channel will continue to traffic to the membrane providing that the Nt remains intact. The Y205 residues are thought to contribute to an 'aromatic cuff' around the mouth of the pore domain which regulates pore dimension and supports selective K^+ uptake (Doyle *et al.*, 1998). In shaker and hERG channels, disruption to this analogous region forces the pore into a permanently inactive C-type gating position (Heginbotham *et al.*, 1994, Fan *et al.*, 1999). Likewise, insertion of the hydrophobic Cys residue (Y205C) into the pore domain promotes the formation of non-specific S-S bonds which can equally stabilise the inactivated state, causing the pore to collapse inwards on itself (Hoshi and Armstrong, 2013). Together, these data offer explanation for the complete lack of current observed at the membrane with the Y205 variants, which are independent of trafficking impairments. This hypothesis of channel instability neatly coincides with our findings of significantly increased expression of the TASK3_Y205 variant channel in the ER despite efficient plasma membrane expression. Misfolded or unstable proteins have been shown to evade the quality control mechanisms enforced during protein production and continue to be trafficked to the membrane however, these proteins often display a decreased half-life (Tizzano *et al.*, 1993). As such, these channels are likely to undergo rapid endocytosis to the ER prior to targeting to the cytosol for degradation (Marcorelles *et al.*, 2014). Considering this finding, it would be insightful to extend this study to include colocalisation studies of the Y205 and G236R variants, with a focus on the late endosomes and lysosomes to determine the degradative fate of these channels.

There is a large body of data available which explores the role of TASK3 channels expressed on the inner mitochondrial membrane due to its malignant implications however, there is little availability of research that investigates the role of mitochondrial TASK3 expression in arousal and wakefulness in association with sleep disorders. Low arousal is one of many symptoms reported in patients with *KCNK9* Imprinting syndrome (Graham *et al.*, 2016). Until now, there was no literature available which explored the expression of the variants associated with this condition in relation to mitochondrial metabolism. Despite finding that the Y205Δ truncated channel was expressed significantly more than the WT, the expression of the G236R and Y205C variants was not. This study was therefore unable to definitively link TASK3_G236R expression in the mitochondria to the low arousal symptoms reported however, it does confirm that the mutant channel can still be trafficked to the mitochondria. It is perhaps more plausible that symptoms of low arousal are likely to be attributed to the loss of GPCR regulation following stimulation by wake-active neurotransmitters histamine and neurotensin in basal forebrain cholinergic neurons and dentate gyrus cells respectively.

TASK1 channels are key participants in the regulation of the resting membrane potential of PASMCs (Olschewski *et al.*, 2006). Reduced expression of TASK1 in PASMCs is now a recognised event in the pathogenesis of PAH (Antigny *et al.*, 2016). TASK1 channel variants, G106R and L214R, are two particularly aggressive homozygous mutations (Navas *et al.*, 2016) which fail to respond to pharmacological interventions that have previously been shown to enhance WT activity (Ma *et al.*, 2013, Cunningham *et al.*, 2019). Like the TASK3_Y205 mutations, I found that the non-functional G106R and L214R TASK1 channel variants were translated and expressed at the plasma membrane as efficiently as the WT channel. Due to the hypoxic events inherent to PAH (Weir *et al.*, 2005), TASK1 expression in the mitochondria was investigated and confirmed for the first time. The expression of the G106R and L214R mutations appeared to be no different to the WT, which implies that the presence of these mutations in the mitochondria do not contribute to the progression of PAH. Despite this finding, it does open an avenue for research into the effect of these mutations on mitochondrial redox signalling when examined under hypoxic conditions, such as those found in PAH.

Together, the connotations of these findings are significant in the development of future therapeutic approaches to both *KCNK9* imprinting syndrome and PAH. Firstly, these findings confirm that trafficking impairments do not account for all the deleterious effects of the G236R mutation; it is more likely the destabilising effect of the insertion of a large hydrophilic residue into a hydrophobic environment in place of a small, uncharged amino acid. Similarly, mutations surrounding Y205 are also likely to contribute to the destabilisation of the pore. Therapeutic strategies aiming to increase TASK3_G236R channel expression at the membrane in the treatment of *KCNK9* Imprinting syndrome could be detrimental to the patient. Indeed, the current through G236R channels can be recovered

pharmacologically through application of fenamates however, such approaches are not likely to rescue GPCR-mediated regulation. Likewise, the G106R and L214R variants of TASK1 also represent loss-of-function channels in which functional currents cannot be restored pharmacologically. Promoting the expression of dysfunctional channels at the plasma membrane may only serve to exacerbate symptoms therefore, in absence of effective pharmaceutical activators, genome editing approaches such as CRISPR/CAS9 technology may be more successful however, these therapies are not yet ready for clinical application.

6.2 Functional characterisation of the TASK3 C-terminus

The function in-relation-to structure studies of transmembrane ion channels have been difficult to accomplish due to the tendency of integral membrane proteins to denature once removed from their native environment. Until recently, no crystal structures for TASK channels had been published (Rödström *et al.*, 2019) and yet they still remain incomplete, lacking the IC terminal regions where much of the channels' regulatory activity occurs. The 6 amino acid 'VLRFLT' motif in the extreme proximal portion of the Ct is critical to the regulation of channel activity by both pharmacological and physiological modulators (Wilke *et al.*, 2014, Veale *et al.*, 2007a, Talley and Bayliss, 2002b), with deletion of the motif altering pH sensitivity and abolishing GPCR regulation (Talley and Bayliss, 2002a). With the location of the motif in the IC Ct domain and the His98 proton sensor in an EC region, alterations to internal gating mechanisms are clearly coupled to EC events however, this motif cannot underpin all the regulatory pathways of this channel (Veale *et al.*, 2007a). Discovery of a novel X-gate identified that the analogous VLRFMT motif in TASK1 is directly involved in channel gating (Rödström *et al.*, 2019), with mutations occurring within and around the motif mirroring the reduced channel activity displayed by the pathogenic TASK3_G236R mutation associated with *KCNK9* Imprinting syndrome (Barel *et al.*, 2008, Veale *et al.*, 2014). Whilst the VLRFLT motif is essential to function, it is unclear whether it behaves as a transducer of signal or a direct binding site. As such, a TASK3 Ct peptide inclusive of the VLRFLT motif was produced in Chapter 4 for the first time.

The GST-TASK3 Ct peptide used in this study was produced both with and without the VLRFLT motif. Regardless of the presence of the hydrophobic motif that is embedded within the plasma membrane, the peptide remained insoluble under physiological conditions. Production of proteins for structural studies commonly see the removal of the terminal regions of integral membrane proteins due to an innate lack of tertiary arrangement and structural irregularity predisposing the protein to aggregation during purification. Indeed, the recombinant expression of the GST-TASK3_(+VLRFLT) Ct resulted in a protein that demonstrated poor solubility and a propensity to precipitate out of solution, stabilising

in conditions significantly different from those considered to be physiologically relevant. Despite the non-physiological conditions in which the peptide was stabilised, it can be postulated that the peptide is unlikely to behave physiologically since it is only a fragment of the full protein.

In expressing the peptide recombinantly, it was deprived of local stabilising interactions otherwise present *in vivo*, promoting peptide unfolding and reduced solubility, as was observed for GST-TASK3_(+VLRFLT). Such interactions have been proven to be central to channel regulation for some K2P channels. Indeed, GPCR modulation of TREK1 is dependent upon the non-specific electrostatic interactions driving the direct association and dissociation of the Ct with the plasma membrane, causing activation and inhibition respectively (Sandoz *et al.*, 2011). Proteins without obvious tertiary arrangement are now often classified as containing regions of 'intrinsic disorder.' IDPRs are commonly located within the flexible cytoplasmic domain of proteins where they are suspected to undergo folding upon contact with a phospholipid membrane as a mechanism for signal transduction (Bürgi *et al.*, 2016). Sequence analysis of TASK3 identified regions of disorder promoting residues neighbouring the VLRFLT motif. Since TASK3 channels are known to be regulated by a wide variety of structurally diverse channel modulators, it is logical to suspect that the TASK3 Ct forms stable complexes through the mechanisms of dynamic conformational selection as opposed to an induced fit binding, supporting the role of the VLRFLT as a transduction motif rather than a binding site. Indeed, the ability of the peptide to remain stable in solution at pH 10 speaks for the resilience of IDPs to maintain functionality in harsh conditions or regain it when returned to physiological conditions (Uversky, 2016, Uversky, 2017, Uversky, 2013, Lee *et al.*, 2019).

Using SRCD in Chapter 5, I show that regardless of conditions, the peptide remained conformationally correct as it continued to interact with the 14-3-3 adaptor protein known to bind directly to the [xRRKS^{p}V] motif (Zuzarte *et al.*, 2009). The direct binding of $G\alpha_{q/11}$ with the TASK3 Ct was also confirmed using CD techniques for the first time. For TRPM8 channels, $G\alpha_{q/11}$ inhibits activity through simultaneous electrostatic binding of its negative switch III loop to positive residues of the Nt as the α3 helix binds to the TRP domain of the Ct (Zhang, 2019). Contrary to TRPM8, GPCR inhibition of TASK3 channels continues mostly unabated in absence of PLC, PKC and DAG (Zhang *et al.*, 2016). Like GPCR regulation of TREK1 relies upon electrostatic interaction of the Ct with the plasma membrane independently of PKC (Sandoz *et al.*, 2011), I propose that $G\alpha_{q/11}$ requires the positively charged residues of the VLRFLT motif for the switch III loop interaction whilst the rigid α3 helix binds to an unknown site within the channel vestibule. This causes a conformational change that allosterically hinders the electrostatic interaction with the inner leaflet of the plasma membrane, dissociating the Ct as a mechanism of channel inhibition. As such, the effect of pore-altering mutations like G236R could impede the access of the $G\alpha_{q/11}$ α3 helix from stabilising the interaction, preventing the

transduction of signal to the SF.

Since I was unable to obtain SRCD data for the GST-TASK3_(-VLRFLT) construct during the scope of this PhD, the function of the VLRFLT motif as a binding site or a transducer could not be confirmed. As such, the next logical step would be to carry out these experiments, although the data presented here would lean towards the function as a transducer. With the work in this study conducted only on a fragment of the full protein, the findings of this thesis are not directly relatable to cellular mechanisms occurring *in vivo* or *in vitro* and instead provide hypotheses to explore new avenues of research including confirmation of the Ct IDPRs and determination of induced-fit or conformational selectivity binding mechanisms. Unfortunately, biochemical and biophysical techniques can only go so far in describing the functions of an integral membrane protein. Alone, these techniques provide little information regarding the three-dimensional structure and the complex interactions occurring at a molecular level that support channel activity. Therefore, the most effective future experiments would focus upon the encapsulation of full-length TASK3 protein from a native membrane environment into a membrane mimetic such as the phospholipid nanodisc for crystallisation studies. Such approaches provide a stable environment for *in vitro* biophysical characterisation, flexibility for conformational changes and retain local interactions which are key to channel regulation.

6.3 Concluding Remarks

Loss-of-function pathological variants of TASK channels are associated with conditions like PAH and *KCNK9* Imprinting syndrome. With limited structural information available, the identification of key regulatory processes is paramount to establishing therapeutic strategies for the treatment of these conditions and many more. In this study, imaging and electrophysiological techniques determined that the reduction in TASK3_G236R current observed in *KCNK9* Imprinting syndrome is a direct result of both trafficking impairments and structural abnormalities as demonstrated by reduced membrane expression but a continued ability to associate with activated $G\alpha_{q/11}$ despite losing GPCR-mediation inhibition. The consequences of TASK3 mutations including (Y205C and Y205Δ) are therefore presumably linked to the destabilisation of the channel pore, preventing transduction of IC regulatory signals to the SF. As such, therapeutic strategies aiming to increase mutant channel expression at the membrane in the treatment of *KCNK9* Imprinting syndrome could be detrimental to the patient. Similarly, loss-of-function TASK1 mutations associated with PAH (G106R and L214R) are dysfunctional whilst trafficking is unaffected. Despite demonstrating the localisation of TASK1 channels in the mitochondria for the first time, this study was unable to link the pathogenic variants to the hypoxic

events involved in the progression of PAH. More work is required to investigate the role of TASK1 mutations in mitochondrial redox signalling under hypoxic conditions.

Finally, this study produced a TASK3 Ct peptide inclusive of the VLRFLT motif critical to GPCR regulation, which appeared to be intrinsically disordered in nature and conformationally correct as I confirm the direct binding of $G\alpha_{q/11}$. In absence of a crystal structure containing this motif, we can only hypothesise the role of the VLRFLT motif in GPCR regulation however, the work included within this thesis provides the foundations for further exploration.

Appendix 1

1.1 Application of DTNB to tsA201 cells expressing Y205C had little effect on the current.

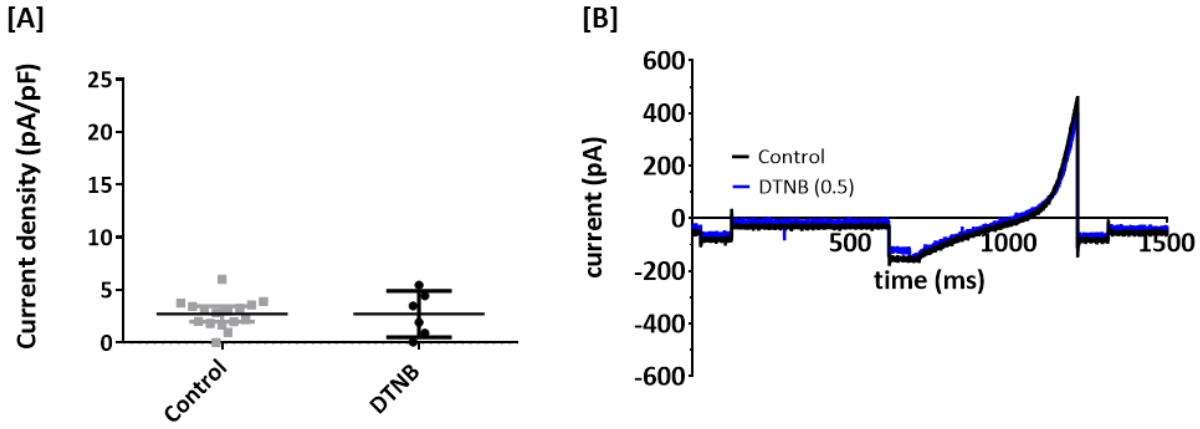

Figure 88 Cysteine modifying agent -5"-Dithio-bis(2-nitrobenzoic acid) (DTNB or Ellman's reagent), reacts with free sulfhydryl side chains of cysteine to form an S-S bond between the protein and a thionitrobenzoic acid (TNB) residue, was applied to see if it was able to recover any current through the Y205C mutant channel. Application of DTNB to the cells resulted in a yellow colour been observed but was found to have little effect on the current

[A] a comparison of current density when the mutated channel is in control solution and in a solution containing 0.5 mM DTNB. No significant difference (P > 0.05, 95% CI = -1.6 to 1.6) was observed between current recorded in control solution (2.72 pA pF^{-1} (n=16, 95% CI = 1.9 to 3.5)) and in 0.5 mM DTNB (2.71 pA pF^{-1} (n = 6, 95% CI = 0.5 to 4.9)); [B] is averaged raw data traces (n=16) from cells in control (black line) and in DTNB (n=6) (blue line), when transiently expressed in tsA201 cells. This work was carried out by Dr E L Veale.

1.2 MTSES had no effect on Y205C mutant channels

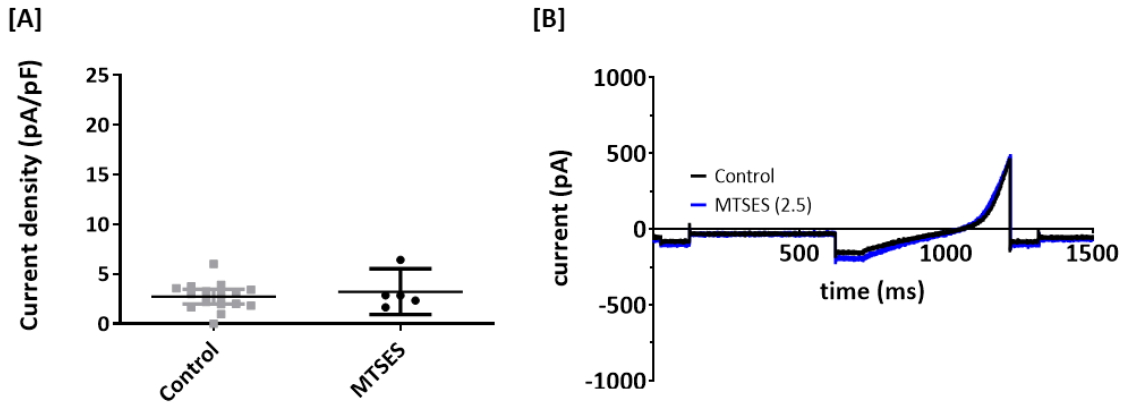

Figure 89 Methanethiosulfonates (MTS) are sulfhydryl-reactive compounds that form mixed disulfide linkages and are commonly used to study cysteine residues on proteins. Sodium (2-sulfonatoethyl) methanethiosulfonate (MTSES) is a negatively charged, membrane impermeant MTS. It is highly reactive with ionized thiolates and targets sulfhydryl groups accessible from the aqueous medium. MTSES had no effect on Y205C mutant channels, which suggests that 205C is either not accessible from the extracellular side or is already cross linked with the 205C on the other monomer or a different cysteine

[A] A comparison of current density when the mutated channel is in control solution and in a solution containing 2.5 mM MTSES. No significant difference (P > 0.05, 95% CI = -1.1 to 2.1) was observed between current recorded in control solution (2.7 pA pF^{-1} (n=16, 95% CI = 1.9 to 3.5)) and in 2.5 mM MTSES (3.2 pA pF^{-1} (n = 5, 95% CI = 0.93 to 5.5)); [B] averaged raw data traces (n=16) from cells in control (black line) and in MTSES (n=5) (blue line), when transiently expressed in tsA201 cells. This work was carried out by Dr E L Veale.

1.3 DTT acted only to reduced current at more positive potentials, where we observe activation of a voltage-gated channel.

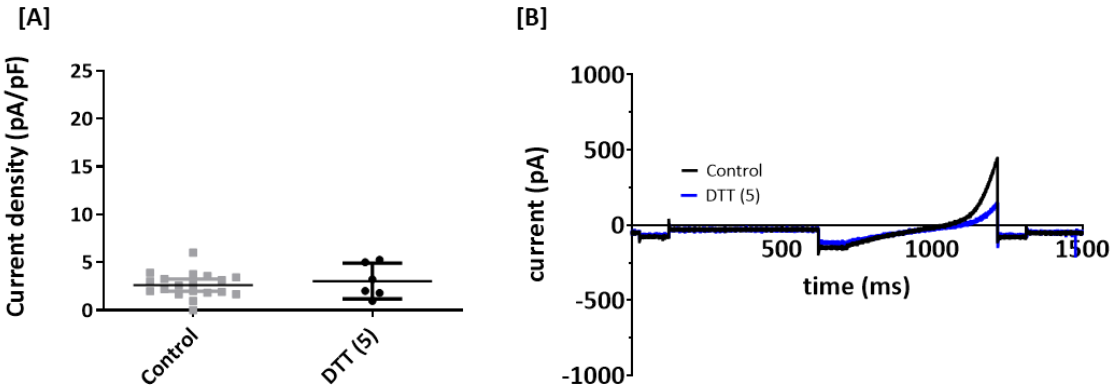

Figure 90 As MTSES had no effect on the protein, we then went on to look at whether the 205 cysteines' had formed intermolecular disulphide bonds between subunits, which had closed the channel. To do this we used the disulphide reducing agent, dithiothreitol (DTT).

[A] a comparison of current density when the mutated channel is in control solution and in a solution containing 5 mM DTT. No significant difference (P > 0.05, 95% CI = -0.95 to 1.79) was observed between current recorded in control solution (2.6 pA pF^{-1} (n=19, 95% CI = 1.9 to 3.2)) and in 5 mM DTT (3.0 pA pF^{-1} (n = 6, 95% CI = 1.2 to 4.9)); [C] averaged raw data traces (n=19) from cells in control (black line) and in DTT (n=6) (blue line), when transiently expressed in tsA201 cells. This work was carried out by Dr E L Veale.

Appendix 2

2.1 SEC of un-concentrated flow through from GST

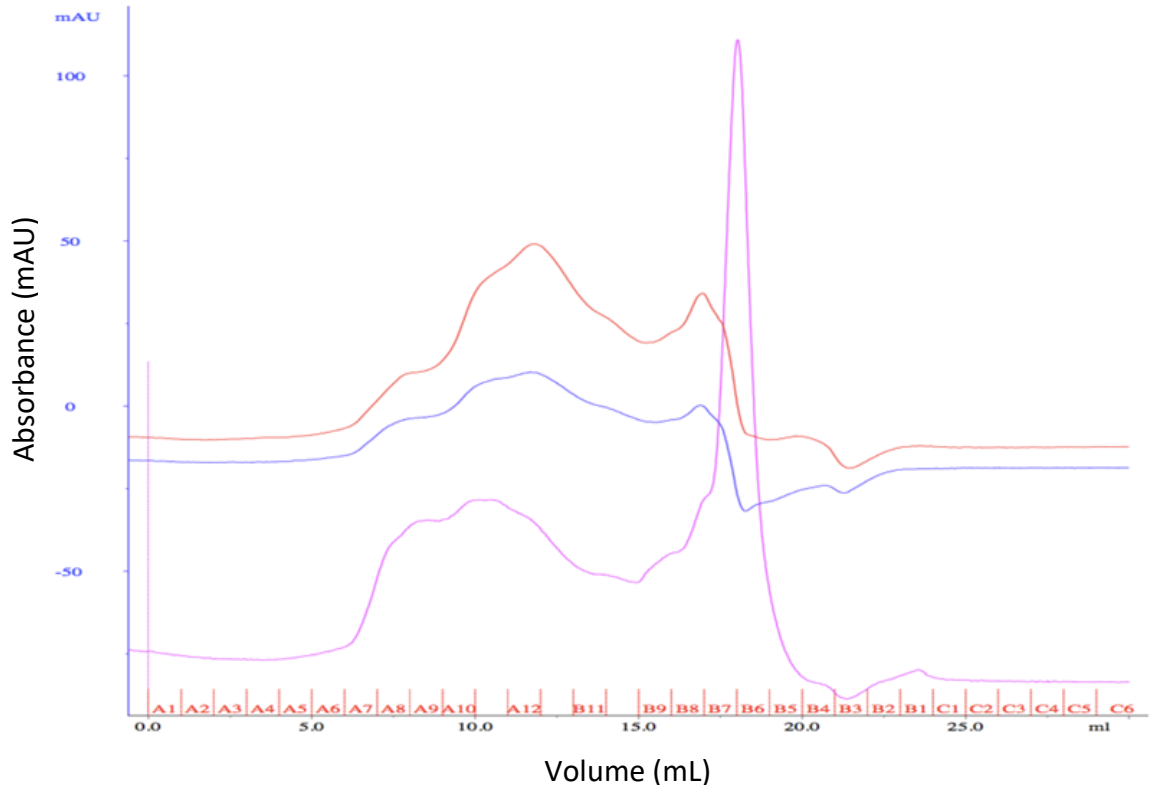

Figure 91 SEC of un-concentrated FT from GST column (Figure 45).

SEC was carried out on the GST column (un-concentrated) FT using the Superdex 75 10/300 GL, as it appeared to contain the full-length protein (see Figure 49) and the elution rate of Ovalbumin (43 kDa) was used as a reference elution rate. Red trace: 260 nm; blue trace: 280 nm and pink trace: 230 nm absorbance. Two minor peaks present at the approximate reference Ovalbumin elution volume (11 mL). The 260 nm reading suggests intense DNA contamination, but sample is too dilute.

2.2 QC confirms new preparation is in a whole state

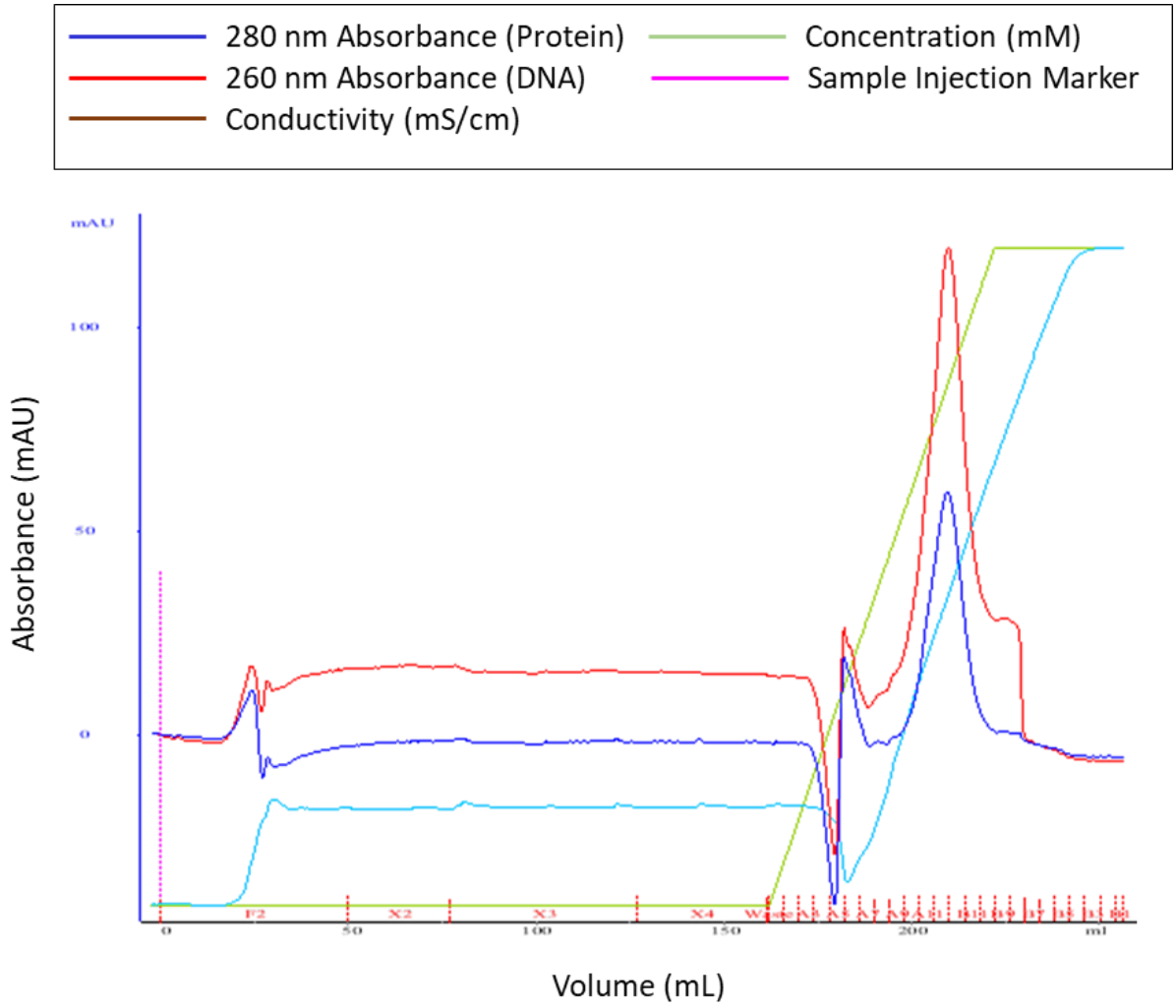

Figure 92 Strong QC of the remaining refolded protein confirms the protein remains in a whole state

The protein began to elute at approximately 60% of sample B application (green trace) and the protein eluted fully at approximately 400 mM NaCl (light blue). Fractions A11-B11 were collected for analysis (Figure 59)

Appendix 3

3.1 Microscopy Solutions

Solution	Recipe
2% Paraformaldehyde (PFA)	Add 5 mL (1X) PBS Add ddH_2O to a volume of 30 mL Heat solution to approx. 80°C (do not boil) Add 1g PFA and 1 mL (5M) NaOH, aspirate to dissolve Add 900 µL (5M) HCl Add HCl dropwise to pH 6.8 (use pH strips) Q.S. to 250 mL with ddH_2O and filter

3.2 In-cell/On-cell Western Blot

Solution	Recipe
2% Paraformaldehyde	*See above*
TBS	0.2 M TRIS Base (121.14 g/mol) 1.5 M NaCl (58.44 g/mol) Q.S. to 500 mL with ddH_2O
0.1% Tween-20 PBS (TBST) Wash buffer	100 mL of (10X) TBS 900 mL ddH_2O 1 mL Tween-20
0.1% Triton-X-100 Permeabilisation buffer	10 µL Triton-X-100 10 mL (1X) PBS
5% Bovine serum blocking buffer	150 mL TBST 7.5g non-fat dry milk

3.3 Protein Production and Purification Solutions

Solution	Recipe
Super optimal broth with catabolite repression (SOC) media (250 mL)	5g Bactotryptone 1.25g Bactoyeast extraxt 0.5 mL (5M) NaCl 0.625 mL (1M) KCl 2.5 mL (1M) $MgCl_2$ 2.5 mL (1M) $MgSO_4$ 5 mL (1M) Glucose Q.S. to 250 mL with ddH_2O and filtered
Resolubilisation buffer: Urea (8M)	20 mM (1X) PBS (pH 7.5) (1M) 150 mM NaCl (5M) 480g Urea (60 g/mol) Q.S. to 1 L with ddH_2O
Resolubilisation buffer: Guanidinium Hydrochloride (6M)	50 mM MES (2-(*N*-morpholino)ethanesulfonic acid) buffer (pH 6.5) (5M) 150mM NaCl (5M) 573.78g Guanidinium (95.63 g/mol) Q.S. to 1 L with ddH_2O
2X Sample buffer	100 mM TRIS (pH 6.8) 2% SDS 100 mM DTT (dithiothreitol) 0.015% β-Mercaptoethanol 15% Glycerol 1 x Small spatula Bromophenol-Blue Q.S. to 1 L with ddH_2O
Staining solution	0.25% R250 Coomassie (2.5 g/L) 10% Acetic acid 40% Methanol Q.S. with ddH_2O
De-staining solution	10% Acetic acid 20% Methanol Q.S. with ddH_2O
10% Polyethylenimine (w/v)	Add 10mL of polyethylenimine to 70 mL ddH_2O and titrate solution to pH 7.9 with (5M) HCl Q.S. To 100mL with ddH_2O and filter
Arginine refolding buffer	20 mM (1X) NAP (Nucleic acid preservation buffer) (1M) 200 mM Arginine (174.2 g/mol) 150mM NaCl (5M) Q.S. to 50 mL with ddH_2O
10 mM Elution buffer (pH 8)	50 mM TRIS (pH 8) (1M) 10 mM Reduced glutathione (307.32 g/mol) Q.S. with ddH_2O
Rat lysate buffer (Zuzarte *et al.*, 2009)	1% Triton-X-100 150 mM NaCl 10 mM TRIS-HCl Protease inhibitor cocktail Q.S. to 50 mL with ddH_2O

Solution (*cont.*)	Recipe (*cont.*)
Wash buffer	20 mM PBS (pH 7.5) 150 mM NaCl 1M Urea 1% Triton-X-100
Strong anion exchange (Buffer A) (pH 10)	25 mM HEPES 70 mM NaCl 20 mM NaOH Q.S. to 500 mL with ddH_2O
Strong anion exchange (Buffer B) (pH 10)	25 mM HEPES 1 M NaCl 20 mM NaOH Q.S. to 500 mL with ddH_2O
Digestion buffer (pH 8)	50 mM TRIS-HCl 150 mM NaCl 1 mM EDTA (ethylenediaminetetraacetic acid) 1 mM DTT 0.01 % Triton-X-100
10 X Cleavage buffer (pH 7)	50 mM TRIS-HCl 150 mM NaCl 5 mM EDTA 1 mM DTT 0.1% Triton-X-100

3.4 Electrophysiology Solutions

Solution	Recipe
External Solution	145 mM NaCl 2.5 mM KCl 3 mM $MgCl_2$ 1 mM $CaCl_2$ 10 mM HEPES (pH adjusted to 7.4 with 1 M NaOH)
Internal Solution	150 mM KCl 3 mM $MgCl_2$ 5 mM EGTA 10 mM HEPES (pH adjusted to 7.4 with 1 M KOH)

References

AEBI, M., BERNASCONI, R., CLERC, S. & MOLINARI, M. 2010. N-glycan structures: recognition and processing in the ER. *Trends Biochem Sci,* 35**,** 74-82.

AGGARWAL, S. K. & MACKINNON, R. 1996. Contribution of the S4 segment to gating charge in the Shaker K+ channel. *Neuron,* 16**,** 1169-77.

AGNEW, W. S., LEVINSON, S. R., BRABSON, J. S. & RAFTERY, M. A. 1978. Purification of the tetrodotoxin-binding component associated with the voltage-sensitive sodium channel from Electrophorus electricus electroplax membranes. *Proceedings of the National Academy of Sciences of the United States of America,* 75**,** 2606-10.

ALLENE, C. & COSSART, R. 2010. Early NMDA receptor-driven waves of activity in the developing neocortex: physiological or pathological network oscillations? *The Journal of Physiology,* 588**,** 83-91.

AMBADIPUDI, S. & ZWECKSTETTER, M. 2016. Targeting intrinsically disordered proteins in rational drug discovery. *Expert Opin Drug Discov,* 11**,** 65-77.

ANDRES-ENGUIX, I., CALEY, A., YUSTOS, R., SCHUMACHER, M. A., SPANU, P. D., DICKINSON, R., MAZE, M. & FRANKS, N. P. 2007. Determinants of the anesthetic sensitivity of two-pore domain acid-sensitive potassium channels: molecular cloning of an anesthetic-activated potassium channel from Lymnaea stagnalis. *J Biol Chem,* 282**,** 20977-90.

ANTIGNY, F., HAUTEFORT, A., MELOCHE, J., BELACEL-OUARI, M., MANOURY, B., RUCKER-MARTIN, C., PECHOUX, C., POTUS, F., NADEAU, V., TREMBLAY, E., RUFFENACH, G., BOURGEOIS, A., DORFMULLER, P., BREUILS-BONNET, S., FADEL, E., RANCHOUX, B., JOURDON, P., GIRERD, B., MONTANI, D., PROVENCHER, S., BONNET, S., SIMONNEAU, G., HUMBERT, M. & PERROS, F. 2016. Potassium Channel Subfamily K Member 3 (KCNK3) Contributes to the Development of Pulmonary Arterial Hypertension. *Circulation,* 133**,** 1371-85.

APPENZELLER-HERZOG, C. & HAURI, H.-P. 2006. The ER-Golgi intermediate compartment (ERGIC): in search of its identity and function. *Journal of Cell Science,* 119**,** 2173.

ARAI, M. 2018. Unified understanding of folding and binding mechanisms of globular and intrinsically disordered proteins. *Biophysical Reviews,* 10**,** 163-181.

ARCHER, S. L., HUANG, J., HENRY, T., PETERSON, D. & WEIR, E. K. 1993. A redox-based O2 sensor in rat pulmonary vasculature. *Circ Res,* 73**,** 1100-12.

ARCHER, S. L., WILL, J. A. & WEIR, E. K. 1986. Redox status in the control of pulmonary vascular tone. *Herz,* 11**,** 127-41.

ASHMOLE, I., GOODWIN, P. A. & STANFIELD, P. R. 2001. TASK-5, a novel member of the tandem pore K+ channel family. *Pflugers Archiv : European journal of physiology,* 442**,** 828-33.

ASHMOLE, I., VAVOULIS, D. V., STANSFELD, P. J., MEHTA, P. R., FENG, J. F., SUTCLIFFE, M. J. & STANFIELD, P. R. 2009. The response of the tandem pore potassium channel TASK-3 (K 2P 9.1) to voltage: gating at the cytoplasmic mouth. *J Physiol,* 58720**,** 4769-4783.

AUTZEN, H. E., MYASNIKOV, A. G., CAMPBELL, M. G., ASARNOW, D., JULIUS, D. & CHENG, Y. 2018. Structure of the human TRPM4 ion channel in a lipid nanodisc. *Science,* 359**,** 228-232.

AZMI, N., NORMAN, C., SPICER, C. H. & BENNETT, G. W. 2006. Effects of a neurotensin analogue (PD149163) and antagonist (SR142948A) on the scopolamine-induced deficits in a novel object discrimination task. *Behav Pharmacol,* 17**,** 357-62.

BABCOCK, J. J. & LI, M. 2014. Deorphanizing the human transmembrane genome: A landscape of uncharacterized membrane proteins. *Acta Pharmacologica Sinica,* 35**,** 11-23.

BABU, M. M. 2016. The contribution of intrinsically disordered regions to protein function, cellular complexity, and human disease. *Biochemical Society Transactions,* 44**,** 1185.

BAGRIANTSEV, S. N., CLARK, K. A., MINOR, D. L. & JR 2012. Metabolic and thermal stimuli control K(2P)2.1 (TREK-1) through modular sensory and gating domains. *The EMBO journal,* 31**,** 3297-308.

BAGRIANTSEV, S. N., PEYRONNET, R., CLARK, K. A., HONORÉ, E., MINOR, D. L. & JR 2011. Multiple modalities converge on a common gate to control K2P channel function. *The EMBO Journal,* 30**,** 3594.

BALLANYI, K. & BUCK, L. T. 2004. Protective role of neuronal KATP channels in brain hypoxia. *The Journal of experimental biology,* 207**,** 3201-12.

BANDO, Y., HIRANO, T. & TAGAWA, Y. 2014. Dysfunction of KCNK potassium channels impairs neuronal migration in the developing mouse cerebral cortex. *Cerebral Cortex*.

BANDULIK, S., PENTON, D., BARHANIN, J. & WARTH, R. 2010. TASK1 and TASK3 potassium channels: determinants of aldosterone secretion and adrenocortical zonation. *Horm Metab Res,* 42**,** 450-7.

BANDULIK, S., TAUBER, P., PENTON, D., SCHWEDA, F., TEGTMEIER, I., STERNER, C., LALLI, E., LESAGE, F., HARTMANN, M., BARHANIN, J. & WARTH, R. 2013. Severe Hyperaldosteronism in Neonatal Task3 Potassium Channel Knockout Mice Is Associated With Activation of the Intraadrenal Renin-Angiotensin System. *Endocrinology,* 154**,** 2712-2722.

BANEYX, F. 1999. Recombinant protein expression in Escherichia coli. *Curr Opin Biotechnol,* 10**,** 411-21.

BANG, H., KIM, Y. & KIM, D. 2000. TREK-2, a new member of the mechanosensitive tandem-pore K+ channel family. *The Journal of biological chemistry,* 275**,** 17412-9.

BAREL, O., SHALEV, S. A., OFIR, R., COHEN, A., ZLOTOGORA, J., SHORER, Z., MAZOR, G., FINER, G., KHATEEB, S., ZILBERBERG, N. & BIRK, O. S. 2008. Maternally inherited Birk Barel mental retardation dysmorphism syndrome caused by a mutation in the genomically imprinted potassium channel KCNK9. *Am J Hum Genet,* 83**,** 193-9.

BAYBURT, T. H. & SLIGAR, S. G. 2010. Membrane protein assembly into Nanodiscs. *FEBS letters,* 584**,** 1721-7.

BAYLISS, D. A. & BARRETT, P. Q. 2008. Emerging roles for two-pore-domain potassium channels and their potential therapeutic impact. *Trends Pharmacol Sci,* 29**,** 566-75.

BEETON, C., PENNINGTON, M. W., WULFF, H., SINGH, S., NUGENT, D., CROSSLEY, G., KHAYTIN, I., CALABRESI, P. A., CHEN, C. Y., GUTMAN, G. A. & CHANDY, K. G. 2005. Targeting effector memory T cells with a selective peptide inhibitor of Kv1.3 channels for therapy of autoimmune diseases. *Mol Pharmacol,* 67**,** 1369-81.

BEETON, C., WULFF, H., BARBARIA, J., CLOT-FAYBESSE, O., PENNINGTON, M., BERNARD, D., CAHALAN, M. D., CHANDY, K. G. & BERAUD, E. 2001. Selective blockade of T lymphocyte K(+) channels ameliorates experimental autoimmune encephalomyelitis, a model for multiple sclerosis. *Proc Natl Acad Sci U S A,* 98**,** 13942-7.

BEETON, C., WULFF, H., STANDIFER, N. E., AZAM, P., MULLEN, K. M., PENNINGTON, M. W., KOLSKI-ANDREACO, A., WEI, E., GRINO, A., COUNTS, D. R., WANG, P. H., LEEHEALEY, C. J., B, S. A., SANKARANARAYANAN, A., HOMERICK, D., ROECK, W. W., TEHRANZADEH, J., STANHOPE, K. L., ZIMIN, P., HAVEL, P. J., GRIFFEY, S., KNAUS, H. G., NEPOM, G. T., GUTMAN, G. A., CALABRESI, P. A. & CHANDY, K. G. 2006. Kv1.3 channels are a therapeutic target for T cell-mediated autoimmune diseases. *Proc Natl Acad Sci U S A,* 103**,** 17414-9.

BEN-ABU, Y., ZHOU, Y., ZILBERBERG, N. & YIFRACH, O. 2009. Inverse coupling in leak and voltage-activated K+ channel gates underlies distinct roles in electrical signaling. *Nature Structural & Molecular Biology,* 16**,** 71-79.

BERNSTEIN, J. 1912. Die lehre von den elektrischen vorgangen in organismus, auf moderener grundlage dargestellt. *Elektrobiologie*.

BERTHELEME, N., CHAE, P. S., SINGH, S., MOSSAKOWSKA, D., HANN, M. M., SMITH, K. J., HUBBARD, J. A., DOWELL, S. J. & BYRNE, B. 2013. Unlocking the secrets of the gatekeeper: Methods for stabilizing and crystallizing GPCRs. *Biochimica et Biophysica Acta (BBA) - Biomembranes,* 1828**,** 2583-2591.

BERTRAND, C. A. & FRIZZELL, R. A. 2003. The role of regulated CFTR trafficking in epithelial secretion. *Am J Physiol Cell Physiol,* 285**,** C1-18.

BESANA, A., BARBUTI, A., TATEYAMA, M. A., SYMES, A. J., ROBINSON, R. B. & FEINMARK, S. J. 2004. Activation of protein kinase C epsilon inhibits the two-pore domain K+ channel, TASK-1, inducing repolarization abnormalities in cardiac ventricular myocytes. *The Journal of biological chemistry,* 279**,** 33154-60.

BISTA, P., MEUTH, S. G., KANYSHKOVA, T., CERINA, M., PAWLOWSKI, M., EHLING, P., LANDGRAF, P., BORSOTTO, M., HEURTEAUX, C., PAPE, H. C., BAUKROWITZ, T. & BUDDE, T. 2012. Identification of the muscarinic pathway underlying cessation of sleep-related burst activity in rat thalamocortical relay neurons. *Pflugers Arch,* 463**,** 89-102.

BITTNER, S., BOBAK, N., HERRMANN, A. M., GOBEL, K., MEUTH, P., HOHN, K. G., STENNER, M. P., BUDDE, T., WIENDL, H. & MEUTH, S. G. 2010a. Upregulation of K2P5.1 potassium channels in multiple sclerosis. *Ann Neurol,* 68**,** 58-69.

BITTNER, S., BUDDE, T., WIENDL, H. & MEUTH, S. G. 2010b. From the Background to the Spotlight: TASK Channels in Pathological Conditions. *Brain Pathology,* 20**,** 999-1009.

BITTNER, S., MEUTH, S. G., GÖBEL, K., MELZER, N., HERRMANN, A. M., SIMON, O. J., WEISHAUPT, A., BUDDE, T., BAYLISS, D. A., BENDSZUS, M. & WIENDL, H. 2009. TASK1 modulates inflammation and neurodegeneration in autoimmune inflammation of the central nervous system. *Brain,* 132**,** 2501-2516.

BLIN, S., BEN SOUSSIA, I., KIM, E.-J., BRAU, F., KANG, D., LESAGE, F. & BICHET, D. 2016. Mixing and matching TREK/TRAAK subunits generate heterodimeric K2P channels with unique properties. *Proceedings of the National Academy of Sciences of the United States of America,* 113**,** 4200-5.

BONIFACINO, J. S. & TRAUB, L. M. 2003. Signals for sorting of transmembrane proteins to endosomes and lysosomes. *Annu Rev Biochem,* 72**,** 395-447.

BORGIA, A., BORGIA, M. B., BUGGE, K., KISSLING, V. M., HEIDARSSON, P. O., FERNANDES, C. B., SOTTINI, A., SORANNO, A., BUHOLZER, K. J., NETTELS, D., KRAGELUND, B. B., BEST, R. B. & SCHULER, B. 2018. Extreme disorder in an ultrahigh-affinity protein complex. *Nature,* 555**,** 61-66.

BORODINSKY, L. N., ROOT, C. M., CRONIN, J. A., SANN, S. B., GU, X. & SPITZER, N. C. 2004. Activity-dependent homeostatic specification of transmitter expression in embryonic neurons. *Nature,* 429**,** 523-530.

BORTONE, D. & POLLEUX, F. 2009. KCC2 Expression Promotes the Termination of Cortical Interneuron Migration in a Voltage-Sensitive Calcium-Dependent Manner. *Neuron,* 62**,** 53-71.

BOUCHERAT, O., CHABOT, S., ANTIGNY, F., PERROS, F., PROVENCHER, S. & BONNET, S. 2015. Potassium channels in pulmonary arterial hypertension. *Eur Respir J,* 46**,** 1167-77.

BOUDIN, H., LAZAROFF, B., BACHELET, C. M., PELAPRAT, D., ROSTENE, W. & BEAUDET, A. 2000. Immunologic differentiation of two high-affinity neurotensin receptor isoforms in the developing rat brain. *J Comp Neurol,* 425**,** 45-57.

BOYER, H. W. & ROULLAND-DUSSOIX, D. 1969. A complementation analysis of the restriction and modification of DNA in Escherichia coli. *Journal of molecular biology,* 41**,** 459-72.

BRICKLEY, S. G., ALLER, M. I., SANDU, C., VEALE, E. L., ALDER, F. G., SAMBI, H., MATHIE, A. & WISDEN, W. 2007. TASK-3 two-pore domain potassium channels enable sustained high-frequency firing in cerebellar granule neurons. *J Neurosci,* 27**,** 9329-40.

BROCK, C., BOUDIER, L., MAUREL, D., BLAHOS, J. & PIN, J.-P. 2005. Assembly-dependent Surface Targeting of the Heterodimeric GABA B Receptor Is Controlled by COPI but Not 14-3-3. *Molecular Biology of the Cell,* 16**,** 5572-5578.

BROHAWN, S. G., DEL MÁRMOL, J. & MACKINNON, R. 2012. Crystal structure of the human K2P TRAAK, a lipid-and mechano-sensitive K + ion channel. *Science,* 335**,** 436-441.

BROICHER, T., WETTSCHURECK, N., MUNSCH, T., COULON, P., MEUTH, S. G., KANYSHKOVA, T., SEIDENBECHER, T., OFFERMANNS, S., PAPE, H. C. & BUDDE, T. 2008. Muscarinic ACh receptor-mediated control of thalamic activity via G(q)/G (11)-family G-proteins. *Pflugers Arch,* 456**,** 1049-60.

BUCHHALTER, J. R. 1993. Animal models of inherited epilepsy. *Epilepsia,* 34 Suppl 3**,** S31-41.
BUCKLER, K. J. 1997. A novel oxygen-sensitive potassium current in rat carotid body type I cells. *The Journal of physiology,* 498 (Pt 3**,** 649-62.
BUCKLER, K. J., WILLIAMS, B. A. & HONORE, E. 2000. An oxygen-, acid- and anaesthetic-sensitive TASK-like background potassium channel in rat arterial chemoreceptor cells. *The Journal of Physiology,* 525**,** 135.
BURDAKOV, D., JENSEN, L. T., ALEXOPOULOS, H., WILLIAMS, R. H., FEARON, I. M., O'KELLY, I., GERASIMENKO, O., FUGGER, L. & VERKHRATSKY, A. 2006. Tandem-Pore K+ Channels Mediate Inhibition of Orexin Neurons by Glucose. *Neuron,* 50**,** 711-722.
BÜRGI, J., XUE, B., UVERSKY, V. N. & VAN DER GOOT, F. G. 2016. Intrinsic Disorder in Transmembrane Proteins: Roles in Signaling and Topology Prediction. *PLOS ONE,* 11**,** e0158594.
BUTLER, M. G., HOSSAIN, W., SULSONA, C., DRISCOLL, D. J. & MANZARDO, A. M. 2015. Increased plasma chemokine levels in children with Prader–Willi syndrome. *American Journal of Medical Genetics Part A,* 167**,** 563-571.
CAPERA, J., SERRANO-NOVILLO, C., NAVARRO-PEREZ, M., CASSINELLI, S. & FELIPE, A. 2019. The Potassium Channel Odyssey: Mechanisms of Traffic and Membrane Arrangement. *Int J Mol Sci,* 20.
CARTIER, E. A., CONTI, L. R., VANDENBERG, C. A. & SHYNG, S. L. 2001. Defective trafficking and function of KATP channels caused by a sulfonylurea receptor 1 mutation associated with persistent hyperinsulinemic hypoglycemia of infancy. *Proc Natl Acad Sci U S A,* 98**,** 2882-7.
CAVALIERI, D., DOLARA, P., MINI, E., LUCERI, C., CASTAGNINI, C., TOTI, S., MACIAG, K., DE FILIPPO, C., NOBILI, S., MORGANTI, M., NAPOLI, C., TONINI, G., BACCINI, M., BIGGERI, A., TONELLI, F., VALANZANO, R., ORLANDO, C., GELMINI, S., CIANCHI, F., MESSERINI, L. & LUZZATTO, L. 2007. Analysis of gene expression profiles reveals novel correlations with the clinical course of colorectal cancer. *Oncology research,* 16**,** 535-48.
CHEMIN, J., GIRARD, C., DUPRAT, F., LESAGE, F., ROMEY, G. & LAZDUNSKI, M. 2003. Mechanisms underlying excitatory effects of group I metabotropic glutamate receptors via inhibition of 2P domain K+ channels. *The EMBO journal,* 22**,** 5403-11.
CHEMIN, J., PATEL, A. J., DUPRAT, F., LAURITZEN, I., LAZDUNSKI, M. & HONORÉ, E. 2005. A phospholipid sensor controls mechanogating of the K+ channel TREK-1. *The EMBO journal,* 24**,** 44-53.
CHEN, X., TALLEY, E. M., PATEL, N., GOMIS, A., MCINTIRE, W. E., DONG, B., LIX VIANA, F., GARRISON, J. C. & BAYLISS, D. A. 2006. Inhibition of a background potassium channel by Gq protein alpha-subunits. *Proceedings of the National Academy of Sciences of the United States of America,* 103**,** 3422-3427.
CHENG, W. W., MCCOY, J. G., THOMPSON, A. N., NICHOLS, C. G. & NIMIGEAN, C. M. 2011. Mechanism for selectivity-inactivation coupling in KcsA potassium channels. *Proc Natl Acad Sci U S A,* 108**,** 5272-7.
CHOE, S. 2002. Potassium channel structures. *Nature Reviews Neuroscience,* 3**,** 115-121.
CLARKE, C. E., VEALE, E. L., WYSE, K., VANDENBERG, J. I. & MATHIE, A. 2008. The M1P1 loop of TASK3 K2P channels apposes the selectivity filter and influences channel function. *Journal of Biological Chemistry*.
COBBOLD, C., MONACO, A. P., SIVAPRASADARAO, A. & PONNAMBALAM, S. 2003. Aberrant trafficking of transmembrane proteins in human disease. *Trends in Cell Biology,* 13**,** 639-647.
COBLITZ, B., SHIKANO, S., WU, M., GABELLI, S. B., COCKRELL, L. M., SPIEKER, M., HANYU, Y., FU, H., AMZEL, L. M. & LI, M. 2005. C-terminal recognition by 14-3-3 proteins for surface expression of membrane receptors. *The Journal of biological chemistry,* 280**,** 36263-72.
COHEN, A., BEN-ABU, Y. & ZILBERBERG, N. 2009. Gating the pore of potassium leak channels. *European Biophysics Journal,* 39**,** 61-73.
COLE, K. S. 1949. Dynamic electrical characteristics of the squid axon membrane. *Arch. Sci. Physiol,* 3**,** 253-258.

CONCHA, G., BUSTOS, D., ZÚÑIGA, R., CATALÁN, M. A. & ZÚÑIGA, L. 2018. The Insensitivity of TASK-3 K2P Channels to External Tetraethylammonium (TEA) Partially Depends on the Cap Structure. *Int J Mol Sci.*

CONTRERAS, J. E., SRIKUMAR, D. & HOLMGREN, M. 2008. Gating at the selectivity filter in cyclic nucleotide-gated channels. *Proceedings of the National Academy of Sciences of the United States of America,* 105**,** 3310-4.

CORDERO-MORALES, J. F., CUELLO, L. G., ZHAO, Y., JOGINI, V., CORTES, D. M., ROUX, B. & PEROZO, E. 2006. Molecular determinants of gating at the potassium-channel selectivity filter. *Nat Struct Mol Biol,* 13**,** 311-8.

COULON, P., KANYSHKOVA, T., BROICHER, T., MUNSCH, T., WETTSCHURECK, N., SEIDENBECHER, T., MEUTH, S. G., OFFERMANNS, S., PAPE, H. C. & BUDDE, T. 2010. Activity Modes in Thalamocortical Relay Neurons are Modulated by G(q)/G(11) Family G-proteins - Serotonergic and Glutamatergic Signaling. *Front Cell Neurosci,* 4**,** 132.

CUELLO, L. G., JOGINI, V., CORTES, D. M. & PEROZO, E. 2010. Structural mechanism of C-type inactivation in K+ channels. *Nature,* 466**,** 203-208.

CUNNINGHAM, K. P., HOLDEN, R. G., ESCRIBANO-SUBIAS, P. M., COGOLLUDO, A., VEALE, E. L. & MATHIE, A. 2019. Characterization and regulation of wild-type and mutant TASK-1 two pore domain potassium channels indicated in pulmonary arterial hypertension. *Journal of Physiology,* 597**,** 1087-1101.

CZIRJAK, G. & ENYEDI, P. 2002. TASK-3 dominates the background potassium conductance in rat adrenal glomerulosa cells. *Mol Endocrinol,* 16**,** 621-9.

CZIRJÁK, G. & ENYEDI, P. 2002. Formation of functional heterodimers between the TASK-1 and TASK-3 two-pore domain potassium channel subunits. *Journal of Biological Chemistry*.

CZIRJÁK, G. & ENYEDI, P. 2003. Ruthenium red inhibits TASK-3 potassium channel by interconnecting glutamate 70 of the two subunits. *Molecular pharmacology,* 63**,** 646-52.

CZIRJÁK, G., PETHEO, G. L., SPÄT, A. & ENYEDI, P. 2001. Inhibition of TASK-1 potassium channel by phospholipase C. *American journal of physiology. Cell physiology,* 281**,** C700-8.

DANIELLI, J. F. & DAVSON, H. 1935. A contribution to the theory of permeability of thin films. *Journal of Cellular and Comparative Physiology,* 5**,** 495-508.

DAVIDSON, W. S., JONAS, A., CLAYTON, D. F. & GEORGE, J. M. 1998. Stabilization of alpha-synuclein secondary structure upon binding to synthetic membranes. *J Biol Chem,* 273**,** 9443-9.

DAVIES, L. A., HU, C., GUAGLIARDO, N. A., SEN, N., CHEN, X., TALLEY, E. M., CAREY, R. M., BAYLISS, D. A. & BARRETT, P. Q. 2008. TASK channel deletion in mice causes primary hyperaldosteronism. *Proceedings of the National Academy of Sciences,* 105**,** 2203-2208.

DE LA CRUZ, I. P., LEVIN, J. Z., CUMMINS, C., ANDERSON, P. & HORVITZ, H. R. 2003. sup-9, sup-10, and unc-93 may encode components of a two-pore K+ channel that coordinates muscle contraction in Caenorhabditis elegans. *J Neurosci,* 23**,** 9133-45.

DE LECEA, L., CARTER, M. E. & A, A. 2012. Shining Light on Wakefulness and Arousal. *Biological Psychiatry,* 71**,** 1046-1052.

DEB, P., SHARMA, S. & HASSAN, K. M. 2010. Pathophysiologic mechanisms of acute ischemic stroke: An overview with emphasis on therapeutic significance beyond thrombolysis. *Pathophysiology,* 17**,** 197-218.

DECHER, N., WEMHÖNER, K., RINNÉ, S., NETTER, M. F., ZUZARTE, M., ALLER, M. I., KAUFMANN, S. G., LI, X. T., MEUTH, S. G., DAUT, J., SACHSE, F. B. & MAIER, S. K. G. 2011. Knock-Out of the Potassium Channel TASK-1 Leads to a Prolonged QT Interval and a Disturbed QRS Complex. *Cellular Physiology and Biochemistry,* 28**,** 77-86.

DECOURSEY, T. E., CHANDY, K. G., GUPTA, S. & CAHALAN, M. D. 1984. Voltage-gated K+ channels in human T lymphocytes: a role in mitogenesis? *Nature,* 307**,** 465-8.

DEIANA, A., FORCELLONI, S., PORRELLO, A. & GIANSANTI, A. 2019. Intrinsically disordered proteins and structured proteins with intrinsically disordered regions have different functional roles in the cell. *bioRxiv***,** 646901.

DEUTSCH, C. 2002. Potassium channel ontogeny. *Annual review of physiology,* 64**,** 19-46.

DIB, H., TAMBY, M. C., BUSSONE, G., REGENT, A., BEREZNÉ, A., LAFINE, C., BROUSSARD, C., SIMONNEAU, G., GUILLEVIN, L., WITKO-SARSAT, V., HUMBERT, M. & MOUTHON, L. 2012. Targets of anti-endothelial cell antibodies in pulmonary hypertension and scleroderma. *European Respiratory Journal,* 39**,** 1405.

DIETRICH, A., KALWA, H., ROST, B. R. & GUDERMANN, T. 2005. The diacylglycerol-sensitive TRPC3/6/7 subfamily of cation channels: functional characterization and physiological relevance. *Pflügers Archiv - European Journal of Physiology,* 451**,** 72-80.

DORAY, B., MISRA, S., QIAN, Y., BRETT, T. J. & KORNFELD, S. 2012. Do GGA adaptors bind internal DXXLL motifs? *Traffic,* 13**,** 1315-25.

DORSAM, R. T. & GUTKIND, J. S. 2007. G-protein-coupled receptors and cancer. *Nat Rev Cancer,* 7**,** 79-94.

DOSZTANYI, Z., CHEN, J., DUNKER, A. K., SIMON, I. & TOMPA, P. 2006. Disorder and sequence repeats in hub proteins and their implications for network evolution. *J Proteome Res,* 5**,** 2985-95.

DOYLE, D. A., CABRAL, J. M. J. M., PFUETZNER, R. A., KUO, A., GULBIS, J. M., COHEN, S. L., CHAIT, B. T., MACKINNON, R., DOYLE, D. A., CABRAL, J. M. J. M., PFUETZNER, R. A., KUO, A., GULBIS, J. M., COHEN, S. L., CHAIT, B. T. & MACKINNON, R. 1998. The Structure of the Potassium Channel : Molecular Basis of K + Conduction and Selectivity. 280**,** 69-77.

DUNKER, A. K., LAWSON, J. D., BROWN, C. J., WILLIAMS, R. M., ROMERO, P., OH, J. S., OLDFIELD, C. J., CAMPEN, A. M., RATLIFF, C. M., HIPPS, K. W., AUSIO, J., NISSEN, M. S., REEVES, R., KANG, C., KISSINGER, C. R., BAILEY, R. W., GRISWOLD, M. D., CHIU, W., GARNER, E. C. & OBRADOVIC, Z. 2001. Intrinsically disordered protein. *J Mol Graph Model,* 19**,** 26-59.

DUNPHY, J. T. & LINDER, M. E. 1998. Signalling functions of protein palmitoylation. *Biochim Biophys Acta,* 1436**,** 245-61.

DUPRAT, F., LAURITZEN, I., PATEL, A. & HONORÉ, E. 2007. The TASK background K2P channels: chemo- and nutrient sensors. *Trends in Neurosciences,* 30**,** 573-580.

DUPRAT, F., LESAGE, F., FINK, M., REYES, R., HEURTEAUX, C. & LAZDUNSKI, M. 1997. TASK, a human background K+ channel to sense external pH variations near physiological pH. *The EMBO journal,* 16**,** 5464-71.

EHLING, P., BITTNER, S., BOBAK, N., SCHWARZ, T., WIENDL, H., BUDDE, T., KLEINSCHNITZ, C. & MEUTH, S. G. Open Access RESEARCH Two pore domain potassium channels in cerebral ischemia: a focus on K 2P 9.1 (TASK3, KCNK9). Experimental & Translational Stroke Medicine, 2010. 14.

EHLING, P., GÖB, E., BITTNER, S., BUDDE, T., LUDWIG, A., KLEINSCHNITZ, C. & MEUTH, S. G. Ischemia-induced cell depolarization: does the hyperpolarization-activated cation channel HCN2 affect the outcome after stroke in mice? , 2013.

ELLGAARD, L., MOLINARI, M. & HELENIUS, A. 1999. Setting the standards: quality control in the secretory pathway. *Science,* 286**,** 1882-8.

ENYEDI, P., BRAUN, G. & CZIRJÁK, G. 2012. TRESK: The lone ranger of two-pore domain potassium channels. *Molecular and Cellular Endocrinology,* 353**,** 75-81.

ENYEDI, P. & CZIRJAK, G. 2010. Molecular Background of Leak K + Currents: Two-Pore Domain Potassium Channels. *Physiol Rev,* 90**,** 559-605.

FAN, J. S., JIANG, M., DUN, W., MCDONALD, T. V. & TSENG, G. N. 1999. Effects of outer mouth mutations on hERG channel function: a comparison with similar mutations in the Shaker channel. *Biophys J,* 76**,** 3128-40.

FEKETE, S., BECK, A., VEUTHEY, J.-L. & GUILLARME, D. 2015. Ion-exchange chromatography for the characterization of biopharmaceuticals. *Journal of Pharmaceutical and Biomedical Analysis,* 113**,** 43-55.

FELICIANGELI, S., CHATELAIN, F. C., BICHET, D. & LESAGE, F. 2015. The family of K2P channels: salient structural and functional properties. *The Journal of physiology,* 593**,** 2587-603.

FICKER, E., DENNIS, A. T., OBEJERO-PAZ, C. A., CASTALDO, P., TAGLIALATELA, M. & BROWN, A. M. 2000. Retention in the endoplasmic reticulum as a mechanism of dominant-negative current suppression in human long QT syndrome. *J Mol Cell Cardiol,* 32**,** 2327-37.

FINK, M., DUPRAT, F., LESAGE, F., REYES, R., ROMEY, G., HEURTEAUX, C. & LAZDUNSKI, M. 1996. Cloning, functional expression and brain localization of a novel unconventional outward rectifier K+ channel. *The EMBO journal,* 15**,** 6854-62.

FISCHER, E. 1894. Einfluss der Configuration auf die Wirkung der Enzyme. *Berichte der deutschen chemischen Gesellschaft,* 27**,** 2985-2993.

FITZPATRICK, K., WINROW, C. J., GOTTER, A. L., MILLSTEIN, J., ARBUZOVA, J., BRUNNER, J., KASARSKIS, A., VITATERNA, M. H., RENGER, J. J. & TUREK, F. W. 2012. Altered sleep and affect in the neurotensin receptor 1 knockout mouse. *Sleep,* 35**,** 949-56.

FULLER, P. M., SHERMAN, D., PEDERSEN, N. P., SAPER, C. B. & LU, J. 2011. Reassessment of the structural basis of the ascending arousal system. *J Comp Neurol,* 519**,** 933-56.

GABASHVILI, I. S., SOKOLOWSKI, B. H. A., MORTON, C. C. & GIERSCH, A. B. S. 2007. Ion Channel Gene Expression in the Inner Ear. *Journal of the Association for Research in Otolaryngology,* 8**,** 305-328.

GAINE, S. & MCLAUGHLIN, V. 2017. Pulmonary arterial hypertension: tailoring treatment to risk in the current era. *Eur Respir Rev,* 26.

GAMPER, N. & SHAPIRO, M. S. 2007. Regulation of ion transport proteins by membrane phosphoinositides. *Nature Reviews Neuroscience,* 8**,** 921-934.

GEORGE, M. P., CHAMPION, H. C., SIMON, M., GUYACH, S., TARANTELLI, R., KLING, H. M., BROWER, A., JANSSEN, C., MURPHY, J., CARNEY, J. P., MORRIS, A., GLADWIN, M. T. & NORRIS, K. A. 2013. Physiologic changes in a nonhuman primate model of HIV-associated pulmonary arterial hypertension. *Am J Respir Cell Mol Biol,* 48**,** 374-81.

GHOFRANI, H. A., HUMBERT, M., LANGLEBEN, D., SCHERMULY, R., STASCH, J. P., WILKINS, M. R. & KLINGER, J. R. 2017. Riociguat: Mode of Action and Clinical Development in Pulmonary Hypertension. *Chest,* 151**,** 468-480.

GIANNI, S., DOGAN, J. & JEMTH, P. 2014. Distinguishing induced fit from conformational selection. *Biophys Chem,* 189**,** 33-9.

GIRARD, C., TINEL, N., TERRENOIRE, C., ROMEY, G., LAZDUNSKI, M. & BORSOTTO, M. 2002. p11, an annexin II subunit, an auxiliary protein associated with the background K+ channel, TASK-1. *The EMBO Journal,* 21**,** 4439-4448.

GIRERD, B., PERROS, F., ANTIGNY, F., HUMBERT, M. & MONTANI, D. 2014. KCNK3: new gene target for pulmonary hypertension? *Expert Rev Respir Med,* 8**,** 385-7.

GOLDSTEIN, S. A., BOCKENHAUER, D., O'KELLY, I. & ZILBERBERG, N. 2001. Potassium leak channels and the KCNK family of two-P-domain subunits. *Nature reviews. Neuroscience,* 2**,** 175-84.

GOLDSTEIN, S. A. N., BAYLISS, D. A., KIM, D., LESAGE, F., PLANT, L. D. & RAJAN, S. 2005. International Union of Pharmacology. LV. Nomenclature and molecular relationships of two-P potassium channels. *Pharmacological reviews,* 57**,** 527-40.

GOOD, N. E., WINGET, G. D., WINTER, W., CONNOLLY, T. N., IZAWA, S. & SINGH, R. M. M. 1966. Hydrogen Ion Buffers for Biological Research*. *Biochemistry,* 5**,** 467-477.

GRAETHER, S. P. 2019. Troubleshooting Guide to Expressing Intrinsically Disordered Proteins for Use in NMR Experiments. *Frontiers in Molecular Biosciences,* 5.

GRAHAM, J. M., ZADEH, N., KELLEY, M., TAN, E. S., LIEW, W., TAN, V., DEARDORFF, M. A., WILSON, G. N., SAGI-DAIN, L. & SHALEV, S. A. 2016. KCNK9 Imprinting Syndrome—Further Delineation of a Possible Treatable Disorder. *American Journal of Medical Genetics,* 170A**,** 2632-2637.

GRUSS, M., MATHIE, A., LIEB, W. R. & FRANKS, N. P. 2004. The Two-Pore-Domain K⁺ Channels TREK-1 and TASK-3 Are Differentially Modulated by Copper and Zinc. *Molecular Pharmacology,* 66**,** 530-537.

GSPONER, J., FUTSCHIK, M. E., TEICHMANN, S. A. & BABU, M. M. 2008. Tight Regulation of Unstructured Proteins: From Transcript Synthesis to Protein Degradation. *Science,* 322**,** 1365.

GUAGLIARDO, N. A., YAO, J., HU, C., SCHERTZ, E. M., TYSON, D. A., CAREY, R. M., BAYLISS, D. A. & BARRETT, P. Q. 2012. TASK-3 Channel Deletion in Mice Recapitulates Low-Renin Essential Hypertension. *Hypertension,* 59**,** 999-1005.

GURNEY, A. M., OSIPENKO, O. N., MACMILLAN, D., MCFARLANE, K. M., TATE, R. J. & KEMPSILL, F. E. 2003. Two-pore domain K channel, TASK-1, in pulmonary artery smooth muscle cells. *Circ Res,* 93**,** 957-64.

HAAS, H. & PANULA, P. 2003. The role of histamine and the tuberomamillary nucleus in the nervous system. *Nature Reviews Neuroscience,* 4**,** 121-130.

HAMMARSTRÖM, M., HELLGREN, N., VAN DEN BERG, S., BERGLUND, H. & HÄRD, T. 2002. Rapid screening for improved solubility of small human proteins produced as fusion proteins in Escherichia coli. *Protein Sci.*

HANCOCK, J. F., PATERSON, H. & MARSHALL, C. J. 1990. A polybasic domain or palmitoylation is required in addition to the CAAX motif to localize p21ras to the plasma membrane. *Cell,* 63**,** 133-9.

HARPER, S. & SPEICHER, D. W. 2011. Purification of proteins fused to glutathione S-tranferase. *Methods Mol Biol,* 681**,** 259-80.

HE, Y., WANG, K. & YAN, N. 2014. The recombinant expression systems for structure determination of eukaryotic membrane proteins. *Protein Cell.*

HEGINBOTHAM, L., LU, Z., ABRAMSON, T. & MACKINNON, R. 1994. Mutations in the K+ channel signature sequence. *Biophysical journal,* 66**,** 1061-7.

HEGINBOTHAM, L. & MACKINNON, R. 1992. The aromatic binding site for tetraethylammonium ion on potassium channels. *Neuron,* 8**,** 483-91.

HEITZMANN, D., DERAND, R., JUNGBAUER, S., BANDULIK, S., STERNER, C., SCHWEDA, F., EL WAKIL, A., LALLI, E., GUY, N., MENGUAL, R., REICHOLD, M., TEGTMEIER, I., BENDAHHOU, S., GOMEZ-SANCHEZ, C. E., ALLER, M. I., WISDEN, W., WEBER, A., LESAGE, F., WARTH, R. & BARHANIN, J. 2008. Invalidation of TASK1 potassium channels disrupts adrenal gland zonation and mineralocorticoid homeostasis. *Embo j,* 27**,** 179-87.

HELMS, J. B. & ROTHMAN, J. E. 1992. Inhibition by brefeldin A of a Golgi membrane enzyme that catalyses exchange of guanine nucleotide bound to ARF. *Nature,* 360**,** 352-354.

HEMNES, A. R. & HUMBERT, M. 2017. Pathobiology of pulmonary arterial hypertension: understanding the roads less travelled. *Eur Respir Rev,* 26.

HIBINO, H., INANOBE, A., FURUTANI, K., MURAKAMI, S., FINDLAY, I. & KURACHI, Y. 2010. Inwardly Rectifying Potassium Channels: Their Structure, Function, and Physiological Roles. *Physiological Reviews,* 90**,** 291-366.

HILL, N. S., CAWLEY, M. J. & HEGGEN-PEAY, C. L. 2016. New Therapeutic Paradigms and Guidelines in the Management of Pulmonary Arterial Hypertension. *J Manag Care Spec Pharm,* 22**,** S3-21.

HILLE, B. 1975. The receptor for tetrodotoxin and saxitoxin. A structural hypothesis. *Biophys J,* 15**,** 615-9.

HILLE, B. 2001. Ion channels of excitable membranes. 814.

HODGKIN A. L., H. A. F., KATZ B. 1949. Ionic currents underlying activity in the giant axon of the squid. *J. Physiol,* 116**,** 424-448.

HODGKIN, A. L. & HUXLEY, A. F. 1952. A quantitative description of membrane current and its application to conduction and excitation in nerve. *The Journal of physiology,* 117**,** 500-44.

HODGKIN, A. L. & KATZ, B. 1949. The effect of sodium ions on the electrical activity of giant axon of the squid. *J Physiol,* 108**,** 37-77.

HODGKIN, A. L. & KEYNES, R. D. 1955. The potassium permeability of a giant nerve fibre. *The Journal of physiology,* 128**,** 61-88.

HOGGART, C. J., VENTURINI, G., MANGINO, M., GOMEZ, F., ASCARI, G., ZHAO, J. H., TEUMER, A., WINKLER, T. W., TŠERNIKOVA, N., LUAN, J. A., MIHAILOV, E., EHRET, G. B., ZHANG, W., LAMPARTER, D., ESKO, T., MACÉ, A., RÜEGER, S., BOCHUD, P.-Y., BARCELLA, M., DAUVILLIERS, Y., BENYAMIN, B., EVANS, D. M., HAYWARD, C., LOPEZ, M. F., FRANKE, L., RUSSO, A., HEID, I.

M., SALVI, E., VENDANTAM, S., ARKING, D. E., BOERWINKLE, E., CHAMBERS, J. C., FIORITO, G., GRALLERT, H., GUARRERA, S., HOMUTH, G., HUFFMAN, J. E., PORTEOUS, D., GENERATION SCOTLAND, C., THE LIFELINES COHORT, S., THE, G. C., MORADPOUR, D., IRANZO, A., HEBEBRAND, J., KEMP, J. P., LAMMERS, G. J., AUBERT, V., HEIM, M. H., MARTIN, N. G., MONTGOMERY, G. W., PERAITA-ADRADOS, R., SANTAMARIA, J., NEGRO, F., SCHMIDT, C. O., SCOTT, R. A., SPECTOR, T. D., STRAUCH, K., VÖLZKE, H., WAREHAM, N. J., YUAN, W., BELL, J. T., CHAKRAVARTI, A., KOONER, J. S., PETERS, A., MATULLO, G., WALLASCHOFSKI, H., WHITFIELD, J. B., PACCAUD, F., VOLLENWEIDER, P., BERGMANN, S., BECKMANN, J. S., TAFTI, M., HASTIE, N. D., CUSI, D., BOCHUD, M., FRAYLING, T. M., METSPALU, A., JARVELIN, M.-R., SCHERAG, A., SMITH, G. D., BORECKI, I. B., ROUSSON, V., HIRSCHHORN, J. N., RIVOLTA, C., LOOS, R. J. F. & KUTALIK, Z. 2014. Novel Approach Identifies SNPs in SLC2A10 and KCNK9 with Evidence for Parent-of-Origin Effect on Body Mass Index. *PLOS Genetics,* 10**,** e1004508.

HOLCOMB, J., SPELLMON, N., ZHANG, Y., DOUGHAN, M., LI, C. & YANG, Z. 2017. Protein crystallization: Eluding the bottleneck of X-ray crystallography. *AIMS Biophys,* 4**,** 557-75.

HONORE, E. 2007. The neuronal background K2P Channels: Focus on TREK1. *Nature Reviews,* 8**,** 251-261.

HONORÉ, E., MAINGRET, F., LAZDUNSKI, M. & PATEL, A. J. 2002. An intracellular proton sensor commands lipid- and mechano-gating of the K(+) channel TREK-1. *The EMBO journal,* 21**,** 2968-76.

HOSHI, T. & ARMSTRONG, C. M. 2013. C-type inactivation of voltage-gated K⁺ channels: Pore constriction or dilation? *The Journal of General Physiology,* 141**,** 151.

HUMBERT, M., LAU, E. M., MONTANI, D., JAIS, X., SITBON, O. & SIMONNEAU, G. 2014. Advances in therapeutic interventions for patients with pulmonary arterial hypertension. *Circulation,* 130**,** 2189-208.

HWANG, I. & PARK, S. 2008. Computational design of protein therapeutics. *Drug Discov Today Technol,* 5**,** e43-8.

HWANG, P. M., PAN, J. S. & SYKES, B. D. 2014. Targeted expression, purification, and cleavage of fusion proteins from inclusion bodies in Escherichia coli. *FEBS Lett,* 588**,** 247-52.

IAKOUCHEVA, L. M., BROWN, C. J., LAWSON, J. D., OBRADOVIC, Z. & DUNKER, A. K. 2002. Intrinsic disorder in cell-signaling and cancer-associated proteins. *J Mol Biol,* 323**,** 573-84.

IAKOUCHEVA, L. M., RADIVOJAC, P., BROWN, C. J., O'CONNOR, T. R., SIKES, J. G., OBRADOVIC, Z. & DUNKER, A. K. 2004. The importance of intrinsic disorder for protein phosphorylation. *Nucleic Acids Res,* 32**,** 1037-49.

IRWIN, M. 1931. Can protein act as a carrier in penetration. *Exp Biol Med,* 29**,** 342-342.

JAHN, R. & SCHELLER, R. H. 2006. SNAREs--engines for membrane fusion. *Nat Rev Mol Cell Biol,* 7**,** 631-43.

KADAMUR, G. & ROSS, E. M. 2013. Mammalian Phospholipase C. *Annual Review of Physiology,* 75**,** 127-154.

KAMATO, D., THACH, L., BERNARD, R., CHAN, V., ZHENG, W., KAUR, H., BRIMBLE, M., OSMAN, N. & LITTLE, P. J. 2015. Structure, Function, Pharmacology, and Therapeutic Potential of the G Protein, Gα/q,11. *Front Cardiovasc Med,* 2.

KANANURA, C., SANDER, T., RAJAN, S., PREISIG-MULLER, R., GRZESCHIK, K. H., DAUT, J., DERST, C. & STEINLEIN, O. K. 2002. Tandem pore domain K(+)-channel TASK-3 (KCNK9) and idiopathic absence epilepsies. *Am J Med Genet,* 114**,** 227-9.

KARPLUS, P. A. & SCHULZ, G. E. 1985. Prediction of chain flexibility in proteins. *Naturwissenschaften,* 72**,** 212-213.

KARSCHIN, C., WISCHMEYER, E., PREISIG-MÜLLER, R., RAJAN, S., DERST, C., GRZESCHIK, K.-H., DAUT, J. & KARSCHIN, A. 2001. Expression Pattern in Brain of TASK-1, TASK-3, and a Tandem Pore Domain K+ Channel Subunit, TASK-5, Associated with the Central Auditory Nervous System. *Molecular and Cellular Neuroscience,* 18**,** 632-648.

KEMP, P. J., PEERS, C., LEWIS, A. & MILLER, P. 2004. Regulation of recombinant human brain tandem P domain K+ channels by hypoxia: a role for O2 in the control of neuronal excitability? *Journal of Cellular and Molecular Medicine,* 8**,** 38-44.

KHAZIPOV, R. & LUHMANN, H. J. 2006. Early patterns of electrical activity in the developing cerebral cortex of humans and rodents. *Trends in Neurosciences,* 29**,** 414-418.

KILISCH, M., LYTOVCHENKO, O., ARAKEL, E. C., BERTINETTI, D. & SCHWAPPACH, B. 2016. A dual phosphorylation switch controls 14-3-3-dependent cell surface expression of TASK-1. *Journal of cell science,* 129**,** 831-42.

KILISCH, M., LYTOVCHENKO, O., SCHWAPPACH, B., RENIGUNTA, V. & DAUT, J. 2015. The role of protein-protein interactions in the intracellular traffic of the potassium channels TASK-1 and TASK-3. *Pflugers Arch,* 467**,** 1105-20.

KIM, C. J., CHO, Y. G., JEONG, S. W., KIM, Y. S., KIM, S. Y., NAM, S. W., LEE, S. H., YOO, N. J., LEE, J. Y. & PARK, W. S. 2004. Altered expression of KCNK9 in colorectal cancers. *APMIS,* 112**,** 588-94.

KIM, D.-S., KIM, J.-E., KWAK, S.-E., CHOI, H.-C., SONG, H.-K., KIMG, Y.-I., CHOI, S.-Y. & KANG, T.-C. 2007. Up-regulated astroglial TWIK-related acid-sensitive K+ channel-1 (TASK-1) in the hippocampus of seizure-sensitive gerbils: A target of anti-epileptic drugs. *Brain Research,* 1185**,** 346-358.

KIM, D., CAVANAUGH, E. J., KIM, I. & CARROLL, J. L. 2009a. Heteromeric TASK-1/TASK-3 is the major oxygen-sensitive background K+ channel in rat carotid body glomus cells. *The Journal of physiology,* 587**,** 2963-75.

KIM, J.-E., KWAK, S.-E. & KANG, T.-C. 2009b. Upregulated TWIK-related acid-sensitive K+ channel-2 in neurons and perivascular astrocytes in the hippocampus of experimental temporal lobe epilepsy. *Epilepsia,* 50**,** 654-663.

KIM, Y., BANG, H. & KIM, D. 2000. TASK-3, a New Member of the Tandem Pore K Channel Family. *Journal of Biological Chemistry,* 275**,** 9340-9347.

KLEINSCHNITZ, C., MEUTH, S. G., KIESEIER, B. C. & WIENDL, H. 2007. Immunotherapeutic approaches in MS: update on pathophysiology and emerging agents or strategies 2006. *Endocr Metab Immune Disord Drug Targets,* 7**,** 35-63.

KOIKE-TANI, M., COLLINS, J. M., KAWANO, T., ZHAO, P., ZHAO, Q., KOZASA, T., NAKAJIMA, S. & NAKAJIMA, Y. 2005. Signal transduction pathway for the substance P-induced inhibition of rat Kir3 (GIRK) channel. *J Physiol,* 564**,** 489-500.

KOMURO, H. & RAKIC, P. 1993. Modulation of neuronal migration by NMDA receptors. *Science (New York, N.Y.),* 260**,** 95-7.

KOO, E. H. & SQUAZZO, S. L. 1994. Evidence that production and release of amyloid beta-protein involves the endocytic pathway. *J Biol Chem,* 269**,** 17386-9.

KOO, G. C., BLAKE, J. T., TALENTO, A., NGUYEN, M., LIN, S., SIROTINA, A., SHAH, K., MULVANY, K., HORA, D., JR., CUNNINGHAM, P., WUNDERLER, D. L., MCMANUS, O. B., SLAUGHTER, R., BUGIANESI, R., FELIX, J., GARCIA, M., WILLIAMSON, J., KACZOROWSKI, G., SIGAL, N. H., SPRINGER, M. S. & FEENEY, W. 1997. Blockade of the voltage-gated potassium channel Kv1.3 inhibits immune responses in vivo. *J Immunol,* 158**,** 5120-8.

KOSOLAPOV, A. & DEUTSCH, C. 2003. Folding of the voltage-gated K+ channel T1 recognition domain. *The Journal of biological chemistry,* 278**,** 4305-13.

KOSZTKA, L., RUSZNAK, Z., NAGY, D., NAGY, Z., FODOR, J., SZUCS, G., TELEK, A., GONCZI, M., RUZSNAVSZKY, O., SZENTANDRASSY, N. & CSERNOCH, L. 2011. Inhibition of TASK-3 (KCNK9) channel biosynthesis changes cell morphology and decreases both DNA content and mitochondrial function of melanoma cells maintained in cell culture. *Melanoma Res,* 21**,** 308-22.

KUMAR, R. & GRAHAM, B. 2018. How does inflammation contribute to pulmonary hypertension? *European Respiratory Journal,* 51**,** 1702403.

KUPERSHMIDT, S., YANG, T., CHANTHAPHAYCHITH, S., WANG, Z., TOWBIN, J. A. & RODEN, D. M. 2002. Defective human Ether-a-go-go-related gene trafficking linked to an endoplasmic reticulum retention signal in the C terminus. *J Biol Chem,* 277**,** 27442-8.

LAH, J. J. & LEVEY, A. I. 2000. Endogenous presenilin-1 targets to endocytic rather than biosynthetic compartments. *Mol Cell Neurosci,* 16**,** 111-26.

LAMBERT, N. A. 2008. Dissociation of heterotrimeric g proteins in cells. *Sci Signal,* 1**,** re5.

LASKOWSKI, M., AUGUSTYNEK, B., KULAWIAK, B., KOPROWSKI, P., BEDNARCZYK, P., JARMUSZKIEWICZ, W. & SZEWCZYK, A. 2016. What do we not know about mitochondrial potassium channels? *Biochimica et Biophysica Acta (BBA) - Bioenergetics,* 1857**,** 1247-1257.

LASZLO, K., TOTH, K., KERTES, E., PECZELY, L., OLLMANN, T. & LENARD, L. 2010. Effects of neurotensin in amygdaloid spatial learning mechanisms. *Behav Brain Res,* 210**,** 280-3.

LAURITZEN, I., ZANZOURI, M., HONORÉ, E., DUPRAT, F., EHRENGRUBER, M. U., LAZDUNSKI, M. & PATEL, A. J. 2003. K+-dependent Cerebellar Granule Neuron Apoptosis. *Journal of Biological Chemistry,* 278**,** 32068-32076.

LAZARENKO, R. M., WILLCOX, S. C., SHU, S., BERG, A. P., JEVTOVIC-TODOROVIC, V., TALLEY, E. M., CHEN, X. & BAYLISS, D. A. 2010. Motoneuronal TASK channels contribute to immobilizing effects of inhalational general anesthetics. *The Journal of neuroscience : the official journal of the Society for Neuroscience,* 30**,** 7691-704.

LEACH, N. T., SUN, Y., MICHAUD, S., ZHENG, Y., LIGON, K. L., LIGON, A. H., SANDER, T., KORF, B. R., LU, W., HARRIS, D. J., GUSELLA, J. F., MAAS, R. L., QUADE, B. J., COLE, A. J., KELZ, M. B. & MORTON, C. C. 2007. Disruption of diacylglycerol kinase delta (DGKD) associated with seizures in humans and mice. *American journal of human genetics,* 80**,** 792-9.

LEE, A., FAKLER, B., KACZMAREK, L. K. & ISOM, L. L. 2014. More than a pore: ion channel signaling complexes. *The Journal of neuroscience : the official journal of the Society for Neuroscience,* 34**,** 15159-69.

LEE, M. H., KWON, B. S., SON, A., KIM, H. D., KIM, K.-H., LIM, J., KWON, Y.-G., KANG, S. J., LEE, K. B., BYUN, H. Y. & SEONG, L. B. 2019. Stabilization of Intrinsically Disordered DKK2 Protein by Fusion to RNA-Binding Domain. *International Journal of Molecular Sciences,* 20.

LEONARD, R. J., GARCIA, M. L., SLAUGHTER, R. S. & REUBEN, J. P. 1992. Selective blockers of voltage-gated K+ channels depolarize human T lymphocytes: mechanism of the antiproliferative effect of charybdotoxin. *Proc Natl Acad Sci U S A,* 89**,** 10094-8.

LESAGE, F. & BARHANIN, J. 2011. Molecular physiology of pH-sensitive background K(2P) channels. *Physiology (Bethesda),* 26**,** 424-37.

LESAGE, F., GUILLEMARE, E., FINK, M., DUPRAT, F., LAZDUNSKI, M., ROMEY, G. & BARHANIN, J. 1996a. TWIK-1, a ubiquitous human weakly inward rectifying K+ channel with a novel structure. *The EMBO journal,* 15**,** 1004-11.

LESAGE, F. & LAZDUNSKI, M. 2000. Molecular and functional properties of two-pore-domain potassium channels. *Am J Physiol Renal Physiol,* 279**,** F793-801.

LESAGE, F., REYES, R., FINK, M., DUPRAT, F., GUILLEMARE, E. & LAZDUNSKI, M. 1996b. Dimerization of TWIK-1 K+ channel subunits via a disulfide bridge. *The EMBO journal,* 15**,** 6400-7.

LEWIS, R. S. 2001. Calcium signaling mechanisms in T lymphocytes. *Annu Rev Immunol,* 19**,** 497-521.

LI, J., CHEN, C., HE, Q., LI, H., MOYZIS, R. K., XUE, G. & DONG, Q. 2011. Neurotensin receptor 1 gene (NTSR1) polymorphism is associated with working memory. *PLoS One,* 6**,** e17365.

LI, W. & ALDRICH, R. W. 2011. Electrostatic influences of charged inner pore residues on the conductance and gating of small conductance Ca2+ activated K+ channels. *Proc Natl Acad Sci U S A,* 108**,** 5946-53.

LI, Y. 2011. Recombinant production of antimicrobial peptides in Escherichia coli: A review. *Protein Expression and Purification,* 80**,** 260-267.

LIANG, B., SOKA, M., CHRISTENSEN, A. H., OLESEN, M. S., LARSEN, A. P., KNOP, F. K., WANG, F., NIELSEN, J. B., ANDERSEN, M. N., HUMPHREYS, D., MANN, S. A., HUTTNER, I. G., VANDENBERG, J. I., SVENDSEN, J. H., HAUNSO, S., PREISS, T., SEEBOHM, G., OLESEN, S. P., SCHMITT, N. & FATKIN, D. 2014. Genetic variation in the two-pore domain potassium channel, TASK-1, may contribute to an atrial substrate for arrhythmogenesis. *J Mol Cell Cardiol,* 67**,** 69-76.

LIMBERG, S. H., NETTER, M. F., ROLFES, C., RINNE, S., SCHLICHTHORL, G., ZUZARTE, M., VASSILIOU, T., MOOSDORF, R., WULF, H., DAUT, J., SACHSE, F. B. & DECHER, N. 2011. TASK-1 channels may modulate action potential duration of human atrial cardiomyocytes. *Cell Physiol Biochem,* 28**,** 613-24.

LINDING, R., SCHYMKOWITZ, J., ROUSSEAU, F., DIELLA, F. & SERRANO, L. 2004. A comparative study of the relationship between protein structure and beta-aggregation in globular and intrinsically disordered proteins. *J Mol Biol,* 342**,** 345-53.

LIU, C., COTTEN, J. F., SCHUYLER, J. A., FAHLMAN, C. S., AU, J. D., BICKLER, P. E. & YOST, C. S. 2005. Protective effects of TASK-3 (KCNK9) and related 2P K channels during cellular stress. *Brain research,* 1031**,** 164-73.

LIU, X., HASHIMOTO-TORII, K., TORII, M., DING, C. & RAKIC, P. 2010. Gap junctions/hemichannels modulate interkinetic nuclear migration in the forebrain precursors. *The Journal of neuroscience : the official journal of the Society for Neuroscience,* 30**,** 4197-209.

LOEB, J., AND BEUTNER, R.U 1912. Uber die potentialdifferenzen an der unversehrten und verletzten oberflache pflanzlicher und tierische Organe. *Biochem Z,* 41**,** 1-26.

LONG, S. B., CAMPBELL, E. B. & MACKINNON, R. 2005. Crystal structure of a mammalian voltage-dependent Shaker family K+ channel. *Science,* 309**,** 897-903.

LONG, S. B., TAO, X., CAMPBELL, E. B. & MACKINNON, R. 2007. Atomic structure of a voltage-dependent K+ channel in a lipid membrane-like environment. *Nature,* 450**,** 376-82.

LOPES, C. M. B., ROHÁCS, T., CZIRJÁK, G., BALLA, T., ENYEDI, P. & LOGOTHETIS, D. E. 2005. PIP2 hydrolysis underlies agonist-induced inhibition and regulates voltage gating of two-pore domain K+ channels. *The Journal of physiology,* 564**,** 117-29.

LÓPEZ-BARNEO, J., ORTEGA-SÁENZ, P., PARDAL, R., PASCUAL, A. & PIRUAT, J. I. 2008. Carotid body oxygen sensing. *The European respiratory journal,* 32**,** 1386-98.

LOSSI, L., MIOLETTI, S. & MERIGHI, A. 2002. Synapse-independent and synapse-dependent apoptosis of cerebellar granule cells in postnatal rabbits occur at two subsequent but partly overlapping developmental stages. *Neuroscience,* 112**,** 509-523.

MA, L., ROMAN-CAMPOS, D., AUSTIN, E. D., EYRIES, M., SAMPSON, K. S., SOUBRIER, F., GERMAIN, M., TRÉGOUËT, D. A., BORCZUK, A., ROSENZWEIG, E. B., GIRERD, B., MONTANI, D., HUMBERT, M., LOYD, J. E., KASS, R. S. & CHUNG, W. K. 2013. A Novel Channelopathy in Pulmonary Arterial Hypertension. *N Engl J Med,* 369**,** 351-61.

MACHADO, R. D., SOUTHGATE, L., EICHSTAEDT, C. A., ALDRED, M. A., AUSTIN, E. D., BEST, D. H., CHUNG, W. K., BENJAMIN, N., ELLIOTT, C. G., EYRIES, M., FISCHER, C., GRAF, S., HINDERHOFER, K., HUMBERT, M., KEILES, S. B., LOYD, J. E., MORRELL, N. W., NEWMAN, J. H., SOUBRIER, F., TREMBATH, R. C., VIALES, R. R. & GRUNIG, E. 2015. Pulmonary Arterial Hypertension: A Current Perspective on Established and Emerging Molecular Genetic Defects. *Hum Mutat,* 36**,** 1113-27.

MACKENZIE, G., FRANKS, N. P. & BRICKLEY, S. G. 2015. Two-pore domain potassium channels enable action potential generation in the absence of voltage-gated potassium channels. *Pflugers Archiv European Journal of Physiology,* 467**,** 989-999.

MACKINNON, R. 2004. Potassium Channels and the Atomic Basis of Selective Ion Conduction (Nobel Lecture). *Angewandte Chemie International Edition,* 43**,** 4265-4277.

MACKINTOSH, C. 2004. Dynamic interactions between 14-3-3 proteins and phosphoproteins regulate diverse cellular processes. *Biochemical Journal,* 381.

MAINGRET, F., PATEL, A. J., LESAGE, F., LAZDUNSKI, M. & HONORÉ, E. 1999. Mechano- or acid stimulation, two interactive modes of activation of the TREK-1 potassium channel. *The Journal of biological chemistry,* 274**,** 26691-6.

MANT, A., WILLIAMS, S. & O'KELLY, I. 2013a. Acid sensitive background potassium channels K2P3.1 and K2P9.1 undergo rapid dynamin-dependent endocytosis. *Channels (Austin),* 7**,** 288-302.

MANT, A., WILLIAMS, S., RONCORONI, L., LOWRY, E., JOHNSON, D. & O'KELLY, I. 2013b. N-Glycosylation-dependent Control of Functional Expression of Background Potassium Channels K2P3.1 and K2P9.1*. *J Biol Chem.*

MARBLESTONE, J. G., EDAVETTAL, S. C., LIM, Y., LIM, P., ZUO, X. & BUTT, T. R. 2006. Comparison of SUMO fusion technology with traditional gene fusion systems: enhanced expression and solubility with SUMO. *Protein Sci,* 15**,** 182-9.

MARCORELLES, P., FRIOCOURT, G., UGUEN, A., LEDÉ, F., FÉREC, C. & LAQUERRIÈRE, A. 2014. Cystic Fibrosis Transmembrane Conductance Regulator Protein (CFTR) Expression in the Developing Human Brain: Comparative Immunohistochemical Study between Patients with Normal and Mutated CFTR. *Journal of Histochemistry & Cytochemistry,* 62**,** 791-801.

MARMONT, G. J. 1949. Studies on the axon membrane. A new method. *Cell. Comp. Physiol,* 34**,** 351-382.

MATHIE, A. 2007. Neuronal two-pore-domain potassium channels and their regulation by G protein-coupled receptors. *The Journal of physiology,* 578**,** 377-85.

MATHIE, A., REES, K. A., EL HACHMANE, M. F. & VEALE, E. L. 2010. Trafficking of neuronal two pore domain potassium channels. *Current neuropharmacology,* 8**,** 276-86.

MATTSON, M. P. 1997. Cellular actions of beta-amyloid precursor protein and its soluble and fibrillogenic derivatives. *Physiol Rev,* 77**,** 1081-132.

MCLAUGHLIN, S. & ADEREM, A. 1995. The myristoyl-electrostatic switch: a modulator of reversible protein-membrane interactions. *Trends Biochem Sci,* 20**,** 272-6.

MCMAHAN, Z. H. & HUMMERS, L. K. 2013. Systemic sclerosis--challenges for clinical practice. *Nat Rev Rheumatol,* 9**,** 90-100.

MEDHURST, A. D., RENNIE, G., CHAPMAN, C. G., MEADOWS, H., DUCKWORTH, M. D., KELSELL, R. E., GLOGER, I. I. & PANGALOS, M. N. 2001. Distribution analysis of human two pore domain potassium channels in tissues of the central nervous system and periphery. *Molecular Brain Research,* 86**,** 101-114.

MEERA, P., WALLNER, M., SONG, M. & TORO, L. 1997. Large conductance voltage- and calcium-dependent K+ channel, a distinct member of voltage-dependent ion channels with seven N-terminal transmembrane segments (S0-S6), an extracellular N terminus, and an intracellular (S9-S10) C terminus. *Proceedings of the National Academy of Sciences of the United States of America,* 94**,** 14066-71.

MEISSNER, T., BEINBRECH, B. & MAYATEPEK, E. 1999. Congenital hyperinsulinism: molecular basis of a heterogeneous disease. *Hum Mutat,* 13**,** 351-61.

MEUTH, S. G., ALLER, M. I., MUNSCH, T., SCHUHMACHER, T., SEIDENBECHER, T., MEUTH, P., KLEINSCHNITZ, C., PAPE, H. C., WIENDL, H., WISDEN, W. & BUDDE, T. 2006a. The contribution of TWIK-related acid-sensitive K+-containing channels to the function of dorsal lateral geniculate thalamocortical relay neurons. *Mol Pharmacol,* 69**,** 1468-76.

MEUTH, S. G., BITTNER, S., MEUTH, P., SIMON, O. J., BUDDE, T. & WIENDL, H. 2008a. TWIK-related Acid-sensitive K+ Channel 1 (TASK1) and TASK3 Critically Influence T Lymphocyte Effector Functions. *Journal of Biological Chemistry,* 283**,** 14559-14570.

MEUTH, S. G., BUDDE, T., KANYSHKOVA, T., BROICHER, T., MUNSCH, T. & PAPE, H. C. 2003. Contribution of TWIK-related acid-sensitive K+ channel 1 (TASK1) and TASK3 channels to the control of activity modes in thalamocortical neurons. *J Neurosci,* 23**,** 6460-9.

MEUTH, S. G., KANYSHKOV, T., MELZER, N., BITTNER, S., KIESEIER, B. C., BUDDE, T. & WIENDL, H. 2008b. Altered neuronal expression of TASK1 and TASK3 potassium channels in rodent and human autoimmune CNS inflammation. *Neurosci Lett,* 446**,** 133-8.

MEUTH, S. G., KANYSHKOVA, T., MEUTH, P., LANDGRAF, P., MUNSCH, T., LUDWIG, A., HOFMANN, F., PAPE, H. C. & BUDDE, T. 2006b. Membrane resting potential of thalamocortical relay neurons is shaped by the interaction among TASK3 and HCN2 channels. *J Neurophysiol,* 96**,** 1517-29.

MEUTH, S. G., KLEINSCHNITZ, C., BROICHER, T., AUSTINAT, M., BRAEUNINGER, S., BITTNER, S., FISCHER, S., BAYLISS, D. A., BUDDE, T., STOLL, G. & WIENDL, H. 2009. The neuroprotective

impact of the leak potassium channel TASK1 on stroke development in mice. *Neurobiology of Disease,* 33**,** 1-11.

MICHELAKIS, E. D., HAMPL, V., NSAIR, A., WU, X., HARRY, G., HAROMY, A., GURTU, R. & ARCHER, S. L. 2002. Diversity in mitochondrial function explains differences in vascular oxygen sensing. *Circ Res,* 90**,** 1307-15.

MILLER, A. N. & LONG, S. B. 2012. Crystal structure of the human two-pore domain potassium channel K2P1. *Science (New York, N.Y.),* 335**,** 432-6.

MILLER, C. 2000. An overview of the potassium channel family. *Genome Biology,* 1**,** reviews0004.1.

MILLER, D. J. 2004. Sydney Ringer; physiological saline, calcium and the contraction of the heart. *The Journal of physiology,* 555**,** 585-7.

MISONOU, H., MOHAPATRA, D. P., MENEGOLA, M. & TRIMMER, J. S. 2005. Calcium- and Metabolic State-Dependent Modulation of the Voltage-Dependent Kv2.1 Channel Regulates Neuronal Excitability in Response to Ischemia. *Journal of Neuroscience,* 25**,** 11184-11193.

MORALES, J., FISHBURN, C. S., WILSON, P. T. & BOURNE, H. R. 1998. Plasma membrane localization of G alpha z requires two signals. *Mol Biol Cell,* 9**,** 1-14.

MORTON, M. J., O'CONNELL, A. D., SIVAPRASADARAO, A. & HUNTER, M. 2003. Determinants of pH sensing in the two-pore domain K+ channels TASK-1 and -2. *Pflügers Archiv - European Journal of Physiology,* 445**,** 577-583.

MU, D., CHEN, L., ZHANG, X., SEE, L.-H., KOCH, C. M., YEN, C., TONG, J. J., SPIEGEL, L., NGUYEN, K. C. Q., SERVOSS, A., PENG, Y., PEI, L., MARKS, J. R., LOWE, S., HOEY, T., JAN, L. Y., MCCOMBIE, W. R., WIGLER, M. H. & POWERS, S. 2003. Genomic amplification and oncogenic properties of the KCNK9 potassium channel gene. *Cancer Cell,* 3**,** 297-302.

MUSTAIN, W. C., RYCHAHOU, P. G. & EVERS, B. M. 2011. The role of neurotensin in physiologic and pathologic processes. *Curr Opin Endocrinol Diabetes Obes,* 18**,** 75-82.

NADLER, J. V. 2003. The recurrent mossy fiber pathway of the epileptic brain. *Neurochem Res,* 28**,** 1649-58.

NAKAI, W., KONDO, Y., SAITOH, A., NAITO, T., NAKAYAMA, K. & SHIN, H. W. 2013. ARF1 and ARF4 regulate recycling endosomal morphology and retrograde transport from endosomes to the Golgi apparatus. *Mol Biol Cell,* 24**,** 2570-81.

NAKANISHI, S. & OKAZAWA, M. 2006. Membrane potential-regulated Ca2+ signalling in development and maturation of mammalian cerebellar granule cells. *The Journal of physiology,* 575**,** 389-95.

NAVAS, P., TENORIO, J., QUEZADA, C. A., BARRIOS, E., GORDO, G., ARIAS, P., LOPEZ MESEGUER, M., SANTOS-LOZANO, A., PALOMINO DOZA, J., LAPUNZINA, P. & ESCRIBANO SUBIAS, P. 2016. Molecular Analysis of BMPR2, TBX4, and KCNK3 and Genotype-Phenotype Correlations in Spanish Patients and Families With Idiopathic and Hereditary Pulmonary Arterial Hypertension. *Rev Esp Cardiol (Engl Ed),* 69**,** 1011-1019.

NEBENFÜHR, A., RITZENTHALER, C. & ROBINSON, D. G. 2002. Brefeldin A: deciphering an enigmatic inhibitor of secretion. *Plant physiology,* 130**,** 1102-8.

NEGULESCU, P. A., SHASTRI, N. & CAHALAN, M. D. 1994. Intracellular calcium dependence of gene expression in single T lymphocytes. *Proc Natl Acad Sci U S A,* 91**,** 2873-7.

NEHER, E., SAKMANN, B. & STEINBACH, J. H. 1978. The extracellular patch clamp: a method for resolving currents through individual open channels in biological membranes. *Pflugers Archiv : European journal of physiology,* 375**,** 219-28.

NODA, M., SHIMIZU, S., TANABE, T., TAKAI, T., KAYANO, T., IKEDA, T., TAKAHASHI, H., NAKAYAMA, H., KANAOKA, Y., MINAMINO, N., KANGAWA, K., MATSUO, H., RAFTERY, M. A., HIROSE, T., INAYAMA, S., HAYASHIDA, H., MIYATA, T. & NUMA , S. 1984. Primary structure of Electrophorus electricus sodium channel deduced from cDNA sequence. *Nature,* 312**,** 121-127.

NODA, M., TAKAHASHI, H., TANABE, T., TOYOSATO, M., KIKYOTANI, S., FURUTANI, Y., HIROSE, T., TAKASHIMA, H., INAYAMA, S., MIYATA, T. & NUMA, S. 1983. Structural homology of Torpedo californica acetylcholine receptor subunits. *Nature,* 302**,** 528-532.

NOGUEIRA, E. F., GERRY, D., MANTERO, F., MARINIELLO, B. & RAINEY, W. E. 2010. The role of TASK1 in aldosterone production and its expression in normal adrenal and aldosterone-producing adenomas. *Clin Endocrinol (Oxf),* 73**,** 22-9.

NORDSTEDT, C., CAPORASO, G. L., THYBERG, J., GANDY, S. E. & GREENGARD, P. 1993. Identification of the Alzheimer beta/A4 amyloid precursor protein in clathrin-coated vesicles purified from PC12 cells. *J Biol Chem,* 268**,** 608-12.

O'DONOHOE, P. B., HUSKENS, N., TURNER, P. J., PANDIT, J. J. & BUCKLER, K. J. 2018. A1899, PK-THPP, ML365, and Doxapram inhibit endogenous TASK channels and excite calcium signaling in carotid body type-1 cells. *Physiol Rep,* 6**,** e13876.

O'KELLY, I., BUTLER, M. H., ZILBERBERG, N. & GOLDSTEIN, S. A. N. 2002. Forward Transport: 14-3-3 Overcomes ER Retention. *Cell,* 111**,** 577-588.

O'KELLY, I. & GOLDSTEIN, S. A. 2008. Forward Transport of K2p3.1: mediation by 14-3-3 and COPI, modulation by p11. *Traffic,* 9**,** 72-8.

O'KELLY, I. 2015. Endocytosis as a mode to regulate functional expression of two-pore domain potassium (K2P) channels. *Pflügers Archiv - European Journal of Physiology,* 467**,** 1133-1142.

OBSIL, T., GHIRLANDO, R., KLEIN, D. C., GANGULY, S. & DYDA, F. 2001. Crystal structure of the 14-3-3zeta:serotonin N-acetyltransferase complex. a role for scaffolding in enzyme regulation. *Cell,* 105**,** 257-67.

OHINATA, K., SONODA, S., INOUE, N., YAMAUCHI, R., WADA, K. & YOSHIKAWA, M. 2007. beta-Lactotensin, a neurotensin agonist peptide derived from bovine beta-lactoglobulin, enhances memory consolidation in mice. *Peptides,* 28**,** 1470-4.

OLSCHEWSKI, A., LI, Y., TANG, B., HANZE, J., EUL, B., BOHLE, R. M., WILHELM, J., MORTY, R. E., BRAU, M. E., WEIR, E. K., KWAPISZEWSKA, G., KLEPETKO, W., SEEGER, W. & OLSCHEWSKI, H. 2006. Impact of TASK-1 in human pulmonary artery smooth muscle cells. *Circ Res,* 98**,** 1072-80.

ORTEGA-SAENZ, P., LEVITSKY, K. L., MARCOS-ALMARAZ, M. T., BONILLA-HENAO, V., PASCUAL, A. & LOPEZ-BARNEO, J. 2010. Carotid body chemosensory responses in mice deficient of TASK channels. *J Gen Physiol,* 135**,** 379-92.

PANULA, P., CHAZOT, P. L., COWART, M., GUTZMER, R., LEURS, R., LIU, W. L., STARK, H., THURMOND, R. L. & HAAS, H. L. 2015. International Union of Basic and Clinical Pharmacology. XCVIII. Histamine Receptors. *Pharmacol Rev,* 67**,** 601-55.

PANYI, G., VARGA, Z. & GASPAR, R. 2004. Ion channels and lymphocyte activation. *Immunol Lett,* 92**,** 55-66.

PATEL, A. J., HONORE, E., LESAGE, F., FINK, M., ROMEY, G. & LAZDUNSKI, M. 1999. Inhalational anesthetics activate two-pore-domain background K+ channels. *Nature Neuroscience,* 2**,** 422-426.

PATEL, A. J. & LAZDUNSKI, M. 2004. The 2P-domain K + channels: role in apoptosis and tumorigenesis. *Pfl*gers Archiv European Journal of Physiology,* 448**,** 261-273.

PEI, L., WISER, O., SLAVIN, A., MU, D., POWERS, S., JAN, L. Y. & HOEY, T. 2003. Oncogenic potential of TASK3 (Kcnk9) depends on K+ channel function. *Proceedings of the National Academy of Sciences,* 100**,** 7803-7807.

PENTON, D., BANDULIK, S., SCHWEDA, F., HAUBS, S., TAUBER, P., REICHOLD, M., CONG, L. D., EL WAKIL, A., BUDDE, T., LESAGE, F., LALLI, E., ZENNARO, M. C., WARTH, R. & BARHANIN, J. 2012. Task3 potassium channel gene invalidation causes low renin and salt-sensitive arterial hypertension. *Endocrinology,* 153**,** 4740-8.

PERRIER, J.-F., ALABURDA, A. & HOUNSGAARD, J. 2003. 5-HT1A receptors increase excitability of spinal motoneurons by inhibiting a TASK-1-like K+ current in the adult turtle. *The Journal of Physiology,* 548**,** 485-492.

PERRY, J. R., DAY, F., ELKS, C. E., SULEM, P., THOMPSON, D. J., FERREIRA, T., HE, C., CHASMAN, D. I., ESKO, T., THORLEIFSSON, G., ALBRECHT, E., ANG, W. Q., CORRE, T., COUSMINER, D. L., FEENSTRA, B., FRANCESCHINI, N., GANNA, A., JOHNSON, A. D., KJELLQVIST, S., LUNETTA, K. L., MCMAHON, G., NOLTE, I. M., PATERNOSTER, L., PORCU, E., SMITH, A. V., STOLK, L., TEUMER, A., TŠERNIKOVA, N., TIKKANEN, E., ULIVI, S., WAGNER, E. K., AMIN, N., BIERUT, L. J., BYRNE, E. M., HOTTENGA, J. J., KOLLER, D. L., MANGINO, M., PERS, T. H., YERGES-ARMSTRONG, L. M., ZHAO, J. H., ANDRULIS, I. L., ANTON-CULVER, H., ATSMA, F., BANDINELLI, S., BECKMANN, M. W., BENITEZ, J., BLOMQVIST, C., BOJESEN, S. E., BOLLA, M. K., BONANNI, B., BRAUCH, H., BRENNER, H., BURING, J. E., CHANG-CLAUDE, J., CHANOCK, S., CHEN, J., CHENEVIX-TRENCH, G., COLLÉE, J. M., COUCH, F. J., COUPER, D., COVEILLO, A. D., COX, A., CZENE, K., D'ADAMO, A. P., SMITH, G. D., DE VIVO, I., DEMERATH, E. W., DENNIS, J., DEVILEE, P., DIEFFENBACH, A. K., DUNNING, A. M., EIRIKSDOTTIR, G., ERIKSSON, J. G., FASCHING, P. A., FERRUCCI, L., FLESCH-JANYS, D., FLYGER, H., FOROUD, T., FRANKE, L., GARCIA, M. E., GARCÍA-CLOSAS, M., GELLER, F., DE GEUS, E. E., GILES, G. G., GUDBJARTSSON, D. F., GUDNASON, V., GUÉNEL, P., GUO, S., HALL, P., HAMANN, U., HARING, R., HARTMAN, C. A., HEATH, A. C., HOFMAN, A., HOONING, M. J., HOPPER, J. L., HU, F. B., HUNTER, D. J., KARASIK, D., KIEL, D. P., et al. 2014. Parent-of-origin specific allelic associations among 106 genomic loci for age at menarche. *Nature,* 514**,** 92-7.

PETRIC, S., CLASEN, L., VAN WEßEL, C., GEDULDIG, N., DING, Z., SCHULLENBERG, M., MERSMANN, J., ZACHAROWSKI, K., ALLER, M. I., SCHMIDT, K. G. & DONNER, B. C. 2012. In vivo Electrophysiological Characterization of TASK-1 Deficient Mice. *Cellular Physiology and Biochemistry,* 30**,** 523-537.

PFAFF, D. W. & KIEFFER, B. L. 2008. Molecular and biophysical mechanisms of arousal, alertness, and attention. *Annals of the New York Academy of Sciences*.

PIECHOTTA, P. L., RAPEDIUS, M., STANSFELD, P. J., BOLLEPALLI, M. K., ERHLICH, G., ANDRES-ENGUIX, I., FRITZENSCHAFT, H., DECHER, N., SANSOM, M. S. P., TUCKER, S. J., BAUKROWITZ, T., EHRLICH, G., ERHLICH, G., ANDRES-ENGUIX, I., FRITZENSCHAFT, H., DECHER, N., SANSOM, M. S. P., TUCKER, S. J. & BAUKROWITZ, T. 2011. The pore structure and gating mechanism of K2P channels. *The EMBO Journal,* 30268**,** 3607-3619.

PIND, S., RIORDAN, J. R. & WILLIAMS, D. B. 1994. Participation of the endoplasmic reticulum chaperone calnexin (p88, IP90) in the biogenesis of the cystic fibrosis transmembrane conductance regulator. *J Biol Chem,* 269**,** 12784-8.

PLUM, F. & POSNER, J. B. 1972. The diagnosis of stupor and coma. *Contemp Neurol Ser,* 10**,** 1-286.

POCSAI, K., KOSZTKA, L., BAKONDI, G., GÖNCZI, M., FODOR, J., DIENES, B., SZENTESI, P., KOVÁCS, I., FENIGER-BARISH, R., KOPF, E., ZHARHARY, D., SZŰCS, G., CSERNOCH, L. & RUSZNÁK, Z. 2006. Melanoma cells exhibit strong intracellular TASK-3-specific immunopositivity in both tissue sections and cell culture. *Cellular and Molecular Life Sciences,* 63**,** 2364-2376.

PRABHAKAR, N. R. & PENG, Y.-J. 2017. Oxygen Sensing by the Carotid Body: Past and Present. Springer, Cham.

PRAKRIYA, M. & LEWIS, R. S. 2003. CRAC channels: activation, permeation, and the search for a molecular identity. *Cell Calcium,* 33**,** 311-21.

PREININGER, A. M. & HAMM, H. E. 2004. G protein signaling: insights from new structures. *Sci STKE,* 2004**,** re3.

PREVARSKAYA, N., SKRYMA, R. & SHUBA, Y. 2010. Ion channels and the hallmarks of cancer. *Trends Mol Med,* 16**,** 107-21.

QUIRION, R., WELNER, S., GAUTHIER, S. & BEDARD, P. 1987. Neurotensin receptor binding sites in monkey and human brain: autoradiographic distribution and effects of 1-methyl-4-phenyl-1,2,3,6-tetrahydropyridine treatment. *Synapse,* 1**,** 559-66.

RABINOVITCH, M., GUIGNABERT, C., HUMBERT, M. & NICOLLS MARK, R. 2014. Inflammation and Immunity in the Pathogenesis of Pulmonary Arterial Hypertension. *Circulation Research,* 115**,** 165-175.

RAJAN, S., PREISIG-MÜLLER, R., WISCHMEYER, E., NEHRING, R., HANLEY, P. J., RENIGUNTA, V., MUSSET, B., SCHLICHTHÖRL, G., DERST, C., KARSCHIN, A. & DAUT, J. 2002. Interaction with 14-3-3 proteins promotes functional expression of the potassium channels TASK-1 and TASK-3. *The Journal of Physiology,* 545**,** 13-26.

RAJAN, S., WISCHMEYER, E., LIU, G. X., PREISIG-MÜLLER, R., DAUT, J., KARSCHIN, A. & DERST, C. 2000. TASK-3, a novel tandem pore domain acid-sensitive K+ channel. An extracellular histidine as pH sensor. *Journal of Biological Chemistry*.

RAKHADE, S. N. & JENSEN, F. E. 2009. Epileptogenesis in the immature brain: emerging mechanisms. *Nat Rev Neurol,* 5**,** 380-91.

RAPEDIUS, M., FOWLER, P. W., SHANG, L., SANSOM, M. S. P., TUCKER, S. J. & BAUKROWITZ, T. 2007. H bonding at the helix-bundle crossing controls gating in Kir potassium channels. *Neuron,* 55**,** 602-14.

RAWLINGS, ANDREA E. 2016. Membrane proteins: always an insoluble problem? *Biochemical Society Transactions,* 44**,** 790-795.

RENIGUNTA, V., FISCHER, T., ZUZARTE, M., KLING, S., ZOU, X., SIEBERT, K., LIMBERG, M. M., RINNÉ, S., DECHER, N., SCHLICHTHÖRL, G. & DAUT, J. 2014. Cooperative endocytosis of the endosomal SNARE protein syntaxin-8 and the potassium channel TASK-1. *Molecular biology of the cell,* 25**,** 1877-1891.

RENIGUNTA, V., YUAN, H., ZUZARTE, M., RINNE, S., KOCH, A., WISCHMEYER, E., SCHLICHTHORL, G., GAO, Y., KARSCHIN, A., JACOB, R., SCHWAPPACH, B., DAUT, J. & PREISIG-MULLER, R. 2006. The retention factor p11 confers an endoplasmic reticulum-localization signal to the potassium channel TASK-1. *Traffic,* 7**,** 168-81.

RESH, M. D. 1999. Fatty acylation of proteins: new insights into membrane targeting of myristoylated and palmitoylated proteins. *Biochim Biophys Acta,* 1451**,** 1-16.

RITTINGER, K., BUDMAN, J., XU, J., VOLINIA, S., CANTLEY, L. C., SMERDON, S. J., GAMBLIN, S. J. & YAFFE, M. B. 1999. Structural analysis of 14-3-3 phosphopeptide complexes identifies a dual role for the nuclear export signal of 14-3-3 in ligand binding. *Mol Cell,* 4**,** 153-66.

RODRIGUEZ DE TURCO, E. B., TANG, W., TOPHAM, M. K., SAKANE, F., MARCHESELLI, V. L., CHEN, C., TAKETOMI, A., PRESCOTT, S. M. & BAZAN, N. G. 2001. Diacylglycerol kinase epsilon regulates seizure susceptibility and long-term potentiation through arachidonoyl- inositol lipid signaling. *Proceedings of the National Academy of Sciences of the United States of America,* 98**,** 4740-5.

RÖDSTRÖM, K. E. J., KIPER, A. K., ZHANG, W., RINNÉ, S., PIKE, A. C. W., GOLDSTEIN, M., CONRAD, L., DELBECK, M., HAHN, M., MEIER, H., PLATZK, M., QUIGLEY, A., SPEEDMAN, D., SHRESTHA, L., MUKHOPADHYAY, S. M. M., BURGESS-BROWN, N. A., TUCKER, S. J., MUELLER, T., DECHER, N. & CARPENTER, E. P. 2019. A unique lower X-gate in TASK channels traps inhibitors within the vestibule. *bioRxiv***,** 706168.

RUNDÉN-PRAN, E., HAUG, F. M., STORM, J. F. & OTTERSEN, O. P. 2002. BK channel activity determines the extent of cell degeneration after oxygen and glucose deprivation: a study in organotypical hippocampal slice cultures. *Neuroscience,* 112**,** 277-88.

RUSZNÁK, Z., BAKONDI, G., KOSZTKA, L., POCSAI, K., DIENES, B., FODOR, J., TELEK, A., GÖNCZI, M., SZŰCS, G. & CSERNOCH, L. 2008. Mitochondrial expression of the two-pore domain TASK-3 channels in malignantly transformed and non-malignant human cells. *Virchows Archiv,* 452**,** 415-426.

RUTISHAUSER, J. & SPIESS, M. 2002. Endoplasmic reticulum storage diseases. *Swiss Med Wkly,* 132**,** 211-22.

RYAN, J., DASGUPTA, A., HUSTON, J., CHEN, K.-H. & ARCHER, S. L. 2015. Mitochondrial dynamics in pulmonary arterial hypertension. *Journal of molecular medicine (Berlin, Germany),* 93**,** 229-242.

SAEZ-HERNANDEZ, L., PERAL, B., SANZ, R., GOMEZ-GARRE, P., RAMOS, C., AYUSO, C. & SERRATOSA, J. M. 2003. Characterization of a 6p21 translocation breakpoint in a family with idiopathic generalized epilepsy. *Epilepsy Res,* 56**,** 155-63.

SALUTA, M. & BELL, P. A. 1998. Troubleshooting GST Fusion Protein Expression in E.coli. *Life Science News.*

SANDOZ, G., BELL, S. C. & ISACOFF, E. Y. 2011. Optical probing of a dynamic membrane interaction that regulates the TREK1 channel. *Proceedings of the National Academy of Sciences of the United States of America,* 108**,** 2605-10.

SANDOZ, G., THÜMMLER, S., DUPRAT, F., FELICIANGELI, S., VINH, J., ESCOUBAS, P., GUY, N., LAZDUNSKI, M. & LESAGE, F. 2006. AKAP150, a switch to convert mechano-, pH- and arachidonic acid-sensitive TREK K+ channels into open leak channels. *EMBO J.*

SAZGAR, M. & YOUNG, M. G. 2019. Seizures and Epilepsy. *In:* SAZGAR, M. & YOUNG, M. G. (eds.) *Absolute Epilepsy and EEG Rotation Review: Essentials for Trainees.* Cham: Springer International Publishing.

SCAMMELL, T. E., ARRIGONI, E. & LIPTON, J. 2017. Neural Circuitry of Wakefulness and Sleep. *Neuron,* 93**,** 747-65.

SCHEWE, M., NEMATIAN-ARDESTANI, E., SUN, H., MUSINSZKI, M., CORDEIRO, S., BUCCI, G., DE GROOT, B. L., TUCKER, S. J., RAPEDIUS, M. & BAUKROWITZ, T. 2016. A Non-canonical Voltage-Sensing Mechanism Controls Gating in K2P K+ Channels. *Cell*.

SCHLESSINGER, A., SCHAEFER, C., VICEDO, E., SCHMIDBERGER, M., PUNTA, M. & ROST, B. 2011. Protein disorder--a breakthrough invention of evolution? *Curr Opin Struct Biol,* 21**,** 412-8.

SCHONEBERG, T., LIU, J. & WESS, J. 1995. Plasma membrane localization and functional rescue of truncated forms of a G protein-coupled receptor. *J Biol Chem,* 270**,** 18000-6.

SCHOPPA, N. E., MCCORMACK, K., TANOUYE, M. A. & SIGWORTH, F. J. 1992. The size of gating charge in wild-type and mutant Shaker potassium channels. *Science,* 255**,** 1712.

SCHREIBER, M., WEI, A., YUAN, A., GAUT, J., SAITO, M. & SALKOFF, L. 1998. Slo3, a novel pH-sensitive K+ channel from mammalian spermatocytes. *The Journal of biological chemistry,* 273**,** 3509-16.

SCHULTE, U. & FAKLER, B. 2000. Gating of inward-rectifier K+ channels by intracellular pH. *European Journal of Biochemistry,* 267**,** 5837-5841.

SCHWAPPACH, B. 2008. An overview of trafficking and assembly of neurotransmitter receptors and ion channels (Review). *Molecular Membrane Biology,* 25**,** 270-278.

ŠEDIVÁ, M., LAŠŠUTHOVÁ, P., ZÁMEČNÍK, J., SEDLÁČKOVÁ, L., SEEMAN, P. & HABERLOVÁ, J. 2019. Novel variant in the KCNK9 gene in a girl with Birk Barel syndrome. *European Journal of Medical Genetics*.

SEOH, S.-A., SIGG, D., PAPAZIAN, D. M. & BEZANILLA, F. 1996. Voltage-Sensing Residues in the S2 and S4 Segments of the Shaker K+ Channel. *Neuron,* 16**,** 1159-1167.

SHIKANO, S., COBLITZ, B., SUN, H. & LI, M. 2005. Genetic isolation of transport signals directing cell surface expression. *Nature Cell Biology,* 7**,** 985-992.

SHULGA, Y. V., TOPHAM, M. K. & EPAND, R. M. 2011. Regulation and Functions of Diacylglycerol Kinases. *Chemical Reviews,* 111**,** 6186-6208.

SIMEN, A. A., LEE, C. C., SIMEN, B. B., BINDOKAS, V. P. & MILLER, R. J. 2001. The C terminus of the Ca channel alpha1B subunit mediates selective inhibition by G-protein-coupled receptors. *J Neurosci,* 21**,** 7587-97.

SIMONNEAU, G., GATZOULIS, M. A., ADATIA, I., CELERMAJER, D., DENTON, C., GHOFRANI, A., GOMEZ SANCHEZ, M. A., KRISHNA KUMAR, R., LANDZBERG, M., MACHADO, R. F., OLSCHEWSKI, H., ROBBINS, I. M. & SOUZA, R. 2013. Updated clinical classification of pulmonary hypertension. *J Am Coll Cardiol,* 62**,** D34-41.

SMITH, D. B. & JOHNSON, K. S. 1988. Single-step purification of polypeptides expressed in Escherichia coli as fusions with glutathione S-transferase. *Gene,* 67**,** 31-40.

STARCEVIC, M., NAZARIAN, R. & DELL'ANGELICA, E. C. 2002. The molecular machinery for the biogenesis of lysosome-related organelles: lessons from Hermansky-Pudlak syndrome. *Semin Cell Dev Biol,* 13**,** 271-8.

STEELE, D. F., ELDSTROM, J. & FEDIDA, D. 2007. Mechanisms of cardiac potassium channel trafficking. *J Physiol,* 582**,** 17-26.

STEINBERG, E. A., WAFFORD, K. A., BRICKLEY, S. G., FRANKS, N. P. & WISDEN, W. 2015. The role of K2P channels in anaesthesia and sleep. *Pflügers Archiv - European Journal of Physiology,* 467**,** 907-916.

STETEFELD, J., MCKENNA, S. A. & PATEL, T. R. 2016. Dynamic light scattering: a practical guide and applications in biomedical sciences. *Biophys Rev.*

STOJANOVSKI, D., BOHNERT, M., PFANNER, N. & VAN DER LAAN, M. 2012. Mechanisms of protein sorting in mitochondria. *Cold Spring Harb Perspect Biol,* 4.

SUGASE, K., DYSON, H. J. & WRIGHT, P. E. 2007. Mechanism of coupled folding and binding of an intrinsically disordered protein. *Nature,* 447**,** 1021-5.

SUH, B.-C. & HILLE, B. 2008. PIP ₂ Is a Necessary Cofactor for Ion Channel Function: How and Why? *Annual Review of Biophysics,* 37**,** 175-195.

SWANTON, E. & BULLEID, N. J. 2003. Protein folding and translocation across the endoplasmic reticulum membrane. *Mol Membr Biol,* 20**,** 99-104.

SWARTZ, K. J. 2004. Towards a structural view of gating in potassium channels. *Nature Reviews Neuroscience,* 5**,** 905-916.

SYLVESTER, J. T., SHIMODA, L. A., AARONSON, P. I. & WARD, J. P. 2012. Hypoxic pulmonary vasoconstriction. *Physiol Rev,* 92**,** 367-520.

SZABO, I. & ZORATTI, M. 2014. Mitochondrial Channels: Ion Fluxes and More. *Physiological Reviews,* 94**,** 519-608.

SZEWCZYK, A., JARMUSZKIEWICZ, W. & KUNZ, W. S. 2009. Mitochondrial potassium channels. *IUBMB Life,* 61**,** 134-143.

TALLEY, E. M. & BAYLISS, D. A. 2002a. Modulation of TASK-1 (Kcnk3) and TASK-3 (Kcnk9) potassium channels: volatile anesthetics and neurotransmitters share a molecular site of action. *J Biol Chem,* 277**,** 17733-42.

TALLEY, E. M. & BAYLISS, D. A. 2002b. Modulation of TASK-1 (Kcnk3) and TASK-3 (Kcnk9) potassium channels: volatile anesthetics and neurotransmitters share a molecular site of action. *The Journal of biological chemistry,* 277**,** 17733-42.

TALLEY, E. M., LEI, Q., SIROIS, J. E. & BAYLISS, D. A. 2000. TASK-1, a two-pore domain K+ channel, is modulated by multiple neurotransmitters in motoneurons. *Neuron,* 25**,** 399-410.

TALLEY, E. M., SOLORZANO, G., LEI, Q., KIM, D. & BAYLISS, D. A. 2001a. Cns distribution of members of the two-pore-domain (KCNK) potassium channel family. *J Neurosci,* 21**,** 7491-505.

TALLEY, E. M., SOLORZANO, G., LEI, Q., KIM, D. & BAYLISS, D. A. 2001b. Cns distribution of members of the two-pore-domain (KCNK) potassium channel family. *The Journal of neuroscience : the official journal of the Society for Neuroscience,* 21**,** 7491-505.

TAMASKOVIC, R., SIMON, M., STEFAN, N., SCHWILL, M. & PLÜCKTHUN, A. 2012. Chapter five - Designed Ankyrin Repeat Proteins (DARPins): From Research to Therapy. *In:* WITTRUP, K. D. & VERDINE, G. L. (eds.) *Methods in Enzymology.* Academic Press.

TANG, H., DESAI, A. A. & YUAN, J. X. 2016. Genetic Insights into Pulmonary Arterial Hypertension. Application of Whole-Exome Sequencing to the Study of Pathogenic Mechanisms. *Am J Respir Crit Care Med,* 194**,** 393-7.

TAO, X., AVALOS, J. L., CHEN, J. & MACKINNON, R. 2009. Crystal structure of the eukaryotic strong inward-rectifier K+ channel Kir2.2 at 3.1 A resolution. *Science,* 326**,** 1668-74.

TAVERNA, S., TKATCH, T., METZ, A. E. & MARTINA, M. 2005. Differential Expression of TASK Channels between Horizontal Interneurons and Pyramidal Cells of Rat Hippocampus. *Journal of Neuroscience,* 25**,** 9162-9170.

TEMPLE, I. K. 2007. Imprinting in human disease with special reference to transient neonatal diabetes and Beckwith-Wiedemann syndrome. *Endocrine development,* 12**,** 113-23.

THINAKARAN, G. & KOO, E. H. 2008. Amyloid precursor protein trafficking, processing, and function. *J Biol Chem,* 283**,** 29615-9.

TIAN, C., ZHU, R., ZHU, L., QIU, T., CAO, Z. & KANG, T. 2014. Potassium Channels: Structures, Diseases, and Modulators. *Chemical Biology & Drug Design,* 83**,** 1-26.

TIMOFEEV, I. 2011. Neuronal plasticity and thalamocortical sleep and waking oscillations. *Prog Brain Res,* 193**,** 121-44.

TIRADO-SANTIAGO, G., LAZARO-MUNOZ, G., RODRIGUEZ-GONZALEZ, V. & MALDONADO-VLAAR, C. S. 2006. Microinfusions of neurotensin antagonist SR 48692 within the nucleus accumbens core impair spatial learning in rats. *Behav Neurosci,* 120**,** 1093-102.

TIZZANO, E. F., CHITAYAT, D. & BUCHWALD, M. 1993. Cell-specific localization of CFTR mRNA shows developmentally regulated expression in human fetal tissues. *Hum Mol Genet,* 2**,** 219-24.

TOMPA, P. 2009. Bioinformatics Approaches to the Structure and Function of Intrinsically Disordered Proteins. *In:* RIGDEN, D. J. (ed.) *From Protein Structure to Function with Bioinformatics.* Dordrecht: Springer Netherlands.

TRAD, S., AMOURA, Z., BEIGELMAN, C., HAROCHE, J., COSTEDOAT, N., BOUTIN LE, T. H., CACOUB, P., FRANCES, C., WECHSLER, B., GRENIER, P. & PIETTE, J. C. 2006. Pulmonary arterial hypertension is a major mortality factor in diffuse systemic sclerosis, independent of interstitial lung disease. *Arthritis Rheum,* 54**,** 184-91.

TRAPP, S., ALLER, M. I., WISDEN, W. & GOURINE, A. V. 2008. A role for TASK-1 (KCNK3) channels in the chemosensory control of breathing. *J Neurosci,* 28**,** 8844-50.

TSCHUMI, C. W. & BECKSTEAD, M. J. 2019. Diverse actions of the modulatory peptide neurotensin on central synaptic transmission. *Eur J Neurosci,* 49**,** 784-793.

TU, L. & DEUTSCH, C. 1999. Evidence for Dimerization of Dimers in K+ Channel Assembly. *Biophysical Journal,* 76**,** 2004-2017.

TU, L., WANG, J., HELM, A., SKACH, W. R. & DEUTSCH, C. 2000. Transmembrane Biogenesis of Kv1. *Biochemistry,* 39**,** 824-836.

TURNER, P. J. & BUCKLER, K. J. 2013. Oxygen and mitochondrial inhibitors modulate both monomeric and heteromeric TASK-1 and TASK-3 channels in mouse carotid body type-1 cells. *J Physiol,* 591**,** 5977-98.

UVERSKY, V. N. 2013. Unusual biophysics of intrinsically disordered proteins. *Biochim Biophys Acta,* 1834**,** 932-51.

UVERSKY, V. N. 2016. Dancing Protein Clouds: The Strange Biology and Chaotic Physics of Intrinsically Disordered Proteins. *J Biol Chem,* 291**,** 6681-8.

UVERSKY, V. N. 2017. Paradoxes and wonders of intrinsic disorder: Stability of instability. *Intrinsically Disordered Proteins,* 5**,** e1327757.

UVERSKY, V. N., DAVE, V., IAKOUCHEVA, L. M., MALANEY, P., METALLO, S. J., PATHAK, R. R. & JOERGER, A. C. 2014. Pathological unfoldomics of uncontrolled chaos: intrinsically disordered proteins and human diseases. *Chem Rev,* 114**,** 6844-79.

VAN DER LEE, R., LANG, B., KRUSE, K., GSPONER, J., SANCHEZ DE GROOT, N., HUYNEN, M. A., MATOUSCHEK, A., FUXREITER, M. & BABU, M. M. 2014. Intrinsically disordered segments affect protein half-life in the cell and during evolution. *Cell Rep,* 8**,** 1832-1844.

VASSAR, R., BENNETT, B. D., BABU-KHAN, S., KAHN, S., MENDIAZ, E. A., DENIS, P., TEPLOW, D. B., ROSS, S., AMARANTE, P., LOELOFF, R., LUO, Y., FISHER, S., FULLER, J., EDENSON, S., LILE, J., JAROSINSKI, M. A., BIERE, A. L., CURRAN, E., BURGESS, T., LOUIS, J. C., COLLINS, F., TREANOR, J., ROGERS, G. & CITRON, M. 1999. Beta-secretase cleavage of Alzheimer's amyloid precursor protein by the transmembrane aspartic protease BACE. *Science,* 286**,** 735-41.

VEALE, E. L., BUSWELL, R., CLARKE, C. E. & MATHIE, A. 2007a. Identification of a region in the TASK3 two pore domain potassium channel that is critical for its blockade by methanandamide. *British journal of pharmacology,* 152**,** 778-86.

VEALE, E. L., HASSAN, M., WALSH, Y., AL-MOUBARAK, E. & MATHIE, A. 2014. Recovery of Current through Mutated TASK3 Potassium Channels Underlying Birk Barel Syndrome s. *MOLECULAR PHARMACOLOGY Mol Pharmacol,* 85**,** 397-407.

VEALE, E. L., KENNARD, L. E., SUTTON, G. L., MACKENZIE, G., SANDU, C. & MATHIE, A. 2007b. Gaq - Mediated Regulation of TASK3 Two-Pore Domain Potassium Channels: The Role of Protein Kinase C. *Molecular Pharmacology,* 71**,** 1666-1675.

VERKHRATSKY, A., KRISHTAL, O. A. & PETERSEN, O. H. 2006. From Galvani to patch clamp: the development of electrophysiology. *Pflügers Archiv - European Journal of Physiology,* 453**,** 233-247.

VU, M. T., DU, G., BAYLISS, D. A. & HORNER, R. L. 2015. TASK Channels on Basal Forebrain Cholinergic Neurons Modulate Electrocortical Signatures of Arousal by Histamine. *The Journal of neuroscience : the official journal of the Society for Neuroscience*.

VUZMAN, D. & LEVY, Y. 2010. DNA search efficiency is modulated by charge composition and distribution in the intrinsically disordered tail. *Proc Natl Acad Sci U S A,* 107**,** 21004-9.

WALDO, G. L., RICKS, T. K., HICKS, S. N., CHEEVER, M. L., KAWANO, T., TSUBOI, K., WANG, X., MONTELL, C., KOZASA, T., SONDEK, J. & HARDEN, T. K. 2010. Kinetic Scaffolding Mediated by a Phospholipase C–β and Gq Signaling Complex. *Science,* 330**,** 974-80.

WALLACE, B. A. 2009. Protein characterisation by synchrotron radiation circular dichroism spectroscopy. *Q Rev Biophys,* 42**,** 317-70.

WASHBURN, C. P., SIROIS, J. E., TALLEY, E. M., GUYENET, P. G. & BAYLISS, D. A. 2002. Serotonergic Raphe Neurons Express TASK Channel Transcripts and a TASK-Like pH- and Halothane-Sensitive K⁺ Conductance. *The Journal of Neuroscience,* 22**,** 1256.

WATKINS, C. S. & MATHIE, A. 1996. A non-inactivating K+ current sensitive to muscarinic receptor activation in rat cultured cerebellar granule neurons. *J Physiol,* 491**,** 401-12.

WATSON, M. A., YAMADA, M., CUSACK, B., VEVERKA, K., BOLDEN-WATSON, C. & RICHELSON, E. 1992. The rat neurotensin receptor expressed in Chinese hamster ovary cells mediates the release of inositol phosphates. *J Neurochem,* 59**,** 1967-70.

WEDEGAERTNER, P. B. 2012. G Protein Trafficking. *Subcell Biochem,* 63**,** 193-223.

WEI, A., JEGLA, T. & SALKOFF, L. 1996. Eight Potassium Channel Families Revealed by the C. elegans Genome Project. *Neuropharmacology,* 35**,** 805-829.

WEINREB, P. H., ZHEN, W., POON, A. W., CONWAY, K. A. & LANSBURY, P. T. 1996. NACP, A Protein Implicated in Alzheimer's Disease and Learning, Is Natively Unfolded. *Biochemistry,* 35**,** 13709-13715.

WEIR, E. K., LOPEZ-BARNEO, J., BUCKLER, K. J. & ARCHER, S. L. 2005. Acute oxygen-sensing mechanisms. *N Engl J Med,* 353**,** 2042-55.

WEISSMAN, T. A., RIQUELME, P. A., IVIC, L., FLINT, A. C. & KRIEGSTEIN, A. R. 2004. Calcium Waves Propagate through Radial Glial Cells and Modulate Proliferation in the Developing Neocortex. *Neuron,* 43**,** 647-661.

WIEDEMANN, C., BELLSTEDT, P. & GORLACH, M. 2013. CAPITO--a web server-based analysis and plotting tool for circular dichroism data. *Bioinformatics,* 29**,** 1750-7.

WILKE, B. U., LINDNER, M., GREIFENBERG, L., ALBUS, A., KRONIMUS, Y., BÜNEMANN, M., LEITNER, M. G. & OLIVER, D. 2014. ARTICLE Diacylglycerol mediates regulation of TASK potassium channels by Gq-coupled receptors. *Nature Communications,* 5.

WILLIAMS, B. A. & BUCKLER, K. J. 2004. Biophysical properties and metabolic regulation of a TASK-like potassium channel in rat carotid body type 1 cells. *American Journal of Physiology-Lung Cellular and Molecular Physiology,* 286**,** L221-L230.

WILSON, M. S., MENTINK-KANE, M. M., PESCE, J. T., RAMALINGAM, T. R., THOMPSON, R. & WYNN, T. A. 2007. Immunopathology of schistosomiasis. *Immunol Cell Biol,* 85**,** 148-54.

WITSCHAS, K., JOBIN, M.-L., KORKUT, D. N., VLADAN, M. M., SALGADO, G., LECOMTE, S., VLACHOVA, V. & ALVES, I. D. 2015. Interaction of a peptide derived from C-terminus of human TRPA1 channel with model membranes mimicking the inner leaflet of the plasma membrane. *Biochimica et Biophysica Acta (BBA) - Biomembranes,* 1848**,** 1147-1156.

WOOD, K. A., DIPASQUALE, B. & YOULE, R. J. 1993. In situ labeling of granule cells for apoptosis-associated DNA fragmentation reveals different mechanisms of cell loss in developing cerebellum. *Neuron,* 11**,** 621-632.

WRIGHT, P. D., VEALE, E. L., MCCOULL, D., TICKLE, D. C., LARGE, J. M., OCOCKS, E., GOTHARD, G., KETTLEBOROUGH, C., MATHIE, A. & JERMAN, J. 2017. Terbinafine is a novel and selective activator of the two-pore domain potassium channel TASK3. *Biochem Biophys Res Commun,* 493**,** 444-450.

WU, F. & YAO, P. J. 2009. Clathrin-mediated endocytosis and Alzheimer's disease: an update. *Ageing Res Rev,* 8**,** 147-9.

WULFF, H. & ZHOROV, B. S. 2008. K+ channel modulators for the treatment of neurological disorders and autoimmune diseases. *Chem Rev,* 108**,** 1744-73.

XIAO, Z., DENG, P. Y., ROJANATHAMMANEE, L., YANG, C., GRISANTI, L., PERMPOONPUTTANA, K., WEINSHENKER, D., DOZE, V. A., PORTER, J. E. & LEI, S. 2009. Noradrenergic depression of neuronal excitability in the entorhinal cortex via activation of TREK-2 K+ channels. *J Biol Chem,* 284**,** 10980-91.

XIONG, Z. Q. & STRINGER, J. L. 2000. Extracellular pH responses in CA1 and the dentate gyrus during electrical stimulation, seizure discharges, and spreading depression. *J Neurophysiol,* 83**,** 3519-24.

YAFFE, M. B. 2002. How do 14-3-3 proteins work?-- Gatekeeper phosphorylation and the molecular anvil hypothesis. *FEBS Lett,* 513**,** 53-7.

YAMAUCHI, R., WADA, E., KAMICHI, S., YAMADA, D., MAENO, H., DELAWARY, M., NAKAZAWA, T., YAMAMOTO, T. & WADA, K. 2007. Neurotensin type 2 receptor is involved in fear memory in mice. *J Neurochem,* 102**,** 1669-1676.

YAO, J., MCHEDLISHVILI, D., MCINTIRE, W. E., GUAGLIARDO, N. A., ERISIR, A., COBURN, C. A., SANTARELLI, V. P., BAYLISS, D. A. & BARRETT, P. Q. 2017. Functional TASK-3-Like Channels in Mitochondria of Aldosterone-Producing Zona Glomerulosa Cells. *Hypertension (Dallas, Tex. : 1979),* 70**,** 347-356.

YELLEN, G. 2002. The voltage-gated potassium channels and their relatives. *Nature,* 419**,** 35-42.

YOUNG-PEARSE, T. L., BAI, J., CHANG, R., ZHENG, J. B., LOTURCO, J. J. & SELKOE, D. J. 2007. A critical function for beta-amyloid precursor protein in neuronal migration revealed by in utero RNA interference. *J Neurosci,* 27**,** 14459-69.

YU, F. H. & CATTERALL, W. A. 2004. The VGL-Chanome: A Protein Superfamily Specialized for Electrical Signaling and Ionic Homeostasis. *Science Signaling,* 2004**,** re15-re15.

YU, X., FRANKS, N. P. & WISDEN, W. 2018. Sleep and Sedative States Induced by Targeting the Histamine and Noradrenergic Systems. *Frontiers in Neural Circuits,* 12.

YUAN, J. X., ALDINGER, A. M., JUHASZOVA, M., WANG, J., CONTE, J. V., JR., GAINE, S. P., ORENS, J. B. & RUBIN, L. J. 1998. Dysfunctional voltage-gated K+ channels in pulmonary artery smooth muscle cells of patients with primary pulmonary hypertension. *Circulation,* 98**,** 1400-6.

YUILL, K., ASHMOLE, I. & STANFIELD, P. R. 2004. The selectivity filter of the tandem pore potassium channel TASK-1 and its pH-sensitivity and ionic selectivity. *Pflugers Arch,* 448**,** 63-9.

ZHANG, H., DONG, H., CILZ, N. I., KURADA, L., HU, B., WADA, E., BAYLISS, D. A., PORTER, J. E. & LEI, S. 2016. Neurotensinergic Excitation of Dentate Gyrus Granule Cells via G??q-Coupled Inhibition of TASK-3 Channels. *Cerebral Cortex*.

ZHANG, X. 2019. Direct Galphaq Gating Is the Sole Mechanism for TRPM8 Inhibition Caused by Bradykinin Receptor Activation. *Cell Rep,* 27**,** 3672-3683.e4.

ZHANG, X., MAK, S., LI, L., PARRA, A., DENLINGER, B., BELMONTE, C. & MCNAUGHTON, P. A. 2012. Direct inhibition of the cold-activated TRPM8 ion channel by G alpha q. *Nature Cell Biology,* 14.

ZHU, S., NOVIELLO, C. M., TENG, J., WALSH, R. M., KIM, J. J. & HIBBS, R. E. 2018. Structure of a human synaptic GABA-A receptor. *Nature,* 559**,** 67-72.

ZILBERBERG, N., ILAN, N. & GOLDSTEIN, S. A. 2001. KCNKO: opening and closing the 2-P-domain potassium leak channel entails "C-type" gating of the outer pore. *Neuron,* 32**,** 635-48.

ZÚÑIGA, L. & ZÚÑIGA, R. 2016. Understanding the Cap Structure in K2P Channels. *Frontiers in Physiology,* 7**,** 228.

ZUZARTE, M., HEUSSER, K., RENIGUNTA, V., SCHLICHTHÖRL, G., RINNÉ, S., WISCHMEYER, E., DAUT, J., SCHWAPPACH, B. & PREISIG-MÜLLER, R. 2009. Intracellular traffic of the K + channels TASK-1 and TASK-3: role of N- and C-terminal sorting signals and interaction with 14-3-3 proteins. *The Journal of Physiology,* 587**,** 929-952.

ZUZARTE, M., RINNÉ, S., SCHLICHTHÖRL, G., SCHUBERT, A., DAUT, J. & PREISIG-MÜLLER, R. 2007. A Di-Acidic Sequence Motif Enhances the Surface Expression of the Potassium Channel TASK-3. *Traffic,* 8**,** 1093-1100.